UNIVERSITE DE YAOUNDE I
FACULTE DES SCIENCES
CENTRE DE RECHERCHE ET DE FORMATION DOCTORALE EN SCIENCES, TECHNOLOGIES ET GEOSCIENCES

UNITE DE RECHERCHE ET DE FORMATION DOCTORALE PHYSIQUE ET APPLICATIONS

THE UNIVERSITY OF YAOUNDE I
FACULTY OF SCIENCE
POSTGRADUATE SCHOOL OF SCIENCE, TECHNOLOGY AND GEOSCIENCES

RESEARCH AND POSTGRADUATE TRAINING UNIT FOR PHYSICS AND APPLICATIONS

LABORATORY OF NUCLEAR, ATOMIC, MOLECULAR PHYSICS AND BIOPHYSICS

# DYNAMICS OF MATTER-WAVE CONDENSATES: EFFECTS OF QUANTUM FLUCTUATIONS AND THREE-BODY INTERATOMIC INTERACTIONS

**Thesis**

Submitted and defended in fulfillment of the requirements for the degree of

**Doctor of Philosophy** in Physics

**Option** : Atom and Radiation



**By**

**BELOBO BELOBO DIDIER**

**Master of Science in Physics, Option : Atom and Radiation**

**Registration number : 98T301**

**Under the supervision of**

**BEN-BOLIE Germain Hubert**
Associate Professor
University of Yaounde I

and

**KOFANE Timoléon Crépin**
Professor
University of Yaounde I

Année académique 2014 - 2015

Academic year 2014 - 2015

REPUBLIQUE DU CAMEROUN
Paix - Travail – Patrie
**********
UNIVERSITE DE YAOUNDE I
**********
CENTRE DE RECHERCHE ET DE FORMATION DOCTORALE EN SCIENCES, TECHNOLOGIES ET GEOSCIENCES
**********
B.P. : 812 Yaoundé
E-mail : crfd_stg@uy1.uninet.cm

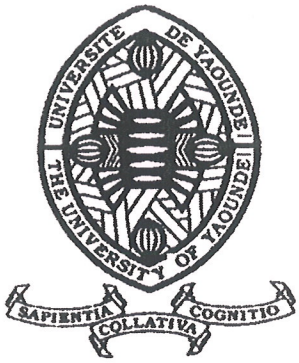


REPUBLIC OF CAMEROON
Peace - Work – Fatherland
**********
THE UNIVERSITY OF YAOUNDE I
**********
POSTGRADUATE SCHOOL OF SCIENCE, TECHNOLOGY AND GEOSCIENCES
**********
Po Box : 812 Yaounde
E-mail : crfd_stg@uy1.uninet.cm

**UNITE DE RECHERCHE ET DE FORMATION DOCTORALE PHYSIQUE ET APPLICATIONS**

**LABORATOIRE DE PHYSIQUE NUCLEAIRE, ATOMIQUE, MOLECULAIRE ET BIOPHYSIQUE**

# ATTESTATION DE CORRECTION

Nous soussignés, **Professeur MANGUELLE-DICOUM Eliézer** et **Professeur OWONO OWONO Luc Calvin**, respectivement Président et Membre du jury de soutenance de thèse de Doctorat/PhD de M. **BELOBO BELOBO Didier**, Matricule 98T301, attestons que l'intéressé a effectué les corrections conformément aux remarques et suggestions des membres du jury.

Cette thèse intitulée «**Dynamics of matter wave condensates: effects of quantum fluctuations and three-body interatomic interactions** », a été présentée et soutenue en vue de l'obtention du diplôme de Doctorat/PhD en Physique.

En foi de quoi la présente attestation lui est délivrée pour servir et valoir ce que de droit.

Yaoundé, le 12 OCT 2015

**Membre**

**Pr OWONO OWONO Luc Calvin**

**Président du Jury**

**Pr MANGUELLE DICOUM Eliézer**

# List of the Permanent Teaching Staff of the Faculty of Science

**ADMINISTRATION**

| | | |
|---|---|---|
| **DEAN** | : | BILONG Paul, Professor |
| **VICE-DEAN/*DPSAA*** Division of Programming and Follow-up of Academic Affairs | : | NJOPWOUO Daniel, Professor |
| **VICE-DEAN/*DSSE*** Division of Admission and Follow-up of Students | : | DONGO Etienne, Professor |
| **VICE-DEAN/*DRC*** Division of Research and Cooperation | : | ESSIMBI ZOBO Bernard, Professor |
| **Head of Division/*DAASR*** Division of Academic Affairs, Admission and Research | : | ABOSSOLO Monique, Senior Lecturer |
| **Head of Division/*DAF*** Administrative and Financial Division | : | NDOYE FOE Marie C. F., Senior Lecturer |

| 1 - DEPARTMENT OF BIOCHEMISTRY(*B.C.*) (41) | | | |
|---|---|---|---|
| 01 | MOUNDIPA FEWOU Paul | Professor | **Head of Department** |
| 02 | OBEN Julius ENYONG | Professor | on duty |
| 03 | BENG *born* NINTCHOM PENLAP V. | Associate Professor | on duty |
| 04 | FEKAM BOYOM Fabrice | Associate Professor | on duty |
| 05 | FOKOU Elie | Associate Professor | on duty |
| 06 | KANSCI Germain | Associate Professor | on duty |
| 07 | MBACHAM Wilfried | Associate Professor | on duty |
| 08 | MINKA Samuel | Associate Professor | on duty |
| 09 | NGUEFACK Julienne | Associate Professor | on duty |
| 10 | ACHU Merci BIH | Senior Lecturer | on duty |
| 11 | ATOGHO Barbara Mma | Senior Lecturer | on duty |
| 12 | BELINGA *born* NDOYE FOE Marie C. F. | Senior Lecturer | **Head *DAF* / FS** |
| 13 | BIGOGA Jude | Senior Lecturer | on duty |
| 14 | BIYITI BI ESSAM *born* AKAM ADA L. F. | Senior Lecturer | *I.G./ MINRESI* |
| 15 | BOUDJEKO Thaddée | Senior Lecturer | on duty |
| 16 | DEMMANO Gustave | Senior Lecturer | on duty |
| 17 | DJOKAM TAMO Rosine | Senior Lecturer | on duty |
| 18 | DJUIDJE NGOUNOUE Marcelline | Senior Lecturer | on duty |
| 19 | EFFA ONOMO Pierre | Senior Lecturer | on duty |
| 20 | EVEHE BEBANDOUE Marie-Solange | Senior Lecturer | on duty |
| 21 | MOFOR *born* TEUGWA Clautilde | Senior Lecturer | *CE SEP/ MINESUP* |
| 22 | NGONDI Judith Laure | Senior Lecturer | on duty |
| 23 | NJAYOU Frédéric Nico | Senior Lecturer | on duty |
| 24 | TCHANA NKOUATCHOUA Angèle | Senior Lecturer | on duty |
| 25 | WAKAM *born* NANA Louise | Senior Lecturer | on duty |
| 26 | AKINDEH MBUH NJI | Assistant | on duty |
| 27 | BEBEE FADIMATOU | Assistant | on duty |
| 28 | BEBOY EDZENGUELE Sara Nathalie | Assistant | on duty |
| 29 | DAKOLE DABOY Charles | Assistant | on duty |
| 30 | DJUIDJE NGOUNOUE Marcelline | Assistant | on duty |
| 31 | DJUIKWO NKONGA Ruth Viviane | Assistant | on duty |
| 32 | DONGMO LEKAGNE Joseph Blaise | Assistant | on duty |
| 33 | KOTUE KAPTUE Charles | Assistant | on duty |
| 34 | FONKOUA Martin | Assistant | on duty |
| 35 | LUNGA Paul KAILAH | Assistant | on duty |
| 36 | MANANGA Marlyse Joséphine | Assistant | on duty |
| 37 | MBONG ANGIE MOUGANDE Mary Ann | Assistant | on duty |
| 38 | MBOUCHE FANMOE Marcelline Joëlle | Assistant | on duty |
| 39 | PACHANGOU NSANGOU Sylvain | Assistant | on duty |
| 40 | Palmer MASUMBE NETONGO | Assistant | on duty |
| 41 | TIENTCHEU DJOKAM Léopold | Assistant | on duty |

| 2 - DEPARTMENT OF ANIMAL BIOLOGY AND PHYSIOLOGY (*B.P.A.*) (45) | | | |
|---|---|---|---|
| 01 | BILONG BILONG Charles Félix | Professor | **Head of Department** |
| 02 | DIMO Théophile | Professor | on duty |
| 03 | FOMENA Abraham | Professor | on duty |
| 04 | KAMTCHOUING Pierre | Professor | on duty |
| 05 | MIMPFOUNDI Remy | Professor | on duty |
| 06 | NGASSAM Pierre | Professor | on duty |
| 07 | NJIOKOU Flobert | Professor | on duty |
| 08 | NOLA Moïse | Professor | on duty |
| 09 | DJIETO Lordon Champlain | Associate Professor | on duty |
| 10 | ESSOMBA née NTSAMA MBALLA | Associate Professor | *MINSANTE* |
| 11 | FOTO MENBOHAN Samuel | Associate Professor | *CT2 MIN. ENERGIE* |
| 12 | KAMGANG René | Associate Professor | *C.S./ MINRESI* |
| 13 | NJAMEN Dieudonné | Associate Professor | on duty |
| 14 | TAN Paul | Associate Professor | on duty |
| 15 | TCHUEM TCHUENTE Louis | Associate Professor | *Coord. Progr./ MINSANTE* |
| 16 | AJEAGAH Gidéon AGHAINDUM | Senior Lecturer | on duty |
| 17 | ALENE Désirée Chantal | Senior Lecturer | on duty |
| 18 | BELLET EDIMO Oscar Roger | Senior Lecturer | on duty |
| 19 | BILANDA Danielle Claude | Senior Lecturer | on duty |
| 20 | DJIOGUE Séfirin | Senior Lecturer | on duty |
| 21 | DZEUFIET DJOMENI Paul Désiré | Senior Lecturer | on duty |
| 22 | GOUNOUE KAMKUMO Raceline | Senior Lecturer | on duty |
| 23 | JATSA MEGAPTCHE Hermine | Senior Lecturer | on duty |
| 24 | KEKEUNOU Sévilor | Senior Lecturer | on duty |
| 25 | MEGNEKOU Rosette | Senior Lecturer | on duty |
| 26 | MONY NTONE Ruth | Senior Lecturer | on duty |
| 27 | NGUEGUIM TSOFACK Florence | Senior Lecturer | on duty |
| 28 | NGUEMBOCK | Senior Lecturer | on duty |
| 29 | TOMBI Jeannette | Senior Lecturer | on duty |
| 30 | ZEBAZE TOGOUET Serge Hubert | Senior Lecturer | on duty |
| 31 | ATSAMO Albert Donatien | Assistant | on duty |
| 32 | ETEME ENAMA Serge | Assistant | on duty |
| 33 | KANDELA KAVAYE Antoine | Assistant | on duty |
| 34 | KOGA MANG'Dobara | Assistant | on duty |
| 35 | LEKEUFACK FOLEFACK Guy Benoît | Assistant | on duty |
| 36 | MAHOB Raymond Joseph | Assistant | on duty |
| 37 | MBENOUN MASSE Paul Serge | Assistant | on duty |
| 38 | MOUNGANG NGAMENI Luciane | Assistant | on duty |
| 39 | MUH Bernice FIEN | Assistant | on duty |
| 40 | MVEYO NDANKEU Yves Patrick | Assistant | on duty |
| 41 | NGOUATEU KENFACK Omer BEBE | Assistant | on duty |
| 42 | NJUA Clarisse YAFI | Assistant | on duty |
| 43 | OBI OBEN Esther | Assistant | on duty |
| 44 | TADU Zéphirin | Assistant | on duty |
| 45 | YEDE | Assistant | on duty |

| 3 - DEPARTMENT OF PLANT BIOLOGY AND PHYSIOLOGY (*B.P.V.*) (25) | | | |
|---|---|---|---|
| 01 | YOUMBI Emmanuel | Professor | **Head of Department** |
| 02 | AMBANG Zachée | Associate Professor | **Vice-Dean/*FSE*** |
| 03 | BELL Joseph Martin | Associate Professor | on duty |
| 04 | DJOCGOUE Pierre François | Associate Professor | on duty |
| 05 | MOSSEBO Dominique Claude | Associate Professor | on duty |
| 06 | YOUMBI Emmanuel | Associate Professor | on duty |
| 07 | ZAPFACK Louis | Associate Professor | on duty |
| 08 | ANGONI Hyacinthe | Senior Lecturer | on duty |
| 09 | BIYE Elvire Hortense | Senior Lecturer | on duty |
| 10 | KENGNE NOUMSI Ives Magloire | Senior Lecturer | on duty |
| 11 | MALLA Armand William | Senior Lecturer | on duty |
| 12 | MBARGA BINDZI Marie Alain | Senior Lecturer | *CEA / MINESUP* |
| 13 | MBOLO Marie | Senior Lecturer | on duty |
| 14 | NDONGO BEKOLO | Senior Lecturer | *CE / MINRESI* |
| 15 | NGODO MELINGUI Jean Baptiste | Senior Lecturer | on duty |
| 16 | NGONKEU MAGAPTCHE Eddy Léonard | Senior Lecturer | on duty |
| 17 | NGOUO Lucas Vincent | Senior Lecturer | on duty |
| 18 | NSOM ZAMO Annie Claude *spouse* PIAL | Senior Lecturer | National Expert/UNESCO |
| 19 | TONFACK Libert Brice | Senior Lecturer | on duty |
| 20 | TSOATA Esaïe | Senior Lecturer | on duty |
| 21 | DJEUANI Astride Carole | Assistant | on duty |
| 22 | MAHBOU SOMO TOUKAM Gabriel | Assistant | on duty |
| 23 | MAFFO MAFFO Nicole Liliane | Assistant | on duty |
| 24 | NGALLE Hermine BILLE | Assistant | on duty |
| 25 | NNANGA MEBENGA Ruth Laure | Assistant | on duty |
| 26 | NOUKEU KOUAKAM Armelle | Assistant | on duty |

| 4 - DEPARTMENT OF INORGANIC CHEMISTRY (*C.I.*) (33) | | | |
|---|---|---|---|
| 01 | NGAMENI Emmanuel | Professor | Director/ *MINESUP* |
| 02 | NJOPWOUO Daniel | Professor | **Vice-Dean/*DPSAA*** |
| 03 | AGWARA ONDOH Moïse | Associate Professor | *I.G./ MINPMEA* |
| 04 | AVOM Jérôme | Associate Professor | Director of *I.A.I* Gabon |
| 05 | BABALE *born* DJAM DOUDOU | Associate Professor | *Chargée de Mission/ P.R.* |
| 06 | DJOUFAC WOUMFO Emmanuel | Associate Professor | on duty |
| 07 | ELIMBI Antoine | Associate Professor | on duty |
| 08 | GHOGOMU Paul MINGO | Associate Professor | Director of PM Cabinet |
| 9 | KETCHA MBADCAM Joseph | Associate Professor | **Head of Department** |
| 10 | LAMINSI Samuel | Associate Professor | on duty |
| 11 | MELO *born* CHINJE Uphie F. | Associate Professor | Director of *MIPROMALO* |
| 12 | NANSEU Charles Péguy | Associate Professor | on duty |
| 13 | NENWA Justin | Associate Professor | on duty |
| 14 | NENWA Justin | Associate Professor | on duty |
| 15 | NDIKONTAR Maurice KOR | Associate Professor | Vice-Dean *UBDA* |
| 16 | NGOMO Horace MANGA | Associate Professor | S.G. of *MINESUP* |
| 17 | YOUNANG Elie | Associate Professor | on duty |
| 18 | BAIZOUMI ZOUA | Senior Lecturer | Head of Unit/ *MINTOUR* |
| 19 | EMADACK Alphonse | Senior Lecturer | on duty |
| 20 | GWET Simon-Pierre | Senior Lecturer | on duty |
| 21 | KEUMEGNE MBOUGUEM Jean Claude | Senior Lecturer | on duty |
| 22 | KONG SAKEO | Senior Lecturer | *C.M./ P.M* |
| 23 | NJIOMOU Chantal *spouse* DJANGANG | Senior Lecturer | on duty |
| 24 | NJOYA Dayirou | Senior Lecturer | on duty |
| 25 | SIGNING Pierre | Senior Lecturer | on duty |
| 26 | ACAYANKA Elie | Senior Lecturer | on duty |
| 27 | CHEUMANI YONA Arnaud | Senior Lecturer | on duty |
| 28 | KAMGANG YOUBI Georges | Senior Lecturer | on duty |
| 29 | NYAMEN Linda Dyorisse | Assistant | on duty |
| 30 | PABOUDAM GBAMBIE Awaou | Senior Lecturer | on duty |
| 31 | TCHAKOUTE KOUAMO Hervé | Senior Lecturer | on duty |
| 32 | BELIBI BELIBI Placide Désiré | Assistant | on duty |
| 33 | NDI Julius NSAMI | Assistant | on duty |

| 5 - DEPARTMENT OF ORGANIC CHEMISTRY (*C.O.*) (34) | | | |
|---|---|---|---|
| 01 | DONGO Etienne | Professor | on duty |
| 02 | GHOGOMU TIH Robert Ralph | Professor | on duty |
| 03 | MBAFOR Joseph | Professor | on duty |
| 04 | NGADJUI TCHALEU B. | Professor | Head of Dept./ *FMBS* |
| 05 | NGOUELA Silvère Augustin | Professor | on duty |
| 06 | NKENGFACK Augustin Ephraïm | Professor | **Head of Department** |
| 07 | NYASSE Barthélemy | Professor | Head of Div./ *MINESUP* |
| 08 | PEGNYEMB Dieudonné Emmanuel | Professor | Head of Div./ *MINESUP* |
| 09 | WANDJI Jean | Professor | on duty |
| 10 | Alex de Théodore ATCHADE | Associate Professor | **CS Rectorat/ UYI** |
| 11 | FOLEFOC Gabriel NGOSONG | Associate Professor | Vice-Dean/ UB |
| 12 | KAPNANG Henriette | Associate Professor | on duty |
| 13 | KEUMEDJIO Félix | Associate Professor | on duty |
| 14 | KOUAM Jacques | Associate Professor | on duty |
| 15 | NOUNGOUE TCHAMO Diderot | Associate Professor | on duty |
| 16 | TCHOUANKEU Jean-Claude | Associate Professor | D.A.A.C. UY I |
| 17 | YANKEP Emmanuel | Associate Professor | on duty |
| 18 | TIH née NGO BILONG E. Anastasie | Associate Professor | on duty |
| 19 | AMBASSA Pantaleon | Senior Lecturer | on duty |
| 20 | EYONG Kenneth OBEN | Senior Lecturer | on duty |
| 21 | KENMOGNE Marguerite | Senior Lecturer | on duty |
| 22 | MBAZOA *born* DJAMA Céline | Senior Lecturer | on duty |
| 23 | MKOUNGA Pierre | Senior Lecturer | on duty |
| 24 | NGO MBING Joséphine | Senior Lecturer | on duty |
| 25 | NGONO BIKOBO Dominique Serge | Senior Lecturer | on duty |
| 26 | NOTE LOUGBOT Olivier | Senior Lecturer | on duty |
| 27 | OUAHOUO WACHE Blandine Marlyse | Senior Lecturer | on duty |
| 28 | TABOPDA KUATE Turibio | Senior Lecturer | on duty |
| 29 | TAGATSING FOTSING Maurice | Senior Lecturer | on duty |
| 30 | ZONDEGOUMBA Ernestine | Senior Lecturer | on duty |
| 31 | FOTSO WABO Ghislain | Assistant | on duty |
| 32 | KAMTO Eutrophe Ledoux | Assistant | on duty |
| 33 | NGINTEDO Dominique | Assistant | on duty |
| 34 | NGOMO Orléans | Assistant | on duty |

| 6 - DEPARTMENT OF COMPUTER SCIENCE (*IN*) (25) | | | |
|---|---|---|---|
| 01 | TCHUENTE Maurice | Professor | *PCA* UB |
| 02 | ATSA ETOUNDI Roger | Associate Professor | Head of Dep., Head of Div./ *MINFOPRA* |
| 03 | FOTSO Pauline Laure | Associate Professor | Vice-Rector/ UDs |
| 04 | FOUDA NDJODO Marcel | Associate Professor | *IA4 MINESUP*/H.O.D *ENS* |
| 05 | NDOUNDAM René | Associate Professor | on duty |
| 06 | CHEDOM FOTSO Donatien | Senior Lecturer | on duty |
| 07 | MELATAGIA YONTA Paulin | Senior Lecturer | on duty |
| 08 | MOTO MPONG Serge Alain | Senior Lecturer | on duty |
| 09 | TINDO Gilbert | Senior Lecturer | on duty |
| 10 | TSOPZE Norbert | Senior Lecturer | on duty |
| 11 | WAKU KOUAMOU Jules | Senior Lecturer | on duty |
| 12 | ABESSOLO ALO'O Gislain | Assistant | on duty |
| 13 | BAYEM Jacques Narcisse | Assistant | on duty |
| 14 | DJOUWE MEFFEJA Merline Flore | Assistant | on duty |
| 15 | DOMGA KOMGUEM Rodrigue | Assistant | on duty |
| 16 | EBELE Serge | Assistant | on duty |
| 17 | HAMZA Adamou | Assistant | on duty |
| 18 | KAMDEM KENGNE Christiane | Assistant | on duty |
| 19 | KAMGUEU Patrick Olivier | Assistant | on duty |
| 20 | KENFACK DONGMO Clauvice Viliane | Assistant | on duty |
| 21 | KOUOKAM KOUOKAM Etienne Appolin | Assistant | on duty |
| 22 | MEYEMDOU Nadège Sylvianne | Assistant | on duty |
| 23 | MONTHE DJIADEU Valery Martial | Assistant | on duty |
| 24 | JIOMEKONG AZANZI Fidel | Assistant | on duty |
| 25 | TAPOMO KENFACK Hyppolite | Assistant | on duty |

| 7 - DEPARTMENT OF MATHEMATICS (*MA*) (35) | | | |
|---|---|---|---|
| 01 | BEKOLLE David | Professor | Vice-Rector/UN |
| 02 | BITJONG NDOMBOL | Professor | *DIDP* UY II |
| 03 | DOSSA COSSY Marcel | Professor | on duty |
| 04 | NGUETSENG Gabriel | Professor | Head of Training Course *IUT-BOIS* UYI |
| 05 | NOUTCHEGUEME Norbert | Professor | on duty |
| 06 | EMVUDU WONO Yves S. | Associate Professor | Head of Unit/ *MINESUP* |
| 07 | NKUIMI JUGNIA Célestin | Associate Professor | on duty |
| 08 | TCHAPNDA NJABO Sophonie Blaise | Associate Professor | on duty |
| 09 | TONGA Marcel | Associate Professor | on duty |
| 10 | WAMON François | Associate Professor | **Head of Department** |
| 11 | AGHOUKENG JIOFACK Jean Gérard | Senior Lecturer | on duty |
| 12 | AYISSI Raoult Domingo | Senior Lecturer | on duty |
| 13 | FOMEKONG Christophe | Senior Lecturer | on duty |
| 14 | KIANPI Maurice | Senior Lecturer | on duty |
| 15 | KIKI Maxime Armand | Senior Lecturer | on duty |
| 16 | MBAKOP Guy Merlin | Senior Lecturer | on duty |
| 17 | MBANG Joseph | Senior Lecturer | on duty |
| 18 | MBIANDA Gilbert | Senior Lecturer | on duty |
| 19 | MENGUE MENGUE David Joe | Senior Lecturer | on duty |
| 20 | NGUIMTSA Charles | Senior Lecturer | on duty |
| 21 | NOUNDJEU Pierre | Senior Lecturer | on duty |
| 22 | TCHANGANG Roger Duclos | Senior Lecturer | on duty |
| 23 | TCHOUNDJA Edgar Landry | Senior Lecturer | on duty |
| 24 | TIAYA TSAGUE N. Anne-Marie | Senior Lecturer | on duty |
| 25 | CHENDJOU Gilbert | Assistant | on duty |
| 26 | DJIADEU NGAHA Michel | Assistant | on duty |
| 27 | MBEHOU Mohamed | Assistant | on duty |
| 28 | MBELE BEDIMA Martin | Assistant | on duty |
| 29 | MBIAKOP Hilaire George | Assistant | on duty |
| 30 | NGUEFACK Bertrand | Assistant | on duty |
| 31 | NIMPA PEFOUKEU Romain | Assistant | on duty |
| 32 | POLA DOUNDOU Emmanuel | Assistant | on duty |
| 33 | TAKAM SOH Patrice | Assistant | on duty |
| 34 | TANG AHANDA Barnabé | Assistant | Head of Serv. *MINPLAMAT* |
| 35 | TETSADJIO TCHILEPECK Mesmin Erick | Assistant | on duty |

| 8 - DEPARTMENT OF MICROBIOLOGY (*MB*) (13) | | | |
|---|---|---|---|
| 01 | ETOA François-Xavier | Professor | **Head of Department**/*CT PM* |
| 02 | ESSIA NGANG Jean Justin | Associate Professor | on duty |
| 03 | NWAGA Dieudonné M. | Associate Professor | on duty |
| 04 | BODA Maurice | Senior Lecturer | on duty |
| 05 | BOYOMO ONANA | Senior Lecturer | on duty |
| 06 | ENO Anna Arey | Senior Lecturer | on duty |
| 07 | ESSONO OBOUGOU Germain Gabriel | Senior Lecturer | on duty |
| 08 | NYEGUE Maximillienne Ascension | Senior Lecturer | on duty |
| 09 | RIWOM Sara Honorine | Senior Lecturer | on duty |
| 10 | SADO KAMDEM Sylvain Leroy | Senior Lecturer | on duty |
| 11 | BOUGNOM Blaise Pascal | Assistant | on duty |
| 12 | NJIKI BIKOÏ Jacky | Assistant | on duty |
| 13 | TCHIKOUA Roger | Assistant | on duty |

| 9 - DEPARTMENT OF PHYSICS (*PH*) (40) | | | |
|---|---|---|---|
| 01 | ESSIMBI ZOBO Bernard | Professor | **Vice-Dean/DRC** |
| 02 | KOFANE Timoléon Crépin | Professor | **Head of Department** |
| 03 | NJOMO Donatien | Professor | on duty |
| 04 | WOAFO Paul | Professor | on duty |
| 05 | NDJAKA Jean Marie Bienvenu | Professor | on duty |
| 06 | BEN-BOLIE Germain Hubert | Associate Professor | on duty |
| 07 | EKOBENA FOUDA Henri Paul | Associate Professor | Head of Dept./ UN |
| 08 | NJANDJOCK NOUCK Philippe | Associate Professor | Head of Serv./ *MINRESI* |
| 09 | NOUAYOU Robert | Associate Professor | on duty |
| 10 | OUMAROU BOUBA | Associate Professor | Rector UY II |
| 11 | PEMHA Elkana | Associate Professor | on duty |
| 12 | TABOD Charles TABOD | Associate Professor | Dean/ UBda |
| 13 | TCHAWOUA Clément | Associate Professor | on duty |
| 14 | ZEKENG Serge Sylvain | Associate Professor | on duty |
| 15 | BIYA MOTTO Frédéric | Senior Lecturer | Gen. Manager of MEKIM Dam |
| 16 | BODO Bernard | Senior Lecturer | on duty |
| 17 | DJUIDJE KENMOE Germaine *spouse* ALOYEM K. | Senior Lecturer | on duty |
| 18 | EDONGUE HERVAIS | Senior Lecturer | on duty |
| 19 | EYEBE FOUDA Jean Sire | Senior Lecturer | on duty |
| 20 | FEWO Serge Ibraïd | Senior Lecturer | on duty |
| 21 | FOUEDJIO David | Senior Lecturer | on duty |
| 22 | HONA Jacques | Senior Lecturer | on duty |
| 23 | MBANE BIOUELE | Senior Lecturer | on duty |
| 24 | MBONO SAMBA Yves Christian U. | Senior Lecturer | on duty |
| 25 | NANA NBENDJO Blaise | Senior Lecturer | on duty |
| 26 | NDOP Joseph | Senior Lecturer | on duty |
| 27 | OBOUNOU Marcel | Senior Lecturer | on duty |
| 28 | SAIDOU | Senior Lecturer | on duty |
| 29 | SIEWE SIEWE Martin | Senior Lecturer | on duty |
| 30 | SIMO Elie | Senior Lecturer | on duty |
| 31 | TABI Conrad Bertrand | Senior Lecturer | on duty |
| 32 | TCHOFFO Fidèle | Senior Lecturer | on duty |
| 33 | VONDOU DERBETINI Appolinaire | Senior Lecturer | on duty |
| 34 | WAKATA *born* BEYA Annie | Senior Lecturer | Head of Serv./ *MINESUP* |
| 35 | WOULACHE Rosalie Laure | Senior Lecturer | on duty |
| 36 | ABDOURAHIMI | Assistant | on duty |
| 37 | CHAMANI Roméo | Assistant | on duty |
| 38 | ENYEGUE A NYAM Françoise *spouse* BELINGA | Assistant | on duty |
| 39 | MBINACK Clément | Assistant | on duty |
| 40 | MBOUSSI NKOMIDIO Aissatou | Assistant | on duty |

| 10 - DEPARTMENT OF EARTH SCIENCE (*S.T.*) (43) | | | |
|---|---|---|---|
| 01 | BILONG Paul | Professor | **Dean/ Head of Department** |
| 02 | NZENTI Jean-Paul | Professor | on duty |
| 03 | BITOM Dieudonné Lucien | Professor | Dean/ UN |
| 04 | FOUATEU Rose *spouse* YONGUE | Associate Professor | on duty |
| 05 | KAMGANG Pierre | Associate Professor | on duty |
| 06 | MEDJO EKO Robert | Associate Professor | *D.I.P.D.* UYI |
| 07 | MVONDO ONDOA Joseph | Associate Professor | on duty |
| 08 | NDAM NGOUPAYOU Jules-Remy | Associate Professor | on duty |
| 09 | NDJIGUI Paul-Désiré | Associate Professor | *C.S.M.M.* |
| 10 | NGOS III Simon | Associate Professor | *D.A.A.C./ UM* |
| 11 | NJILAH Isaac KONFOR | Associate Professor | on duty |
| 12 | NKOUMBOU Charles | Associate Professor | on duty |
| 13 | TEMDJIM Robert | Associate Professor | on duty |
| 14 | ABOSSOLO *born* ANGUE Monique | Senior Lecturer | Head of *DAASR* |
| 15 | BEKOA Etienne | Senior Lecturer | on duty |
| 16 | BISSO Dieudonné | Senior Lecturer | Director of Memve'ele Dam Project |
| 17 | EKOMANE Emile | Senior Lecturer | *CS/MINIMDT* |
| 18 | ESSONO Jean | Senior Lecturer | *C.E.A. MINIMDT* |
| 19 | GANNO Sylvestre | Senior Lecturer | on duty |
| 20 | GHOGOMU Richard TANWI | Senior Lecturer | on duty |
| 21 | LAMILEN BILLA Daniel | Senior Lecturer | on duty |
| 22 | LIENOU Gaston | Senior Lecturer | on duty |
| 23 | MBIDA YEM | Senior Lecturer | *CS/LABOGENIE* |
| 24 | MINYEM Dieudonné | Senior Lecturer | on duty |
| 25 | MOUAFO Lucas | Senior Lecturer | on duty |
| 26 | MOUNDI Amidou | Senior Lecturer | *Insp. 1 MINIMDT* |
| 27 | NGO BIDJECK Louise Marie | Senior Lecturer | on duty |
| 28 | NGUEUTCHOUA Gabriel | Senior Lecturer | on duty |
| 29 | NJILAH Isaac KONFOR | Senior Lecturer | on duty |
| 30 | NYECK Bruno | Senior Lecturer | *Ass. Man./MINIMDT* |
| 31 | ONANA Vincent | Senior Lecturer | on duty |
| 32 | TCHAKOUNTE Jacqueline *spouse* NUMBEM | Senior Lecturer | *CEA/MINRESI* |
| 33 | TCHOUANKOUE Jean-Pierre | Senior Lecturer | on duty |
| 34 | YENE ATANGANA Joseph Q. | Senior Lecturer | Head of Div. *MINFOF* |
| 35 | ZO'O ZAME Philémon | Assistant | S.G. of *MINTP* |
| 36 | ANABA ONANA Achille Basile | Assistant | on duty |
| 37 | FUH Calistus Gentry | Assistant | Sec of State/*MINMIDT* |
| 38 | METANG Victor | Assistant | on duty |
| 39 | NGO BELNOUN Rose Noël | Assistant | on duty |
| 40 | NOMO NEGUE Emmanuel | Assistant | on duty |
| 41 | TCHAPTCHET TCHATO De Pesquidoux I | Assistant | on duty |
| 42 | TEHNA Nathanaël | Assistant | CS/*MINMIDT* |
| 43 | TEMGA Jean Pierre | Assistant | on duty |

**Distribution of the permanent Teaching Staff of the Faculty of Science according to Departments (28 May 2013)**

| Department | Number of Lecturers | | | | |
|---|---|---|---|---|---|
| | **Professors** | **Associate Professors** | **Senior Lecturers** | **Assistants** | **Total** |
| **B.C.** | 02 (0) | 06 (1) | 16 (11) | 16 (7) | **40 (20)** |
| **B.P.A** | 07 (0) | 06 (0) | 14 (7) | 20 (5) | **47 (12)** |
| **B.P.V** | 01 (0) | 06 (0) | 11 (3) | 08 (5) | **26 (08)** |
| **C.I.** | 03 (0) | 14 (2) | 09 (1) | 08 (2) | **34 (05)** |
| **C.O.** | 11 (0) | 06 (1) | 13 (6) | 07 (1) | **37 (08)** |
| **IN** | 01 (0) | 04 (1) | 06 (0) | 15 (4) | **26 (05)** |
| **MA** | 05 (0) | 02 (0) | 19 (1) | 13 (1) | **39 (02)** |
| **MB** | 01 (0) | 02 (0) | 06 (3) | 03 (0) | **12 (03)** |
| **PH** | 03 (0) | 08 (0) | 19 (3) | 09 (1) | **39 (04)** |
| **ST** | 02 (0) | 10 (1) | 20 (3) | 10 (1) | **42 (05)** |
| **Total** | **36 (0)** | **64 (6)** | **133 (38)** | **109 (27)** | **342 (71)** |

That is, a total of: 342 (71) with
- Professors 36 (0)
- Associate Professors 64 (6)
- Senior Lecturers 133 (38)
- Assistants 109 (27)

- ( ) = Number of Women.

# Dedication

This work is dedicated to:

- my dear mother **MBIA Fridoline**
- my dear Father **ONANA BELOBO Didier**
- my beloved sister **BELOBO MBIA Marguerite**.

# Acknowledgments

This thesis has been realized in the Laboratory of Atom and Radiation. I would like to great my supervisor and Head of the lab **Professor BEN-BOLIE Germain Hubert** for his high human qualities, guidance and constant support during this research work. He gave me the opportunity to work in the Atom and Radiation Lab and showed me the way to postgraduate studies. In spite of his huge academic and administrative duties, he always found time to discuss with me and answer my queries. Next, I would like to express my sincere gratitude to my second supervisor, **Professor KOFANE Timoléon Crépin**, Head of the Department of Physics and Laboratory of Mechanics. Before being my Ph.D thesis supervisor, I first met **Professor KOFANE** at the end of my master of science dissertation in 2009. Since that meeting, I have been appreciating his exceptional personality as well as his scientific and human qualities. First and foremost, **Professor KOFANE** is a physicist with a very large culture. His formidable knowledge of problems involving nonlinear physics and his curiosity to new ideas make of him a fascinating seolar: his ideas and suggestions brought clarity and insight to our work. His pedagogic attitude and permanent need of comprehension remain an identification model for me. **Professor KOFANE** has also been a patient supervisor, with the tact and the ability to understand the finer details of theoretical methods. He has guided me through difficult challenges with empathy and patience, and openly shared the excitement of our successes. At the end of this research work, I am aware of having improved largely, scientifically and personally since the beginnings. For the key role I do believe he plays in this evolution, I would like to express my sincere gratitude to **Professor KOFANE**.

I am grateful to **Professor NDJAKA Jean Marie Bienvenu** of the University of Yaounde I and **Professor Alidou Mohamadou** of the University of Maroua, who have accepted to bring their great expertise in reviewing the present thesis. I also express my sincere gratitude to **Professors MANGUELlE- DICOUM Eliézer, and OWONO OWONO Luc Calvin** whose presence in the jury adds luster in this work.

I owe a lot of gratitude to all the teachers of the Department of Physics of the University of Yaounde I and the University of Ngaoundéré. I wish to express special thanks to **Professor EKOBENA FOUDA Henri Paul** and his family for the support and friendship we share.

I have benefited greatly from countless discussions with **Doctor TIOFACK LATCHIO Gaston Camus**. I would like to thank him for putting up with my ignorance. He was always

ready to share his knowledge with me.

I do appreciated fruitful discussions with **Professor MALOMED Boris**, and **Professor SALASNICH Luca** who kindly responded to my querries. Parts of this research work have been done in collaboration with some teachers and students of the Department of Physics of the 'Université des Sciences et techniques de Masuku'. I do appreciate the collaboration of **Professor MOUBISSI Alain Brice, Professor EKOGO Thierry Blanchard, Mr MBOUMBA Maik Delon, Mr LOEMBA MOUANDZA S. Y.**

I would like to thank all the former and the present members of the Laboratory of Atom and Radiation for their help and the friendship I found there. Among them are the member of the teaching staff, **Dr. ELE ABIAMA Patrice, Dr. SAIDO**, and Mr **ABDOURAHIMI**. I am also grateful to all the friends I met during this work at the Department of Physics. I wish to name particularly **Dr. BEYALA JEAN FELIX, Dr. TABI Conrad, Dr. KOL GUY Richard, Dr. MEGNING Arsène, Mr DANG KOKO Adamou**, and Mr **MAINA Ibrahim**.

I wish I expressed here my sincere gratitude to **Miss MBORA Brigitte and her family**, **Mr ONANA Luc and his family** for the support and love they have been giving to my person. I acknowledge the support and friendship of my fellows at the Lab, **ADJABA Jean Liboire, BIEDI Brunel, DIAMARD MORNADJI Rachel, MINKONDA TOULOU Bruno, FOUENANG TIOKENG Herve, TCHAMBA Eric, TANTOH KWALAR Rowland, TICHOUK, KUETCHE TAKOU Bruno, TCHINDA TANANG Romuald**.

I acknowledge the support and encouragement from my brothers **BELOBO NDONGO Raphael Prospère, BELOBO ATANGANA Vincent de Paul, MBOUNI Achille, BELOBO TSOGO François Xavier, MBAZOA Roger, NGOUME Martial, BELOBO AKOUMOU Charles Louis** and my friends **KAKENGNE Elvis Delany, OYONO Jean Daniel, AYISSI Guy Christian, AZEGUE Théophile**.

# Contents

# List of Figures

# List of abbreviations

**GPE**: *Gross-Pitaevskii equation*

# Résumé

Cette thèse décrit la dynamique, le mécanisme de génération et la manipulation des solitons dans les condensats de Bose-Einstein à une ou plusieurs espèces d'atomes, avec interactions interatomiques à deux et ou trois corps, confinés dans des potentiels extérieurs ayant diverses formes géométriques.

Nos investigations commencent avec des condensats confinés dans un potentiel périodique anharmonique variable dont la forme peut être modifiée dans un large intervalle entre les deux cas limites que sont le modèle de Kronig-Penney et son inverse, avec le réseau optique sinusoïdal comme cas intermédiaire. En appliquant l'approche variationnelle avec le critère de stabilité de Vakhitov-Kolokolov, nous dérivons les conditions de stabilité des condensats de Bose-Einstein dans des potentiels périodiques anharmoniques. Les simulations numériques directes de l'équation de Gross-Pitaevskii corroborent les résultats obtenus par l'approche variationelle.

Considérant des versions modifiées de l'équation de Gross-Pitaevskii, nous examinons analytiquement et numériquement l'instabilité modulationnelle des condensats de Bose-Einstein confinés dans des potentiel complexes. Les impacts de certains effets tels que les fluctuations quantiques, la réponse non linéaire retardée du système, et le potentiel linéaire sur l'apparition de l'instabilité ainsi que sur la dynamique des solitons dans les condensats sont clarifiés.

Nous considérons aussi l'équation de Gross-Pitaevskii où les interactions interatomiques à deux et trois corps sont modulées dans le temps, avec des potentiels complexes. En utilisant l'approche variationnelle, et la méthode dite 'F-extension method', nous construisons plusieurs familles de solutions exactes de l'équation de Gross-Pitaevskii qui comprennent entre autres les solitons, les solutions périodiques. La robustesse des solutions analytiques trouvées est confirmée par la persistance temporelle des solutions numériques. Nos solutions ont plusieurs paramètres indépendants qui peuvent être utilisés pour gérer moult propriétés des condensats comme la position, la largeur, la vitesse, l'accélération, et la densité.

***Mots clés:*** *Condensat de Bose-Einstein, équation de Gross-Pitaevskii modifiée, interactions interatomiques à deux et trois corps, approche variationnelle, instabilité modulationnelle, F-expansion method, solutions exactes.*

# Abstract

This thesis describes the dynamics and the underlying mechanism of generating and manipulating solitons in single and mixtures of Bose-Einstein condensates with two- and or three-body interatomic interactions, confined in different external potentials. Our study is based on some Gross-Pitaevskii equations (GPEs) that govern the evolution of Bose-Einstein condensates.

Our investigations start with single condensates loaded in a variable anharmonic periodic potential which shape can be varied within a wide range between the two special limits of the Kronig-Penney model and the inverse Kronig-Penney model, with the sinusoidal optical lattice as an intermediate case. By applying the standard variational approach along with the Vakhitov-Kolokolov criterion, we derive the stability conditions for Bose-Einstein condensates in anharmonic periodic potentials. Full numerical simulations of the GPE finally test the results of the variational approach and show good agreements between both methods.

Considering some modified versions of the GPE, we examine analytically and numerically the modulational instability of Bose-Einstein condensates confined in a complex potential. Important effects such as the quantum fluctuations around the mean-field approximation, the delayed nonlinear response of the condensate, and the linear potential on the onset of instability as well as the dynamics of solitons in Bose-Einstein condensates are clarified.

We also consider the dynamics of Bose-Einstein condensates with time-dependent two- and three-body interatomic interactions confined in complex potentials. By means of the variational approach in addition to the F-expansion method, we construct many families of exact solutions of the GPE which include solitons, periodic solutions among others. The robustness of the analytical solutions found is confirmed by the long time behaviors of the numerical solutions. Our solutions have many free parameters which can be used to manage many features of matter waves in Bose-Einstein condensates such as the position, width, velocity, acceleration, and density.

***Keywords***: *Bose-Einstein condensates, modified Gross-Pitaevskii equation, two- and three-body interatomic interactions, variational approach, modulational instability, modified lens-type transformation, F-expansion method, exact solutions.*

# General Introduction

In the recent past years, one of the major break-through in the field of atomic physics has been the experimental realization of Bose-Einstein condensates in weakly interacting alkali gases [1, 2, 3]. A Bose-Einstein condensate is a new state of matter which is very dilute and at very low temperature, where a macroscopic fraction of the atoms occupy the same quantum level, and behave as a coherent matter wave similar to the coherent light wave produced by a laser. After first experimental production of condensates, there have been a plethora of experimental and theoretical works devoted to the study of properties of these new quantum gases. Among these properties, the physical mechanism of Bose-Einstein condensate solitons (stable solitary waves which propagate in a nonlinear medium) is a relevant aspect, since it is believed that the generation and evolution of Bose-Einstein condensate solitons are important for a number of Bose-Einstein condensate applications such as the observation of quantum phase effects [4, 5, 6], phase transitions from superfluids to Mott insulators [4], quantum computation and quantum information [7], atomic number squeezing [5, 6, 8], transport of matter waves [5], atom lasers [9] and so on. The generation and propagation of coherent matter waves in Bose-Einstein condensates have become an active research topic at the forefront of atomic physics with tremendous achievements both on the theoretical and experimental sides such as dark solitons [10], bright solitons [11], dark-bright solitons [12], vortices [13], vortex lattices [14] just to name a few.

Bose-Einstein condensates are achieved in experiments by confining the bosons of the atomic cloud in external potentials which may take a wide range of geometries. These external trapping potentials can be realized with magnetic fields [15], or counter-propagating laser beams [16] using the so-called optical dipole traps [17]. Magnetic traps that may be either repulsive or attractive with time-dependent strengths are typically harmonic, while the form of optical dipole trap is extremely versatile and manageable by the experimenter since the dipole trap is proportional to the intensity of the laser beams [17]. The special case of light-induced periodic potentials also called optical lattices is a relevant aspect that has been used to unveil rich and interesting new phenomena in condensates [18, 19]. 'Optical supperlattice' potentials which are characterized by two different periods of the underlying laser beams can be realized experimentally [20]. There is also the possibility to combine the magnetic and the optical dipole trap potentials with each other [21, 22] or with other potentials [4, 22]. The external potentials also

offer many possibilities to precisely manipulate and control the dynamics of condensates.

The dynamical behavior of Bose-Einstein condensates at the mean-field limit, as the zero temperature is approached, is governed by the three-dimensional GPE [23, 24] which can also be considered as a nonlinear Schrödinger equation type with an external potential. Though the very diluteness of a condensate gas, atom-atom interactions play a crucial role as they affect the properties of the gas in a dramatic way leading to rich and interesting nonlinear effects. ***Basically, the dynamics of Bose-Einstein condensates can be modeled by the cubic GPE where the cubic nonlinearity is attributed to two-body atom-atom interactions.*** The strength of the cubic nonlinearity is characterized by the s-wave scattering length which can be positive or negative. It has been shown that the scattering length can be tuned to the desired value, and its sign may be turned from a positive to a negative value by using the Feshbach resonance management technique [25]. This has paved the way to manipulating matter waves of condensates with an unprecedent control and enter regimes inaccessible in other physical systems such as solid-state physics. ***The avenue of the management of the scattering length suggests a way to reduce two-body interactions, and bring the gas in a regime where the two-body binding energy may be close to zero, such that the gas may approach the so-called Efimov limit, where three-body interatomic interactions are important. In this case, the dynamics of Bose-Einstein condensates can be modeled by the quintic GPE where the three-body interatomic interactions are accounted by quintic nonlinearities***.

In the recent past years, many works have been dedicated to the investigation of soliton properties of Bose-Einstein condensates with time and or space modulations of the cubic and quintic nonlinearities in confining potentials with different shapes [26, 27]. On the other hand, an important issue of solitons in condensates is their generation. The generation of solitons in Bose-Einstein condensates through the activation of modulational instability has been predicted theoretically [28, 29] and observed experimentally [30, 31] in the framework of the cubic GPE. Due to its potential applications, the modulational instability technique applied in Bose-Einstein condensates has been paid increasing attention and has been studied for different trapping potentials [32, 33, 34].

Advances in trapping techniques for Bose-Einstein condensates have allowed to create multi-component Bose-Einstein condensates where the same atoms with different hyperfine states [35] or different F-spin orientations [36], or different atomic species [37] are currently confined. Many important aspects of mixtures of condensates have been investigated and involved the structure and dynamics of binary Bose-Einstein condensates [38], the formation of domain walls between immiscible species [38, 39], bound states of dark-dark [40], or dark-bright [41], or coupled-vortex [42], and modulational instability [43]. We recall that in some cases, dissipative Bose-Einstein condensate models where a fraction of the atomic cloud is not condensed and which is coupled to the condensed fraction have been reported. This situation results to a coupling between the

Bose-Einstein condensate and a source of uncondensed atoms at the same temperature and to a sink [44, 45, 46, 47]. One may also be interested in the search of solitons in dissipative Bose-Einstein condensate models that may be applied to atom lasers [44, 45, 46].

In literature, many authors have examined the properties of solitons in single and binary Bose-Einstein condensates in optical lattices [19, 48, 49, 50], however modulations of nonlinearities and lattice deformations are seldom taken into account. The generation and structure dynamics of solitons have been studied in single Bose-Einstein condensates at the mean-field level with cubic [27, 33] and cubic-quintic [34] nonlinearities confined in potentials with different shapes via the activation of modulational instability. However, the mean-field is no longer applicable when the density of the Bose-Einstein condensate is relatively high. In this case, some authors have proposed some variant forms of the GPE that integrate quantum fluctuations around the mean-field [51, 52]. In [52], in addition to quantum fluctuations, a shape-dependent confinement correction term stemming from the shape dependence on the interaction potential are introduced in the equation that describes the dynamics of Bose-Einstein condensates. Most previous works do not consider effects of quantum fluctuations and the shape-dependent confinement correction term on the modulational instability of condensates. For multicomponent condensates, especially binary condensates, many properties of solitons have been investigated in systems with only two-body interatomic interactions [**?**]. Effects of the three-body interactions on the generation and structure dynamics of binary Bose-Einstein condensates are not well understood up to now.

In this thesis, we investigate soliton properties of single and binary Bose-Einstein condensates both analytically and numerically in the framework of the GPE, and modified GPEs. We analyze effects of lattice deformations on the stability diagrams of bright solitons in Bose-Einstein condensates. We also study impacts of some important effects such as quantum fluctuations, the dependence on the interaction potential induced by atom-atom interactions, and the three-body interactions on the generation and structure dynamics of bright solitons in conserved and slightly opened dissipative Bose-Einstein condensates. The work is organized as follows.

In chapter 1, we present the general theory and some ideas that are basic to our current understanding of the phenomenon of Bose-Einstein condensation. An emphasis is made on the mean-field regime where the GPE describing the dynamics of inhomogeneous interacting Bose-Einstein gases on the basis of a classical description of the order parameter is derived. A brief summary of methods for the cooling and the trapping of particles, including the laser cooling and the magneto-optical trapping, used to achieve most condensates, is presented.

Chapter 2 describes the analytical and numerical methods used in the investigation of the dynamics of solitons in Bose-Einstein condensates. As analytical methods, we present the variational approach [38, 50], the modified lens-type transformation [34], the linear stability analysis [34], and the F-expansion method [34]. Also are presented some numerical methods such as, the normalized gradient flow with backward Euler plus second-order centered finite difference dis-

cretization with imaginary time propagation scheme [53], the fourth-order Runge-Kutta scheme in the interaction picture [54], the split-step Fourier method [55], and the MATLAB toolbox PDEPE that have been used to numerically integrate different model equations used in this work.

In chapter 3, we present the main results of this thesis. By applying the variational approach, we start by carefully analyzing the stability conditions of single Bose-Einstein condensates in a variable anharmonic optical lattice which shapes may account for lattice deformations in experiments.

In the framework of some modified GPEs, we investigate analytically and numerically the modulational instability of Bose-Einstein condensates in harmonic and complex potentials, in addition to the delayed nonlinear response of the condensate system, and beyond the mean-field approximation.

By means of the variational approach and the F-expansion method, we construct many families of analytical solutions of GPEs with time modulations of the strengths of the two- and three-body interatomic interactions. The stability of the solutions derived is analyzed with the linear stability analysis, and with intensive numerical simulations of corresponding original equations.

The present thesis ends with a general conclusion and provides some future directions that could be investigated.

# Chapter 1

# Generalities on Bose-Einstein Condensation

## 1.1 Introduction

The phenomenon of Bose-Einstein condensation was first predicted in 1924 [56] by Einstein who extended to massive particles a work of Satyendra Nath Bose on the statistics of a gas of photons [57]. Einstein's prediction was made for an ideal gas of non-interacting particles at zero temperature. The first evidence of Bose-Einstein condensation were reported in 1995 [1, 2, 3] in gases of weakly interacting alkalis. The behavior and properties of Bose-Einstein gases are important since Bose-Einstein condensates become a natural ground to test fundamental quantum theories, and may lead to a wide range of technological applications.

In this chapter, we start with the description of non-interacting, and interacting particles boson gases. Then, using the mean-field theory, we present the mathematical formalism that helps understand the dynamics of Bose-Einstein condensates. The time-dependent and time-independent GPEs are derived for single and binary condensates. Some limitations of the mean-field description are underlined and some models that go beyond the mean-field are discussed. The chapter ends with the description of experimental procedures that lead to observations of Bose-Einstein condensates.

## 1.2 Non-interacting and interacting particle Bose-Einstein gases

In classical mechanics, one could exactly follow the evolution of an ensemble of massive particles with the knowledge of those particles' initial positions and momenta. The wavelike nature of electromagnetic fields was described with Maxwell's equations. At the end of the nineteenth century, classical mechanics failed to explain some experimental observations such as the photo-electric effect and the black-body radiation. The explanations of the latter experimental features were made in the framework of a new mechanical formalism known as quantum

mechanics. In quantum mechanics, massive particles and electromagnetic waves are unified as they are fundamentally described by a 'wavefunction'. In contrary to classical mechanics where an individual particle has a well-defined phase-space trajectory, it is not possible to have at the same time the position and momentum of a particle with certainty in quantum mechanics. The wavefunction, $\Psi(r,t)$, is interpreted as the amplitude probability that a massive or non-massive particle is found in position $r$ in space at time $t$.

For a system of N particles, the wavefunction description is extended to a 'many-body wavefunction', $\Psi_{\alpha_1,\alpha_2...}(r_1,r_2,...,t)$, where each particle is labeled by its position $r_m$ and spin $\alpha_m$. The many-body wavefunction describes the amplitude probability to find the particles $m$ at positions $r_m$ at time $t$. For the specific case of identical particles, those particles are indistinguishable. The indistinguishability of particles implies that the interchange of particle labels does not affect any physical observable of the system, and can at most introduce an unmeasurable global phase rotation to the many-body wavefunction as

$$\Psi_{...,\alpha_m,...,\alpha_n,...}(...,r_m,...,r_n,...,t) = \exp(\imath\theta)\Psi_{...,\alpha_n,...,\alpha_m,...}(...,r_n,...,r_m,...,t). \tag{1.1}$$

If the same interchange of particle labels is repeated the original state must be recovered, hence the global phase satisfies the relation $\exp(\imath\theta) = \pm 1$ [55]. The two types of phases correspond to two types of particles observed in nature: fermions which have an antisymmetric wavefunction ($\exp(\imath\theta) = -1$) and half-integer spin and bosons with a symmetric wavefunction ($\exp(\imath\theta) = +1$) and integer spin.

The nature of particles gives rise to dramatic different behaviors. In statistical mechanics, it can be shown that for an ensemble of identical particles at thermal equilibrium $T$, the mean number of particles occupying a single quantum level k with energy $\epsilon_k$ is given by the general expression

$$f(\varepsilon_k) = \frac{1}{Z^{-1}\exp(\beta\epsilon_k) + \nu}, \tag{1.2}$$

where $\beta = \frac{1}{k_B T}$, $k_B$ is the Boltzmann's constant, $Z$ is the fugacity of the system defined by $Z = \exp(\beta\mu)$. The chemical potential $\mu$ represents the energy needed to add one particle or the energy gained by the system as a result of the addition of a single particle at constant volume and entropy [56]. The parameter $\nu$ is a constant that accounts for the indistinguishability of the particles. For gases at very low temperatures, $\nu$ takes the values $+1$ in the quantum statistics of fermions and $-1$ in the quantum statistics of bosons. At higher temperatures, $\nu = 0$ and Eq.(1.2) describes the 'Maxwell-Boltzmann' statistic. We present on Fig. 1 a sketch of the distribution of particles for the two quantum statistics.

In the remainder of this work, we focus our attention on the case of gases of massive bosons. Thus, as the chemical potential $\mu$ approaches the single-particle ground state energy from below $\varepsilon_0$, the population of the ground state increases macroscopically. This phenomenon is nowadays known as Bose-Einstein condensation. Particles that macroscopically occupy the ground state are named Bose-Einstein condensates.

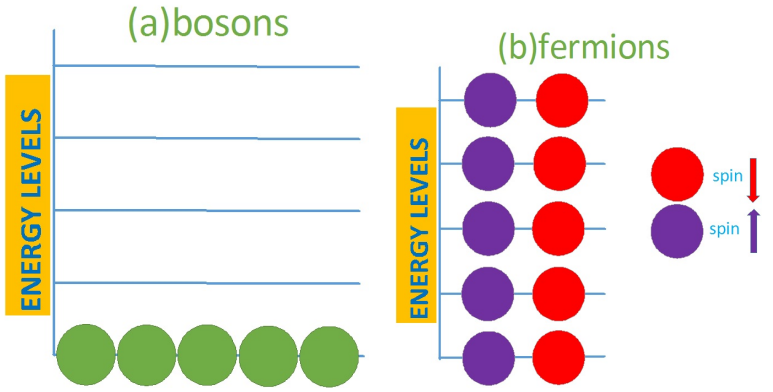


**Figure 1**: Sketch of quantum statistics: bosons versus fermions with weak interactions at T = 0

## 1.3 Bose-Einstein condensates in an ideal gas

A description of Bose-Einstein condensates in an ideal gas is available in many textbooks on statistical mechanics [60]. It is important since it serves as a useful guide to the regime under which Bose-Einstein condensation occurs.

Let us consider a gas of N non-interacting bosons with mass $m$ in a box of volume $\Omega$. The total number of particles at thermal equilibrium can be written as

$$N = \sum_k f_{BE}(\varepsilon_k), \tag{1.3}$$

where $f_{BE}$ corresponds to $\nu = -1$ in Eq.(1.2), $\varepsilon_k$ is the eigenenergy of the $k$th single-particle state. Considering that the function $f_{BE}$ varies slowly compared to the energy spacing between contiguous levels, we replace the discrete summation in Eq.(1.3) by the integral

$$N = N_0 + \int g(\varepsilon) f_{BE}(\varepsilon) d\varepsilon, \tag{1.4}$$

in which $g(\varepsilon_k)$ is the density of states of the system and accounts for the number of quantum levels in the range $d\varepsilon$. The quantity $N_0$ is the number of particles in the ground state of the system. In the semiclassical approximation, the density of state for particles of mass $m$ is given by the following expression

$$g(\varepsilon) = \frac{1}{(2\pi)^3} \int dr \int d\mathbf{k} \delta(\varepsilon - V(r) - \frac{\hbar^2 K^2}{2m}), \tag{1.5}$$

where $V(r)$ represents the external potential, $\delta(z)$ is the Dirac delta function, and $\mathbf{k}$ is the three-dimensional wavevector space. For an infinite square well potential, Eq.(1.5) reduces to

$$g(\varepsilon) = \frac{m^{3/2}\Omega}{\sqrt{2}\pi^2\hbar^3} \sqrt{\varepsilon}. \tag{1.6}$$

It is easy to see from Eq.(1.2) that when $\mu \to 0^-$, the number of particles in the ground state can become very large, i.e., $N_0 = \frac{Z}{(1-Z)}$. In addition, Eq.(1.6) implies that $g(\varepsilon_0 = 0) = 0$ (for the square well), meaning that there is no particle in the ground state of the system. Thus, the semiclassical treatment is not appropriate for the description of the ground state, and this is the reason why the occupation number of the ground state of the system was separated from the integral in Eq.(1.4). Combining the density of state of the square well with a binomial expansion of the Bose-Einstein distribution $f_{BE}$, then performing the integral (1.4) we obtain

$$N = N_0 + \Omega(\frac{mK_BT}{2\pi\hbar^2})^{3/2}G_{3/2}(Z). \tag{1.7}$$

In Eq.(1.7), the second term represents the number of particles in the excited states $N^{ex}$, $G_{3/2}(Z)$ is the Bose-Einstein function defined by

$$G_{3/2}(Z) = \sum_{j=1}^{\infty} \frac{Z^j}{j^{3/2}}, \tag{1.8}$$

over the domain $Z \; \epsilon \; (-\infty, \; 1]$ (so that $N$ remains positive). Maxima of the Bose-Einstein function occur at $Z = 1$. For instance, $G_{3/2}(1) = \zeta(3/2) \approx 2.612$, where $\zeta(x)$ is the Riemann zeta function. From Eq.(1.2), it is easy to see that for $\mu \to 0$, $Z \to 1$, thus for a given temperature $T$, there exists a maximum number of particles that can be contained within the excited single-particles states that can be written as

$$N^{ex}_{max} = 2.612\Omega(\frac{mK_BT}{2\pi\hbar^2})^{3/2}. \tag{1.9}$$

If the total number of particles $N$ exceeds $N^{ex}_{max}$, all the remaining particles must therefore be in the single-particle ground state and form a Bose-Einstein condensate. At higher temperatures, almost all particles are excited. ***Nevertheless, as the system is cooled down, there is a critical temperature*** $T_C$ ***at which*** $N^{ex}_{max} = N$ ***given by***

$$T_C = \frac{2\pi\hbar^2}{mK_B}(\frac{N}{2.612\Omega})^{2/3}. \tag{1.10}$$

Introducing the constant $n = N/\Omega$, and inserting Eq.(1.10) into Eq.(1.7), one finds the variation of the condensate fraction with the temperature

$$\frac{n_0}{n} = 1 - (\frac{T}{T_C})^{3/2}, \tag{1.11}$$

where $n_0 = N_0/\Omega$. ***The Bose-Einstein condensation phenomenon occurs if*** $T \leq T_C$***.***

A simple way to describe the physical significance of Bose-Einstein condensation is to identify the thermal de Broglie wavelength $\lambda_{dB} = \sqrt{\frac{2\pi\hbar^2}{mK_BT}}$ of particles. ***The onset of Bose-Einstein condensation becomes***

$$n\lambda^3_{dB} \leq 2.612. \tag{1.12}$$

***Hence, the phenomenon of Bose-Einstein condensation occurs when the de Broglie wave packets of particles starts overlapping, and their quantum nature become important.***

In most Bose-Einstein condensate experiments, bosons are confined in an external harmonic potential of the form

$$V(r) = \frac{m}{2}(\omega_x^2 x^2 + \omega_y^2 y^2 + \omega_z^2 z^2), \tag{1.13}$$

where $\omega_{x,y,z}$ represent the trapping frequencies or strengths in the cartesian directions $-x$, $-y$, $-z$, respectively. Using the semiclassical method [61], the number of particles reads

$$N = N_0 + (\frac{K_B T}{\hbar\overline{\omega}})^3 G_3(Z), \tag{1.14}$$

where $\overline{\omega} = (\omega_x\omega_y\omega_z)^{1/3}$ is the mean trap frequency. The critical temperature for the onset of Bose-Einstein condensation is

$$T_C = \frac{\hbar\overline{\omega}}{K_B}(\frac{N}{1.202})^{1/3}, \tag{1.15}$$

and the Bose-Einstein condensate fraction is

$$\frac{n_0}{n} = 1 - (\frac{T}{T_C})^3. \tag{1.16}$$

Equation (1.16) is similar to Eq.(1.11) meaning that the ideal BEC gas confined in an harmonic potential and in a free space have analogous behaviors.

## 1.4 Bose-Einstein condensates of interacting particles

The presence of interactions between particles can profoundly modifies the equilibrium state of the system, principally by depleting the condensate fraction. In 1947, using the new idea of second quantization in addition to the many-body field theory, Bogoliubov showed that the introduction of weak particle interactions do not quantitatively have a profound impact on the nature of the condensate [62]. Nevertheless, the low-lying excitations of the condensate were significantly altered, and the predicted phonon spectrum was exactly that assumed by Landau which ensured the stability of the superfluid flow [63].

There are mainly two types of interactions involved in weakly interacting Bose-Einstein condensate gases: the two- and three-body interatomic interactions. The two-body interatomic interactions come from atom-atom interactions and their intensity is characterized by the s-wave scattering length $a_s$. Depending on the atomic specie that forms the Bose-Einstein condensate gas, the scattering length can be positive for repulsive interactions between atoms ($^{87}$Rb, $^{23}$Na), or negative for attractive interactions between atoms ($^{85}$Rb, $^{7}$Li). When the Bose-Einstein condensate system is very diluted, the two-body interactions dominate over the three-body ones [1, 2, 3]. However, in some experiments, the number of three-body interatomic interactions have been increased by using a magnetic field [64, 65, 66, 67]. The three-body interatomic interactions

may become important and are used to describe the dynamics of Bose-Einstein condensates in the Tonks-Girardeau regime where the interatomic interactions are strong [68]. The strength and sign of the scattering length can be varied in Bose-Einstein condensate experiments by using the Feshbach resonance management technique. For Bose-Einstein condensates trapped in magnetic potentials, the scattering length near the Feshbach resonance magnetic field $B_0$ has the form [64, 65, 66, 67, 69]

$$a(B) = a_s(1 - \frac{\Delta}{B - B_0}), \tag{1.17}$$

where $a_s$ is the value of the scattering length far from resonance, whereas $\Delta$ represents the width of the resonance. The scattering length can also be manipulated by means of optical lasers when Bose-Einstein condensates are studied in optical lattices. In this case, the expression of the scattering length is [70]

$$a(x) = a_{s0} + g_1 I/(\delta + I), \tag{1.18}$$

where $a_{s0}$ is the scattering length in the absence of the light signal, $g_1$ is a constant, $\delta$ which may be either positive or negative, measures the resonance detuning. The quantity $I = I_0 \cos^2(2\pi\lambda x)$ accounts for the light intensity with wavelength $\lambda$. The Feshbach resonance technique is a mechanism that can be used to manipulate the interatomic interactions in Bose-Einstein condensates.

## 1.5 Mean-field theory

The description of the dynamics of dilute Bose-Einstein condensed gases starts with the second quantized many-body Hamiltonian for a system of identical bosons. The gas is assumed to be diluted enough such that three-body collisions are rare, and to a good approximation one only considers two-body (pairwise) collisions. The Hamiltonian is given by the well-known Heisenberg picture Hamiltonian

$$\hat{H} = \int d^3\vec{r}\hat{\Psi}^\dagger(\vec{r},t)\hat{H}_{sp}\hat{\Psi}(\vec{r},t) + \frac{1}{2}\int d^3\vec{r}\int d^3\vec{r'}\hat{\Psi}^\dagger(\vec{r},t)\hat{\Psi}^\dagger(\vec{r'},t)U(\vec{r}-\vec{r'})\hat{\Psi}(\vec{r},t)\hat{\Psi}(\vec{r'},t). \tag{1.19}$$

The first term of the Hamiltonian of Eq.(1.19) is a non-interacting Hamiltonian corresponding to an ideal gas and can be diagonalized exactly, while the second term describes two-body interactions via the interatomic potential $U(\vec{r}-\vec{r'})$. The field operators $\hat{\Psi}(\vec{r},t)$ and $\hat{\Psi}^\dagger(\vec{r},t)$ annihilates and creates a single boson of mass $m$ at position $\vec{r}$ and time $t$, respectively, and satisfy the commutation rules

$$\begin{aligned} \left[\hat{\Psi}(\vec{r},t), \hat{\Psi}(\vec{r'},t)\right] &= \left[\hat{\Psi}^\dagger(\vec{r},t), \hat{\Psi}^\dagger(\vec{r'},t)\right] = 0, \\ \left[\hat{\Psi}(\vec{r},t), \hat{\Psi}^\dagger(\vec{r'},t)\right] &= \delta(\vec{r}-\vec{r'}). \end{aligned} \tag{1.20}$$

The single particle Hamiltonian, $H_{sp}$, is expressed as

$$\hat{H}_{sp} = -\frac{\hbar^2}{2m}\nabla^2 + V(\vec{r}), \tag{1.21}$$

where $V(\vec{r})$ is the external potential in which bosons are confined. We normalize the field operator as

$$\hat{N} = \int d^3\vec{r}\hat{\Psi}^\dagger(\vec{r},t)\hat{\Psi}(\vec{r},t), \tag{1.22}$$

where $\hat{N}$ is the number field operator, and obeys the commutation rule $\left[\hat{N},\hat{H}\right]=0$.

Using the Heisenberg picture

$$\imath\hbar\frac{\partial\hat{A}}{\partial t} = \left[\hat{A},\hat{H}\right], \tag{1.23}$$

and assuming that $\hat{A}$ does not have any time dependence, we derive the equation of motion of the field operator as

$$\imath\hbar\frac{\partial\hat{\Psi}(\vec{r},t)}{\partial t} = \hat{H}_{sp}\hat{\Psi}(\vec{r},t) + \int d^3\vec{r'}\hat{\Psi}^\dagger(\vec{r'},t)U(\vec{r}-\vec{r'})\hat{\Psi}(\vec{r'},t)\hat{\Psi}(\vec{r},t). \tag{1.24}$$

We expand the field operator on an infinite orthonormal basis set such that

$$\hat{\Psi}(\vec{r},t) = \sum_n \hat{a}_n(t)\phi_n(t), \tag{1.25}$$

where $\hat{a}_n(t)$ annihilates a boson in mode $n$ at time $t$, and satisfies the equal time boson commutation relations

$$\left[\hat{a}_m,\hat{a}_n\right] = \left[\hat{a}_m^\dagger,\hat{a}\dagger_n\right] = 0, \qquad \left[\hat{a}_m,\hat{a}_n^\dagger\right] = \delta_{mn}, \tag{1.26}$$

in which the time dependence is dropped for clarity. Inserting Eq.(1.25) into Eq.(1.19) and considering that the set $\{\phi_n\}$ represents the eigenvectors of $\hat{H}_{sp}$, we obtain

$$\hat{H} = \sum_n \hbar\omega_n\hat{a}_n^\dagger\hat{a}_n + \frac{1}{2}\sum_{pqmn} < pq|U|mn > \hat{a}_p^\dagger\hat{a}_q^\dagger\hat{a}_m\hat{a}_n, \tag{1.27}$$

with symmetric matrix elements defined as

$$\begin{aligned} < pq|U|mn > \;\; = \;\; & \frac{1}{2}\int d^3\vec{r}\int d^3\vec{r'}\phi_p^*(\vec{r})\phi_q^*(\vec{r'})U(\vec{r}-\vec{r'})\phi_m(\vec{r'})\phi_n(\vec{r}) \\ & +\frac{1}{2}\int d^3\vec{r}\int d^3\vec{r'}\phi_p^*(\vec{r})\phi_q^*(\vec{r'})U(\vec{r}-\vec{r'})\phi_n(\vec{r'})\phi_m(\vec{r}). \end{aligned} \tag{1.28}$$

Equation (1.28) represents direct as well as exchange collisions between bosons. We can then write the Heisenberg equation of motion of an individual mode operator as

$$\imath\hbar\frac{\partial\hat{a_p}}{\partial t} = \hbar\omega_p\hat{a_p} + \sum_{qmn} < pq|U|mn > \hat{a}_q^\dagger\hat{a}_m\hat{a}_n. \tag{1.29}$$

Now, we suppress the free evolution of the operators by setting

$$\tilde{a}_p = \hat{a}_p\exp(\imath\omega t), \tag{1.30}$$

then, Eq.(1.29) becomes

$$\imath\hbar\frac{\partial\tilde{a}_p}{\partial t} = \sum_{qpm} < pq|U|mn > \tilde{a}_p^\dagger\tilde{a}_m\tilde{a}_n\exp[\imath(\omega_p+\omega_q-\omega_m-\omega_n)t]. \tag{1.31}$$

The calculations of matrix elements $< pq|U|mn >$ involve the evaluations of spatial integrals over the bare two-body potential $U(\vec{r}-\vec{r'})$. In dilute gases, the requirement that only two particles are involved in any single scattering event, is consistent with the assumption that the characteristic length scales of the system are much larger than the range of the interparticle scattering potential. ***Since in Bose-Einstein condensate gases one is interested in the large scale behavior of the system, the microscopic details of the scattering trajectories may be neglected provided that the macroscopic field dynamics are correctly described. This means that one can replace the calculations of matrix elements by another theory that correctly recovers the effects of the particle interactions at the microscopic scale.*** Using the hard-sphere interaction approximation, Huang and Yang [71] showed that many features of the scattering could be reproduced using a relatively simple pseudopotential. For ultracold neutral atoms, this idea, to its lowest order, leads to the substitution of the real scattering potential in the Hamiltonian of (1.19) by the zero-range contact potential

$$U(\vec{r}-\vec{r'}) \rightarrow U_0\delta(\vec{r}-\vec{r'}), \tag{1.32}$$

where the interaction strength is [24]

$$U_0 = \frac{4\pi\hbar^2 a_s}{m}. \tag{1.33}$$

However, the contact potential (1.32) is unphysical in the sense that high-energy particles are scattered just as efficiently as low-energy particles. Thus, momentum transfer between atoms will vanish at high momenta. This situation results into ultraviolet divergences in Bose-Einstein condensate theories if the contact potential is simply substituted into the Hamiltonian (1.19). The problem of ultraviolet divergences is often circumvented by assuming that all the high-energy states are unpopulated.

In order to avoid ultraviolet divergences, Morgan [72] has proposed a method that allows the introduction of the contact potential as an approximation of the two-body T-matrix, rather than the direct replacement of the contact potential in the Hamiltonian (1.19). In this approach, the scattering terms of the two-body T-matrix, $T_{2b}$, are interpreted as the amplitude probability that a scattering event between two particles will lead to transitions into a particular set of modes [73]. So, the scattering matrix elements in the Hamiltonian (1.27) are replaced by

$$< pq|U|mn > \rightarrow T_{2b}(pq,mn) \equiv < pq|\hat{T}_{2b}|mn >, \tag{1.34}$$

where the two-body T-matrix governing transitions from modes $p,q$ to modes $m,n$ is defined in terms of the two-body T-operator $\hat{T}_{2b}$. The two-body T-matrix is defined by the Lippmann-Schwinger equation [72, 73]

$$\hat{T}_{2b}(z) = U + U\frac{1}{z-\hat{H}_{sp}}\hat{T}_{2b}(z), \tag{1.35}$$

where $z$ is the energy of the collision. Inserting a complete set of eigenfunctions of $\hat{H}_{sp}$ one obtains

$$\hat{T}_{2b}(z) = U + U \sum_{pq} |pq> \frac{1}{z - \varepsilon_p - \varepsilon_q} < pq|\hat{T}_{2b}(z), \tag{1.36}$$

in which $\varepsilon_p$, $\varepsilon_q$ are single particle energies, $|pq>$ is a two-particle eigenstate describing an intermediate state in a collision.

The mode space is now divided into two subspaces: the low-energy region L that contains all the particles in the system forming our system of interest, and a high-energy region H that contains all the remaining unoccupied levels which are accessed only as intermediate virtual states within individual scattering events, and is supposed to be unpopulated. The boundary is defined as the finite energy cutoff $\varepsilon_{cut}$.

The T-matrix is most easily calculated within an homogeneous field, for which eigenfunctions of $\hat{H}_{sp}$ are simple plane waves. In the limiting case where the volume of the system tends to infinity ($\Omega \to \infty$), the T-matrix takes the form

$$\hat{T}_{2b}(\vec{K'}, \vec{K}, z) = U(\vec{K'} - \vec{K}) + \frac{1}{(2\pi^3)} \int d^3\vec{K''} \frac{U(\vec{K''} - \vec{K'})\hat{T}_{2b}(\vec{K''}, \vec{K'}, z)}{z - (\hbar K'')^2/2\tilde{m}}, \tag{1.37}$$

$$\begin{aligned} U(\vec{K}) &= \int d^3U(\vec{r}) \exp(\imath\vec{K}.\vec{r}), \\ \hat{T}_{2b}(\vec{(K')}, \vec{K}, z) &= \int d^3\vec{r'} \int d^3\vec{r} \exp(-\imath\vec{K'}.\vec{K})\hat{T}_{2b}(\vec{K'}, \vec{K}, z) \exp(\imath\vec{K}.\vec{r}), \end{aligned} \tag{1.38}$$

$\hbar\vec{K}$, $\hbar\vec{K'}$ are the initial and final momenta of two colliding atoms. The parameter $\tilde{m} = m/2$ is the reduced mass, the quantity $z$ has been redefined to include the center of mass energy of two colliding atoms. In the case where the energy and momenta of two colliding atoms are conserved, the homogenous two-body T-matrix can be expanded in terms of the phase shifts $\phi_l(K)$ induced by the interatomic potential for $\delta \to 0$ and $K' \to K$ as [73]

$$\hat{T}_{2b}(\vec{K'}, \vec{K'}, \varepsilon_K + \imath\delta) = -(4\pi\hbar^2/m) \sum_{l=0}^{\infty} \frac{2l+1}{K} \exp(\imath\phi_l(K) P_l(\cos(\theta))), \tag{1.39}$$

where $\varepsilon_K = (\hbar K)^2/2\tilde{m}$ and $\theta$ is the angle between $\vec{K}$ and $\vec{K'}$.

At low energy, i.e. $Ka \ll 1$, only the s-wave scattering process is important. For a hard sphere of radius $a$, the s-wave phase shift reads $\phi_0(K) = -Ka$, such that the quantity $a$ is understood as the scattering length. Hence, Eq.(1.39) reduces to

$$\hat{T}_{2b}(\vec{K'}, \vec{K}, \varepsilon_K + \imath\delta) = \frac{4\pi\hbar^2 a_s}{m} + O(Ka). \tag{1.40}$$

In terms of spatial coordinates, Eq.(1.40) is written as

$$\hat{T}_{2b}(\vec{r'}, \vec{r}, 0) = \frac{4\pi\hbar^2 a_s}{m} \delta(\vec{r'} - \vec{r})\delta(\vec{r}). \tag{1.41}$$

The spatial T-operator (1.41) has the same form as the contact potential (1.32).

Considering that matrix elements of Eq.(1.31) containing only one high index tend to zero, one retrieves the equation of motion of the low-energy state $p$

$$\begin{aligned} \imath\hbar\frac{d\tilde{a}_p}{dt} &= \sum_{qmn}^{L} < pq|U|mn > \tilde{a}_q^\dagger \tilde{a}_m \tilde{a}_n \exp[\imath(\omega_p + \omega_q - \omega_m - \omega_n)t] \\ &+ \sum_{q}^{L}\sum_{mn}^{H} < pq|U|mn > \tilde{a}_q^\dagger \tilde{a}_m \tilde{a}_n \exp[\imath(\omega_p + \omega_q - \omega_m - \omega_n)t], \end{aligned} \tag{1.42}$$

where $\sum_{mn}^{H}$ means that the indices $m$ and $n$ are high, while $L$ means that one uses low-energy states in the summation. Focusing on the evolution of the low-energy state using adiabatic elimination of high energy modes, Morgan has shown that it is possible to replace the second term of the right-hand side of Eq.(1.31) by operators that act only on the low-energy states [69]

$$\imath\hbar\frac{d\tilde{a}_p}{dt} = \sum_{qmn}^{L} < pq|\hat{T}_H|mn > \tilde{a}_q^\dagger \tilde{a}_m \tilde{a}_n \exp[\imath(\omega_p + \omega_q - \omega_m - \omega_n)t]. \tag{1.43}$$

In Eq.(1.43), the operator $\tilde{T}_H$ represents the restricted two-body T-matrix expressed as

$$\hat{T}_H = U + \sum_{pq}^{H} U|pq > \frac{-1}{(\varepsilon_p + \varepsilon_q)} < pq|\hat{T}_H. \tag{1.44}$$

Equation (1.44) only differs from the usual definition of the two-body T-operator of Eq.(1.35) by the fact that the summation is restricted to the high-energy states only. If the cutoff energy is sufficiently low such that $K_{cut}a \ll 1$ ($K_{cut} = (1/\hbar)(2m\varepsilon_{cut})^{0.5}$), then $\tilde{T}_H \approx \tilde{T}_{2b}$.

In order to avoid ultraviolet divergences due to direct replacement of the contact potential into the Hamiltonian of Eq.(1.19), one has to divide the system into the subspaces H and L as above, then replace in all matrix elements $\hat{T}_{2b}$ by $\hat{T}_H$. The resulting effective Hamiltonian of the condensate system is written as

$$\hat{H}_{eff} = \sum_{n}^{L} \hbar\omega_n \hat{a}_n^\dagger \hat{a}_n + \frac{1}{2}\sum_{pqmn}^{L} < pq|\hat{T}_H|mn > \hat{a}_p^\dagger \hat{a}_q^\dagger \hat{a}_m \hat{a}_n. \tag{1.45}$$

When the boundary energy between the subspaces H and L is sufficiently low, the effective T-matrix is approximately the same as the full two-body matrix $T_{2b}$ which in turns is approximately the same as $T_H$ that leads to the same expression to the lowest order of the pseudopotential of Huang and Yang [71]. The contact potential is introduced as an approximation of the two-body T-operator, avoiding ultraviolet divergences.

### 1.5.1 Derivation of the GPE for single Bose-Einstein condensates

The GPE is a nonlinear equation of Schrödinger with an external potential that has been a quite useful tool allowing to describe many static and dynamical properties of Bose-Einstein

condensates at very low temperatures. Its usual derivation follows the mean-field approach based on the Bogoliubov approximation first formulated in 1947 [62].

**(a). Time-dependent GPE**

According to [62], the boson field operator as is decomposed as

$$\hat{\Psi}(\vec{r},t) = \psi(\vec{r},t) + \hat{\delta}(\vec{r},t), \tag{1.46}$$

where $\psi(\vec{r},t) = \left[ < \hat{\Psi}(\vec{r},t) > \right]$ is the expectation value of the boson field operator and is commonly called the *macroscopic wavefunction*. The quantity $\hat{\delta}(\vec{r},t)$ represents the non-condensed part, which, at temperatures well below $T_C$, is actually negligible and accounts for the remaining quantum fluctuations of the field. Inserting Eq.(1.46) into Eq.(1.24) and making use of the contact potential in addition to the fact that $\left\langle \hat{\delta}(\vec{r},t) \right\rangle = 0$, one obtains [74]

$$\imath\hbar\frac{\partial\psi}{\partial t} = \hat{H}_{sp}\psi + U_0|\psi|^2\psi + U_0[< \hat{\delta}^\dagger\hat{\delta} > \psi + < \hat{\delta}\hat{\delta} > \psi^* + < \hat{\delta}^\dagger\hat{\delta}\hat{\delta} >], \tag{1.47}$$

in which the space and time labels are dropped for clarity. ***The terms involving the operator $\hat{\delta}$ can be interpreted as follows: (i) $< \hat{\delta}^\dagger\hat{\delta} >$ is the mean-field of the uncondensed particles acting on the condensate. This term is negligible in the case where almost all particles are condensed; (ii) $< \hat{\delta}\hat{\delta} >$ represents a collision between two uncondensed particles in which one of them is transferred to the condensate. This term is also negligible when the majority of particles are condensed; (iii) $< \hat{\delta}^\dagger\hat{\delta}\hat{\delta} >$ represents the modification of the interaction between two condensate atoms due to virtual processes in which they make transitions to excited states before returning to the condensate. This term vanishes at $T = 0$ [74]. The latter approximation works well at zero temperature, such that for $T \to 0$, we retrieve the time-dependent GPE***

$$\imath\hbar\frac{\partial\psi}{\partial t} = \hat{H}_{sp}\psi + U_0|\psi|^2\psi. \tag{1.48}$$

In Eq.(1.48), $U_0$ is the strength of the two-body interatomic interaction $U_0|\psi|^2\psi$; in term of the nonlinearity, $U_0|\psi|^2\psi$ represents the cubic nonlinearity.

**(b). Time-independent GPE**

At zero temperature, a stationary condensate is described by the GPE, its density is time invariant; thus the Bose-Einstein condensate wavefunction has a spatially uniform phase rotation due to the its energy. The time dependence lies in the global phase, and may be separated from the spatial dependence by using the transformation

$$\psi(\vec{r},t) = \psi(\vec{r})\exp(-\imath\lambda t/\hbar). \tag{1.49}$$

Substituting (1.49) into (1.48) yields the time-independent GPE

$$\lambda\psi(\vec{r}) = \hat{H}_{sp}\psi(\vec{r}) + U_0|\psi(\vec{r})|^2\psi(\vec{r}), \tag{1.50}$$

where the constant $\lambda$ represents the eigenvalue of the condensate. The external potential hidden in $\hat{H_{sp}}$ must be time-independent. The parameter $\lambda$ is the energy required to add or remove the last particle to the condensate whilst ensuring that the normalization condition $n_0 = \int d^3r|\psi(r,t)|^2$ is satisfied. The parameter $\lambda$ is sometimes called the chemical potential and written $\mu$. Rigorously, $\lambda$ is not the chemical potential. When the condensate is at equilibrium with $n_0$ particles, one has the following relation

$$\lambda = \mu + K_B T \ln(1 + 1/n_0). \tag{1.51}$$

As $T \to 0$, the two chemical potentials are equal, i.e., $\lambda = \mu$.

**(c) The Thomas-Fermi solution**

For highly populated Bose-Einstein condensates, the kinetic energy is much smaller than the interaction energy or the potential energy due to the external potential. Hence, neglecting the kinetic energy, the ground state solution of the time-independent GPE (1.50) reads

$$\psi(r) = \sqrt{\frac{\lambda - V(r)}{U_0}} \qquad \lambda > V(r), \tag{1.52}$$

and zero elsewhere. The Thomas-Fermi wavefunction is most accurate where the condensate's density is high, and least accurate toward the system edges, where the kinetic energy dominates. Considering an harmonic confinement

$$V(r) = \frac{m}{2}(\omega_x x^2 + \omega_y y^2 + \omega_z z^2), \tag{1.53}$$

and taking into account the fact that the wavefunction is normalized to $N$, we find the Thomas-Fermi relationship between the condensate eigenvalue and the number of atoms in the system

$$\lambda = (\frac{15NU_0}{64\pi\hbar\bar{\omega}})^{2/5}(\frac{2m\bar{\omega}}{\hbar})^{3/5}, \tag{1.54}$$

where $\bar{\omega} = (\omega_x\omega_y\omega_z)^{1/3}$. Equation (1.52) implies that the spatial extent of the Thomas-Fermi wavefunction, where the condensate density vanishes, corresponds to $\lambda = U_{ext}$, and the surface thus defined is expected to be a good measure of the size of the corresponding time-independent GPE eigenstate. The extent of the condensate which is half of the surface of the edge of the Thomas-Fermi wavefunction along each axis is found to be

$$r_i = (\frac{2\lambda}{m\omega_i})^{1/2}, \tag{1.55}$$

with $i \epsilon \{x, y, z\}$.

**(d). Cubic-quintic GPE**

It is well known that the three-body interactions become important not only for large values of the scattering length, but also for small values close to the ideal gas regime. Moreover,

the three-body interactions also play a crucial role in understanding the Efimov regime, where three bosons form a bound state. Using an effective field theory, the strength of the three-body interactions, which effectively arises from the two-body interactions was derived in [72] and takes the form $384\pi\hbar^2a^4/m(4\pi-3\sqrt{3})\big[\ln(\kappa a)+B\big]$, in which $\kappa$ is a wave number and $B$ a constant calculated numerically. It is shown in [75] that $\kappa$ is an arbitrary value that can be chosen in order to fit experimental data. The constant $B$ in general is a complex number, but its imaginary part is very small in comparison to the real one [22, 23]. The case of a Bose-Einstein condensate at the mean-field regime requires that the strength of the quintic nonlinearity be smaller than the scattering length [75]. The cubic-quintic GPE has the form

$$\lambda\psi(\vec{r}) = \hat{H}_{sp}\psi(\vec{r}) + U_0|\psi(\vec{r})|^2\psi(\vec{r}) + U_1|\psi(\vec{r})|^4\psi(\vec{r}). \tag{1.56}$$

The coefficient $U_1$ represents the strength of the three-body interactions. The cubic-quintic GPE has been useful in the study of the dynamics of Bose-Einstein condensates [34].

### 1.5.2 GPE for binary Bose-Einstein condensates

After first observations of Bose-Einstein condensates made of identical atomic species, mixtures of condensates, the so-called multicomponent condensates have been achieved experimentally. The realization of mixtures of condensates gives rise to investigations in the physics of interacting quantum matter-wave fluids, where interspecies interactions play a major role. These interspecies interactions which characterize the coupling between different condensates in the mixture are amenable to produce new features not observable in single condensates. Among these features, we have complex phase diagrams [36, 77], metastable states [78], vortex transfer dynamics [13, 79], symmetry breaking instabilities [36, 80] and modulational instability [81].

The dynamics of binary Bose-Einstein condensates can be described in the framework of the coupled GPE. In the mean-field picture, the coupled GPE has the following form

$$\imath\hbar\frac{\partial\psi_j(r,t)}{\partial t} = -\frac{\hbar^2}{2m_j}\nabla^2\psi_j(r,t) + V_j(r)\psi_j(r,t) + \sum_{l=1}^{2} U_{jl} \mid \psi_l(r,t) \mid^2 \psi_j(r,t), \qquad j=1,2. \tag{1.57}$$

where $U_{jl} = 2\pi\hbar^2a_{jl}/\mu_{jl}$ $(j,l=1,2)$, $\mu_{jl} = m_jm_l/(m_j+m_l)$ being the reduced mass of an atom $j$ and an atom $l$. Parameters $a_{jl}$ account for the two-body interactions between like and unlike atoms. The strengths of the two-body intraspecies interactions are denoted $U_{jj} = U_j$, while the strengths of the two-body interspecies interactions are denoted $U_{jl} = g$ $(j \neq l)$. This implies that $U_{12} = U_{21} = U$. Equation (1.57) is the generalization of Eq.(1.48) to two-component condensates and can be derived in a similar way.

## 1.6 Limitations of the GPE

### 1.6.1 Bose-Einstein condensates at finite temperatures

In the latter section, the equation describing the dynamics of Bose-Einstein condensates, i.e., the GPE, is derived from the mean-field picture with two major assumptions: (i) the gas is sufficiently diluted and, (ii) the temperature is zero ($T \to 0$), meaning that almost all the gas is in the condensed state. However, in real physical experiments, the temperature is no longer zero. This means that real Bose-Einstein condensate experiments are conducted at finite temperatures where the thermal cloud is present. There are some regimes where the impact of the thermal cloud on the dynamical behavior of the condensate becomes important; for example, the problem of the condensate growth, the heating of the gas under strong external perturbations, or the phase fluctuations exhibited by the condensate in low-dimensional systems. It is believed that future applications of Bose-Einstein condensates such as narrow atomic microfabricated waveguides, integrated atom-interferometry-based sensing devices would also benefit from a good understanding of the behavior of condensates at finite temperatures. Therefore, theoretical models of condensates at finite temperatures are highly needed [82].

### 1.6.2 GPE beyond the mean-field pseudopotential approximation

In deriving the GPE, the contact potential was also assumed to be a constant. This assumption leads to a constant pseudopotential, with many terms neglected. Improved theoretical calculations require that quantum corrections around the mean-field also be taken into account. These quantum corrections bring us to regimes where the constant pseudopotential approximation of the GPE becomes less valid. Many theories that go beyond the GPE have focused on quantum fluctuations. Braaten and Nieto [51] have shown that for a trapped Bose-Einstein gas in the ground state, quantum corrections to the number density $n$ are dominated by quantum fluctuations with wavelengths of order $1/\sqrt{na_s}$. Using diffusion Monte Carlo calculations, Blume and Greene [54] demonstrated that the addition of an effective potential term in the mean-field equation, which accounts for quantum fluctuations leads to a greatly improved description of trapped Bose-Einstein gases. Nevertheless, Cowel *et al.* [83] proved that for homogeneous systems, different potentials having the same scattering length can lead to a vastly different ground-state energy. More, for an inhomogeneous system and for atoms under strong confinement or with a large scattering length, the shape-independent approximation becomes less applicable [84], thus a better description of atom-atom interaction beyond the pseudopotential approximation is needed. Willing to obtain more accurate theoretical predictions, Fu, Wang and Gao [85] introduced a modified form of the GPE which takes into account quantum fluctuations and the shape-dependent confinement correction term that lead to better agreements with diffusion Monte Carlo results. The modified GPE derived by Fu, Wang and Gao [85] has

the following form

$$\begin{aligned} \imath\hbar\frac{\partial\psi(r,t)}{\partial t} &= -\frac{\hbar^2}{2m}\nabla^2\psi(r,t) + V(r)\psi(r,t) \\ &\quad +U_0|\psi(r,t)|^2\psi(r,t) + U_1|\psi(r,t)|^3\psi(r,t) \\ &\quad +U_2\nabla^2(|\psi(r,t)|^2)\psi(r,t), \end{aligned} \tag{1.58}$$

where $U_1 = g\frac{32}{3\sqrt{\pi}}a_s^{\frac{3}{2}}$ and the last term accounts for the shape-dependent confinement correction on the interaction potential with $U_2 = \frac{2}{3}a_s^{2g}$.

## 1.7 Experimental realization of Bose-Einstein condensates

Bose-Einstein condensed gases are nowadays routinely produced in many laboratories around the world. Although each experimental group has its own experimental setup and details, the broad outline is similar. There are three main steps towards the formation of a Bose-Einstein condensate in the laboratory which are (i) laser cooling, (ii) magnetic trapping, and (iii) evaporative cooling. In this section, we give an overview of the experimental procedure in the achievement of Bose-Einstein condensates in experiments.

### 1.7.1 Laser cooling

In this part, we are only interested to the use of a laser light in the cooling of an atomic gas rather than the creation and properties of the laser light itself. In 1975, Hänsch and Schawlow proposed the use of the laser light in order to cool down neutral atoms. The basic idea was to use the momentum transfer resulting from the collision between an atom and a photon to reduce the velocity of the atom.

An atom that absorbs a photon of frequency $\nu$ loses a momentum of an amount of $p = h\nu/c$ ($h$ is the Planck's constant and $c$ is the velocity of light). An atom gains a momentum of the same magnitude when it emits a photon with frequency $\nu$. For two counter-propagating lasers with the same direction acting on an atomic gas sample, the resulting momenta due to many fast absorption and emission events are not the same. This is mainly due to the fact that fluorescent photons are emitted in all directions and their sum averages to zero. Therefore, the momentum of an atom of the gas sample is reduced. The laser cooling is effective provided the Doppler effect is used such that only atoms moving in the laser beam absorb photons. The lasers are tuned to the absorption line (detuning), thus atoms moving counter to a laser beam feel photons of the laser Doppler-shifted into resonance. These atoms lose momentum, i.e. speed, and are cooled down. On the contrary, atoms moving along with the detuned laser are Doppler-shifted far away from resonance and do not absorb any photon, so that they are not cooled down. Figure 2 illustrates the principle of laser cooling.

The cooling of an atomic gas in three dimensions needs the use of three counter-propagating laser beams in the three directions $-x$, $-y$, and $-z$. The three dimensional laser cooling is often

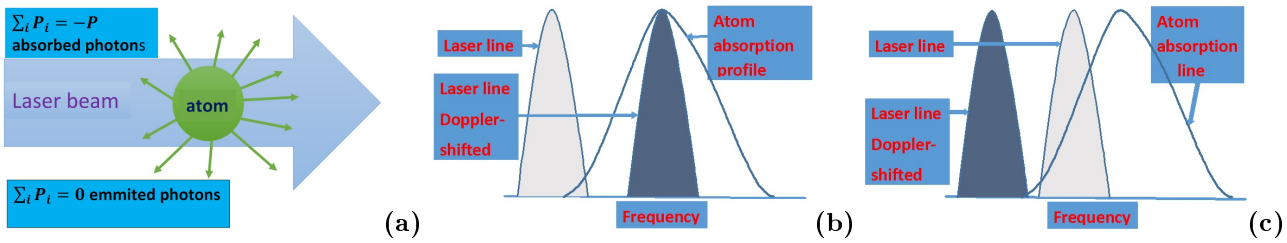


**Figure 2**: Laser cooling of atoms. (a) An atom illuminated by a laser beam absorbs and scatters many photons. (b) Laser frequency tuned below the atom resonance line, the atom moving counter to the laser beam 'feels' a Doppler-shifted frequency laser, absorbs low-energy photons of the laser, emits higher-energy photons at the resonance frequency from its transition line and is slow down. (c) An atom moving along the direction of the laser beam 'feels' the laser frequency Doppler-shifted far away from its maximum absorption line, absorbs few photons and is not cooled down.

referred to as optical molasses because the behavior of atoms in optical molasses is similar to their behavior in viscous liquids. The laser cooling mechanism is limited because the cooling rate reduces with the loss of speed of atoms. The laser cooling stops when the velocity gains by an atom as it emits a photon compensates the loss of velocity due to the scattering process. There are many other cooling mechanisms that can be used instead of the laser cooling such as the Zeeman slowing process. The reader interested in further details of laser cooling and trapping is referred to one of the following review papers [86].

### 1.7.2 Magnetic trapping

After pre-cooling, atoms are transferred into a magnetic trap. The most common used magnetic trap in condensate experiments is the magneto-optical trap potential first realized in 1987 by Ketterle, Davis, Martin, and Pritchard [87].

Though the laser cooling can bring the atomic sample to very low temperatures, due to random Brownian motion, atoms can escape out of the laser regions. The Magneto-optical trap combines the optical molasses with an appropriate external magnetic field which induces a spatial force that pushes back atoms to the center of the trapping potential. This process enables to maintain atoms in the external trap.

The magneto-optical trap consists of three pairs of counter-propagating laser beams, slightly red-detuned below the atomic resonance with opposite circular polarisations that create the optical molasses within a vacuum chamber. The laser beams are superimposed on a magnetic quadrupole field produced by a pair of anti-Helmholtz coils outside the optical molasses. The quadrupole magnetic field vanishes at the center of the two coils. The magnetic field gradient linearly increases from the trap center in any direction. The trap works because the Zeeman sublevels of an atom displaced from the center of the trap are shifted by the local magnetic field in such a way that the atom tunes into resonance with the laser field moving in the opposite direction. The net force resulting onto the atom is thus always towards the origin. Due to the Doppler shift, it appears a velocity-dependent force. The result is to cool and trap a sample

of atoms in the region at the center of the magnetic field. In addition to cool the atoms, the magneto-optical trap also confines the atoms and compresses them to higher densities. Figure 3 displays a schematic of the magneto-optical trap and the principle used to confine neutral atoms. In panel (b) of Fig. 3, a laser beam polarized $\sigma^+$, causes a transition of an atom from

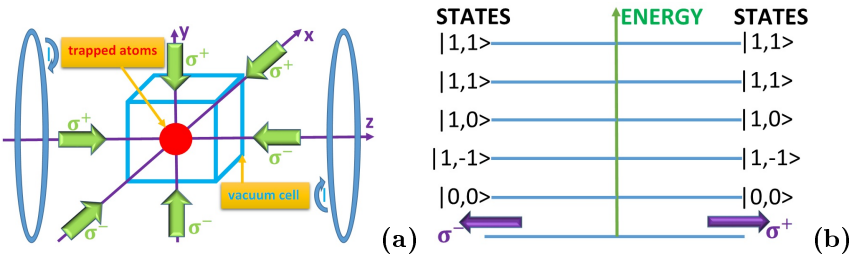


**Figure 3**: (a) Schematic of the magneto-optical trap. (b) Sketch of energy diagram indicating why trapping of atoms occurs.

the ground state $|0,0>$ to the excited state $|1,1>$, while the laser beam polarized $\sigma^-$ brings an atom from the ground state to the excited state $|1,-1>$. The presence of the magnetic field produced by the anti-Helmholtz magnetic coils (see Fig. 4(a)) shifts the degeneracy of the Zeeman sublevels of the atom. When an atom moves away from the center of the magnetic trap, for example to the left, the laser beam polarized $\sigma^-$ enters to resonance with the atomic substate $|1,-1>$ such that it preferentially absorbs polarized $\sigma^-$ photons over polarized $\sigma^+$ photons arriving from the counter direction. The atom feels a pressure due to the two counter propagating laser beams which pushes the atom back towards the center of the trap. A similar behavior is observed if the atoms moves out in any direction from the center of the trap. The magnetic trap is symmetric such that the atoms remain confined at the center of the trap. There are many trapping potentials that can be realized in order to produce Bose-Einstein condensates. A review of these can be found in [88].

### 1.7.3 Evaporative cooling

Evaporative cooling is done by continuously removing the high-energy tail of the thermal distribution from the trap. The evaporated atoms carry away more than the average energy, which means that the temperature of the remaining atoms decreases.

The magnetic trap works on diamagnetic atoms which are polarized in the Zeeman substate $|m=-1>$. On the contrary, paramagnetic atoms polarized in the Zeeman substate $|m=1>$ will be attracted to the higher magnetic fields outside the trapping region. A radio-frequency field acting onto the cold atomic sample can be used to induce transitions between magnetic substates and converts atoms into a high-field seeking state, and thus be selectively ejected from the system. The frequency of the radio-frequency field is chosen such that only atoms with enough energy move to the edge of the magnetic potential well come into resonance with the radio-frequency field. Figure 4 displays a sketch of the principle of evaporative cooling technique.

Figure 4 shows that the most energetic atoms are removed from the magnetic trap. In fact, atoms

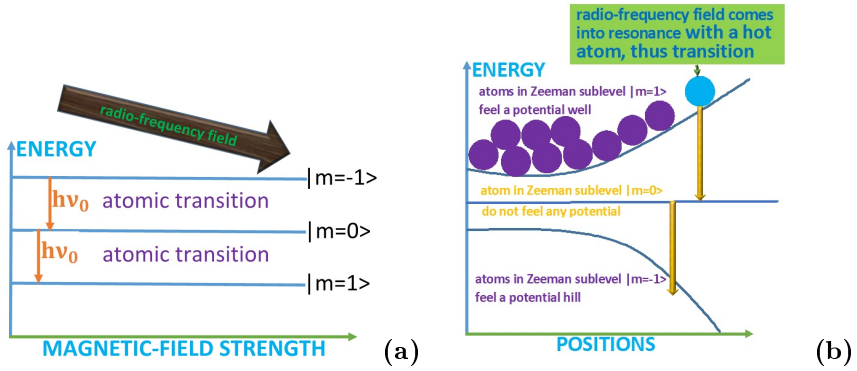


**Figure 4**: (a) Atomic Zeeman sublevels. (b) Principle of evaporative cooling.

in the magnetic trap are diamagnetic, i.e., in the Zeeman sublevel $|m = 1 >$, since have lower energy in weaker magnetic fields. Hence, such atoms are attracted to weaker magnetic fields. On the contrary, atoms in the Zeeman sublevel $|m = -1 >$ are paramagnetic, i.e., are attracted to higher magnetic fields. When most energetic atoms in the Zeeman sublevel ($|m = 1 >$) come into resonance with a radio-frequency field with frequency $\nu_0$, they undergo transitions from the substate $|m = 1 >$ to $|m = 0 >$, and from $|m = 0 >$ to $|m = -1 >$. The most diamagnetic atoms are selectively transformed into paramagnetic atoms, then removed from the magnetic trap. After many binary elastic collisions, the remaining atoms in the magnetic trap rethermalize and undergo a lower temperature towards the formation of a Bose-Einstein condensate.

However, the evaporative cooling presents a pitfall because at the center of the magneto-optical trap the magnitude of the magnetic field is zero. Thus, at the center of the trap, magnetic substates are not Zeeman-split, so, polarized atoms can undergo spontaneous Majorana spin-flip transitions to untrapped $m_F$ states. The problem is worse at lower temperatures as cold atoms spend more time at the center of the trap where the magnetic field vanishes. To overcome this problem, two approaches were implemented. The time-orbiting potential was developed at the Joint Institute Laboratory of Astrophysics [89]. In the time-orbiting potential trap, a rapidly rotating bias field is added to the static quadrupole field, so that on average the atoms experience a harmonic potential. At any time the zero of the magnetic field circulates about the center of the trap, removing hot atoms rather than cold ones. The second approach has been implemented at the Massachusetts Institute of Technology, where an Ioffe-Pritchard type trap with no region with vanishing magnetic field was built [90]. We display in Fig. 5 an image of the first condensate obtained by the team of Wieman and Cornell [1].

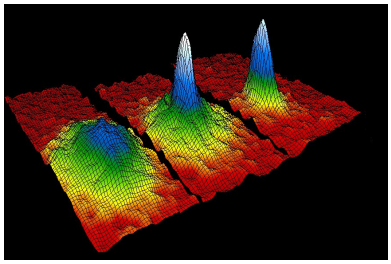

**Figure 5**: Images of the velocity distribution of rubidium atoms during Bose-Einstein condensation. The left frame corresponds to a gas at a temperature just above condensation; the center frame, just after the appearance of the condensate; the right frame, after further evaporation leaves a sample of nearly pure condensate

## 1.8 Conclusion

We have dealt with generalities on Bose-Einstein condensation in this chapter. At first, we have described both non-interacting, and interacting particles boson gases. Then, using the mean-field theory, the time-dependent, and time-independent GPEs for single and binary condensates have been derived. Some limitations of the mean-field description, and discussions about some models that go beyond the mean-field picture have also been presented. At the end of the chapter, we have presented an overview of experimental procedures that lead to observation of Bose-Einstein condensates.

In this thesis, we are interested in the generation via modulational instability and the dynamics of coherent matter waves in Bose-Einstein condensates. The next chapter is devoted to the description of some analytical and numerical methods used to investigate the dynamics of solitons in Bose-Einstein condensates.

# Chapter 2

# Analytical and Numerical Methods for the Quest of Solitons

## 2.1 Introduction

The experimental observation of Bose-Einstein condensates of trapped atomic vapors has allowed investigations of some fundamental concepts of atomic physics and condensed matter physics [91]. There has been an increase of experimental and theoretical activities devoted to the quest of nonlinear excitations in Bose-Einstein condensates such as Josephson oscillations and macroscopic quantum tunneling [92], Faraday waves [93], compactons [94], solitons [10, 11, 12], vortices [13] and vortex lattices [14], grey solitons [95], gap solitons [27], rogue waves [96] and so on. The phenomenon of Bose-Einstein condensation provides unique opportunities to study many quantum properties of matter waves. Among these properties, the physical mechanism of Bose-Einstein condensate soliton is a relevant aspect, since it is believed that the generation and evolution of solitons in condensates are important for a number of condensates applications [4, 5, 6, 7, 8]. The generation and structure dynamics of solitons in condensates may be done via the modulational instability mechanism [26, 28, 32, 33, 34]. In addition, many soliton properties of condensates may be explained with exact analytical solutions of the GPE. So, finding exact solutions of the GPE is a task of relative importance. For example, exact solutions may (i) help to choose appropriate experimental parameters, (ii) provide a way of probing the validity of the GPE at higher densities, (iii) help to analyze the stability of condensates, (iv) check the numerical analysis of the GPE, and (v) help to explain the formation and the propagation of different kind of patterns in condensates as well as their long-time evolution. However, The validity of exact analytical solutions found by mathematical means should be confirmed by some numerical integrations of the original equation. Thus, the investigation of dynamical properties of Bose-Einstein condensates requires both analytical and numerical treatments.

The generation of bright solitons in Bose-Einstein condensates is usually studied with the linear stability analysis [26, 28, 32, 33, 34]. Numerous analytical methods have been used to

exactly solve the GPE. Among these methods are the inverse scattering transform method [97], the Darboux transformation method [98], the Hirota bilinear method [99], the Painlevé analysis [100], the $(\frac{G'}{G})$-expansion method [101], the homotopy analysis method [102], the variational approach [38, 50], the F-expansion method which includes the tanh-function and the extended tanh-function methods [34], and many others.

This chapter describes the analytical and numerical methods used in the investigation of the dynamics of solitons in Bose-Einstein condensates. We present the variational approach, the modified lens-type transformation [34], the linear stability analysis, the F-expansion method. The numerical methods presented include the normalized gradient flow with Backward Euler centered finite difference scheme [53], the split-step Fourier method [55], the fourth order Runge-Kutta in the interaction picture method [54], and the MATLAB toolbox PDEPE.

## 2.2 The variational approach

The study of solitons in nonlinear partial differential equations is strongly related to the inverse scattering transform theory. The inverse scattering transform introduces two types of solutions of nonlinear partial differential equations which are solitons and radiations [103]. The radiations are dispersing and decaying type solutions. Nevertheless, true physical examples of exact solitons found with the inverse scattering transform are uncommon since an exact soliton is usually embedded with a significant fraction of radiation [104]. Hence, in real physical situations, it is necessary to develop an approximation that leads to sufficiently accurate explicit results.

The corresponding variational approach was first introduced in the quest of solitons in plasma physics by Bondeson, Lisak and Anderson [105]. The latter paper paved the way to investigations of soliton dynamics in many areas of physics such as fiber optics [106]. A review of the variational approach with its applications in different media was proposed by Malomed [107]. The Variational approach is an approximate method whose objective is to reduce the complex dynamics described by partial differential equations to a relatively simple system of a few ordinary differential equations. In applying the variational approach, one first has to reformulate the underlying equation (here Eq.(2.1)) in a variational form, then choose an ansatz of the field configuration sought for. The ansatz has some unknown variables which are allowed to be functions of the evolutional variable, and characterize important features of the solution looked for. The set of ordinary differential equations for the unknown variables is derived via the standard variational approach procedure by minimizing the action functional $S(U, U^*)$. The action has the form $S = \int L d\varrho$, $\varrho$ being the evolution variable, and $L$ the effective lagrangian. $L$ may be written in term of the lagrangian density $\ell$ as $L = \int \ell d\varrho'$, where $\varrho'$ is the transverse coordinate.

Let us consider the one dimensionless GPE described as

$$\begin{aligned} \imath\frac{\partial\psi(x,t)}{\partial t}+\frac{\partial^2\psi(x,t)}{\partial x^2}+2a|\psi(x,t)|^2\psi(x,t)-(\alpha x^2+\lambda x)\psi(x,t) &= \imath\gamma\psi(x,t) \\ &= R(\psi,\psi^*). \end{aligned} \quad (2.1)$$

The left-hand side of Eq.(2.1) is the conservative part, while in the right-hand side $R$ represents the dissipative part. In Eq.(2.1), $t$ and $x$ are measured in units of $\frac{2}{\omega_\perp}$ and $a_\perp$, respectively. The quantities $a_\perp=\sqrt{\frac{\hbar}{m\omega_\perp}}$ and $\omega_\perp$ represent the harmonic oscillator length and frequency in the two orthogonal directions, respectively. The parameter $m$ is the atomic mass. The quantity $2a$ is the strength of the two-body interatomic interactions. The parameter $\alpha$ represents the strength of the harmonic potential, while the term $\lambda x$ may take into account some linear potentials. The quantity $\gamma$ is a parameter related to the exchange of atoms between the condensate and the uncondensed fraction of the thermal cloud. Positive values of $\gamma$ correspond to the physical situation where atoms are fed into the condensate from the thermal background or injected into the condensate from a reservoir by a pumping mechanism [45]. Negative values of $\gamma$ are related to atoms escaping out of the condensate due to dipolar relaxation. In this case, the magnetic dipole-dipole interaction between the magnetic moments of two colliding atoms makes one or both atoms emerge from the collision in a different spin state, a process that induces an increase of the temperature of the condensate resulting to the expulsion of many atoms out of the trap. Generally speaking, the dissipative mechanism corresponding to $\gamma$ negative is spatially dependent. The specific case where the rate of exchange of atoms is constant means that the size of the uncondensed fraction of atoms is larger than that of the condensate. The rate of exchange of atoms is characterized by a temporal scale $\zeta$ which is the time interval between subsequent events of adding or removing individual atoms from the atomic ensemble. The mean-field approximation remains valid if $\zeta$ is negligible, i.e., $\zeta\omega_\perp \ll 1$, which is verified for typical configurations where $\omega_\perp = 2\pi\times 360$ Hz and $\zeta\sim 4\mu s$. This means that $|\gamma|$ is small.

In order to apply the VA, we choose an ansatz with a Gaussian form

$$\psi(x,t)=A(t)\exp(-\frac{x^2}{2W(t)^2}+\imath(k(t)x+\frac{b(t)x^2}{2}+\phi(t))), \quad (2.2)$$

where $A$, $W$, $k$, $b$, and $\phi$ represent the amplitude, width, linear phase shift, chirp, and homogeneous phase, respectively, and stand for the variational parameters. Equation (2.1) may be formulated in a variational form corresponding to the Lagrangian density $\ell=\ell_C+\ell_R$, where

$$\ell_C=\frac{\imath}{2}[\psi(x,t)^*_t\psi(x,t)-\psi(x,t)_t\psi(x,t)^*]+|\psi(x,t)|^2-a|\psi(x,t)|^4+(\alpha x^2+\lambda x)|\psi(x,t)|^2, \quad (2.3)$$

corresponds to the Lagrangian density of the conservative part, and $\ell_R$ has the property $\delta\ell_R/\delta\psi^*=-R(\psi(x,t),\psi(x,t)^*)$. By applying the Euler-Lagrange equation to $\ell$ with respect to $\psi^*$, we obtain

$$[\frac{\partial\ell}{\partial\psi^*}-\frac{d}{dt}(\frac{\partial\ell}{\partial\psi^*_t})]=[\frac{\partial\ell_C}{\partial\psi^*}-\frac{d}{dt}(\frac{\partial\ell_C}{\partial\psi^*_t})]-R(\psi,\psi^*)=0, \quad (2.4)$$

which leads to Eq.(2.1). The variational principle that corresponds to Eq.(2.4) is

$$\delta \int_0^t L' dt = \delta \int_0^t (L_C + L_R) dt = 0, \tag{2.5}$$

with $L_C = \int dx \ell_C$, $L'$, and $L_C$ being the effective Lagrangian corresponding to $\ell$ and $\ell_C$, respectively. The variational equations are calculated from the formula

$$\frac{d}{dt}\frac{\partial L_C}{\partial Q_t} - \frac{\partial L_C}{\partial Q} = -\int [R\frac{\partial \psi(x,t)^*}{\partial Q} + R^*\frac{\partial \psi(x,t)}{\partial Q}]dx, \tag{2.6}$$

where $Q$ stands for a variational parameter ($A$, $W$, $k$, $b$, and $\phi$). Inserting Eq.(2.2) into Eq.(2.3) and integrating over the spatial coordinate yield the explicit expression of the conservative effective Lagrangian

$$L_C = N[\phi_t + k^2 + \frac{1}{4}(b_t + 2b^2 + 2\alpha)W^2 + \frac{1}{2W^2} - \frac{aN}{\sqrt{2\pi W}}]. \tag{2.7}$$

The parameter $N = \int |\Psi(x,t)|^2 dx = \sqrt{\pi} W A^2$ is the number of atoms in the condensate. Substituting Eq.(2.2) and Eq.(2.7) into Eq.(2.6) leads to the following system of ordinary differential equations

$$\begin{aligned} b &= \frac{W_t}{2W} + \gamma, \\ k &= 0, \\ W_{tt} + 4\gamma W_t &= \frac{4}{W^3} - 4\gamma^2 W - \frac{4aN}{\sqrt{2\pi}W^2} - 4\alpha W, \\ \phi_t &= \frac{2aN}{\sqrt{2\pi}W} - \frac{1}{2W^2} - k^2 - \frac{1}{4}(b_t + 2b^2 + 2\alpha)W^2. \end{aligned} \tag{2.8}$$

Looking for soliton solutions, $W_t = W_{tt} = 0$, the residual variational equations become

$$\begin{aligned} b &= \gamma \\ k &= 0 \\ \pi\sqrt{3}aWN + \pi\sqrt{6\pi}(\alpha + \gamma^2)W^4 - \pi\sqrt{6\pi} &= 0 \\ \phi_t &= \frac{2aN}{\sqrt{2\pi}W} - \frac{1}{2W^2} - \frac{1}{2}(\gamma^2 + \alpha)W^2. \end{aligned} \tag{2.9}$$

Solitons are stable if the Vakhitov-Kolokolov criterion is satisfied, i.e., $-\frac{d\phi_t}{dN} < 0$. Thus, the stability criterion (for $\gamma = 0$) may be written as

$$-\frac{2a}{\sqrt{2\pi}W} < 0. \tag{2.10}$$

As an approximate method, the results obtained with the variational approach should be compared with direct numerical integrations of the underlying model equation. The comparison is necessary for only some important variational parameters. In other words, the validity of the variational approach is tested by a comparison with a direct numerical simulation of the original

partial differential equation(s). This issue is important in the study of the stability of solitons for two main reasons: the shape of the ansatz chosen may miss at least one unstable mode in such a way that the variational approach prediction is numerically unstable; in addition, in some cases, the variational approach introduces a 'false instability' that the soliton does not have in reality. Though its drawbacks, the variational approach remains a very efficient technique for producing analytical or semi-analytical results for complex dynamical models [107].

## 2.3 The modified lens-type transformation

The lens transformation is the optics appellation of the mathematical *pseudo-conformal* transformation used to study symmetries of nonlinear Schrödinger equation types [108]. The lens transformation and its variant forms have also been used to hide the space dependence of external fields in order to facilitate the study of modulational instability in Bose-Einstein condensates [32, 34], and to derive the integrability condition of the GPEs [99, 34]. The standard lens transformation has been widely used, hence we present here a variant form that is useful for GPEs with complex external potentials.

We consider the GPE described by Eq.(2.1), and introduce the modified lens-type transformation [34]

$$\psi(x,t) = \frac{1}{\sqrt{l(t)}}\Phi(X,T)\exp[\eta(t) + \imath f(t)Z(x,t)], \tag{2.11}$$

where $T(t)$, $\eta(t)$, $\sigma(t)$, and $f(t)$ are real scaling functions of time $t$ to be determined later, $X = \frac{x}{l(t)}$, and $Z(x,t) = x^2 + \sigma(t)x$. The transformation (2.11) is analogous to the lens transformation [32, 99] and has been used in some Bose-Einstein condensate problems [32, 34, 100] and mainly differs from the lens transformation because of the inclusion of the functions $\eta(t)$ and $\sigma(t)$. For simplicity and without loss of generality we choose $t_0 = 0$ (initial time), $l(0) = 1$, $\eta(0) = 0$. The function $l(t)$ helps to preserve the scaling. By setting [34, 100]

$$\begin{aligned}
\frac{dT}{dt} &= \frac{1}{l^2(t)},\\
\frac{dl}{dt} &= 4f(t)l(t),\\
\frac{df}{dt} &= -4f^2(t) - \alpha(t),\\
\frac{d\sigma}{dt} &= \frac{-\lambda(t) + \sigma(t)\alpha(t)}{f(t)},\\
\frac{d\eta}{dt} &= \gamma.
\end{aligned} \tag{2.12}$$

Equation (2.1) in terms of the new variables $X$ and $T$ is converted to

$$\begin{aligned}
\imath\frac{\partial\Phi(X,T)}{\partial T} &= -\frac{\partial^2\Phi(X,T)}{\partial X^2} - 2\imath f(t)l(t)\sigma(t)\frac{\partial\Phi(X,T)}{\partial X} + f^2(t)l^2(t)\sigma^2(t)\Phi(X,T)\\
&\quad -2a(t)l(t)\exp(2\eta(t))|\Phi(X,T)|^2\Phi(X,T).
\end{aligned} \tag{2.13}$$

We recall that the spatial dependence of the external potential is hidden in Eq.(2.13). This equation is relatively simple to manipulate than Eq.(2.1) with the external potential.

The modified lens-type transformation is effective when one has explicit expressions of the functions $T(t)$, $f(t)$, $l(t)$, $\sigma(t)$, $\eta(t)$. The set of ordinary differential equations (2.12) is rather difficult to solve analytically, so we restrict ourselves to the simple case where the functions $\alpha(t)$, $\lambda(t)$, $\sigma(t)$ are non-vanishing constants, respectively. In this case, the solution of the last equation of the set (2.12) is $\sigma = \frac{\lambda}{\alpha}$, meaning that $\sigma$ is the ration of the strength of the linear potential over the strength of the quadratic potential. The solution of the last equation of the set (2.12) is $\eta(t) = \lambda t$. The solutions of the first three equations of the set (2.12) depend on the sign of the strength of the external potential $\alpha$, and may be found with a computer algebra software such as MAPLE. For positive values of $\alpha$, the explicit solutions of the first three equations of the set (2.12) are

$$\begin{aligned} f(t) &= -\frac{\sqrt{\alpha}}{2}\tan(2\sqrt{\alpha}t), \\ l(t) &= |\cos(2\sqrt{\alpha}t)|, \\ T(t) &= \frac{1}{2\sqrt{\alpha}}\tan(2\sqrt{\alpha}t). \end{aligned} \tag{2.14}$$

In the case of negative values of $\alpha$, explicit expressions of the functions $f(t)$, $T(t)$, and $l(t)$ are given by

$$\begin{aligned} f &= \pm\frac{1}{2}\sqrt{-\alpha} \\ l(t) &= \exp(2ft) \\ T(t) &= \frac{1-\exp(-8ft)}{8ft}. \end{aligned} \tag{2.15}$$

The expression of $f(t)$ in Eq.(2.14) implies that the presence of the quadratic potential induces the creation of a periodic nonlinear frequency shift. One then concludes that the function $f(t)$ characterizes the periodic oscillations of the nonlinear phase coming from the presence of the quadratic potential. This leads to the creation of a current. Due to the similarity transformation (2.11) and the constraints (2.12), the solution $f(t)$ in Eq.(2.14) induces a time-periodic driving term in Eq.(2.1) with frequency $4\sqrt{\alpha}$, which is the oscillation frequency naturally following from the Ehrenfest theorem. According to Eq.(2.14), these oscillations have singularities at each time $t_n = \frac{(2n+1)\pi}{4\sqrt{\alpha}}$, ($n$ is a positive or negative integer). For each $t_n$, there is a phase divergence that could be understood from the Ehrenfest theorem. The presence of the quadratic potential induces a current which periodically changes its direction as a consequence of the Ehrenfest theorem. The change of the current direction is accompanied by the phase singularity [32]. We circumvent these singularities by taking into account only real physical times belonging to the interval $[0, \frac{\pi}{4\sqrt{\alpha}}[$.

The modified lens-type transformation is related to all experimental parameters of the external potential, i.e., $\alpha$, $\lambda$, and $\gamma$. The explicit expressions of the function variables of the modified

lens-type transformation allow to shuffle between the real and the rescaled variables, respectively. The modified lens-type transformation may also be used to analyze the integrability condition of the GPEs [34, 109].

## 2.4 The linear stability analysis

In this section, we present the linear stability analysis of plane waves in the framework of Eq.(2.1), with the objective to derive the modulational instability criterion. The aim of the linear stability analysis is to slightly perturb the envelop of a continuous plane wave and check if this perturbation increases or not. So, let us consider the following ansatz

$$\Phi = (\Phi_0 + \delta\Phi)\exp[-\imath\int_0^T \Theta(T')dT'], \tag{2.16}$$

where, $\Theta(T) = f^2(t)l^2(t)\sigma^2(t) + \Phi_0^2(2a(t)\exp(2\eta(t)) - 12\Phi_0^2\tau\exp(4\eta(t)))$, accounts for the nonlinear frequency shift, $\delta\Phi(X,T)$ is the complex amplitude of the perturbation and $\Phi_0$ is a real constant. We insert Eq.(2.16) into Eq.(2.13) and keep only first-order terms in $\delta\Phi$ and its complex conjugate $\delta\Phi^*$. After a little algebra, the governing equation describing the dynamics of the perturbation is

$$\imath\frac{\partial\delta\Phi}{\partial T} = -\frac{\partial^2\delta\Phi}{\partial X^2} - 2\imath f(t)l(t)\sigma(t)\frac{\partial\delta\Phi(X,T)}{\partial X} + \Delta(t)(\delta\Phi + \delta\Phi*) + \frac{\partial\delta\Phi^*}{\partial X}), \tag{2.17}$$

with $\triangle(t) = -2a\Phi_0^2(t)l(t)\exp(2\eta(t))$. We suppose that the functions $U$ and $V$ are the real and the imaginary parts of the perturbation ($\delta\Phi = U + \imath V$), respectively, and take the forms [34]

$$\begin{aligned} U &= Re\{U_0\exp[-\imath(KX - \int_0^T \Omega(T')dT')]\} \\ V &= Im\{V_0\exp[-\imath(KX - \int_0^T \Omega(T')dT')]\}, \end{aligned} \tag{2.18}$$

where $KX - \int_0^T \Omega(T')dT'$ represents the phase of the modulation, $K$ is the wave number, and $\Omega(T)$ is the frequency of the modulation. Inserting Eq.(2.18) into Eq.(2.17) then, separating the real and the imaginary parts give rise to a system of two coupled equations in $U$ and $V$, respectively. The determinant of the system provides the dispersion relation

$$\Omega^2 - 4Kf(t)l(t)\sigma(t) - K^2(K^2 + 2\Delta(t) - 4f^2(t)l^2(t)\sigma^2(t))\Phi_0^2 = 0. \tag{2.19}$$

If the frequency of the modulation is a complex number, the system becomes unstable under modulation, and the gain of instability is $\exp(\Omega_i)$, where $\Omega_i$ is the imaginary part of $\Omega$. This implies that the discriminant of Eq.(2.19) is negative. Hence, the modulational instability criterion is

$$|K| < 2\exp(\eta(t))\Phi_0\sqrt{a(t)l(t) + 8\tau\exp(2\eta(t))\Phi_0^2}. \tag{2.20}$$

We can evaluate the gain of modulational instability with the formula

$$G = \Re(\sqrt{K^2(4a(t)l(t)\exp(2\eta(t))\Phi_0^2 - K^2)}). \tag{2.21}$$

It may take a certain period of time after which the instability ceases to be dominant in the system. The critical time $t_C$ after which an instability is no longer dominant in the system is the solution of the following implicit equation $K^2 - 4a(t_C)l(t_C)\exp(2\eta(t_C))\Phi_0^2 = 0$. The value of $t_C$ may be obtained with MAPLE. With the linear stability analysis just performed, one needs explicit expressions of the functions $f$, $l$, $T$, and $\sigma$. These expressions are provided in the previous section.

The linear stability analysis is a successful tool in deriving the modulational instability criterion and growth rate, thus regions of parameters where solitons are likely to be observed. Nevertheless, the linear stability analysis becomes less valid at larger times far from the initial state. This can be understood because one has to neglect higher order terms by keeping only linear ones in the linear stability analysis theory. The linear stability analysis fails to provide any dynamical information beyond the instability points. For this reason, direct numerical integrations of the original equation should be carried in order to investigate the properties of the solitons generated at longer times.

## 2.5 The F-expansion method

The F-expansion method [34, 111] is a powerful technique used to construct analytical solutions of nonlinear partial differential equations. First we give an outline of the method.

Let us consider a nonlinear partial differential equation with dependent variable $u$, and independent variables $x = (x_1, x_2, ...x_l, t)$ of the form

$$P(u, u_x, u_t, u_{xx}, u_{xt}, u_{tt}, ...) = 0. \tag{2.22}$$

**First step:** Seek traveling solutions of Eq.(2.22) by taking

$$u(x) = u(\xi), \qquad \xi = k_1x_1 + k_2x_2 + ... + k_lx_l + \omega t, \tag{2.23}$$

where $k_1$, $k_2$,..., $k_l$, and $\omega$ are constants to be determined later. Substituting Eq.(2.23) into Eq.(2.22) leads to an ordinary differential equation for $u(\xi)$

$$P(u, u', u'', ...) = 0. \tag{2.24}$$

**Second step:** Assume a solution $u(\xi)$ of the form

$$u(\xi) = a_0 + \sum_{i=1}^{n} a_i F^i(\xi). \tag{2.25}$$

The function $F(\xi)$ satisfies a nonlinear ordinary differential equation which has known exact solutions referred to as auxiliary equation. There are many types of auxiliary equations that

may be used such as the Riccati equation $u' = A + u^3$, auxiliary ordinary equation $u'^2 = Bu^2 + Cu^2 + Du^4$, first kind elliptic equation $u'^2 = A + Bu^2 + Du^4$, the generalized Riccati equation $u' = r + pu + qu^2$ and so on [111]. The types of the solutions of the auxiliary equation give their names to particular methods. For example, if the auxiliary equation admits tanh functions as solutions, the method could be referred to as the tanh-function method [112], or the Jacobi elliptic functions method if one considers the Jacobi function solutions of the auxiliary equation [103]. The F-expansion method can be thought of as a generalization of the Jacobi function method [114]. Recently, different extensions of the F-expansion method have been proposed [34, 114, 115]. In the generalized F-expansion method the solution is sought for a traveling solution of the form

$$u(\xi) = a_0 + \sum_{i=-n}^{n} a_i F^i(\xi). \tag{2.26}$$

**Third step:** Insert the trial solution of Eq.(2.25) into Eq.(2.24) and determine the value of $n$ by balancing the highest nonlinear term with the highest partial derivative of $u$.

**Fourth Step:** Insert Eq.(2.25) along with the auxiliary equation into Eq.(2.24) and collect all coefficients of $F'(\xi)F^j(\xi)$. Setting all coefficients to zero yields a set of over-determined ordinary differential equations for the coefficients of the auxiliary equation. Then, solve this set of over-determined equations with MAPLE.

**Fifth step:** Use the solutions of the auxiliary equation, and insert them along with the solutions of the set of ordinary differential equations found in the fourth step to get analytical solutions of the nonlinear partial differential equation (2.23).

Let us illustrate the above algorithm with the following cubic-quintic nonlinear Schrödinger equation

$$\imath\frac{\partial\Psi(x,t)}{\partial t} = -c\frac{\partial^2\Psi(x,t)}{\partial x^2} - (\pm) \mid \Psi(x,t) \mid^2\Psi(x,t) + \chi_0 \mid \Psi(x,t) \mid^4\Psi(x,t). \tag{2.27}$$

Equation (2.27) may be derived by applying a modified lens-type transformation to a cubic-quintic GPE with time varying coefficients [34]. The parameters $c$ and $\chi_0$ are real constants.

We assume that $\Psi(x,t)$ has the amplitude-phase form and may be written as

$$\Psi(x,t) = Q(\xi)\exp[i\theta(x,t)], \tag{2.28}$$

where $Q$ represents the amplitude part and $\theta$ accounts for the phase part. The new variables $\xi$ and $\theta$ have the forms

$$\xi = k_0x - \omega_0t, \qquad \theta(x,t) = kx - \omega t. \tag{2.29}$$

Parameters $k_0$, $k$, $\omega_0$, and $\omega$ are real constants which account for width, linear frequency shift, velocity, homogenous phase of the wavefunction $\Psi(x,t)$, respectively. Substituting Eqs.(2.28)-(2.29) into Eq.(2.27), then separating the real and the imaginary parts, respectively reads the

following set of ordinary differential equations with respect to $Q$

$$(\omega - ck^2)Q + Q^3 - \chi_0 Q^5 + ck_0 \frac{d^2Q}{d\xi^2} = 0, \tag{2.30}$$

$$(\omega_0 - 2ckk_0)\frac{d^2Q}{d\xi^2} = 0. \tag{2.31}$$

Assuming the constraint

$$\omega_0 = 2ckk_0, \tag{2.32}$$

means that we only need to solve Eq.(2.30). Thus, in the following, we focus our attention on deriving solutions of Eq.(2.30). Assuming that the function $Q$ has the following form

$$Q(\xi) = \sum_{i=0}^{M} a_i F^i(\xi), \tag{2.33}$$

where M is a positive integer, and the function $F$ is the solution of the general Bernoulli equation (which is the auxiliary equation)

$$\frac{dF}{d\xi} = aF(\xi) + bF^{\lambda}(\xi), \tag{2.34}$$

parameters $a$, $b$, $\lambda$ being real constants which will be determined later, with $\lambda \neq 1$. Introducing Eq.(2.34) into Eq.(2.27) and using the homogeneous balance between the highest order derivative and nonlinear terms, respectively, yield $\lambda = 2M + 1$. Since $\lambda \neq 1$, then $M \geq 1$. Let us consider the simple case where $M = 1$, and $\lambda = 3$, we have

$$Q(\xi) = a_0 + a_1 F(\xi), \qquad \frac{dF}{d\xi} = aF(\xi) + bF^3(\xi). \tag{2.35}$$

Inserting Eq.(2.35) into Eq.(2.27) and collecting coefficients of powers $F^i(\xi)$, then setting each coefficient to zero, yield a set of over-determined algebraic equations for the unknowns $a_0$, $a_1$, $a$, $b$, and $\omega$. Solving this set of over-determined equations with the aid of MAPLE leads to the following solutions

$$a_0 = 0, \tag{2.36}$$

$$a = \frac{-\sqrt{3}}{4k_0\sqrt{c}\sqrt{\chi_0}}, \tag{2.37}$$

$$b = \pm\frac{a_1^2\sqrt{\chi_0}}{k_0\sqrt{3c}}, \tag{2.38}$$

$$\omega = \frac{-3 + 16ck^2\chi_0}{16\chi_0}. \tag{2.39}$$

Equations (2.36)-(2.39) imply that $c > 0$, and $\chi_0 > 0$. Using the solutions of the general Bernoulli equation (2.28) for $\lambda = 3$ given in the Appendix A [115], we derive analytical solutions of Eq.(2.27)

$$\Psi_{1j}(x,t) = a_1 F_{1j}(\xi)\exp[\imath\theta(x,t)], \qquad j = 1, 2, 3. \tag{2.40}$$

The F-expansion method and extended F-expansion methods are powerful techniques used to construct analytical solutions of nonlinear partial differential equations that appear in mathematical physics. In the next chapter, we will employ the F-expansion method with different auxiliary equations, i.e., the Ricatti equation, the Lenard equation, the hyperbolic equation whose solutions are given in the Appendices B, C, D, and E, respectively.

## 2.6 Numerical methods

The linear stability analysis becomes less valid at lager times because the amplitudes of the carrier waves may exponentially grow in the unstable region. Approximate analytical solutions such as those constructed with methods like the variational approach, the F-expansion method and extended F-expansion methods, always have practical limits since as approximate solutions, these ones neglect some aspects of the exact solution. Besides, in real physical experiments, there are some imperfections that shall perturb the system under consideration. These imperfections shall induce a small amount of perturbation that may destroy exact unstable solutions, which will not be observed in experiments. For these reasons, the and approximate analytical solutions are compared with exact numerical solutions of the nonlinear partial differential equation under study. In this thesis, we have used different numerical methods in order to integrate model equations of GPE type under investigation.

### 2.6.1 The continuous normalized gradient flow with backward Euler centered finite difference

We begin with the presentation of the continuous normalized gradient flow with Backward Euler centered finite difference scheme developed by Bao and Du [53] for integration of the GPE of types

$$\imath\Psi_t(\mathbf{x},t) = -\frac{1}{2}\triangle\Psi(\mathbf{x},t) + V(\mathbf{x},t)\Psi(\mathbf{x},t) + \beta|\Psi(\mathbf{x},t)|^2\Psi(\mathbf{x},t), \quad t>0, \quad \mathbf{x}\epsilon\Theta\subseteq\mathbb{R}^d \quad (2.41)$$

where $\triangle$ represents the Laplacian in $d$-dimensions, with the initial condition $\Psi(\mathbf{x},t)=0$, $\mathbf{x}\ \epsilon\ \Xi=\partial\Theta$, $t\geq 0$. The term $\Theta$ represents a subset of $\mathbb{R}^d$, $V(\mathbf{x},t)$ accounts for an external potential with free geometry, and $\beta$ is a real constant. It is shown in [53] that the continuous normalized gradient flow for a stationary solution of Eq.(2.41), $\Psi(\mathbf{x},t)=\phi(\mathbf{x},t)\exp(-\imath\mu t)$, where $\mu$ is the chemical potential, has the form

$$\begin{aligned}\phi_t(\mathbf{x},t) &= \frac{1}{2}\triangle\phi(\mathbf{x},t) - V(\mathbf{x},t)\phi(\mathbf{x},t) - \beta|\phi(\mathbf{x},t)|^2\phi(\mathbf{x},t) + \mu_\phi(t)\phi(\mathbf{x},t), \quad \mathbf{x} \quad \epsilon\Theta, \quad t>0,\\ \phi(\mathbf{x},t) &= 0, \quad \mathbf{x}\epsilon\Theta, \phi(\mathbf{x},0)=\phi_0(\mathbf{x}), \quad \mathbf{x}\epsilon\Xi. \end{aligned} \quad (2.42)$$

The term $\mu_\phi(t) = \frac{1}{||\phi(.,t)||^2}\int_\Theta[\frac{1}{2}|\nabla\phi(\mathbf{x},t)|^2 + V(x)\phi^2(\mathbf{x},t) + \beta\phi^4(\mathbf{x},t)]$. Let us define the spatial mesh size $h=\Delta\mathbf{x}>0$ as $h=(b-a)/M$, $M$ being an even positive integer. The time step is $k=\Delta t>0$, and the grid points and time steps are $\mathbf{x}_j = a+jh$, $j=0,...,M$, $t_n=nk$,

$n = 0, 1, ....$ Then, the backward Euler for time discretization and second-order centered finite difference for spatial derivatives are used. The detail scheme is

$$\begin{aligned} \frac{\phi_j^* - \phi_j^n}{k} &= \frac{1}{2h^2}[\phi_{j+1}^* - 2\phi_j^* + \phi_{j-1}^*] + V(\mathbf{x}_j)\phi_j^* - \beta(\phi_j^n)^2\phi_j^* \quad j = 1, ..., M-1 \\ \phi_0^* &= \phi_M^* \quad = 0, \quad \phi_j^0 = \phi_0(\mathbf{x}_j), \quad j = 0, 1, ..., M \\ \phi_j^{n+1} &= \frac{\phi_j^*}{||\phi^*||}, \quad j = 0, ..., M, \quad n = 0, 1, ... \end{aligned} \tag{2.43}$$

The norm is defined as $||\phi^*||^2 = h\sum_{j=1}^{M-1}(\phi_j^*)^2$.

The normalized gradient flow with backward scheme has been proven to be more efficient in computing the Bose-Einstein condensate ground state solution than other methods such as the Cranck-Nicholson scheme [53].

### 2.6.2 The split-step Fourier method

The split-step Fourier method is a pseudo-spectral numerical method which is used to solve nonlinear partial differential equations. In this numerical scheme, the solution is computed in small steps, and the linear and the nonlinear parts are treated separately. In addition, it is necessary to compute two Fourier transforms with this numerical scheme. In order to describe the split-step Fourier method, we consider the following dimensionless GPE

$$\imath\frac{\partial\Psi(x,t)}{\partial t} = C\frac{\partial^2\Psi(x,t)}{\partial x^2} + V(x)\Psi(x,t) + g|\Psi(x,t)|^2\Psi(x,t), \tag{2.44}$$

where $C$, $V(x)$, and $g$ are allowed to take real values. However, the method remains efficient for complex values of $C$, $V(x)$, and $g$. The method consists of splitting the equation to solve into a linear and a nonlinear parts. So we rewrite (2.44) in terms of two operators as

$$\frac{\partial\Psi}{\partial t} = [\hat{D} + \hat{N}]\Psi. \tag{2.45}$$

The operator $\hat{D}$ is the linear part. In fact, the operator $\hat{D}$ contains all spatial derivative terms with respect to the linear dependent variable $\Psi$. The operator $\hat{N}$ represents the nonlinear part of the equation under study. Equation (2.45) may be split in two different parts. A linear part

$$\frac{\partial\Psi_D}{\partial t} = \hat{D}\Psi_D. \tag{2.46}$$

In the case of Eq.(2.45), we have the relation $\frac{\partial\Psi_D}{\partial t} = -\imath C\frac{\partial^2\Psi(x,t)}{\partial x^2} = \hat{D}\Psi_D$. The second part is the nonlinear one which is

$$\frac{\partial\Psi_N}{\partial t} = \hat{N}\Psi_N. \tag{2.47}$$

The form of the nonlinear operator in Eq.(2.45) is $\hat{N} = -\imath(V(x) + g|\Psi(x,t)|^2)$.

Equations (2.46) and (2.47) taken separately have analytical solutions, but Eq.(2.45) does not in general have any analytical solutions. However, taking a 'small' step in time, $dt$, then the

two parts may be treated separately with only a 'small' numerical error. Therefore, one may first take a small nonlinear step,

$$\Psi_N(x, t + dt) = \exp[-\imath(V(x) + g|\Psi|^2)dt]\Psi_N(x, t), \tag{2.48}$$

which is the analytical solution of Eq.(2.47) at time $t + dt$, starting from a known solution at time $t$. The analytical solution of Eq.(2.48) is first computed in the frequency domain such that one first applies a Fourier transform

$$\tilde{\Psi}_D(\omega, t) = \int_{-\infty}^{+\infty} \Psi_D \exp[\imath(\omega - \omega_0)dt], \tag{2.49}$$

where $\omega_0$ is the center frequency of the pulse solution. The solution of Eq.(2.46) at time $t + dt$ reads

$$\tilde{\Psi}_D(\omega, t + dt) = \exp[\imath C(\omega - \omega_0)^2 dt]\tilde{\Psi}_D(\omega, t). \tag{2.50}$$

One derives $\Psi_D(\omega, t + dt)$ by taking the inverse fourier transform of $\tilde{\Psi}_D(\omega, t + dt)$.

The formal solution of Eq.(2.45) is written as

$$\Psi(x, t) = \exp[\imath(\hat{D} + \hat{N})t]\Psi(x, 0). \tag{2.51}$$

The operators $\hat{D}$ and $\hat{N}$ do not commute in general. Applying the Baker-Hausdorff formula up to the second order for a small step $dt$, Eq.(2.51) becomes

$$\Psi(x, t + dt) \approx \exp(\imath\hat{D}dt) \exp(\imath\hat{N})dt)\Psi(x, t). \tag{2.52}$$

One should notice that the operator $\hat{D}$ is always computed in the frequency domain, while $\hat{N}$ may be computed in the real physical space at time $t$. To advance the solution in time to a step $dt$, one first computes the Fourier transform of $\exp(\imath\hat{N})dt\Psi(x, t)$, then calculates the product involving $\hat{D}$ and $\hat{N}$ in the frequency domain, applies the inverse fourier transform in order to come back to the real physical space. The algorithm of the method is the following

$$\Psi(x, t + dt) = F^{-1}[\exp -\imath dt\omega F[\exp(\imath\hat{N})\Psi(x, t)]]. \tag{2.53}$$

The Fourier transform of the dispersion part may be computed with the fast Fourier transform algorithm. This allows the split-step Fourier method to be faster than finite difference methods. The split-step Fourier method is accurate to the second order of the step size $dt$. There are modifications of the split-step Fourier method that may be used to improve the accuracy such as the symmetrized split-step Fourier method [55].

### 2.6.3 The fourth order Runge-Kutta in the interaction picture method

The fourth order Runge-Kutta in the interaction picture method [54] is a numerical scheme used for nonlinear partial differential equations that combines the fourth order Runge-Kutta method with the Fourier method [54]. The solution is advanced in time with the fourth order

Runge-Kutta method, with all spatial derivatives computed in the frequency domain by the Fourier transform of derivatives.

The fourth order Runge-Kutta method is a numerical method appropriate for ordinary differential equations [54, 55]. Let us consider the following ordinary differential equation

$$\frac{du(x,t)}{dt} = A(u(x,t),x,t). \tag{2.54}$$

Equation (2.54) is associated with the initial condition $u(x,0)$. The algorithm of the fourth order Runge-Kutta scheme is

$$\begin{aligned} u(x,t+dt) &= u(x,t) + [L_1 + 2L_2 + 2L_3 + L_4]/6, \\ L_1 &= A(u(x,t),x,t)dt, \\ L_2 &= A(u(x,t) + L_1/2, x, t + dt/2)dt, \\ L_3 &= A(u(x,t) + L_2/2, x, t + dt/2)dt, \\ L_4 &= A(u(x,t) + L_3, x, t + dt)dt. \end{aligned} \tag{2.55}$$

The implementation of the fourth order Runge-Kutta scheme is straightforward. In order to set the fourth order Runge-Kutta scheme for partial differential equations, one has to find a way of evaluating the spatial derivatives by numerical means. The fast Fourier transform algorithm is a very fast means of calculating spatial derivatives and is accurate for machine precision. The Fourier transform of a derivative $\Psi^{(n)}(x)$ is $F[\Psi^{(n)}(x)] = (\imath\omega)^n\psi(\omega)$.

The algorithm of the fourth order Runge-Kutta in the interaction picture method for nonlinear partial differential equations of types $\frac{\partial\Psi}{\partial t} = (\hat{D} + \hat{G})\Psi$, is

$$\begin{aligned} \Psi^I \leftarrow &= \hat{D}(\Psi), \\ L_1 \leftarrow &= \hat{D}[\hat{G}(\Psi,t)], \\ t \leftarrow &= t + dt/2, \\ L_2 \leftarrow &= [\hat{G}(\Psi + L_1/2, t)], \\ L_3 \leftarrow &= [\hat{G}(\Psi + L_2/2, t)], \\ t \leftarrow &= t + dt/2, \\ L_4 \leftarrow &= \hat{G}[\hat{D}(\Psi^I + L_3, t)], \\ \Psi \leftarrow &= \hat{D}\Psi^I + [L_1 + 2(L_2 + L_3)]/6 + L_4/6. \end{aligned} \tag{2.56}$$

The operator $\hat{D}$ is the differential operator part of the nonlinear partial differential equation under study, while the operator $\hat{G}$ is the normal part of the nonlinear partial differential equation and may contain nonlinear terms.

The basic algorithm for the fourth order Runge-Kutta in the interaction picture method has been developed by Ballagh and coworkers in [54] where a detail description of the method can be found. The fourth order Runge-Kutta in the interaction picture method has a certain

number of advantages which are: fourth order in step size, stable, relatively few fast fourier transforms, relatively low memory consumption. The fourth order Runge-Kutta in the interaction picture method applies only to nonlinear partial differential equations with diagonal dispersion operators $\hat{D}$.

### 2.6.4 The PDEPE MATLAB toolbox

PDEPE is the MATLAB toolbox for the numerical integration of initial-boundary value problems for systems of parabolic and elliptic partial differential equations in the one space variable and time. PDEPE solves partial differential equations of the form

$$C(x,t,u,u_x)u_t = x^{-m}\frac{\partial}{\partial x}\left[x^m F(x,t,u,u_x)\right] + S(x,t,u,u_x), \tag{2.57}$$

in which the time and space variables lie the regions $t_0 \leq t \leq t_f$ and $a \leq x \leq b$ ($a$ and $b$ being finite real numbers), respectively. In Eq.(2.57), $F$ is the flux term, $S$ the source term, and the parameter $m = 0$, corresponding to a slab symmetry, i.e., to no symmetry (neither cylindrical nor spherical). The initial condition for all $t = t_0$ is $u(x,t_0) = u_0(x_0)$. For all $t$ and either $x = a$ or $x = b$, the solution satisfies boundary conditions of the form

$$p(x,t,u) + q(x,t)f(x,t,u,u_x) = 0, \tag{2.58}$$

where elements of $q$ are either identically zero or never zero. The PDEPE toolbox does not admit neither complex numbers nor complex variables. If one wants to solve a nonlinear partial differential equation where the dependent variable or the coefficients are complex numbers, the first step is to express the dependent variable as the sum of the real and imaginary parts as $u = u_R + \imath u_I$. Taking this in consideration gives rise to a coupled system of equations for Eqs.(2.57)-(2.58), and for the initial condition.

The PDEPE toolbox uses a time step adaptive Runge-Kutta Feldberg algorithm. PDEPE has many options and may be used to solve many types of partial differential equations. A detail of what can be done with PDEPE can be found in the MATLAB help for PDEPE.

## 2.7 Conclusion

In this chapter, we have presented some analytical and numerical methods used in the study of the dynamics of Bose-Einstein condensates. Among the analytical methods described are the variational approach, the modified lens-type transformation, the linear stability analysis, and the F-expansion method. We have shown that the variational approach allows to construct approximate analytical solutions of partial differential equations such as the GPE, and if combined with the Vakhitov-Kolokolov criterion leads to the stability criterion of solutions. It is also demonstrated that the modified lens-type transformation allows to transform the original GPE with an explicit space dependence of the trapping potential to a more tractable form in

which the spatial dependence of the external potential is hidden. The linear stability analysis presented here helps to investigate the modulational instability of plane waves. The F-expansion method is a powerful tool that may be used to construct many families of analytical solutions of nonlinear partial differential equations such as the GPE. The results obtained with the analytical methods need to be compared to exact numerical simulations of the original equations. Exact numerical solutions can be constructed by means of different numerical schemes. We have outlined some numerical methods for partial differential equations such as the normalized gradient flow with backward Euler centered finite difference scheme, the split-step Fourier method, the fourth order Runge-Kutta in the interaction picture method, and the MATLAB toolbox PDEPE.

In the following, we will apply the latter methods in order to elucidate some important effects like the influence of the quantum fluctuations around the mean field, the nonlinear delayed response of the condensates have on the dynamics of solitons in condensates.

# Chapter 3

# Results and Discussion

## 3.1 Introduction

The phenomenon of Bose-Einstein condensation provides unique opportunities to test fundamental quantum theories, and to study many quantum properties of matter waves. For example, Bose-Einstein condensates can be used for the dramatic slowing down of a light pulse [118] in view of storage of coherent optical information with application to quantum information processing [119]. Recently, a condensate made of photons has been realized [120]. It is believed that the possibility of producing photon Bose-Einstein condensates could help further shrink of electronic devices. In 2011, an experience proved the possibility (in term of precise control) of starting and stopping at will, the rotation of the superfluid state in a toroidal sodium condensate medium [121]. The frictionless rotating quantum matter wave actually simulates the role of electrons (Cooper pairs) in superconductivity, and thus opens the door for possible utilization of condensates as essential circuit elements for future means to afford the efficient transformation and transmission of energy. Bose-Einstein condensed gases in optical lattices are also claimed to be good candidates in the route to quantum computers [122, 123, 124, 125]. Condensates provide an unprecedent opportunity to study properties of collective excitations of quantum matter in a macroscopic scale. Further, coherent structures in condensates are good candidates for many applications such as matter-wave transport, atomic number squeezing, atomic chips made of condensates, creation of coherent matter-wave structures and so on. Solitons can be created in condensates [10, 11, 12, 27, 95] and are an active field of research [49, 126, 127, 128, 129, 130].

In this chapter, we investigate the stability of solitons of single and binary Bose-Einstein condensates with two- and or three-body interatomic interactions modulated in time. In Sect. I, by means of the variational approach, we analyze the stability of bright solitons in single condensates loaded in linear optical lattices. Then, the structure dynamics of bright solitons in single and binary condensates are studied in detail via the modulational instability process in Sect. II. Effects of some important physical aspects like quantum fluctuations, the three-body interatomic interactions, on the stability of condensate are examined. Approximate analytical

solutions of single condensates with time-variations of the two- and three-body interatomic interactions, confined in a time-dependent complex potential are constructed in Sec. III.

## 3.2 Stability of matter-wave condensates in optical lattices

### 3.2.1 Model and analytical results

In this section, we study the stability of bright solitons of the one dimensional cubic GPE with a variable anharmonic nonsinusoidal optical lattice of the form [131, 132, 133]

$$\begin{aligned} V(x) &= V_0[1+s-(1-s^2)(\cos(2kx)+s\cos(4kx)+...+s^{n-1}\cos(n2kx))] \\ &= V_0[1+s-(1-s^2)\sum_{n=1} s^{n-1}\cos(n2kx)]. \end{aligned} \tag{3.1}$$

This particular potential presents a number of advantages for analysis. First, its shape may be scaled by the parameter $s$, with $-1 < s < 1$, while the maximum amplitude remains constant at $2V_0$. Second, for $s > 0$, the nonsinusoidal potential has the shape of sharp wells separated by flat wide barriers (see Fig. 6(a), for $s = 0.8$, $s = 0.5$, $s = 0.3$), the potential reduces to the familiar sine-wave potential through a continuous variation when the parameter s goes to zero (see Fig. 6(b), for $s = 0$), while for $s < 0$, it has flat bottoms separated by thin barriers (see Fig. 6(c), for $s = -0.8$, $s = -0.5$, $s = -0.3$). The parameter $k$ in this case is the wave number of the optical lattice.

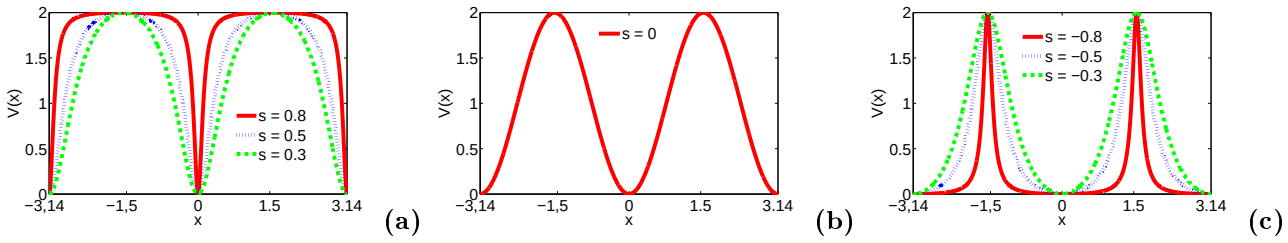


**Figure 6**: Deformability of the periodic potential, Eq.(3.1), with respect to the shape parameter for (a) $s = 0.8$ (solid line), $s = 0.5$ (dotted line), $s = 0.3$ (dash-dotted line); (b) $s = 0$. (c) $s = -0.8$ (solid line), $s = -0.5$ (dotted line), $s = -0.3$ (dash-dotted line), with $V_0 = 1$ and $k = 1$.

We consider the one dimensional cubic dimensionless GPE with the external potential of Eq.(3.1)

$$\imath\frac{\partial\psi(x,t)}{\partial t} = [-\frac{1}{2}\frac{\partial^2}{\partial x^2} + V(x) + g_{1D}|\psi(x,t)|^2]\psi(x,t). \tag{3.2}$$

In Eq.(3.2), $g_{1D}$ is the strength in one dimension of the cubic nonlinearity related to the s-wave scattering length $a_s$ through $g_{1D} = 2\frac{|a_s|}{a_0}$. Here $a_0 = \sqrt{\frac{\hbar}{m\omega_\perp}}$ is the transverse harmonic oscillator length, while $\omega_\perp$ represents the harmonic oscillator in the transverse directions. Equation (3.2) is obtained by introducing the rescaled variables $x \leftarrow kx$, $t \leftarrow (\hbar k^2/2m)t$, $V_0 \leftarrow V_0(\hbar^2k^2/2m)$,

$\psi \leftarrow \psi/\sqrt{n_0}$, where $n_0$ is the density of the condensate, then the dimensional reduction is done as in [134].

We focus our attention to stationary solutions of Eq.(3.2), to this end, we follow the standard procedure and introduce a chemical potential $\mu$ to account for nonlinearity-induced phase shift of the stationary solutions. Assuming that $\psi(x,t) = \phi(x)\exp(-\imath\mu t)$, Eq.(3.2) becomes

$$[-\frac{1}{2}\frac{\partial^2}{\partial x^2}+V_0[1+s-(1-s^2)(\cos(2kx)+s\cos(4kx)+...+s^{n-1}\cos(n2kx))]+g_{1D}|\phi|^2]\phi(x,t) = \mu\phi(x,t). \tag{3.3}$$

In order to derive the stability criterion of stationary bright soliton solutions of Eq.(3.3), we resort the variational approach presented in the former chapter and choose the following ansatz

$$\phi = A(t)\exp[-\frac{x^2}{2W^2(t)} + \imath(\phi(t) + \frac{b(t)x^2}{2})]. \tag{3.4}$$

The effective Lagrangian is

$$L_{1D} = N_{1D}[-\dot{\phi}-\frac{1}{4}\frac{1}{W^2}-\frac{1}{4}W^2(\dot{b}+b^2)-\frac{1}{2\sqrt{2}}A^2g_{1D}-V_0[1+s-(1-s^2)\sum_{n=1}s^{n-1}\exp(-n^2k^2W^2)]]. \tag{3.5}$$

Using the Euler-Lagrange equations, we derive the variational equations [133]

$$\begin{aligned}
&N_{1D} = A^2\sqrt{\pi}W,\\
&\frac{g_{1D}N_{1D}}{\sqrt{2\pi}} = 4V_0(1-s^2)k^2W^3\sum_{n=1}s^{n-1}n^2\exp(-n^2k^2W^2) - \frac{1}{W},\\
&\dot{\phi} = -\mu_{1D} = -[\frac{g_{1D}N_{1D}}{\sqrt{2\pi}W} + \frac{1}{4W^2} + V_0[1+s-(1-s^2)\sum_{n=1}s^{n-1}\exp(-n^2k^2W^2)]].
\end{aligned} \tag{3.6}$$

A noteworthy property of the last equation of the set (3.6) is that there exists a minimal norm $N_{1Dmin}$, that depends on the value of the shape parameter $s$, for a given strength $V_0$ of the linear optical lattice. The value of W, $W_{min}$, that minimizes the norm is obtained by solving the following implicit equation

$$4V_0k^2(1-s^2)W^4\sum_{n=1}s^{n-1}n^2(3-2k^2n^2W^2)\exp(-n^2k^2W^2)+1 = 0. \tag{3.7}$$

Considering the second equation of the set (3.6), a stationary solution exists provided that the norm $N_{1D}$ is positive; for a fixed value of the shape parameter $s$, we determine the critical strength of the linear optical lattice as

$$V_{0crit} = \frac{1}{4k^2W_{min}^4(1-s^2)\sum_{n=1}s^{n-1}n^2\exp(-n^2k^2W_{min}^2)}. \tag{3.8}$$

In fact, for too large or too small values of the shape parameter $s$, if $V_0 < V_{0crit}$, there is one localized state and if $V_{0crit} < V_0$, there are three localized states, one unstable and two stable, some of them present a gap region where there is no solution as $V_0$ increases ($V_{0crit} < V_0$).

For all other values of the shape parameter $s$, if $V_0 < V_{0crit}$, there are three localized states, one unstable and two stable, and for $V_{0crit} < V_0$, there are three localized states with a gap region where the solution does not exist. This gap region gradually increases with $V_0$ (in the case $V_{0crit} < V_0$). We display in Fig. 7 the variation of the number of atoms $N_{1D}$ as a function of the width $W$ for fixed values of the shape parameter $s$.

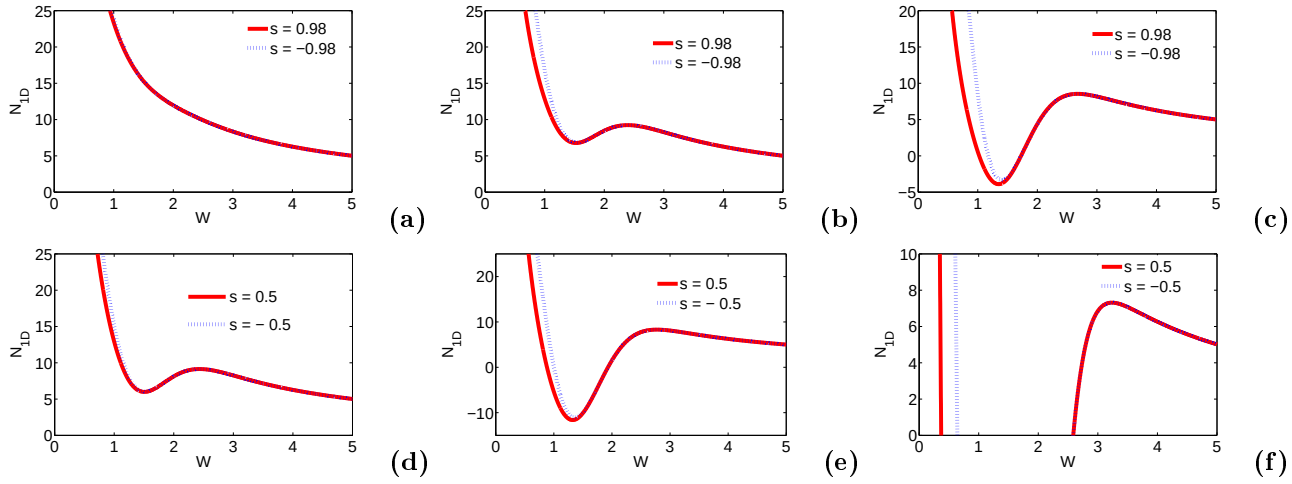


**Figure 7**: (a) $V_{0crit} = 3.5 > V_0 = 1$, stable soliton for very large or small widths. (b) $V_0 = 7 > V_{0crit} = 3.5$, 2 stable and one unstable regions. (c) $V_0 = 14$. (d)-(f) $V_0 = 0.4 < V_{0crit} = 0.62$, medium values of $s$. (d) if $V_0 < V_{0crit}$ 2 stable and one unstable regions. (e) $V_0 > V_{0crit}$, 2 stable and one unstable regions, and a gap region with no soliton. The width of the gap region enlarges with $V_0$ as in (f). Other parameters are $g_{1D} = -0.1$, $k = 1$.

From the second equation of the set (3.6), it is expected that the branches of $N_{1D}(W)$ with negative slopes are stable, i.e., $W < W_{min}$, has negative slopes and therefore are stable. The other branches ($W > W_{min}$) appear to be unstable [11] (Sakaguchi and Malomed). More precisely, for $s = \pm 0.98$, when $V_0 < V_{0crit} \approx 3.5$, $V_0 = 1$ (see Fig. 7(a)), there is one localized state that is stable, and when $V_{0crit} < V_0$, there are three localized states: with $V_0 = 7$ (see Fig. 7(b)), two branches of solution are stable ($W < 1.53$ and $W > 2.29$) and one is unstable ($1.53 < W < 2.29$); with $V_0 = 14$ (see Fig. 7(c)), there are three localized states with a gap region. For $s = 0.98$ (see Fig. 7(c)), one branch of solution is unstable ($1.71 < W < 2.56$) and two branches are stable ($W < 1.03$ and $W > 2.56$). For $s = -0.98$ (see Fig. 7(c)), one branch of solution is unstable ($1.18 < W < 2.56$) and two branches are stable ($W < 1.18$ and $W > 2.56$). Considering intermediate values of $s$, there are always three localized states with a gap region increasing with $V_0$ as one can see in Figs. 7(d)-(f) where $s = \pm 0.5$. For $V_0 < V_{0crit} \approx 0.62$, there are three localized states; with $V_0 = 0.4$ (see Fig. 7(d)), the branch of solution with $1.51 < W < 2.4$ is unstable, while the others ($W < 1.51$ and $W > 2.4$) are stable; when $V_{0crit} < V_0$, there are three localized states: $s = 0.5$, with $V_0 = 1$, (see Fig. 7(e)), the branch of solution with $1.93 < W < 2.68$ is unstable, while the others ($W < 0.87$ and $W > 2.68$) are stable; with $V_0 = 6$, (see Fig. 7(f)), the branch of solution with $2.58 < W < 3.12$ is unstable,

while the others ($W < 0.36$ and $W > 3.12$) are stable; $s = -0.5$, with $V_0 = 1$ (see Fig. 7(e)), the branch of solution with $1.93 < W < 2.68$ is unstable, while the others ($W < 1$ and $W > 2.68$) are stable; with $V_0 = 6$, (see Fig. 7(f)), the branch of solution with $2.58 < W < 3.12$ is unstable, while the others ($W < 0.63$ and $W > 3.12$) are stable.

An additional evidence for the existence of solitons can be obtained from the second equation of the set (3.6) which can be considered as describing the motion of a unit-mass particle with the coordinate $W(t)$ in the effective potential

$$U(W) = \frac{1}{2W^2} + \frac{g_{1D}N_{1D}}{\sqrt{2\pi}W} + 2V_0(1-s^2)\sum_{n=1} s^{n-1}\exp(-n^2k^2W^2). \tag{3.9}$$

Now, we discuss the effective potential structures of the attractive condensate. Figure 3 shows some results for different values of the shape parameter $s$, with the values of $V_0$, $k$, $g_{1D}$, and $N_{1D}$ fixed. Solitons in the attractive condensate exist if the effective potential (Eq.(3.9)) possesses a local minimum. In particular, for $V_0 = 1$, $k = 1$ and $g_{1D} = -0.1$, the effective potential (see Fig. 8) possesses a local minimum both for $s < 0$ (Fig. 8(a)) and for $s > 0$ (Figs. 8(b)-(c)). One also realizes in Fig. 8(a) where $s < 0$ that with the increase of the shape parameter $s$, the effective potential wells' depths gradually reduce. This means that small negative $s$ more stabilized the system that larger ones. Regarding the shape of the linear linear optical lattice in Fig. 6(c), the stabilization of a soliton requires a more confining external potential.

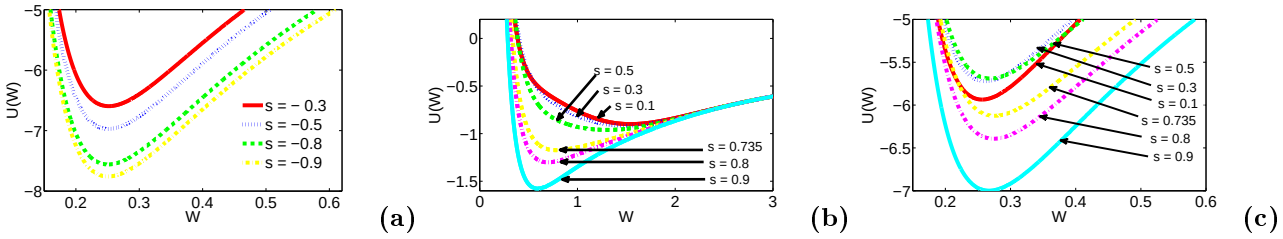


**Figure 8**: Effective potential versus width. (a) ($s < 0$), $N_{1D} = 100$. (b) ($s > 0$), $N_{1D} = 50$. (c) ($s > 0$), $N_{1D} = 100$. Small negative $s$ more stabilize the soliton. For $s > 0$, if $s \geq 0.735$ and $N_{1D} \leq 70$, the stability of the soliton increases with increasing values of $s$. For $s < 0.735$ and $N_{1D} > 70$, the stability increases with decreasing values of $s$. Other parameters are $g_{1D} = -0.1$, $k = 1$, $V_0 = 1$.

Things are slightly different in the case where $s > 0$. For medium values of $N_{1D}$ ($N_{1D}$ lower or around $\approx 70$), with the decrease of the value of the shape parameter $s$, the effective potential wells' depths gradually reduce (see Fig. 8(b)). Hence, for medium values of the number of atoms $N_{1D}$, large values of the shape parameter $s$ increase the stability of the system. But, as well as the number of atoms $N_{1D}$ becomes large ($N_{1D} \geq 100$), for $s < 0.735$, with the increase of the shape parameter $s$, the effective potential wells' depths gradually reduce, while for $s \geq 0.735$, with the decrease of the shape parameter $s$, the effective potential wells' depths gradually reduce (see Fig. 8(b)). For positive values of $s$, the stability of bright solitons is sensitive to the number of atoms in the condensate. The results obtained in Fig. 3 are in good agreement with those of

Fig. 7. From the above stability analysis, there are two important features of the linear optical lattice that can be used to stabilize the system: the shape parameter $s$, and the strength of the linear optical lattice $V_0$. These parameters can be controlled externally in current condensate experiments.

The above stability analysis does not include the dependence $\mu(N)$. Although $\mu$ is not a directly observable quantity, these dependences are important too. According to the Vakhitov-Kolokolov criterion, solutions families which meet the condition

$$\frac{d\mu_{1D}}{dN_{1D}} = \frac{g_{1D}}{\sqrt{2\pi}W} < 0, \tag{3.10}$$

may be stable, while the others with $\frac{d\mu_{1D}}{dN_{1D}} > 0$ should be unstable. From, the Vakhitov-Kolokolov criterion of Eq.(3.10), all solutions are stable.

### 3.2.2 Numerical simulations

We test the predictions obtained with the variational approach by comparisons with the exact numerical solution of Eq.(3.2). The numerical scheme used is the normalized gradient flow with backward Euler centered finite difference with imaginary time propagation [53]. A key point is the use of absorption on the boundaries of the spatial domain of integration. In our study, the spatial grid is $x = [-24, 24]$ with 512 points, and a time step $\Delta t = 0.0027$. A small amount of random white noise is inserted in order to detect any instability that may be seeded in a solution. We insert into Eq.(3.2) the solution given by Eq.(3.4) at initial time $t = 0$. Presented in Fig. 9(a) ($s = 0.98$) and Fig. 9(b) ($s = -0.98$) are the spatiotemporal evolutions of the wavefunction for parameters corresponding to those in Fig. 7(a). The initial condition

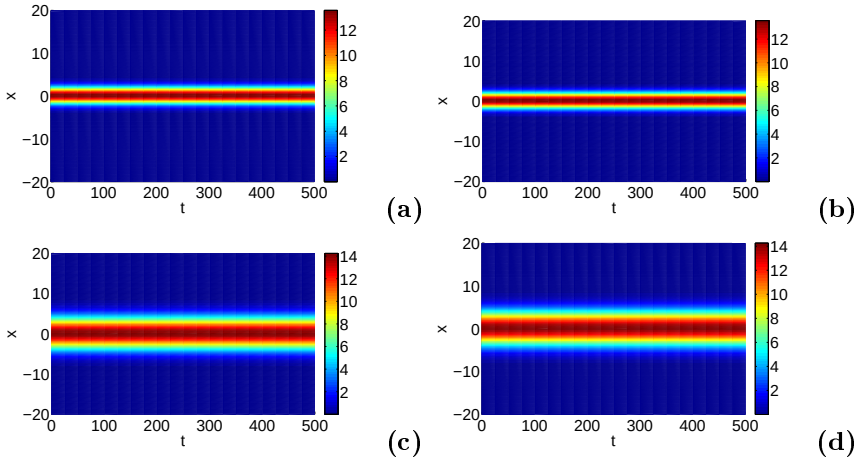


**Figure 9**: Spatiotemporal evolution of stable solitons. (a) $s = 0.98$, $W = 2$, $N_{1D} = 11.95$, $V_0 = 1$. (b) $s = -0.98$, $W = 2$, $N_{1D} = 11.95$, $V_0 = 1$. (c) $s = 0.5$, $W = 4$, $N_{1D} = 6.26$, $V_0 = 0.4$. (d) $s = -0.5$, $W = 4$, $N_{1D} = 2.26$, $V_0 = 0.4$. In all panels $g_{1D} = -0.1$.

evolves with time without any dispersion nor disintegration; it maintains its shape and lasts

longer. We can then say that the exact numerical solutions of Figs. 9(a)-(b) are linearly and dynamically stable. These results are in full agreement with the prediction of the variational approach. We also display in Fig. 9(c) ($s = 0.5$) and Fig. 9(d) ($s = -0.5$) the numerical solutions for parameters chosen as in Fig. 7(d) with $W = 4$, $N_{1D} = 6.26$ that correspond to the second stable region. Once again, the agreement between the variational approach and the exact numerical solutions is quite good.

## 3.3 Modulational instability of single and binary Bose-Einstein condensates

### 3.3.1 Modulational instability of Bose-Einstein condensates beyond the Fermi pseudopotential

**(a). Theoretical Model and linear stability analysis**

Only a few works have studied the modulational instability of condensates beyond the mean-field picture [135]. In order to investigate effects of the quantum fluctuations and the complex potential [136] on the modulational instability in condensates, our starting point is the modified three-dimensional GPE introduced by Fu *et al.* [137]

$$\begin{aligned} \imath\hbar\frac{\partial\bar{\psi}(\bar{x},\bar{y},\bar{z},\bar{t})}{\partial\bar{t}} &= -\frac{\hbar^2}{2m}\nabla^2\bar{\psi}(\bar{x},\bar{y},\bar{z},\bar{t}) + V(\bar{x},\bar{y},\bar{z})\bar{\psi}(\bar{x},\bar{y},\bar{z},\bar{t}) \\ &+g|\bar{\psi}(\bar{x},\bar{y},\bar{z},\bar{t})|^2\bar{\psi}(\bar{x},\bar{y},\bar{z},\bar{t}) + g_1|\bar{\psi}(\bar{x},\bar{y},\bar{z},\bar{t})|^3\bar{\psi}(\bar{x},\bar{y},\bar{z},\bar{t}) \\ &+ g_2\nabla^2(|\bar{\psi}(\bar{x},\bar{y},\bar{z},\bar{t})|^2)\bar{\psi}(\bar{x},\bar{y},\bar{z},\bar{t}), \end{aligned} \tag{3.11}$$

where $g = \frac{4\pi\hbar^2 a_s}{m}$, m being the mass of atoms. The fourth term on the right-hand side of Eq.(3.11) represents the inclusion of quantum fluctuations with $g_1 = g\frac{32}{3\sqrt{\pi}}a_s^{\frac{3}{2}}$ and the last term accounts for the shape-dependent confinement correction on the interaction potential with $g_2 = \frac{2}{3}a_s^2 g$. The external potential is [138]

$$\begin{aligned} V(\bar{x},\bar{y},\bar{z},\bar{t}) &= \frac{1}{2}m(\omega_{\bar{x}}^2\alpha_1^2(\bar{t})\bar{x}^2 + \omega_{\bar{y}}^2\alpha_2^2(\bar{t})\bar{y}^2 + \omega_{\bar{z}}^2\alpha_3^2(\bar{t})\bar{z}^2) \\ &+\frac{1}{2}\omega\sqrt{m\hbar\omega}(\lambda_1(\bar{t})\bar{x} + \lambda_2(\bar{t})\bar{y} + \lambda_3(\bar{t})\bar{z}) + \frac{\imath\hbar\omega}{2}\gamma(\bar{t}), \end{aligned} \tag{3.12}$$

where $\alpha_1(\bar{t})$, $\alpha_2(\bar{t})$, $\alpha_3(\bar{t})$ represent the strengths of the parabolic background; $\lambda_1(\bar{t}), \lambda_2(\bar{t}), \lambda_3(\bar{t})$ characterize the Earth's gravitational field or some linear potentials, and $\omega_{\bar{x}} \equiv \alpha_1(\bar{t})\omega$, $\omega_{\bar{y}} \equiv \alpha_2(\bar{t})\omega$, $\omega_{\bar{z}} \equiv \alpha_3(\bar{t})\omega$ are the angular frequencies, in the $-\bar{x}$, $-\bar{y}$, $-\bar{z}$ directions, respectively, $\omega$ being the angular frequency. The parameter related to feeding or loss of atoms is $\gamma(t)$. It is convenient to manipulate Eq.(3.12) in its dimensionless form. Thus, in terms of the dimensionless variables $x = \frac{\bar{x}}{a}$, $y = \frac{\bar{y}}{a}$, $z = \frac{\bar{z}}{a}$, $t = \frac{\omega}{2}\bar{t}$, $\bar{\psi}(x,y,z,t) \to \sqrt{\frac{2a^3}{N}}\tilde{\psi}$ ($N = \int|\psi|^2 dxdydz$ is the number

of atoms in the condensate), $a = \sqrt{\frac{\hbar}{m\omega}}$ (harmonic oscillator length), Eq.(3.11) becomes

$$\begin{aligned} \imath\frac{\partial\tilde{\psi}}{\partial t} &= [-\nabla^2 + \alpha_1^2(t)x^2 + \alpha_2^2(t)y^2 + \alpha_3^2(t)z^2 + \lambda_1(t)x + \lambda_2(t)y + \lambda_3(t)z + \imath\gamma(t) + \\ &\quad \tilde{g}|\tilde{\psi}|^2 + \tilde{g_1}|\tilde{\psi}|^3 + \tilde{g_2}\nabla^2(|\tilde{\psi}|^2)]\tilde{\psi}, \end{aligned} \tag{3.13}$$

with $\tilde{g} = 4\pi N\frac{a_s}{a}$, $\tilde{g_1} = \frac{128\sqrt{\pi}}{3\sqrt{2}}N^{\frac{3}{2}}(\frac{a_s}{a})^{\frac{5}{2}}$, and $\tilde{g_2} = \frac{8\pi N}{3}(\frac{a_s}{a})^3$. In the case where the condensate is strongly confined in the transverse directions defined here by the plane $(y, z)$, Eq.(3.13) reduces to a quasi-one dimensionless form. In order to derive the one dimensional form of Eq.(3.13), we assume that the condensate remains confined to the ground state in the transverse directions and consider the ansatz [138]

$$\tilde{\psi}(x, y, z, t) = \psi(x, t)\psi_0(y)\psi_0(z)\exp[-\imath(\alpha_2 + \alpha_3)], \tag{3.14}$$

with $\psi_0(y) = (\frac{\alpha_2}{\pi})^{\frac{1}{4}}\exp(\frac{-\alpha_2 y^2}{2})$, $\psi_0(z) = (\frac{\alpha_3}{\pi})^{\frac{1}{4}}\exp(\frac{-\alpha_3 z^2}{2})$, $\psi_0(y)$ and $\phi_0(z)$ being normalized to unity. Introducing Eq.(3.14) into Eq.(3.13), then multiplying by the left by $\psi_0(y)$ and $\psi_0(z)$ and integrating over $y$ and $z$ in space yield the dimensionless one dimensional form of Eq.(3.11)

$$\imath\frac{\partial\psi}{\partial t}(x,t) = [-\frac{\partial^2}{\partial x^2} + \alpha_1^2(t)x^2 + \lambda_1(t)x + \imath\gamma(t) + g'|\psi(x,t)|^2 + g_1'|\psi|^3 + g_2'\frac{\partial^2}{\partial x^2}(|\psi(x,t)|^2)]\psi(x,t), \tag{3.15}$$

where

$$\begin{aligned} g' &= 2N\frac{a_s}{a}\sqrt{\alpha_2\alpha_3}[1 - \frac{2}{3}(\frac{a_s}{a})^2(\alpha_2 + \alpha_3)] \\ g_1' &= \frac{128\sqrt{2}}{15\pi}N^{\frac{3}{2}}(\frac{a_s}{a})^{\frac{5}{2}}(\alpha_2\alpha_3)^{\frac{3}{4}} \\ g_2' &= \frac{4N}{3}(\frac{a_s}{a})^3\sqrt{\alpha_2\alpha_3}. \end{aligned} \tag{3.16}$$

Making the changes $\alpha_1^2(t) = \alpha(t)$ and $\lambda_1(t) = \lambda(t)$, Eq.(3.15) can be rewritten as

$$\imath\frac{\partial\psi}{\partial t}(x,t) = [-\frac{\partial^2}{\partial x^2} + \alpha(t)x^2 + \lambda(t)x + \imath\gamma(t) + g'|\psi(x,t)|^2 + g_1'|\psi(x,t)|^3 + g_2'\frac{\partial^2}{\partial x^2}(|\psi(x,t)|^2)]\psi(x,t). \tag{3.17}$$

The three-dimensional equation (3.11) is the modified GPE beyond the mean-field picture, however since we are interested in its one dimensional form, in the remainder of the work Eq.(3.17) is referred to as the modified GPE I.

Now, we examine the modulational instability of the modified GPE I. Following the method adopted in chapter 2, we use the modified lens-type transformation given by Eq.(2.11) with the constraints of Eq.(2.12) to cast Eq.(3.17) in the new rescaled variables $X$ and $T$

$$\imath\frac{\partial\Phi}{\partial T} = -\frac{\partial^2\Phi}{\partial X^2} - 2\imath k(t)\frac{\partial\Phi}{\partial X} + k^2(t)\Phi + g'(t)|\Phi|^2\Phi + g_1'(t)|\Phi|^3\Phi + g_2'(t)|\Phi|^2_{XX}\Phi, \tag{3.18}$$

with $k(t) = f(t)l(t)\sigma(t)$, $g'(t) = g'l(t)\exp(2\eta(t))$, $g_1'(t) = g_1'\sqrt{l(t)}\exp(3\eta(t))$ and $g_2'(t) = \frac{g_2'}{l(t)}\exp(2\eta(t))$.

We proceed by performing a linear stability analysis with the ansatz of Eq.(2.16) and taking into account the fact that

$$\Theta(T) = k^2(t) + \Phi_0^2[g'(t) + \Phi_0 g_1'(t)], \tag{3.19}$$

leads to the equation describing the dynamics of the perturbation

$$\imath\frac{\partial\delta\Phi}{\partial T} = -\frac{\partial^2\delta\Phi}{\partial X^2} - 2\imath k(t)\frac{\partial\Phi}{\partial X} + \Delta(t)(\delta\Phi + \delta\Phi*) + g_2'(t)\Phi_0^2(\frac{\partial\delta\Phi}{\partial X^2} + \frac{\partial\delta\Phi*}{\partial X^2}). \tag{3.20}$$

In Eq.(3.20) $\Delta(t) = \Phi_0^2[g'(t) + \frac{3}{2}g_1'(t)\Phi_0]$. Then, with the perturbation given by Eq.(2.18) we retrieve the time-dependent dispersion relation

$$\Omega^2 - 4k(t)K\Omega + 4k^2(t)K^2 - K^4\Delta'(t) - 2K^2\Delta(t) = 0. \tag{3.21}$$

The modulational instability criterion reads

$$K^2[K^2\Delta'(t) + 2\Delta(t)] < 0, \tag{3.22}$$

and the gain of modulational instability G is

$$G = |Im(\sqrt{K^2[K^2\Delta'(t) + 2\Delta(t)]})|. \tag{3.23}$$

The explicit expressions of the functions $f(t)$, $l(t)$, $T(t)$ are given by Eq.(2.14). In the case where the condensate loses atoms ($\gamma < 0$), the modulational instability growth rate increases with increasing $\gamma$, for a fixed value of $\alpha$. This means that the atoms loss enhances the modulational instability of the condensate. One can see this behavior in Figs. 10(a)-(b) where the modulational instability growth rate is plotted as a function of the wave number $K$, for three negative values of $\gamma$. In Fig. 10(a) we realize that the gain increases as $\gamma$ increases. Furthermore, for small enough values of $\gamma$, the amplitude of the gain of the modulational instability globally decreases with time as shown in Fig. 10(b). But, for large enough values of $\gamma$, our model, as it will be shown below, fails to fit the numerical results and the modulational instability growth rate is deeply affected by the atoms loss.

In the case where the condensate gains atoms ($\gamma > 0$), the feeding of atoms enhances the loss of stability of the condensate. This behavior is depicted in Fig. 10(c) where the gain of instability is drawn as a function of the wave number $K$, for three different values of $\gamma$, and $\alpha$ being fixed. The gain increases with increasing values of $\gamma$. A comparison of Figs. 10(a)-(b) and Fig. 10(c) shows that the amplitude of the gain is larger for a condensate in the feeding regime than when the condensate loses atoms. This implies that adding atoms to the condensate enhances the instability than removing atoms from the condensate.

**(b). Numerical simulations of the modified GPE I**

In order to confirm our previous analytical results, we integrate numerically the full modified GPE I with the split-step Fourier method. The initial condition is

$$\psi(x,0) = \phi_{TF}[\Phi_0 + \varepsilon\cos(Kx)], \tag{3.24}$$

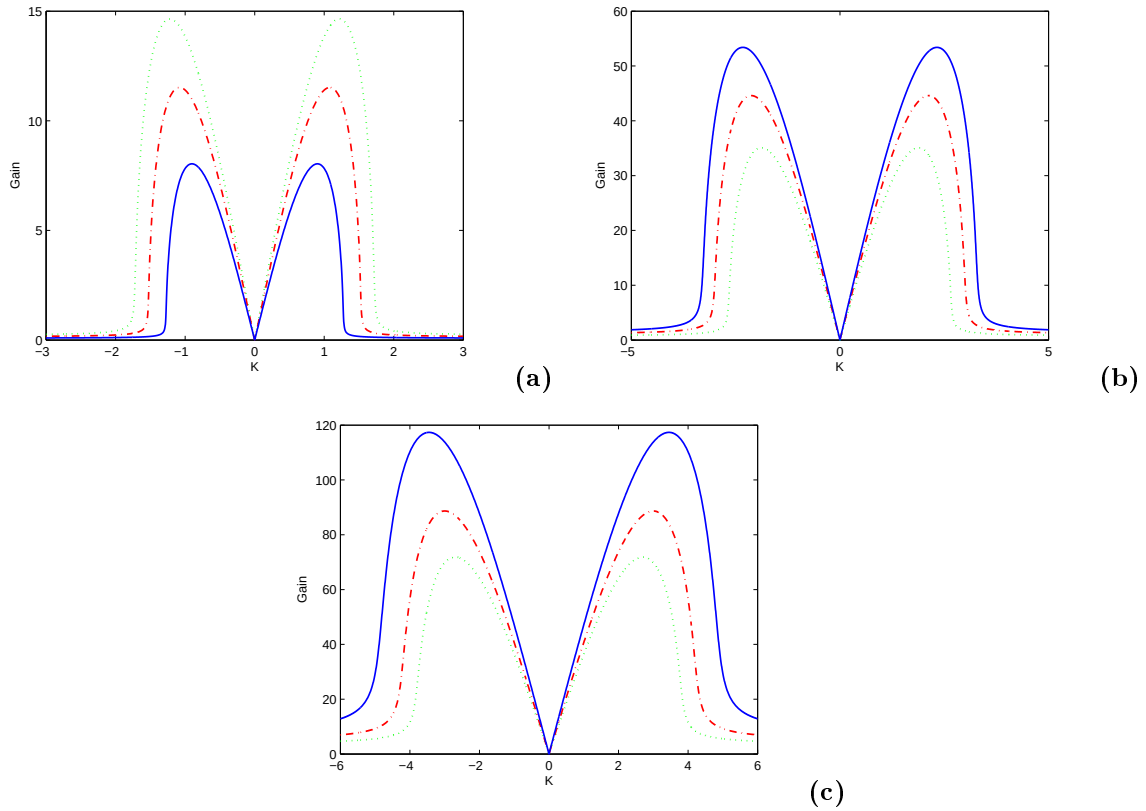


**Figure 10**: Gain of instability versus $K$. (a) $\alpha = 0.00001$ (weak confinement) for small values of $\gamma$, $\gamma = -0.01$ dotted line, $\gamma = -0.012$ dash-dotted line, $\gamma = -0.015$ solid line, $N = 5$, $\Phi_0 = 10$, $t = 60$. (b) $\alpha = 0.001$ (strong confinement), $\gamma = -0.019$ dotted line, $\gamma = -0.015$ dash-dotted line, $\gamma = -0.012$ solid line, $N = 20$, $\Phi_0 = 40$, $t = 30$. (c) $\alpha = 0.001$ (strong confinement), $\gamma = 0.008$ solid line, $\gamma = 0.004$ dash-dotted line, $\gamma = 0.001$ dotted line, $\Phi_0 = 40$, $N = 20$, $t = 35$. Other parameters are $a_s = -2.75$ nm, $a = 1.576.10^3$ nm.

where $\phi_{TF} \simeq 1 - \frac{1}{2}\alpha x^2$ is the background wavefunction in the Thomas-Fermi approximation [108, 128, 131].

The detection of the occurrence of instability may be done by investigating the maxima amplitude of the initial plane wave. We first emphasize on the impact of the exchange of atoms, thus we turn off the linear potential ($\lambda = 0$). Let us first consider the case where the condensate loses atoms. Figure 6 (parameters correspond to those in Figs. 5) represents temporal evolutions of the maxima amplitude, $Max_x|\psi(x,t)|^2$, for three different values of $\gamma$. In Fig. 11(a), the density of the condensate increases with $\gamma$ but, globally reduces with time increasing. The amplitude of the condensate first gradually varies and then starts oscillating at random, thus giving an account of instability. This result is in good agreement with the analytical predictions. The modulational instability sets in at a critical time $t_C = 18$. For large enough values of $\gamma$, Fig. 11(b) shows that the density of the condensate increases with increasing values of $\gamma$. A result that does not corroborate its theoretical counterpart, as mentioned above. Thus, the linear stability analysis is not sufficient for the description of the modulational instability growth rate

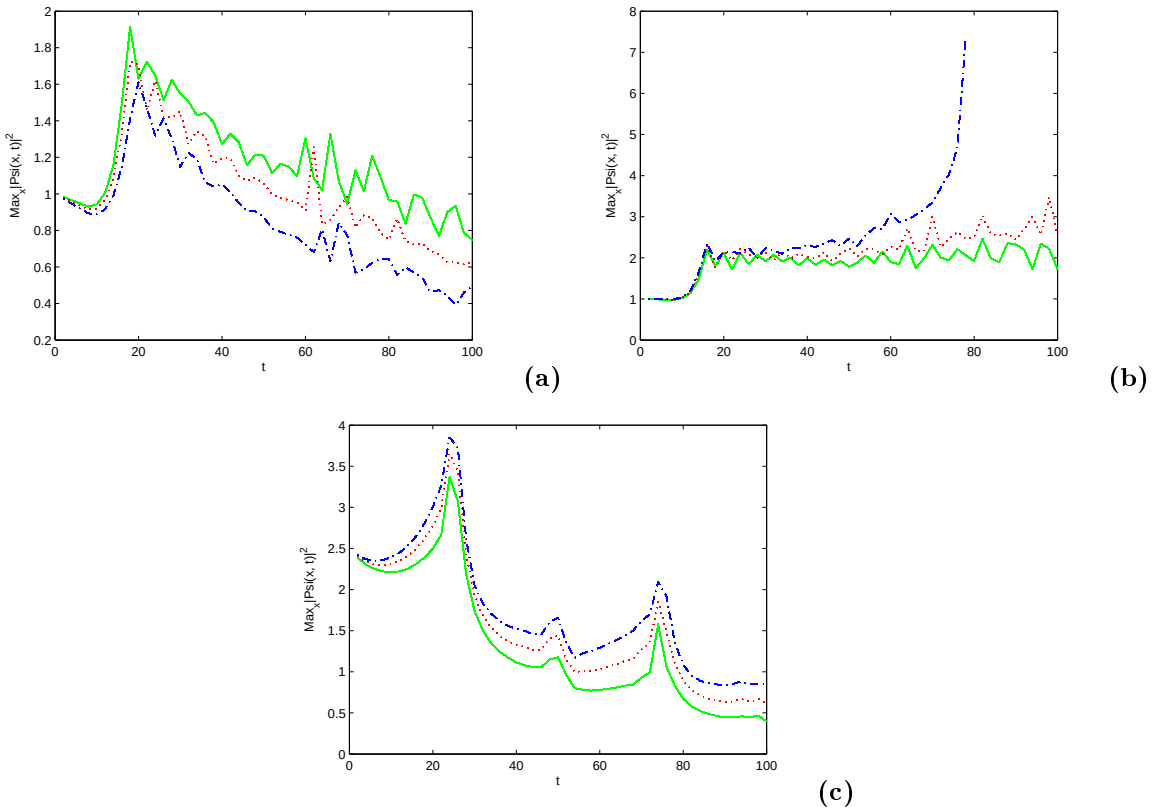


**Figure 11**: Temporal evolution of the maxima amplitude $Max_x|\psi(x,t)|^2$ for three different values of $\gamma$, when the condensate loses atoms. (a) $\alpha = 0.00001$ (small values of $\gamma$) $\gamma = -0.01$ solid line, $\gamma = -0.012$ dotted line, $\gamma = -0.015$ dash-dotted line, $N = 5$. (b) $\alpha = 0.00001$ (large enough values of $\gamma$) $\gamma = -0.004$ solid line, $\gamma = -0.003$ dotted line, $\gamma = -0.002$ dash-dotted line, $N = 5$. (c) $\alpha = 0.001$, $\gamma = -0.019$ solid line, $\gamma = -0.015$ dotted line, $\gamma = -0.012$ dash-dotted line, $N = 20$. Other parameters are $\lambda = 0$, $a_s = -2.75$ nm, $a = 1.576.10^3$ nm, $K = 1.5$, $\varepsilon = 0.001$.

for larger values of $\gamma$. For a too large value of $\gamma$, the generated pulses are destroyed after a shorter time of propagation. This means that for too large values of the parameter characterizing the loss of atoms, the generated solitons will propagate with shorter lifetimes. Hence, one may infer from Fig. 11(b) that the atoms loss does not reduce the number of atoms in the condensate for too large values of $\gamma$. This may be due to the fact that quantum fluctuations are more important since in the absence of quantum fluctuations, it was proved in [139] that the amplitude of the condensate reduces with time when the condensate loses atoms. Moreover, Fig. 8(b) proves that the instability sets in at a critical time $t_C = 16$, while for too large values of $\gamma$, $t_C = 18$ in Fig. 11(a), confirming that the increase of $\gamma$ enhances the loss of stability. When the strength of the external potential is strong, the condensate is compressed at the beginning of the propagation, then, after a gradual variation, the maximal amplitude starts oscillating randomly and globally decreases with time. Figure 11(c) depicts this behavior that is in good accordance with the analytical study. In order to investigate the dynamics of the condensate, one should plot the spatiotemporal evolution of the original wavefunction given by Eq.(3.17). As assumed in the

theoretical study, the initial plane wave transforms into a train of solitons. Figures 12(a)-(b) display some samples of trains of pulses. However, the magnitude of the pulses globally decreases

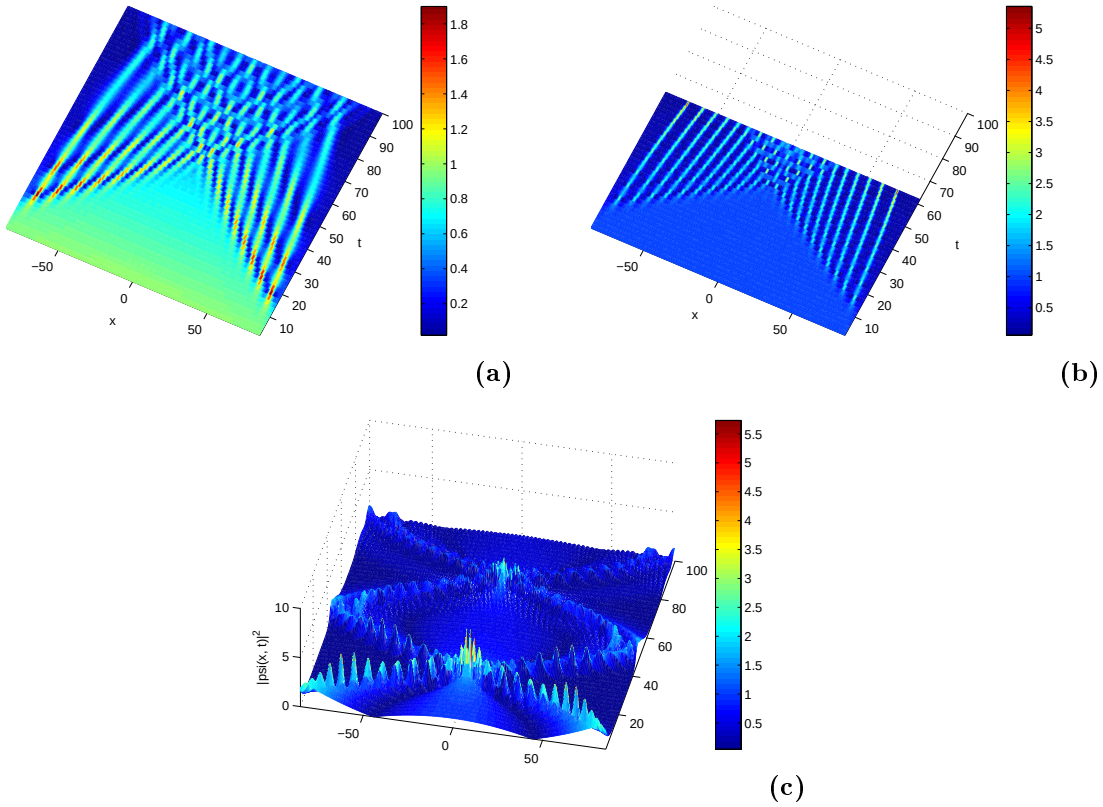


**Figure 12**: Spatiotemporal evolution of modulated plane waves, in the loss regime. (a) $\alpha = 0.00001$ (weak confinement, for small value of $\gamma$) $\gamma = -0.01$, $N = 5$. (b) $\alpha = 0.00001$ (weak confinement, for a large value of $\gamma$) $\gamma = -0.001$, $N = 5$. (c) $\alpha = 0.001$ (strong confinement) $\gamma = -0.01$, $N = 20$. Other parameters are $\lambda = 0$, $a_s = -2.75$ nm, $a = 1.576.10^3$ nm, $K = 1.5$, $\varepsilon = 0.001$.

with time in Fig. 12(a), where $\gamma$ is relatively small. The number of pulses increases with time, due to the collisions among pulses. The train of solitons is symmetric around the center of the spatial coordinate $x = 0$. In Fig. 12(b), $\gamma$ is relatively large and we observe that the magnitude of the wave increases with time. The train of solitons has a shorter lifetime than in the case where $\gamma$ is small. Hence, a proper choice of the value of $\gamma$, that should be relatively small, may enhance the lifetime of a train of solitons. Figure 12(c) also portrays the spatiotemporal evolution of the condensate submitted to a stronger confinement; in this case, the train of solitons oscillates around the spatial axis' center $x = 0$ and the number of pulses grows with time.

We proceed by considering the case where the condensate is fed with atoms, $\gamma > 0$. Feeding atoms to the condensate has three major effects on the structure dynamics of solitons: (i) a reduction of the lifetime of solitons, (ii) an enhancement of the occurrence of modulational instability, and (iii) an increase of the magnitude of the wavefunctions of solitons generated.

Figure 13(a) ($\gamma = 0.001$, $t_C = 16$) and Fig. 13(b) ($\gamma = 0.01$, $t_C = 14$) exhibit these features. An increase of $\gamma$ enhances the occurrence of solitons and shortens their lifetime.

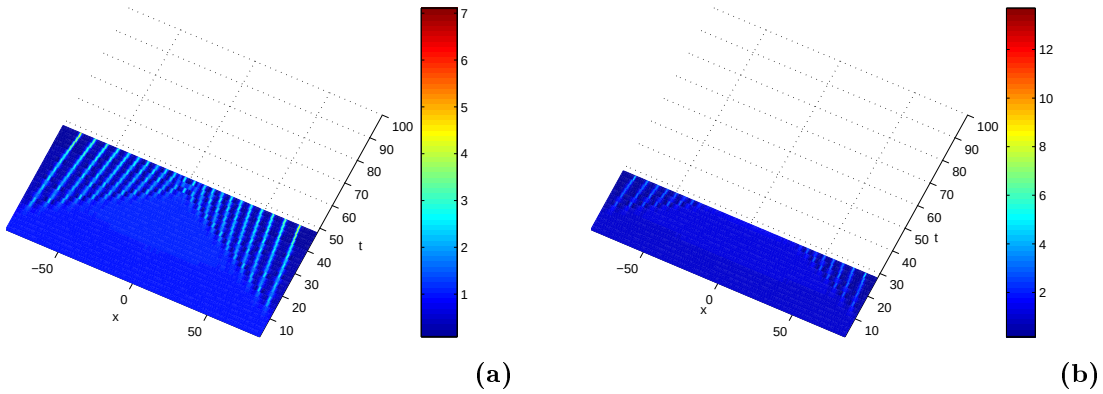


**Figure 13**: Spatiotemporal evolution of modulated solitary plane waves, in the the case where the condensate gains atoms. (a) $\gamma = 0.001$, (b) $\gamma = 0.01$. The other parameters are $\alpha = 0.00001$, $\lambda = 0$, $a_s = -2.75$ nm, $a = 1.576.10^3$ nm, $K = 1.5$, $\varepsilon = 0.001$.

Our analytical development fails to provide any information about effects of the linear potential. However, further numerical simulations show that the linear potential brings three new effects which are the deviation of the trail of trains of solitons, an enhancement of the occurrence of instability, and a reduction of the lifetime of solitons generated for large values of $\lambda$. In Figs. 14(a)-(b) ((a): deviation of the trail of solitons backward with $\lambda = 0.01$, (b) deviation forward of the trail of solitons with $\lambda = -0.01$) $t_C = 4$, while $t_C = 18$ when $\lambda = 0$ in Fig. 12(a). Figures 14(c)-(d) show evidence of the reduction of the lifetime of solitons that emerge due to modulational instability. In Figs. 14(c)-(d) the harmonic confinement and the exchange of atoms are switched off to facilitate interpretations. It is clear that large values of $\lambda$ shorten the lifetime of solitons.

### 3.3.2 Delayed nonlinear response of condensates with three-body interatomic interactions

#### (a1). Theoretical model and analytical results

In order to introduce the model, we start with a one dimensional cubic GPE with harmonic confinement [140]

$$\imath\frac{\partial q(x,t)}{\partial t} + \frac{\partial^2 q(x,t)}{\partial x^2} + 2a(t)|q(x,t)|^2 q(x,t) - \alpha x^2 q(x,t) = 0, \tag{3.25}$$

where the time $t$ and the spatial coordinate $x$ are measured in units of $\frac{2}{\omega_\perp}$ and $a_\perp$, $\omega_\perp$ and $a_\perp$ being the harmonic oscillators frequency and length in the transverse directions, respectively. The strength of the harmonic confinement $\alpha$ which can be positive (attractive potential) or negative (repulsive potential) satisfies $|\alpha|^{\frac{1}{2}} = \frac{|\omega_0|}{\omega_\perp} << 1$, where $\omega_0$ is the harmonic oscillator

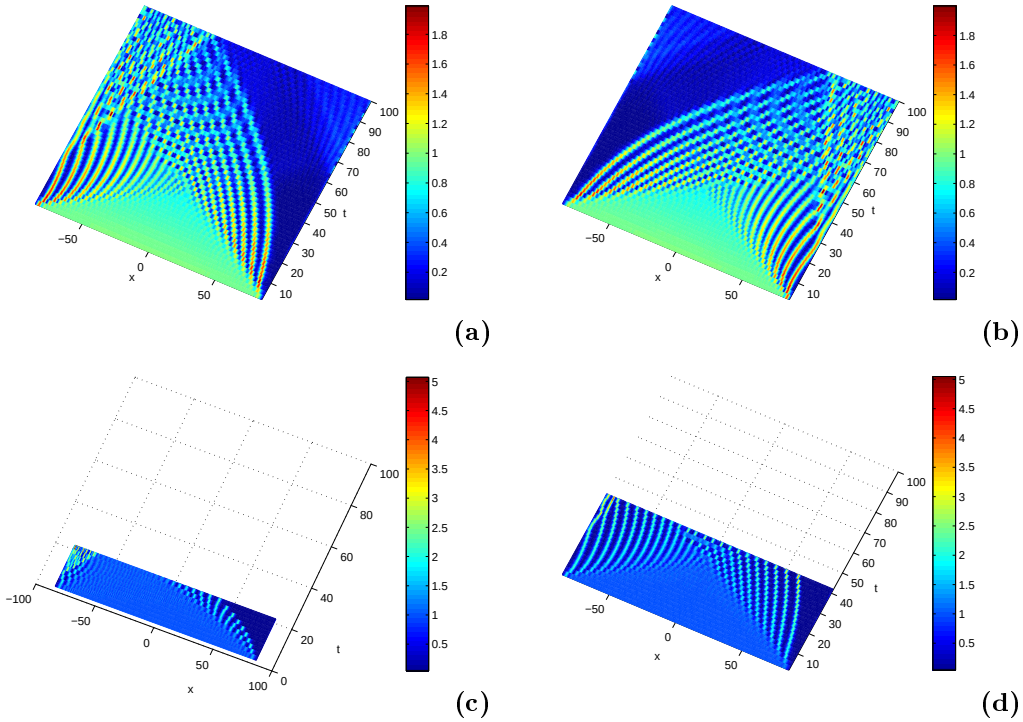


**Figure 14**: Effects of the linear potential on the dynamics of solitons. $\alpha = 0.00001$ for (a) $\lambda = 0.01$ and (b) $\lambda = -0.01$. $\alpha = 0$ for (c) $\lambda = 0.01$ and (d) $\lambda = 0.1$. Other parameters are $\alpha = 0.00001$, $\lambda = 0$, $a_s = -2.75$ nm, $a = 1.576.10^3$ nm, $K = 1.5$, $\varepsilon = 0.001$, $N = 5$.

frequency in the axial direction, and $m$ represents the mass of an atom. The time dependent s-wave scattering length $a(t)$ has the form: $a(t) = a_0 \exp(\lambda t)$, with $\alpha = \frac{\lambda^2}{4}$, $a_0 > 0$ [141] representing the attractive two-body interatomic interaction strength in the absence of time modulation of atom-atom interactions.

Recently, using an appropriate additional phase imprint on the wavefunction, Kumar, Radha, and Wadati [140] (see Eq.(3.35) below) derived a new GPE

$$\begin{aligned} &\imath\frac{\partial\psi(x,t)}{\partial t} + \frac{\partial^2\psi(x,t)}{\partial x^2} + 2a(t)|\psi(x,t)|^2\psi(x,t) - \alpha x^2\psi(x,t) + 12\tau|\psi(x,t)|^4\psi(x,t) \\ &+ 4\imath\sqrt{\tau}(|\psi(x,t)|^2)_x\psi(x,t) = 0 \end{aligned} \tag{3.26}$$

where $\tau$ is the strength of the three-body interatomic interactions and is a real number here. The three-body interatomic interactions may be attractive ($\tau > 0$) or repulsive ($\tau < 0$). Here, we focus on attractive three-body interatomic interactions. The last term of the right hand side of Eq.(3.26), $(|\psi(x,t)|^2)_x\psi(x,t)$, represents the delayed nonlinear response of the condensate system [140]. In the following, Eq.(3.26) is referred to as the modified GPE II. In the context of nonlinear fiber optics, the delayed nonlinear response term is the stimulated Raman scattering [118] term which has been intensively studied [118, 142], and has many applications. For instance, the Stimulated Raman scattering process may be used to realize longer transmission

distances in optical fibers [118, 142], and fiber amplifiers [142]. More, the Stimulated Raman scattering process may also be used for lumped and for distributed amplification in communication systems, as well as a wavelength conversion [142]. Another application of Stimulated Raman scattering in nonlinear optics is the realization of fiber-based Raman lasers which can be tuned over a wide range of frequencies [118]. The atomic counterpart of the laser, the so-called 'atomic laser', has been paid much attention due to the experimental realization of Bose-Einstein condensates [1, 2, 3]. There is also an atomic version of the Stimulated Raman scattering process which was observed or used in some condensate experiments [143, 144, 145, 146]. Nevertheless, the delayed nonlinear response term in the modified GPE II does not accounts for the atomic Stimulated Raman scattering process, but is part of the three-body interatomic interactions term in addition to the quintic term.

We are interested in the modulational instability of the modified GPE II. So, the spatial dependence of the external potential is hidden by using the modified lens-type transformation of Eq.(2.11) [32, 147] with $\eta(t) = \sigma(t) = 0$, such that Eq.(3.26) becomes

$$\begin{aligned} \imath\frac{\partial\Phi(X,T)}{\partial T} &= -\frac{\partial^2\Phi(X,T)}{\partial X^2} + g(t)|\Phi(X,T)|^2\Phi(X,T) - 12\tau|\Phi(X,T)|^4\Phi(X,T) \\ &\quad -4\imath\sqrt{\tau}(|\Phi(X,T)|^2)_X\Phi(X,T), \end{aligned} \tag{3.27}$$

with $g(t) = -2a(t)l(t)$. Our rescaled equation is a cubic-quintic GPE with an additional term, $-4\imath\sqrt{\tau}(|\phi(X,T)|^2)_X\phi(X,T)$, representing the delayed nonlinear response. The next step consists of performing a linear stability analysis using Eq.(2.16), in this case, $\Theta(T) = \Phi_0^2(g(t) - 12\tau\Phi_0^2)$, while the perturbation satisfies the relation

$$\imath\frac{\partial\delta\Phi}{\partial T} = -\frac{\partial^2\delta\Phi}{\partial X^2} + \Delta(t)(\delta\Phi + \delta\Phi*) - 4\imath\sqrt{\tau}\Phi_0^2(\frac{\partial\delta\Phi}{\partial X} + \frac{\partial\delta\Phi^*}{\partial X}), \tag{3.28}$$

where $\triangle(t) = \Phi_0^2(g(t) - 24\tau\Phi_0^2)$. Assuming the complex form described by Eq.(2.18) for the amplitude of the perturbation, the dispersion relation is obtained

$$\Omega^2 - 8\sqrt{\tau}\phi_0^2K\Omega - K^2(K^2 + 2\Delta(t)) = 0. \tag{3.29}$$

The modulational instability criterion reads

$$K^2 - 4a(t)l(t)\phi_0^2 - 32\tau\phi_0^4 < 0, \tag{3.30}$$

while the gain of instability is

$$G = |\sqrt{K^2(4a(t)l(t)\phi_0^2 + 32\tau\phi_0^4 - K^2)}|. \tag{3.31}$$

A straightforward analysis of Eqs.(3.30)-(3.31) shows that the unstable modes domain enlarges and the gain of instability increases when one takes into account the three-body interatomic interactions ($\tau \neq 0$). Thus, the three-body interatomic interactions destabilize the condensate. On the other hand, setting the strength of the two-body interatomic interactions to a minimum

value in Eq.(3.31) may have a stabilizing effect on the condensate system. This result is consistent with exact solutions of the modified GPE II reported in [140]. It is important to remind as pointed out in [136] that the instability occurs in the rescaled variables coordinates $X$ and $T$. So, we analyze the modulational instability in the new coordinates $X$ and $T$.

**(a1.1). Modulational instability of the modified GPE II in an attractive potential ($\alpha > 0$)**

The explicit expressions of the functions $f(t), l(t), T(t)$ used to characterize the modulational instability criterion and growth rate are given by Eq.(2.14). For positive values of $\lambda$ with time increasing scattering length ($a(T) = a_0 \exp(\lambda T), \lambda > 0$), the gain of instability increases. Hence, the increase of the scattering length more destabilizes the condensate. On the contrary, a time reduction of the scattering length ($a(T) = a_0 \exp(\lambda T), \lambda < 0$), softens the instability. The external potential also alters the loss of stabilitily of the system. When the scattering length is constant, i.e., $a(T) = a_0$, small values of $\lambda$ enhance the instability of the condensate as shown in Fig. 15.

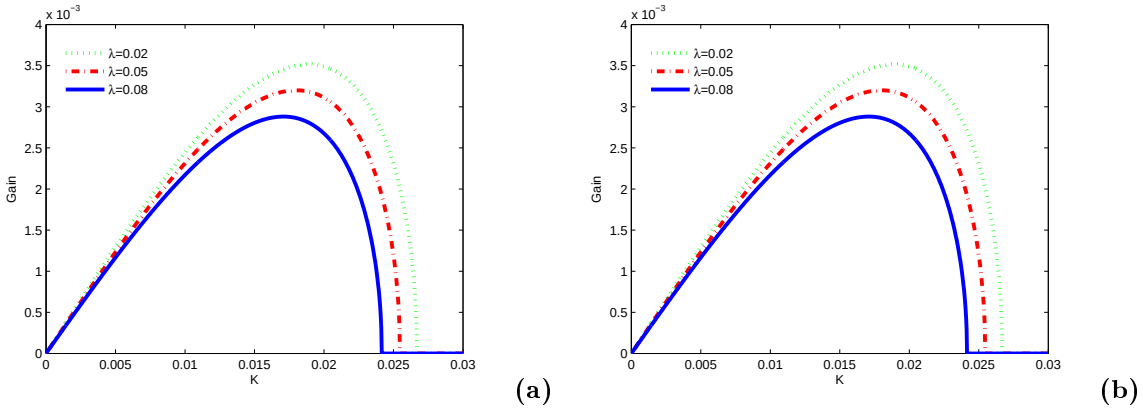


**Figure 15**: Influence of the attractive potential on the instability gain. (a) Attractive potential ($\alpha < 0$). (b) Repulsive potential ($\alpha > 0$). Other parameters are $a = a_0 \exp(\lambda T), \lambda > 0$ at $T = 5$, $a_0 = 0.001$, $\phi_0 = 1$, $\lambda = 0.02$ (dotted line), $\lambda = 0.05$ (dash-dotted line), $\lambda = 0.08$ (solid line).

**(a1.2). Modulational instability of the modified GPE II in a repulsive potential ($\alpha < 0$)**

The explicit expressions of the functions $f(t), l(t), T(t)$ used to characterize the modulational instability criterion and growth are given by Eq.(2.15). First, let us consider the case where $f$ is negative. The gain of instability is a constant that is not affected by the strength of the external potential nor to time $T$. This result is not confirmed by the direct numerical simulations as we will see below. The linear stability analysis is not sufficient to explain the gain of instability when $f < 0$. For positive values of $f$, Fig. 15(b) implies that small positive values of $f$ increase the instability of the condensate.

**(b). Numerical simulations of the modified GPE II**

Our numerical simulations were performed both in the absence and the presence of the three-body interatomic interactions. Different diagrams are obtained, showing the influence of the three-body interaction on the modulational instability of the condensate system. The numerical scheme used is the split-step Fourier method.

**(b1). Impact of the three-body interatomic interactions in the case of an attractive potential**

We start our numerical simulations by inserting through the system the initial condition given by Eq.(3.27). It appears from a comparison of Figs. 16(a)-(b) where the maxima amplitude $Max_x|\psi(x,t)|^2$ are plotted versus time $t$ that the inclusion of the three-body interatomic interactions enhances the instability and its occurrence in the condensate. Furthermore, the increase of the strength of the two-body interatomic interactions plays a destabilizing role (compare Fig. 16(a) $a(t) = a_0$, and Fig. 16(b) $a(t) = a_0 \exp(\lambda t)$). These effects of the two- and three-body interatomic interactions recover well the analytical ones as mentioned above.

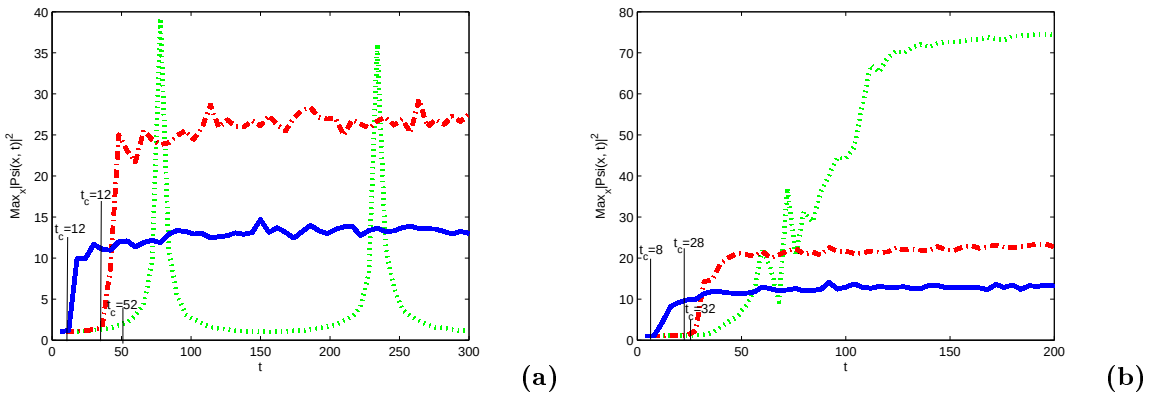


**Figure 16**: Temporal evolution of the maxima amplitude for 3 different values of $\tau$, with $\lambda = 0.02$. (a) Constant scattering length. (b) Time increasing scattering length. $\tau = 0$ (dotted line), $\tau = 0.01$ (dash-dotted line), $\tau = 0.07$ (solid line). Other parameters are $a_0 = 0.001$, $\phi_0 = 1$, $K = 0.01$, and $\varepsilon = 0.001$.

We check the impact of the three-body interatomic interactions on the long time dynamics of solitons that emerge through the activation of modulational instability by plotting the spatiotemporal evolution of the original wavefunction. Figure 17 displays the evolution of the condensate's density. A parallel between Fig. 17(a) ($\tau = 0$) with 12 solitons created and Fig. 17(b) ($\tau = 0.01$) shows that the inclusion of the three-body interatomic interactions drastically modifies the trail of the train of solitons generated and increases their lifetime. Increasing the strength of the three-body interatomic interactions induces a growth of the number of solitons, meanwhile reducing the average distance between two neighbor solitons of the train as can be seen in Fig. 17(c) ($\tau = 0.07$). Another effect of including the three-body interatomic interactions is that it straightens all solitons created via modulational instability (see Figs. 17(a)-(c)).

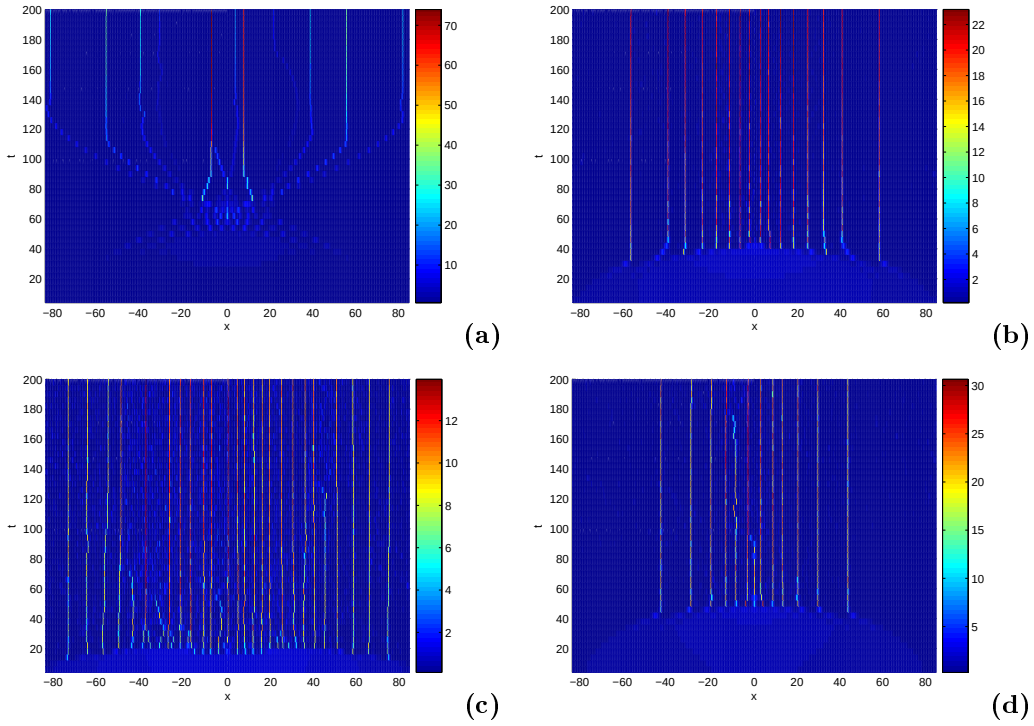


**Figure 17**: Spatiotemporal evolution of the condensate's density. (a) $a = a_0 \exp(\lambda t), \lambda > 0, \tau = 0$. (b) $a = a_0 \exp(\lambda t), \lambda > 0, \tau = 0.01$. (c) $a = a_0 \exp(\lambda t), \lambda > 0, \tau = 0.07$. (d) $a = a_0, \tau = 0.01$. Other parameters are $a_0 = 0.001$, $\Phi_0 = 1$, $K = 0.01$, and $\varepsilon = 0.001$.

Comparing Fig. 17(c) (16 solitons created) and Fig. 17(d) ($a(t) = a_0$, only 13 solitons created), we deduce that the time increasing scattering length has a destabilizing effect on the system. The external potential also destabilizes the condensate as depicted in Fig. 18, where one also realizes that stronger confinement of the condensate enhances the onset of instability.

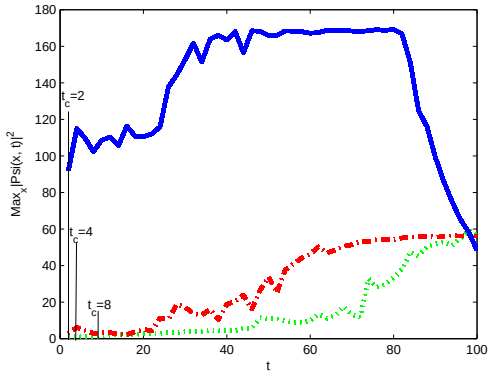


**Figure 18**: Time evolution of the maxima amplitude, $\tau = 0.0001$ with $a = a_0 \exp(\lambda t)$, $\lambda = 0.02$ (dotted line), $\lambda = 0.05$ (dash-dotted line), $\lambda = 0.08$ (solid line). Other parameters are $a_0 = 0.001$, $\Phi_0 = 1$, $K = 0.01$, and $\varepsilon = 0.001$.

**(b2). Impact of the three-body interatomic interactions in the case of a repulsive potential**

For the case of a repulsive trapping potential, we employ the following initial condition [32, 129]

$$\psi(x, 0) = (\Phi_0 + \varepsilon cos(Kx)) \exp(\imath f x^2). \tag{3.32}$$

Let us begin with the case of $f < 0$. The overall behavior of the time variation of maxima amplitude in Fig. 19(a) teaches us that small values of the expulsive potential, with $f < 0$, more destabilize the condensate. This result is not in accordance with the linear stability analysis as mentioned above. An explanation is that, due to the presence of the external potential, the dynamics of the external potential mixes with the original wave number of the perturbation [32, 33], a process called excitation of modulational unstable modes [141].

For $f < 0$, the gain of instability increases as the strength of the trapping potential reduces. Nevertheless, a comparison of Figs. 19(a)-(b) ($f > 0$) leads to the fact that negative values of $f$ more enhance the instability than positive ones. Once the condensate is set into motion, Figs. 19(c)-(d) show that solitons generated are distributed over all the axial axis, evolve asymmetrically, and their number is higher than in the previous cases. By increasing the strength of the external potential, the three-body interatomic interactions only deviate the trail of the train of solitons forward (towards $+x$-direction) on the axial potential (compare Fig. 19(d) where $\lambda = 0.002$, $\tau = 0.0001$ with Fig. 19(e) where $\lambda = 0.002$ and $\tau = 0$). Moreover, for larger values of the strength of the external potential, reducing the strength of the external potential induces the reduction of the density of the condensate as well as the number of solitons created as can

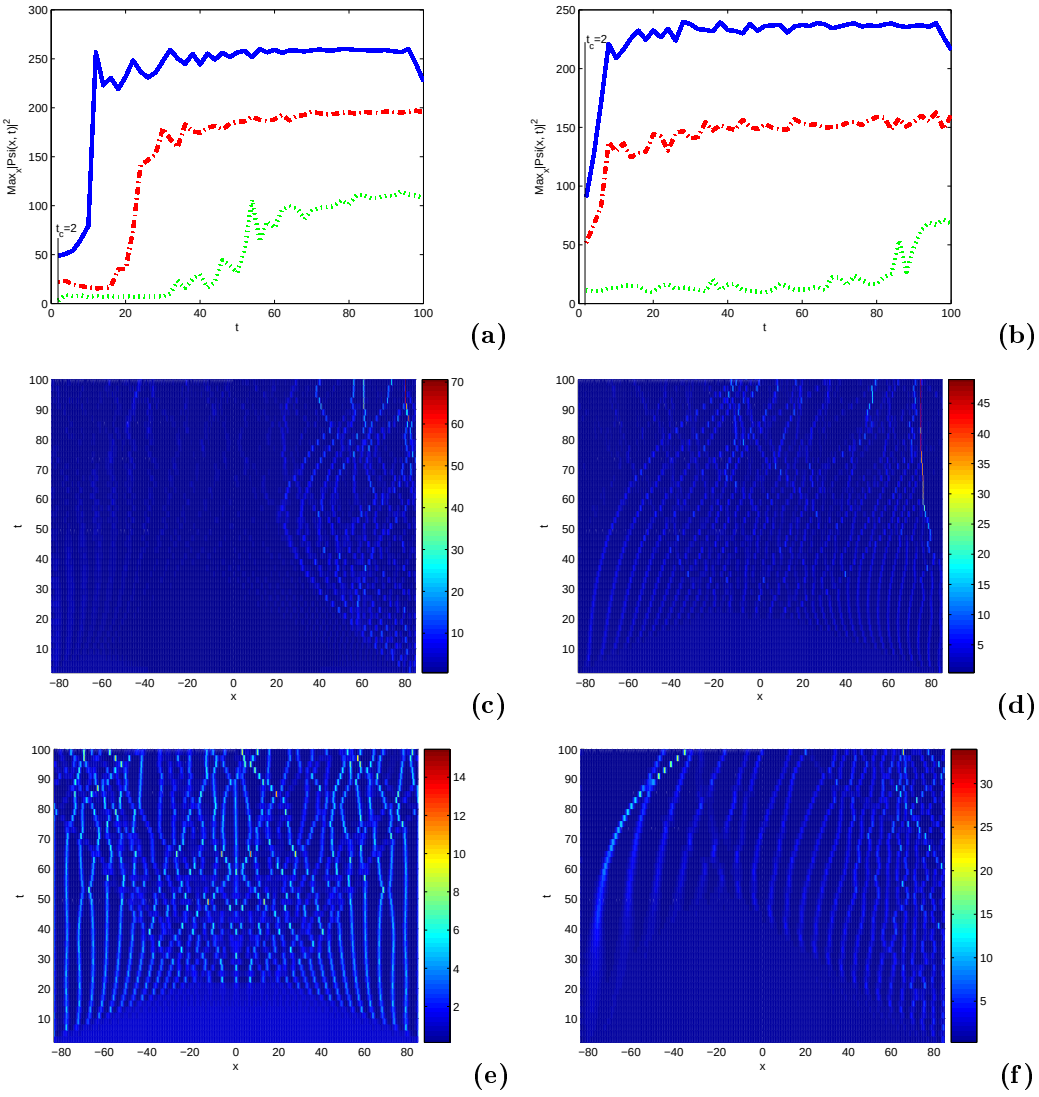


**Figure 19**: Time evolution of maxima amplitude for $a = a_0 \exp(\lambda t), \lambda > 0$, $\tau = 0.0001$, $\lambda = 0.02$ (dotted line), $\lambda = 0.04$ (dash-dotted line), $\lambda = 0.06$ (solid line), (a) $f < 0$, (b) $f > 0$. (c)-(f) Spatiotemporal evolution of the density. (c) $\lambda = 0.002$, $\tau = 0.0001$. (d) $\lambda = 0.002$, $\tau = 0$. (e) $\lambda = 0.006$, $\tau = 0.0001$. Other parameters are $a_0 = 0.001$, $\Phi_0 = 1$, $K = 0.01$, and $\varepsilon = 0.001$.

be seen in Fig. 19(f) ($\lambda = 0.006$).

### 3.3.3 Three-body interatomic interactions beyond the GPE

#### (a). Theoretical model and analytical results

In most models of Bose-Einstein condensates that go beyond the mean-field limit, only corrections around the mean-field are taken into account [51, 52, 72, 74, 75], but the three-body interatomic interactions are not considered. As already mentioned, the three-body interatomic interactions can play an important role in the description of the static and the dynamic properties of condensates. Therefore, inclusion of the three-body interatomic interactions to the governing equation of condensates beyond the mean-field limit is necessary.

In order to derive our modified GPE, we start with the unidimensional reduction of the three-dimensional GPE with two-body interatomic interactions obtained by Tiofack *et al.* [135] which is a reduced version of Eq.(3.17)

$$\begin{aligned} \imath\frac{\partial q(x,t)}{\partial t} &= [-\frac{\partial^2}{\partial x^2} + \alpha(t)x^2 + g'|q(x,t)|^2 + g'_1|q(x,t)|^3 + \\ & g'_2\frac{\partial^2}{\partial x^2}(|q(x,t)|^2)]q(x,t). \end{aligned} \tag{3.33}$$

We introduce an additional phase imprint into the wavefunction $q(x,t)$ as [133]

$$\psi(x,t) = q(x,t)\exp(2\imath\theta(x,t)), \tag{3.34}$$

in which $\theta(x,t)$ is the phase imprint on the old wave function $q(x,t)$. The phase imprint is then engineered as [133]

$$\begin{aligned} \frac{\partial\theta(x,t)}{\partial x} &= -\sqrt{\tau}|\psi(x,t)|^2, \\ \frac{\partial\theta(x,t)}{\partial t} &= \imath\sqrt{\tau}(\psi(x,t)\frac{\partial\psi(x,t)^*}{\partial x} - \psi(x,t)^*\frac{\partial\psi(x,t)}{\partial x}) + 4\tau|\psi(x,t)|^4. \end{aligned} \tag{3.35}$$

The parameter $\tau$ as in Eq.(3.27) describes the strength of the three-body interatomic interactions. Inserting Eqs.(3.34)-(3.35) into Eq.(3.33), we derive for the new wavefunction $\psi(x,t)$, the new modified GPE [149]

$$\begin{aligned} \imath\frac{\partial\psi(x,t)}{\partial t} &= \big[-\frac{\partial^2}{\partial x^2} + \alpha(t)x^2 + g'|\psi(x,t)|^2 + g'_1|\psi(x,t)|^3 + g'_2\frac{\partial^2}{\partial x^2}(|\psi(x,t)|^2) \\ & -12\tau|\psi(x,t)|^4 - 4\imath\sqrt{\tau}\frac{\partial}{\partial x}(|\psi(x,t)|^2)\big]\psi(x,t). \end{aligned} \tag{3.36}$$

Equation (3.36) is a modified GPE that goes beyond the mean-field picture and contains both the two- and three-body interatomic interaction terms. In the following, Eq.(3.36) is referred to as the modified GPE III. One has noticed that in Eq.(3.36), the three-body interatomic interactions consist of a quintic term plus the delayed nonlinear response of the condensate.

Willing to study the modulational instability of the modified GPE III, we follow the procedure adopted above. First, the modified lens-type transformation given by Eq.(2.11) ($\eta(t) = \sigma(t) = 0$) with the constraints of Eq.(2.12) are invoked to ease the calculations. Equation (3.36) in terms of the rescaled variables $X$ and $T$ reads

$$\begin{aligned} \imath\frac{\partial\Phi(X,T)}{\partial T} &= \big[-\frac{\partial^2}{\partial X^2} + g(t)|\Phi(X,T)|^2 + g_1(t)|\Phi(X,T)|^3 \\ &+g_2(t)\frac{\partial^2}{\partial X^2}(|\Phi(X,T)|^2) - 12\tau|\Phi(X,T)|^4 \\ &-4\imath\sqrt{\tau}\frac{\partial}{\partial X}(|\Phi(X,T)|^2)\big]\Phi(X,T), \end{aligned} \tag{3.37}$$

with $g(t) = g'l(t)$, $g_1(t) = g_1'\sqrt{l(t)}$, and $g_2(t) = \frac{g_2'}{l(t)}$. The linear stability analysis is then performed with the ansatz of Eq.(2.16). The perturbation in this case obeys the partial differential equation

$$\begin{aligned} \imath\frac{\partial\delta\Phi}{\partial T} &= -\frac{\partial^2\delta\Phi}{\partial X^2} + \Delta(t)(\delta\Phi + \delta\Phi*) + g_2(t)\Phi_0^2(\frac{\partial\delta\Phi}{\partial X^2} + \frac{\partial\delta\Phi*}{\partial X^2}) - 4\imath\sqrt{\tau}\Phi_0^2(\frac{\partial\delta\Phi}{\partial X} \\ &+\frac{\partial\delta\Phi^*}{\partial X}). \end{aligned} \tag{3.38}$$

The parameter $\Delta(t) = (g(t) + \frac{3}{2}g_1(t)\Phi_0 - 24\tau\Phi_0^2)\Phi_0^2$. Then, considering that the perturbation is a complex quantity, the dispersion relation calculated is

$$\Omega^2 - 16\sqrt{\tau}\Phi_0^2K\Omega - K^2(K^2(1 - g_2(t)\Phi_0^2) + 2\Delta(t)) = 0. \tag{3.39}$$

The modulational instability criterion is expressed as

$$K^2(K^2(1 - g_2(t)\phi_0^2) + 2\Delta(t)) < 0, \tag{3.40}$$

while the gain of instability is given by

$$G = \sqrt{K^2[K^2(-1 + g_2(t)\Phi_0^2) - 2\Delta(t)]}. \tag{3.41}$$

**(a1). Modulational instability of the modified GPE III with attractive confinement**

The solution given by Eq.(2.14) is inserted into Eq.(3.41). We visualize in Fig. 20 the variation of the gain of instability against the unstable modes $K$, at time $t = 5$. Analyzing Fig. 20, we understand from panel (a) that the three-body interatomic interactions favor the instability of the system, while from panel (b) we deduce that small attractive confinements enhance the instability of the condensate. However, in Fig. 20 the unstable modes region is restricted to a finite interval, while all modes were found to be modulationally unstable for the modified GPE I. Therefore, inclusion of the three-body interatomic interactions corresponding to the modified GPE III stabilizes the system. A similar result was reported in [34, 150].

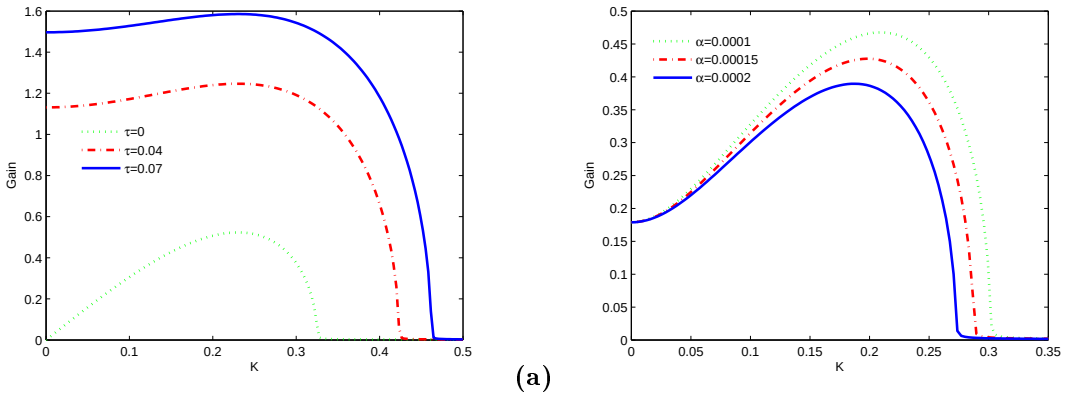


**Figure 20**: Modulational unstable growth rate as a function of modes $K$. (a) $t = 5$, $\alpha = 0.00001$, $\tau = 0$ dotted line, $\tau = 0.04$ dashed-dotted line, $\tau = 0.07$ solid line. The instability increases with the strength of the three-body interactions. (b) $t = 30$, $\tau = 0.001$, $\alpha = 0.0001$ dotted line, $\alpha = 0.00015$ dashed-dotted line, $\alpha = 0.0002$ solid line. The instability is much pronounced with small values of $\alpha$. Other parameters are $a_s = -2.75$ nm, $a = 1.576.10^3$ nm, $\varepsilon = 0.001$, $N = 5$.

**(a2). Modified GPE III for a trapless condensate or a condensate in a repulsive potential**

In the latter subsection, the gain of instability depends on the explicit form of the function $l(t)$ which, depends on the particular solution of the Riccati equation $\frac{df}{dt} = -4f^2 - \alpha$ (see Eq.(2.12)). In fact, the general form of the Riccati equation is [144]

$$\frac{df}{dt} = a_0 + a_1 f + a_2 f^2, \tag{3.42}$$

where $a_0$, $a_1$, $a_2 \in \mathbb{R}$, and $a_2 \neq 0$ are real constants. Equation (3.40) reduces to the special Riccati equation of the set (2.12) if one chooses $a_0 = -\alpha$, $a_1 = 0$, and $a_2 = -4$. In this case, the general solution of Eq.(3.42) is [144]

$$\begin{aligned}
f_1 &= -\frac{1}{-4t + t0}, \quad \alpha = 0 \\
f_{21} &= \frac{\zeta\sqrt{-\alpha}}{2}, \quad \alpha < 0 \\
f_{22} &= \frac{\sqrt{-\alpha}}{2}\tanh(2\sqrt{-\alpha}t - \frac{\zeta\ln(t_0)}{2}), \quad t_0 > 0, \quad \alpha < 0 \\
f_{23} &= \frac{\sqrt{-\alpha}}{2}\coth(2\sqrt{-\alpha}t - \frac{\zeta\ln(-t_0)}{2}), \quad t_0 > 0, \quad \alpha < 0 \\
f_{31} &= -\frac{\sqrt{\alpha}}{2}\tan(2\sqrt{\alpha}t + t_0), \quad \alpha > 0 \\
f_{32} &= \frac{\sqrt{\alpha}}{2}\tan(2\sqrt{\alpha}t + t_0), \quad \alpha > 0,
\end{aligned} \tag{3.43}$$

where $\zeta = \pm 1$, and $t_0$ is an arbitrary real constant. Solving the second equation of the set (2.12) yields the following explicit expressions of the function $l(t)$

$$\begin{aligned}
l_1(t) &= \mid C_1(4t - t_0) \mid, \quad \alpha = 0 \\
l_{21}(t) &= \mid C_2 \exp(-2\zeta\sqrt{-\alpha}t) \mid, \quad \alpha < 0 \\
l_{22}(t) &= \mid C3 \cosh(2\sqrt{-\alpha}t - \frac{\zeta \ln(t_0)}{2}) \mid, \quad t_0 > 0, \quad \alpha < 0 \\
l_{23}(t) &= \mid \frac{C_4}{\sqrt{\coth(2\sqrt{-\alpha}t - \frac{\zeta \ln(-t_0)}{2}) - 1}} \mid, \quad t_0 > 0, \quad \alpha < 0 \\
l_{31}(t) &= \mid C_5 \cos(x + t_0) \mid, \quad \alpha > 0 \\
l_{32}(t) &= \mid C_6 \sin(x + t_0) \mid, \quad \alpha > 0,
\end{aligned} \tag{3.44}$$

coefficients $C_i$ $(i = 1, 2, 3, 4, 5, 6)$ being arbitrary real constants. The solutions given by Eq.(3.43) with Eq.(3.44) provide a systematic set of solutions of the modulational instability gain, for a condensate trapped in an attractive or in a repulsive potentials. Besides, the fifth equation of the set (3.44) reduces to the solution obtained above when the free parameters are $C_5 = 1$, and $t_0 = 0$. In the previous works [32, 33, 34, 135, 138, 147], the case where the external potential is turned off cannot be investigated analytically, since the solution of the Riccati equation used is the same as above. In the next, we restrict our study to two relevant special cases: (i) the external potential is switched off, (ii) the external potential is repulsive ($\alpha < 0$).

We first consider the situation where the external potential is turned off, i.e., $\alpha = 0$. In this case, $l(t) = l_1(t)$. In the absence of the three-body interactions, the condensate remains stable, while the inclusion of the three-body interactions destabilizes the system. This feature is depicted in Fig. 21(a). For a condensate in a repulsive potential, we select the case where

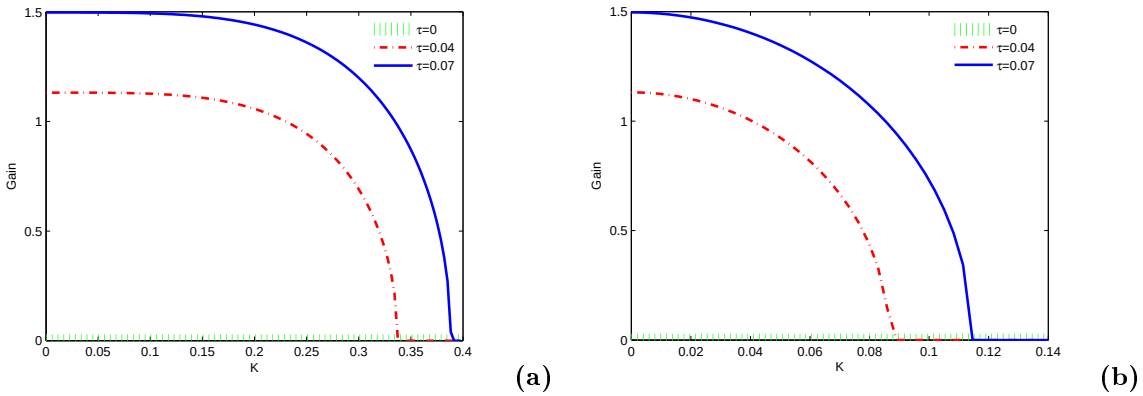


**Figure 21**: Instability gain versus $K$. $\tau = 0$ dotted line, $\tau = 0.04$ dashed-dotted line, and $\tau = 0.07$ solid line. (a) Absence of an external confinement $\alpha = 0$, $C_3 = 1$, $t_0 = 1$. (b) Presence of attractive potential $\alpha = 4$. Other parameters are $a_s = 5.77$ nm, $a = 300.10^3$ nm. $\varepsilon = 0.001$, $N = 5$, $C_1 = 1$.

$l(t) = l_{22}(t)$, with $C_3 = 1$. The amplitude of the gain of instability does not change, but the

unstable modes region shrinks as can be seen by comparing Fig. 21(b) (instability gain versus unstable modes $K$, with $\alpha = -4$, $t = 2$, $t_0 = 1$) and Fig. 21(a).

**(b). Numerical simulations of the modified GPE III**

In this part, we make full numerical integrations of the modified GPE III with the split-step Fourier method in order check the accuracy of the linear stability analysis and investigate the time evolution of solitons generated via modulational instability.

Let us start with the case where the external potential is attractive. We use Eq.(3.24) as initial condition and insert it through Eq.(3.36). An examination of Fig. 22(a) (parameters correspond to Fig. 20(a)) where the time evolution of maxima amplitude are plotted for three different values of $\tau$ reveals that the inclusion of the three-body interatomic interactions enhances the loss of stability as predicted by the linear stability analysis. A parallel between Fig.

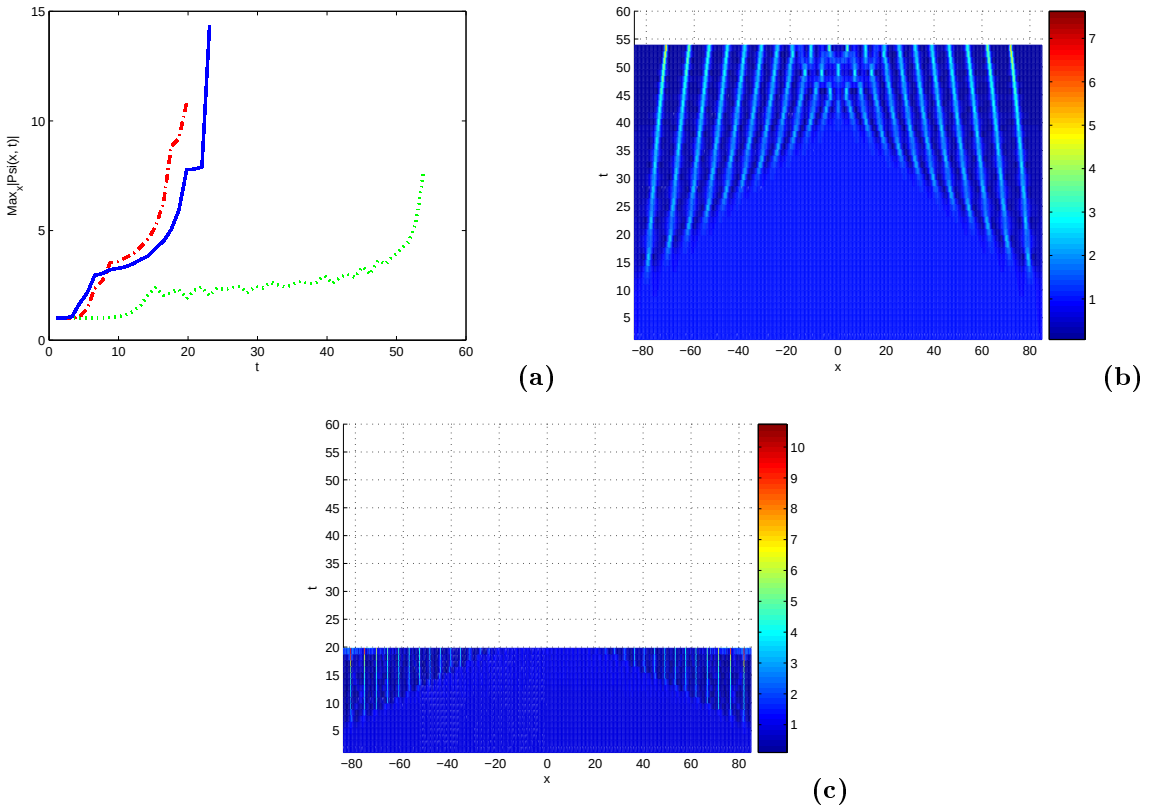


**Figure 22**: (a) Temporal evolution of maxima amplitude for $\tau = 0$ dotted line, $\tau = 0.04$ dashed-dotted line, $\tau = 0.07$ solid line. (b)-(c) Spatiotemporal evolution of the density. (b) $\tau = 0$. (c) $\tau = 0.04$. Other parameters are the same as in Fig. 20(a) with $K = 0.0001$.

22(b) ($\tau = 0$) and Fig. 22(c) ($\tau = 0.04$) shows that the three-body interatomic interactions reduces the lifetime, their appearance, and the number of solitons generated due to modulational instability. In Fig. 22(b) $t_C = 13$ with 23 solitons, while $t_C = 6.6$ with 28 solitons in Fig. 22(c).

The results obtained for modulational instability is sensitive to the type of initial condition used. One important aspect of the study of modulational instability is the possibility to create many solitons at the same time. In order to increase the number of solitons generated, we introduce a new initial condition given by [142]

$$\psi(x,0) = (1 - \frac{1}{2}\alpha x^2)(100\tanh(Kx)\cos(x) + 0.001\cos(x)). \tag{3.45}$$

The factor, 100 in front of the expression $\tanh(Kx)\cos(x)$ is used only for convenience. Figure 23(a) portrays the spatiotemporal evolution of the magnitude of the wavefunction for $\alpha = 0.0001$, $\tau = 0.001$. In comparison with previous results, the number of solitons generated

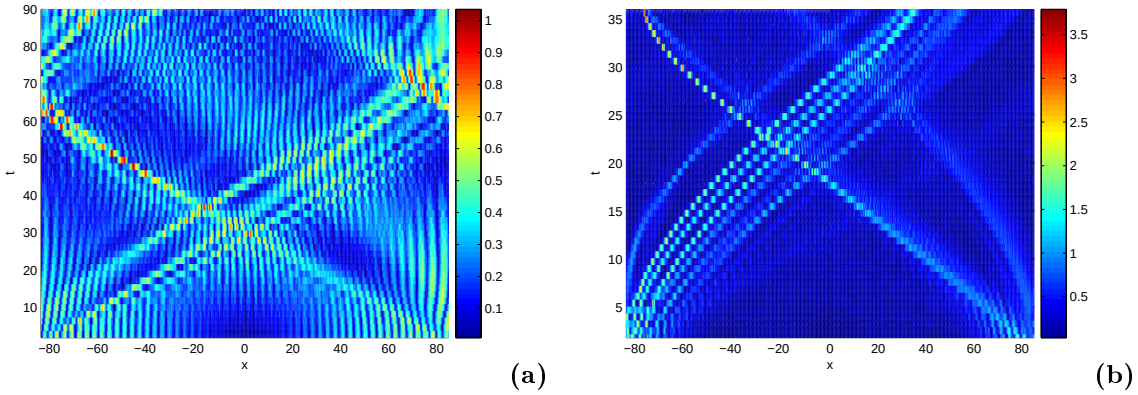


**Figure 23**: Spatiotemporal evolution of the magnitude of the wavefunction corresponding to the initial condition (3.43). (a) $\alpha = 0.0001$, (b) $\alpha = 0.0009$. Other parameters are the same as in Fig. 20(a) with, $\tau = 0.001$, $K = 0.0001$.

has significantly increased. Nevertheless, an increase of the strength of the external potential shortens the lifetime of solitons created (see Fig. 23(b) with $\alpha = 0.0009$, $\tau = 0.001$).

We continue by investigating numerically the modulational instability of the modified GPE III in the absence of external potential, and in the presence of a repulsive. The initial condition for the numerical simulations is $\psi(x,0) = 10^{-6}(1 - \frac{1}{2}\alpha x^2)(100\tanh(Kx)\cos(x) + 0.001\cos(x))$. For a trapless condensate, analyzing Fig. 24(a) (time variation of maxima amplitude), we deduce that the three-body interatomic interactions favor the loss of stability and the appearance of solitons. Once again, the linear stability analysis and the numerical results agree well. In the case of a repulsive confining potential, all solitons generated correspond to straight lines. Thus, we infer that the repulsive potential straightens solitons created.

### 3.3.4 Modified GPE II with complex potential

The modified GPE II is a derivative GPE type which has recently emerged, and its solitonic properties are not largely studied. We resort the analytical method of the first section and apply it to the modified GPE II with the complex potential corresponding to Eq.(3.12). We focus on the cases of attractive and repulsive condensates with constant scattering length, the harmonic

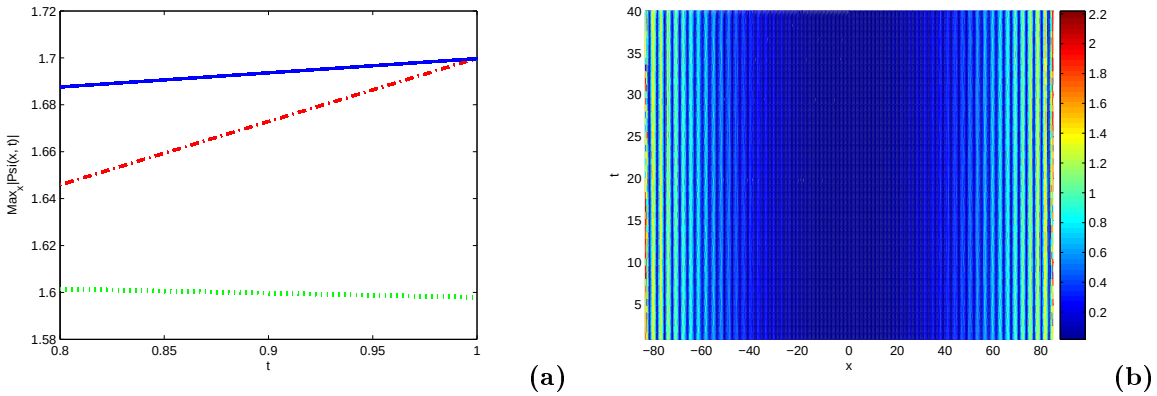


**Figure 24**: (a) Temporal evolution of maxima amplitude for $\tau = 0$ dotted line, $\tau = 0.04$ dashed-dotted line, and $\tau = 0.07$ solid line, $\alpha = -4$. (b) Spatiotemporal evolution of the wavefunction, $\alpha = -4$, $\tau = 0.07$.

part of the complex potential being attractive. An important aspect of modulational instability is the critical time $t_C$ after which an instability ceases to be dominant. It is obtained by solving the following implicit equation with MAPLE [152]

$$K^2 - 4a(t_C)l(t_C)\exp(2\gamma t_C)\phi_0^2 - 32\tau\exp(4\gamma t_C)\phi_0^4 = 0. \tag{3.46}$$

The modulational instability criterion is

$$|K| < 2\exp(\gamma t)\phi_0\sqrt{a(t)l(t) + 8\tau\exp(2\gamma t)\phi_0^2}, \tag{3.47}$$

and the gain of instability is given by

$$G = \Re(\sqrt{K^2(4a(t)l(t)\exp(2\gamma t)\phi_0^2 + 32\tau\exp(4\gamma t)\phi_0^4 - K^2)}). \tag{3.48}$$

Figure 25 displays the variation of the critical time $t_C$ as a function of unstable modes $K$. For a condensate receiving atoms (see Fig. 25(a)), the critical time increases with decreasing values of $K$. Besides, for a fixed value of $K$, $t_C$ increases with decreasing values of $\gamma$. This observation means that smaller values of $\gamma$ allow instability to develop for relatively longer times, in opposition to larger ones. Similar effects are also observed when the condensate looses atoms (see Fig.25(b)).

The analytical study also predicts the occurrence of modulational instability in repulsive condensates. Effects of the exchange of atoms are qualitatively the same with the case of attractive condensates [152]. The critical time in repulsive condensates increases with increasing values of $K$. Yet, the development of instability is shorter in attractive condensates. One notices this feature by making a comparison between Fig. 25(c) ($a < 0$) and Fig. 25(a) ($a > 0$).

We perform numerical integrations of the modified GPE II with the potential given by Eq.(3.12) and compare the results with the predictions of the linear stability analysis. The numerical scheme is the split-step Fourier method. We only focus on positive values of $\gamma$. For

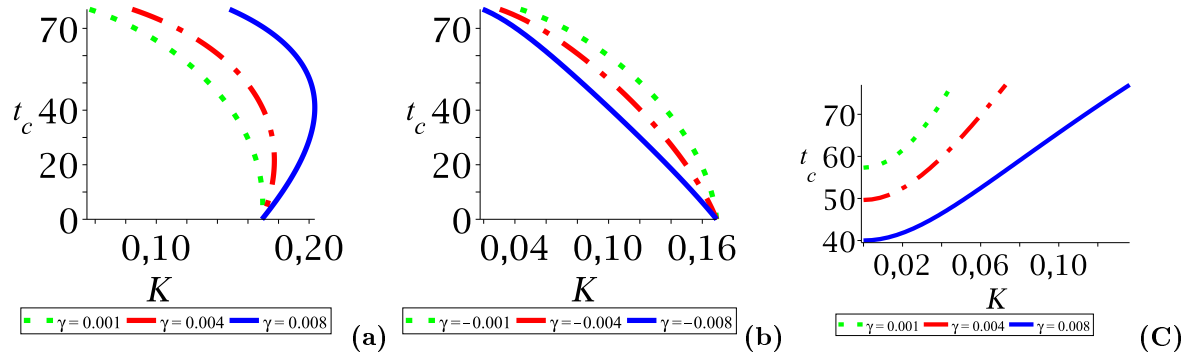


**Figure 25**: Critical time $t_C$ as a function of modes $K$. The condensate is attractive in (a) and (b), but repulsive in (c). (a) $\gamma = 0.001$ dotted line, $\gamma = 0.004$ dash-dotted line, $\gamma = 0.008$ solid line. (b) $\gamma = -0.003$ dotted line, $\gamma = -0.03$ dash-dotted line, $\gamma = -0.06$ solid line. (c) $a_0 = -0.00049$, $\Phi_0 = 3.5$, $\gamma = 0.001$ dotted line, $\gamma = 0.004$ dash-dotted line, $\gamma = 0.008$ solid line. Other parameters are $\alpha = 0.0001$, $\tau = 0.00001$.

attractive condensates, the initial condition used is

$$\psi(x,t) = (\Phi_0 + 0.01\exp(-iKx)). \tag{3.49}$$

We have observed in our numerical calculations that the critical time $t_C$ increases with decreasing values of $\gamma$ [152]. We detect the value of $t_C$ as the time after which no more solitons emerge. For the typical case of $\gamma = 0.001$ and $K = 0.12$, with other parameters corresponding to those in Fig. 25(a), the numerical value of $t_C$ is 56, while the analytical prediction is $\approx 57.52$. The relative error in the determination of $t_C$ amounts to $\approx 2.64_o/^o$, a value sufficiently small, such that the agreement between the numerical and the analytical predictions can be considered to be quite good [152]. The exchange of atoms has dramatic effects on the behavior of solitons generated. A parallel among Fig. 26(a) ($\gamma = 0.001$), Fig. 26(b) ($\gamma = 0.04$), and Fig. 26(c) ($\gamma = 0.08$) shows that, large values of $\gamma$ also affect the dynamics of the modulated solitons in three different ways: (i) the number of solitons created increases, (ii) a radical change of the shape of solitons (that emerge due to modulational instability) which are all straightened, (iii) a significant reduction of the lifetime of solitons generated. The physical origin of the smallness

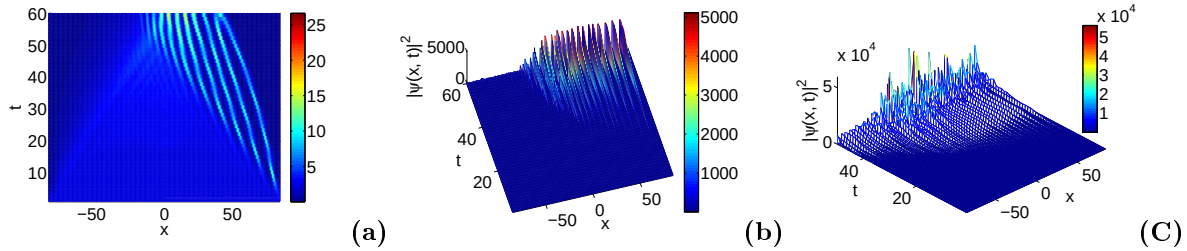


**Figure 26**: Spatiotemporal evolution of the condensate's density. (a) $\gamma = 0.001$, (b) $\gamma = 0.04$, (c) $\gamma = 0.08$. Larger values of $\gamma$ straiten solitons emerging due to the development of MI (compare panels (a) and (b)). (c) Explosion of the condensate due to high feeding rate. In all panels, other parameters are the same as in Fig. 25(a).

of the soliton lifetime at a high rate feeding regime may be explained as follows: many atoms

are injected into the condensate such that its density 'exponentially' increases. The number of collisions in the condensate 'exponentially' increase too, this process results in the rapid growth of the temperature due to the thermal agitation, and the condensate finally explodes when the temperature exceeds the critical temperature needed for condensation. Thus, using a pumping process, we can produce high density condensates which are important for some condensate applications [153] such as atomic number squeezing, quantum tunneling. However, the rate of the pumping process may not be too high (see Fig. 26(c)).

For repulsive condensates, direct numerical simulations allow us to observe the effects of the repulsive atom-atom interactions. The initial condition implemented here is Eq.(3.24). We can see in Fig. 27 the spatiotemporal evolution of the density of the original wavefunction. We

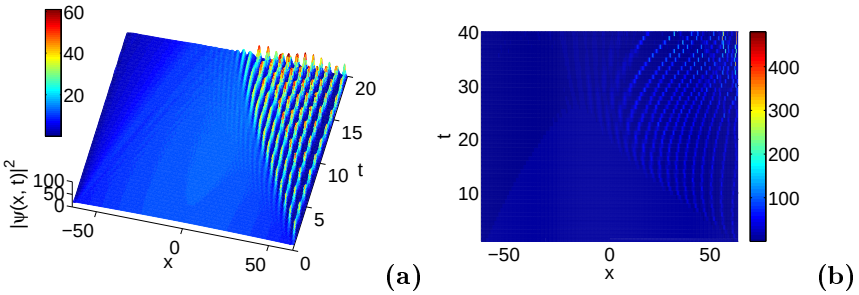


**Figure 27**: Spatiotemporal evolution of the condensate's density. (a) generation of breather solitons. (b) deviation of the trail of breather solitons to the right due to repulsive interactions in the condensate. Parameters are $a_0 = -0.00049$, $\Phi_0 = 3.5$, $\varepsilon = 0.01$, $K = 0.12$, $\tau = 0.00001$, $\gamma = 0.001$

observe in Fig. 27(a) that a train of breather solitons is created, while Fig. 27(b) shows that the trail of the train of bright solitons is deviated towards the right. Since parameters in Figs. 27(a)-(b) are the same as in Fig. 25(a) except $a_0 = 0.003$, we suggest that the repulsive two-body interatomic interactions are responsible for the curvature to the right of the train of solitons observed. This is a salient feature of repulsive condensates that shows a clear difference in the dynamics with attractive condensates that move towards the left side of the axial potential.

With the inclusion of the linear potential, we understand that it can be used to alleviate, or either stop the instability of the system arising due to the small perturbation. The initial envelop wave only oscillates, but does not break up into a train of solitons. Figure 28(a) represents an envelop wave stabilized by the linear potential. Hence, the linear potential can be used in the management of the stability of matter waves. Nevertheless, the creation of solitons is possible, although the linear stability analysis becomes less valid. We display in Fig. 28(b) a train of five solitons created by a strong perturbation of the initial continuous wave. What is fascinating with the train of solitons generated in Fig. 28(b), is that the dynamics of solitons are quite similar with the dynamics of approximate analytical solutions obtained with the variational analysis developed below.

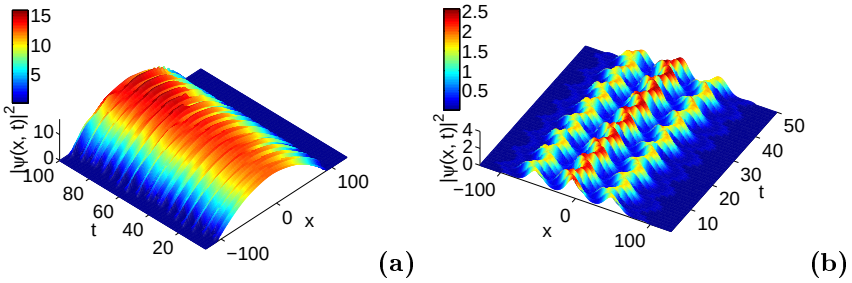


**Figure 28**: Spatiotemporal evolution of the condensate's density. (a) $a_0 = -0.00049$, $\Phi_0 = 3.5$, $\varepsilon = 0.01$ $\lambda = 2$; the linear potential alleviates the instability of an unstable continuous envelop wave. (b) $a_0 = -0.00049$, $\phi_0 = 1$, $\varepsilon = 0.5$ $\lambda = 2$; generation of multiple solitons by a strong perturbation. Other parameters are the same as in Fig. 27(b).

### 3.3.5 Patterns formation in two-component condensates with three-body interatomic interactions

**(a). Model and analytical results**

We consider two-component Bose-Einstein condensates with two- and three-body interatomic interactions, in the framework of the coupled mean-field GPEs, for the macroscopic wavefunctions of the two-species

$$\begin{aligned} \imath\frac{\partial\psi_j(r,t)}{\partial t} &= -\frac{\eta_{1j}}{2}\nabla^2\psi_j(r,t) + \sum_{l=1}^{2} g_{jl} \mid \psi_l(r,t) \mid^2 \psi_j(r,t) + \sum_{l=1}^{2} \chi_{jl} \mid \psi_l(r,t) \mid^4 \psi_j(r,t) \\ &\quad +2\chi_{j(3-j)} \mid \psi_{3-j}(r,t) \mid^2 \mid \psi_j(r,t) \mid^2 \psi_j(r,t), \qquad j = 1,2. \end{aligned} \tag{3.50}$$

where $\nabla^2 \equiv \frac{\partial^2}{\partial x^2} + \frac{\partial^2}{\partial y^2} + \frac{\partial^2}{\partial z^2}$. Equations (3.50) have been reduced to a dimensionless form as in [39] by setting $\hbar = 1$. The energy and length units are $\hbar\omega_1/2$, and $\sqrt{\hbar/(m_1\omega_1)}$, respectively. The quantities $\omega_j$, and $m_j$ represent the frequencies of the traps and the mass of each specie, respectively. The wave functions are normalized as $N_j = \int_{-\infty}^{+\infty} \mid \psi_j(r,t) \mid^2 dr$, $N_j$ being the number of particles of the specie $j$. The two-body interatomic interaction coefficients are $g_{jl} = 4\pi(a_{jl}/\sqrt{\hbar/(m_1\omega_1)})(m_1/\mu_{jl})$, with $\mu_{jl} = m_j m_l/(m_j + m_l)$. Parameters $a_{jl}$ account for the two-body interatomic interactions between like and unlike species. In the following, the strengths of the two-body intraspecies interactions are denoted $g_{jj} = g_j$, while the strengths of the two-body interspecies interactions are denoted $g_{jl} = g$ $(j \neq l)$. This implies that $g_{12} = g_{21} = g$. The coefficients $\chi_{jl}$ characterize the intensity of the quintic nonlinearities between like and unlike species. For the sake of simplicity, the quintic intraspecies nonlinearities shall be written as $\chi_{jj} = \chi_j$, and the quintic interspecies nonlinearities shall take the form $\chi_{jl} = \chi$ $(j \neq l)$. This means that $\chi_{12} = \chi_{21} = \chi$. The external potentials in which each specie is confined are dropped in Eqs.(3.50), meaning that the effects of the potentials on the boundaries are negligible [39, 43]. In such a situation, the size of the boundaries of the two condensates are much smaller than that of the Thomas-Fermi radius [39, 43]. Equations (3.50) describe the dynamics of two-component condensates with two- and three-body interatomic interactions. In the absence of the three-body

interatomic interactions, the set (3.50) is reduced to the coupled cubic GPEs governing the evolution of two-component condensates with only two-body interatomic interactions [39, 43]. In what follows, we consider that the two-component condensate is loaded in a one dimensional setting, such that Eqs.(3.50) become

$$\begin{aligned}
\imath\frac{\partial\psi_1(x,t)}{\partial t} &= -\frac{1}{2}\frac{\partial^2}{\partial x^2}\psi_1(x,t) + g_1 \mid \psi_1(x,t)\mid^2 \psi_1(x,t) + g \mid \psi_2(x,t)\mid^2 \psi_1(x,t) \\
&\quad +\chi_1 \mid \psi_1(x,t)\mid^4 \psi_1(x,t) + \chi \mid \psi_2(x,t)\mid^4 \psi_1(x,t) \\
&\quad +2\chi \mid \psi_1(x,t)\mid^2 \mid \psi_2(x,t)\mid^2 \psi_1(x,t) \qquad (3.51)\\
\imath\frac{\partial\psi_2(x,t)}{\partial t} &= -\frac{\eta}{2}\frac{\partial^2}{\partial x^2}\psi_2(x,t) + g_2 \mid \psi_2(x,t)\mid^2 \psi_2(x,t) + g \mid \psi_1(x,t)\mid^2 \psi_2(x,t) \\
&\quad +\chi_2 \mid \psi_2(x,t)\mid^4 \psi_2(x,t) + \chi \mid \psi_1(x,t)\mid^4 \psi_2(x,t) + \\
&\quad 2\chi \mid \psi_2(x,t)\mid^2 \mid \psi_1(x,t)\mid^2 \psi_2(x,t),
\end{aligned}$$

where the mass ration is defined as $\eta_{1j} = m_1/m_j$ such that $\eta_{11} = 1$, $\eta_{12} = \eta$ [43]. Equations (3.49) can be derived from the Hamiltonian given by [154]

$$H = H_{\psi_1} + H_{\psi_2} + H_{int}, \qquad (3.52)$$

where

$$H_{\psi_1} = \int (\frac{1}{2}|\nabla\psi_1|^2 + \frac{1}{2}g_1|\psi_1|^4 + \frac{1}{3}\chi_1|\psi_1|^6)dr, \qquad (3.53)$$

$H_{\psi_2}$ has a same form as $H_{\psi_1}$ except that the field $\psi_1$ is replaced by the field $\psi_2$, and the interaction part of the Hamiltonian takes the form

$$H_{int} = \int [-g|\psi_1|^2|\psi_2|^2 + \chi(|\psi_1|^4|\psi_2|^2 + |\psi_1|^2|\psi_2|^4)]dr. \qquad (3.54)$$

In order to study the modulational instability of the coupled GPEs given by Eq.(3.51), we consider perturbed plane wave solutions of each component of the form

$$\psi_j(x,t) = (\mid \psi_j^0 \mid + \varepsilon_j(x,t))\exp(\imath\phi_j(t)), \qquad j = 1,2, \qquad (3.55)$$

where $\mid \psi_j^0 \mid$ ($\mid \psi_j^0 \mid^2 = n_j$) is a real constant number, $\varepsilon_j(x,t)$ accounts for a small complex perturbation of the wave envelop with, $\varepsilon_j(x,t) << \mid \psi_j^0 \mid$, and $\phi_j(t)$ is the time-dependent phase shift. Performing a linear stability analysis with $\phi_j(t) = -(g_j n_j + g n_{3-j} + \chi_j n_j^2 + \chi n_{3-j}^2)$ [155], we derive the partial differential equations of the perturbations

$$\begin{aligned}
&\imath\frac{\partial\varepsilon_j}{\partial t} + \frac{\eta_{1j}}{2}\frac{\partial^2}{\partial x^2}\varepsilon_j - g_j n_j(\varepsilon_j + \varepsilon_j^*) - g n_{3-j}^{1/2} n_j^{1/2}(\varepsilon_{3-j} + \varepsilon_{3-j}^*) - 2\chi_j n_j^2(\varepsilon_j + \varepsilon_j^*) \\
&-2\chi n_{3-j}^{1/2} n_j^{1/2}(n_{3-j} + n_j)(\varepsilon_{3-j} + \varepsilon_{3-j}^*) - 2\chi n_{3-j} n_j(\varepsilon_j + \varepsilon_j^*) = 0, \qquad (3.56)
\end{aligned}$$

for $j = 1, 2$. Then, we assume that each perturbation satisfies the relation

$$\varepsilon_j = u_j\cos(Kx - \Omega t) + \imath v_j\sin(Kx - \Omega t), \qquad (3.57)$$

where $u_j$ and $v_j$ are real constants, and apply the procedure used above. The dispersion relation yields

$$(\Omega^2 - E_1)(\Omega^2 - E_2) = X^2, \tag{3.58}$$

with

$$\begin{aligned} E_j &= \frac{1}{4}K^2(K^2 + 4g_j n_j \eta_{1j} + 8n_j^2 \eta_{1j}\chi_j + 8\chi n_{3-j} n_j), \quad j = 1, 2 \\ X^2 &= 4n_1 n_2 \eta K^4 [\frac{1}{4}g^2 + \chi(n_1 + n_2)(g + \chi(n_1 + n_2))]. \end{aligned} \tag{3.59}$$

The pure gain of instability is

$$G = [-\frac{1}{2}(E_1 + E_2) + \frac{1}{2}\sqrt{(E_1 + E_2)^2 + 4(X^2 - E_1 E_2)}]^{1/2}. \tag{3.60}$$

Equations (3.58) and (3.60) are the generalizations to cubic-quintic coupled GPEs of the dispersion relation and the purely growing instability gain, respectively, obtained in [43] in the case of two-component condensates with only two-body interatomic interactions. Basically, the three-body interatomic interactions may be attractive ($\chi_j < 0$, $\chi < 0$) or repulsive ($\chi_j > 0$, $\chi > 0$), $j = 1, 2$. This means that, even in the absence of all the interspecies interactions, $\Omega_j = \pm\sqrt{E_j}$ ($j = 1, 2$) may be a pure imaginary number. Hence, the inclusion of the three-body interatomic interactions destabilizes the system.

For repulsive three-body intraspecies interactions, the pure gain vanishes when the strength of the three-body interspecies interactions lies in the region $[-\chi^1, +\chi^1]$ (the expression of $\chi^1$ is given in Appendix F). An inspection of Fig. 29(a) which displays the gain of instability as

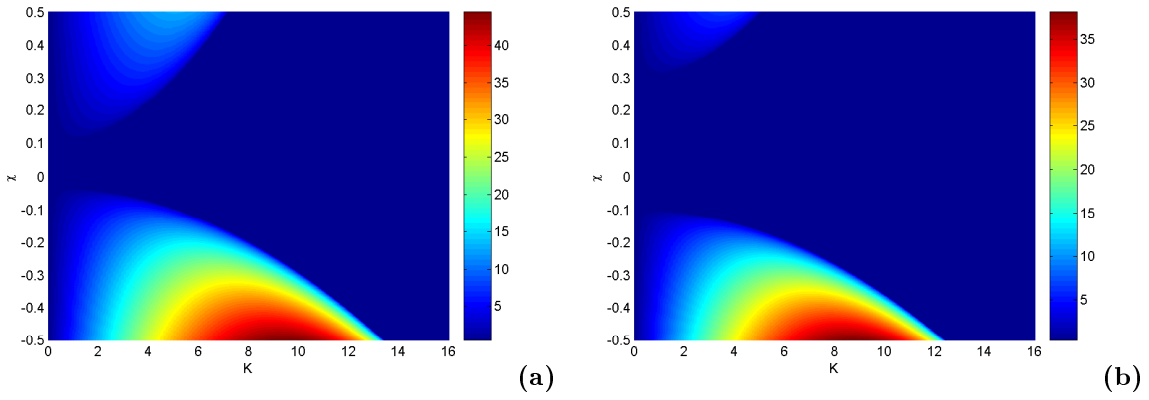


**Figure 29**: Instability gain versus $K$ and $\chi$, with repulsive three-body intraspecies interactions. (a) $\chi_1 = \chi_2 = 0.1$. (b) $\chi_1 = \chi_2 = 0.2$. Other parameters are $g_1 = g_2 = g = 0$, $n_1 = n_2 = 4$, $\eta = 1$.

functions of the three-body intraspecies interactions $\chi$ and the wave numbers $K$, with $\chi_1 = \chi_2 = 0.1$ shows that small attractive and large repulsive three-body interspecies interactions enhance the instability of the two-component condensate, respectively. Furthermore, increasing the strengths of the three-body intraspecies interactions not only reduces the amplitude of the gain and the unstable wave numbers region, but also enlarges the gap region where the gain

vanishes, as one can see in Fig. 29(b) ($\chi_1 = \chi_2 = 0.3$). Hence, repulsive three-body intraspecies interactions alleviate the instability of the two-component condensate.

For the case where the three-body intraspecies interactions are both attractive, Fig. 30 presents the modulational instability gain for $\chi_1 = \chi_2 = -0.1$. A Comparison of Fig. 29(a) and Fig. 30(a) and an analysis of Fig. 30(b) ($\chi_1 = \chi_2 = -0.3$) indicate that attractive three-body intraspecies interactions appear to more destabilize the two-component condensate system than repulsive ones.

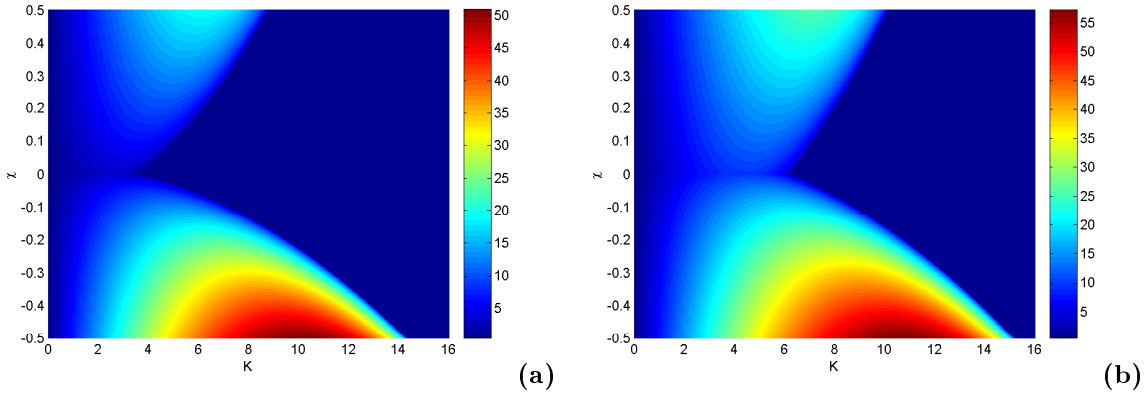


**Figure 30**: Instability versus $K$ and $\chi$, with attractive three-body intraspecies interactions. (a) $\chi_1 = \chi_2 = 0.1$. (b) $\chi_1 = \chi_2 = 0.2$. Other parameters are $g_1 = g_2 = g = 0$, $n_1 = n_2 = 4$, $\eta = 1$.

A parallel between Figs. 30 and 31 confirms that the competition between the two- and three-body interatomic interactions drastically modifies the modulational instability gain spectra. Moreover, attractive two-body interspecies interactions enlarge the unstable modes region and values of the three-body interspecies interactions for which the mixture is unstable (compare Fig. 31(a) ($g < 0$) and Fig. 31(b) ($g > 0$)).

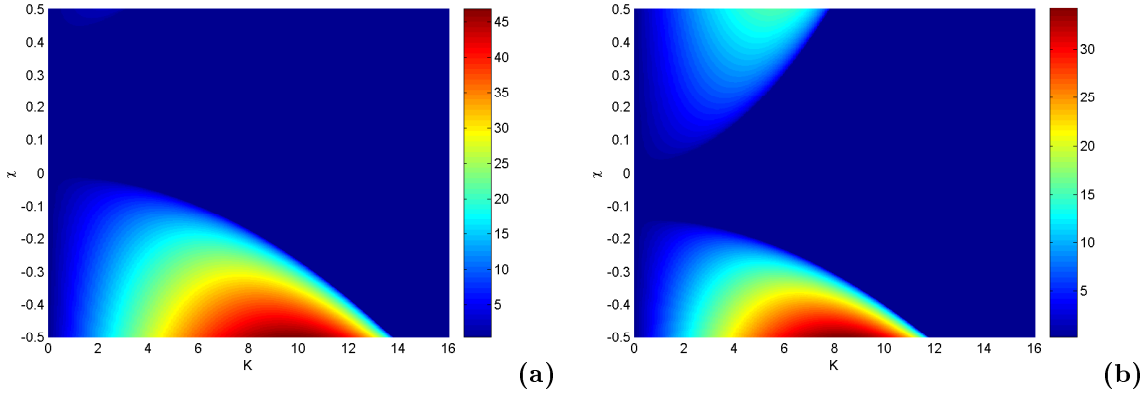


**Figure 31**: (a) $g = -1.6$. (b) $g = 1.6$. Other parameters are the same as those in Fig. 24(a) except $g_1 = 1.1$, $g_2 = 0.9$.

**(b). Numerical simulations of two-component condensates with two- and three-body interatomic interactions**

Direct numerical integrations of Eqs. (3.51) are performed, with the MATLAB toolbox PDEPE with vanishing flux boundary conditions on the spatial domain of integration. The initial conditions are uniform waves periodically perturbed

$$\psi_j(x,t) = 1 + \varepsilon \cos(Kx), \qquad j = 1, 2. \tag{3.61}$$

We plot in Fig. 32 the temporal evolution of the maxima amplitude, for four different values of the strengths of the three-body interspecies interactions, the values of the strengths of the three-body intraspecies interactions being fixed. The global behavior of maxima amplitude in Fig. 32(a) ($\chi_1 = \chi_2 = 0.1$) implies that small attractive three-body interspecies constants more favor the loss of stability than large repulsive ones. Furthermore, a comparison of Figs. 32(a)-(b) shows that an increase of the strength of the repulsive three-body intraspecies interactions soften the instability. These results are in good agreement with their analytical counterparts. In the case of binary condensates with attractive three-body intraspecies interactions (see Figs. 32(c)-(d)), since the magnitudes of maxima amplitude are higher than those in Figs. 32(a)-(b), one deduces that attractive three-body intraspecies interactions increase the instability, while repulsive ones soften the instability. This result once again corroborates the analytical prediction. The modulational instability of the two-component condensate is also affected by the inclusion of the two- and three-body interactions. In Fig. 32(e) where parameters correspond to those in Fig. 31, the binary condensate is more destabilized with attractive two-body interspecies coupling constants than with repulsive ones. A similar feature has been obtained with the linear stability analysis.

Plotting the maxima amplitude one can identify the most unstable component of the mixture as in Fig. 33 where parameters are the same as Fig. 29(a) except $\chi_2 = -0.1$. In Fig. 33(a) the second component with attractive three-body intraspecies interactions is more unstable than the first one with repulsive three-body intraspecies interactions. In Fig. 33(b) the component with attractive two-body interactions is much unstable than the one with repulsive two-body interspecies interactions. For parameters corresponding to Fig. 29, Fig. 34(a) ($\mid \psi_1(x,t) \mid^2$) and Fig. 34(b) ($\mid \psi_1(x,t) \mid^2$) illustrate that the densities in each component of the mixture have almost the same behavior, exhibit mutual interactions, and emerge after the critical time $t_C \approx 60$. In the case where the three-body intraspecies interactions have opposite signs, the instability of the system increases and solitons appear earlier ($t_C \approx 37.24$) as depicted by Figs. 34(c)-(d).

An observation of Fig. 35(a) where $g_1 = 1.1$, $g_2 = 0.9$, $g = -1.6$, $\chi_1{=}\chi_2{=}\chi{=}0$, and Fig. 35(b) with same parameters as in Fig. 35(a) except $\chi_1 = \chi_2 = 0.1$, $\chi = 0$, shows that the inclusion of repulsive three-body intraspecies interactions not only induces the loss of stability of the mixture, but also modifies the trail of trains of solitons generated. At the beginning of

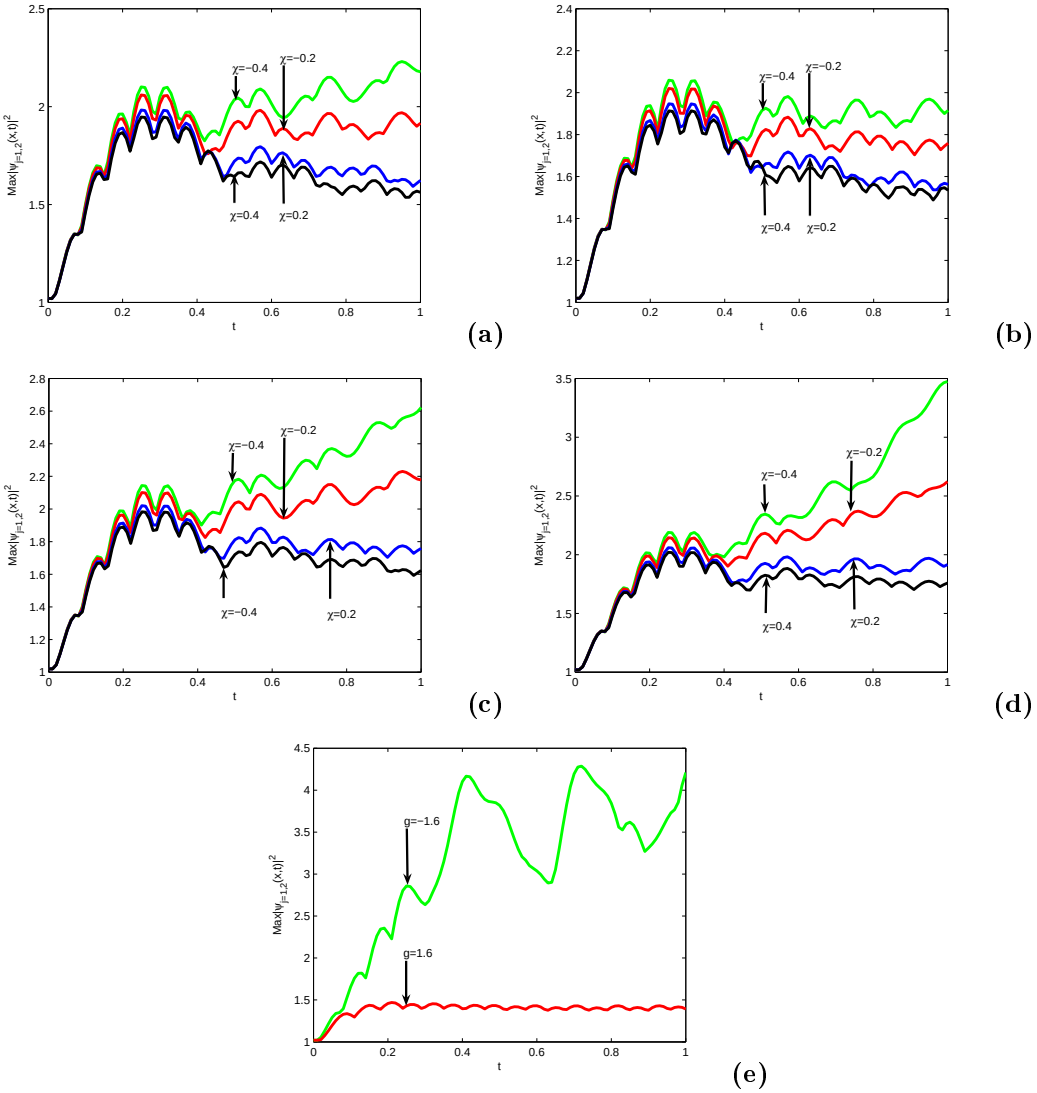


**Figure 32**: Temporal evolution of maxima amplitude. (a) $\chi_1 = \chi_2 = 0.1$. (b) $\chi_1 = \chi_2 = 0.2$. (c) $\chi_1 = \chi_2 = -0.1$. (d) $\chi_1 = \chi_2 = -0.2$. (a)-(b) Same parameters as in Fig. 29. (c)-(d) Same parameters as in Fig. 30. Other parameters in panel (e) are as in Fig. 31.

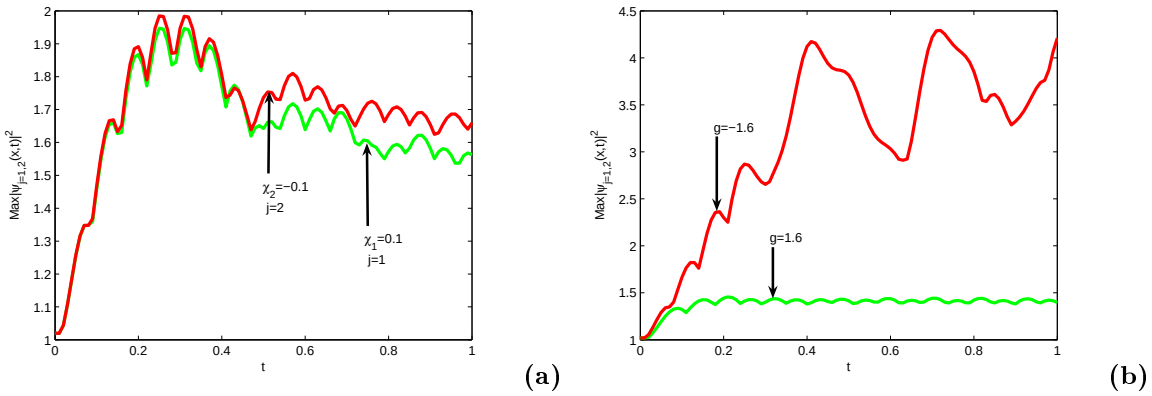


**Figure 33**: Temporal evolution of maxima amplitude $Max|\psi_j(x,t)|^2$. The second component with $\chi_2 = -0.1$ appears to be the most unstable. Other parameters selected are identical to those in Fig. 29(a).

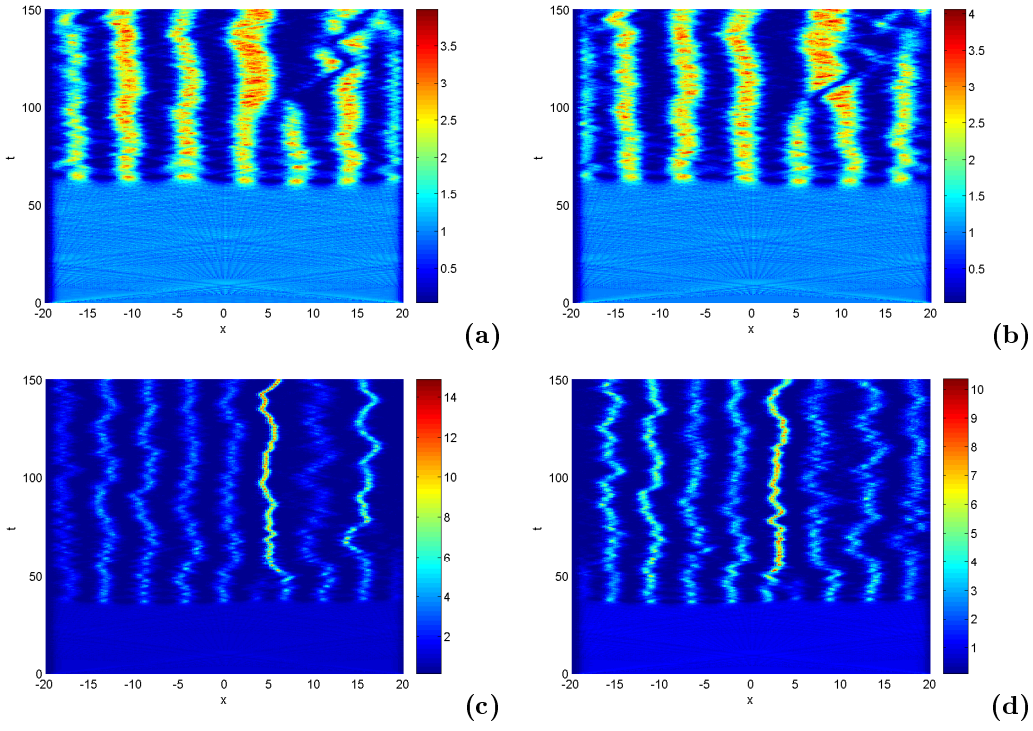


**Figure 34**: Density $|\psi_j(x,t)|^2$ plots of the two components of the binary condensate. (a) $j = 1$, (b) $j = 2$. (c) $j = 2$, $\chi_2 = 0.1$. (d) $j = 1$, $\chi_1 = 0.1$. Other parameters used are the same as in Fig. 31(a).

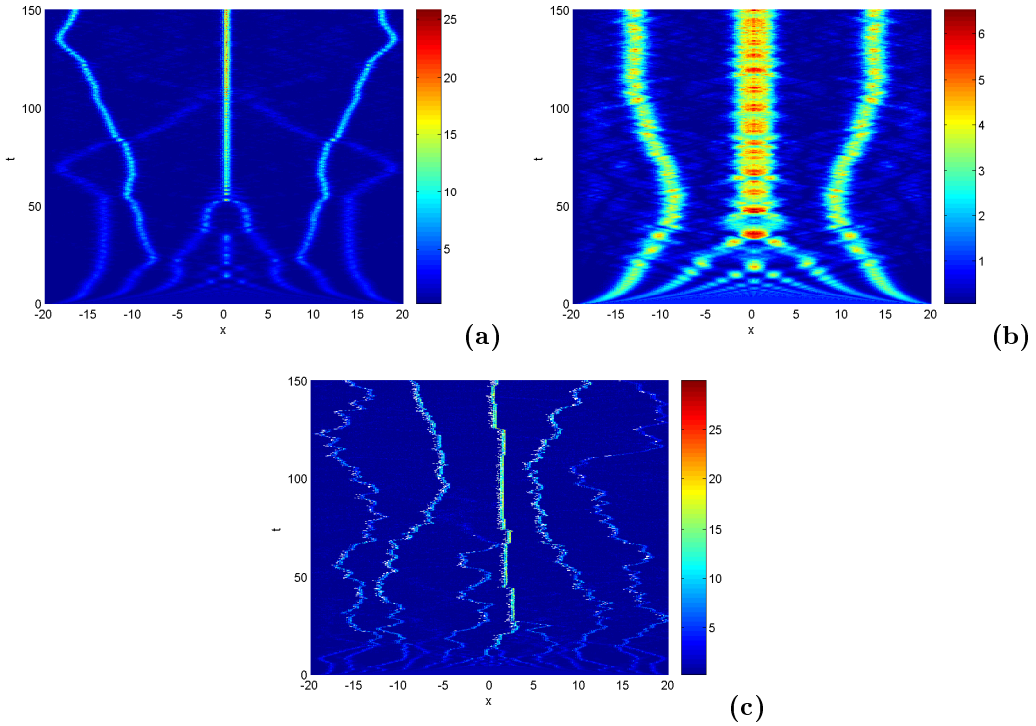


**Figure 35**: Evolution of the density of component 1. (a) $\chi_1 = \chi_2 = \chi = 0$. (b) $\chi_1 = \chi_2 = -0.1$, $\chi = 0$. (c) $\chi_1 = \chi_2 = 0.1$, $\chi = -0.4$. In all panels, $g_1 = 1.1$, $g_2 = 0.9$, $g = -1.6$.

the evolution (see Fig. 35(a)), the train of solitons evolve symmetrically around the center of the spatial domain, i.e., $x = 0$, and solitons are almost regularly spaced, while in Fig. 35(b), the trail of the train of solitons is altered, and the number of solitons is higher. Solitons that are near the center of the cigar-axis attract each others and collide elastically, their collisions yield a soliton which amplitude increases with time. This process suggests a compression of solitons that are near the position $x = 0$, due to multiple superpositions. For the solitons at the edges of the train, they separate with their neighbors, and move away from the center of the train as time increases. The inclusion of three-body interspecies interactions more destabilizes the mixture as one can see in Fig. 35(c) where we have added $\chi = -0.4$. A comparison of Figs. 35(a)-(c) shows that the inclusion of three-body interspecies interactions breaks up the symmetry of the train of solitons, and increases the number of solitons created. As time increases, solitons created collide, the collisions giving rise to the superposition of wavefunctions, increasing the density of the solitons created which number drastically reduces (see Fig. 35(c)).

In the previous cases, the mass ratio, $\eta$, was fixed at $\eta = 1$, meaning that the binary condensate consists of two identical atomic species in two different spin states. In a binary condensate made of two-different atomic species, $\eta$ can be greater than 1. In such a case, a scrutiny analysis of Fig. 36 where $\eta = 2$ proves that an increase of the mass ration brings non trivial effects which are (i) a destabilization of the mixture, (ii) the distortion of the trail of

the train of solitons emerging after the development of modulational instability. Similar results have been reported in [43].

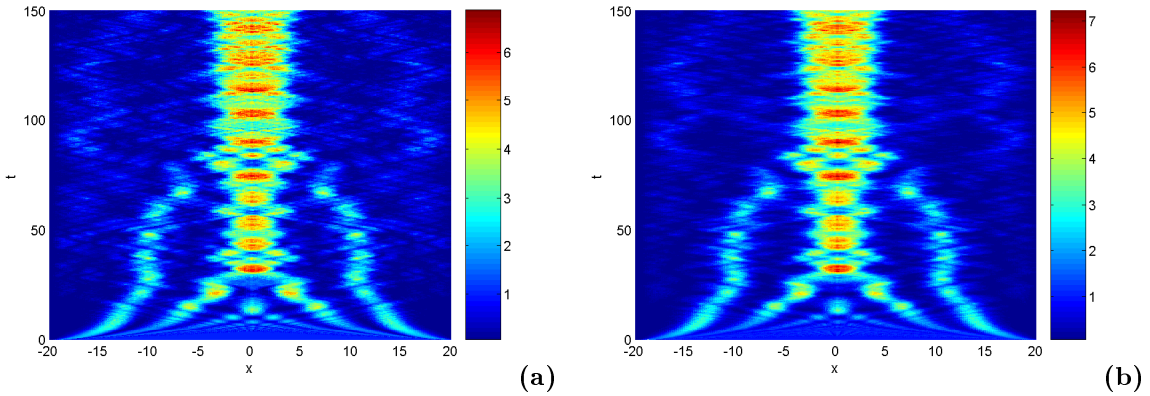


**Figure 36**: Effects of the mass ration $\eta = 2$ on the dynamics of the bright soliton structures. Contour plots of (a) $\mid \psi_1(x,t) \mid^2$, (b) $\mid \psi_2(x,t) \mid^2$. Other parameters are as in Fig. 35(d).

The modulational instability induced patterns are highly sensitive to the intensity of the two-body intraspecies interactions, though one takes into account the three-body interactions. As depicted by Figs. 37(a)-(b) where $g_1 = 0.9$, $g_2 = 1$, and $g = -1.6$, a small change of the strengths of the two-body intraspecies interactions significantly modifies the shape of the train of solitons in comparison to that obtained in Fig. 36(b). Furthermore, changing the sign of the two-body interspecies interactions induces a radical change on soliton patterns that emerge due to modulational instability as confirmed by the contour plot of the densities in both the components displayed in Figs. 37(c)-(d). Besides, the competition between repulsive and attractive three-body intraspecies interactions may straightens all the solitons created as shown in Fig. 38, where $g = -1.2$, $\chi_1 = 0.1$, and $\chi_2 = -0.1$.

Equation (3.50) represents the general form of two- and three-body interactions in two-component systems and was first introduced in [154] in the context of fiber optics. It has been shown that solitons with equal masses always attract each other in two- and three-dimensional geometries. This part of the work considers a one dimensional geometry, as one can see in Figs. 35(d)-(f), in Fig. 33 as well as in Figs. 37(a)-(b), the interactions among solitons with the same masses are attractive for solitons located near the center of the axial potential. A result consistent with the prediction of [154]. In addition, according to the work of [154], the interaction between two solitons with different masses may be attractive or repulsive depending on sign of the two-body interspecies interactions alias cross-phase modulation. The latter interaction is attractive for a repulsive two-body cross-phase modulation, while it is repulsive for attractive two-body cross-phase modulation. The three-body cross-phase modulation interactions are only a small correction. Such a similar feature is observed in Fig. 35(d) where the interactions between the heavy solitons at the border of the train with the light ones are repulsive (the two-

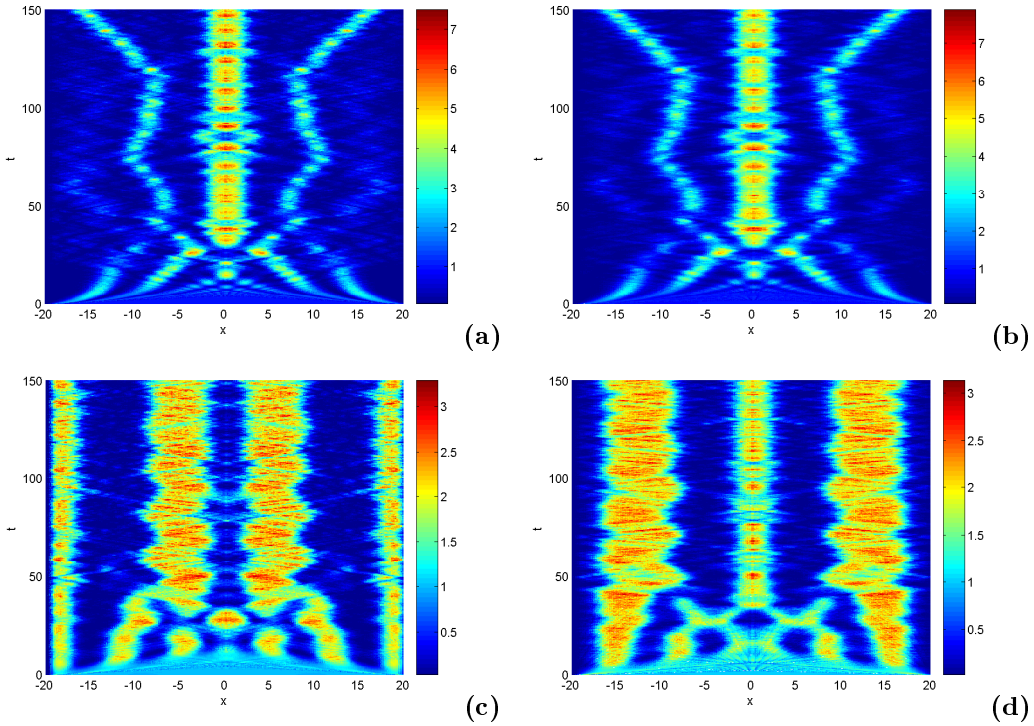


**Figure 37**: (a) $\mid \psi_1(x,t) \mid^2$, $g_1 = 0.9$, $g_2 = 1$, $g = -1.6$, $\chi_1 = \chi_2 = 0.1$, $\chi = 0$. (b) $\mid \psi_2(x,t) \mid^2$ with same parameters as in (a). (c) $\mid \psi_1(x,t) \mid^2$, (d) $\mid \psi_2(x,t) \mid^2$, same parameters as in (a) except $\chi = 1.6$.

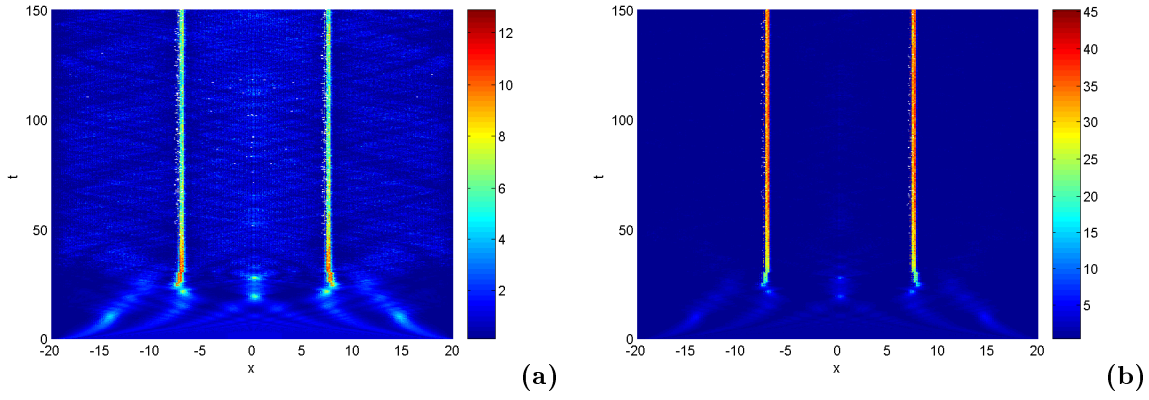


**Figure 38**: Contour plots of densities. (a) $\mid \psi_1(x,t) \mid^2$, (b) $\mid \psi_2(x,t) \mid^2$. Parameters are $\eta = 1$, $K = \frac{1}{3}$, $g_1 = g_2 = 1$, $\chi_1 = 0.1$, $\chi_2 = -0.1$ $g = -1.2$, and $\chi = 0$.

body interspecies interactions are attractive). However, in some cases, the interaction between heavy and light solitons does not follow the type of two-body interspecies interactions. In Fig. 36, the interactions between the light solitons at the edges of the train with the heavy soliton at center of the train is attractive, though attractive two-body interspecies interactions. The analytical results obtained in [154] is no longer valid. The same situation also applies for the interactions among light and heavy solitons of Fig. 37. The three-body interactions significantly contribute to modify the type of interactions among solitons in the train. An explanation may be the following: in [154] a linear superposition of solitons in each component is considered, while in our numerical simulations, in the unstable regions, nonlinear perturbations are no longer negligible. Indeed, perturbations arising from three-body interactions may grow and lead to a profound modification of the effective interaction potential between heavy and light solitons. This issue needs more analytical clarifications in future works.

## 3.4 Exact dynamics of Bose-Einstein condensates with two- and three-body interatomic interactions

It is well known that the three-body interactions can play an important role on the dynamics of condensates [33, 34, 156]. Since the seminal work of Serking and Hasegawa [157], many works have been devoted to the construction of new soliton solutions of nonlinear Schrödinger equation types with versatile time, space, or space-time nonlinearities [34, 119, 157, 158, 159].

### 3.4.1 Stable Bright solitons in the delayed nonlinear response of Bose-Einstein condensates

We aim to construct analytical bright soliton solutions of the modified GPE II with a complex potential. To this end, we resort the variational approach presented in chapter 2 and rewrite the modified GPE II in the appropriate form

$$\begin{aligned} &\imath\frac{\partial\psi(x,t)}{\partial t}+\frac{\partial^2\psi(x,t)}{\partial x^2}+2a(t)|\psi(x,t)|^2\psi(x,t)\\ &-(\alpha x^2+\lambda x)\psi(x,t)+12\tau|\psi(x,t)|^4\psi(x,t)\\ &=\imath(\gamma-4\sqrt{\tau}(|\psi(x,t)|^2)_x)\psi(x,t)\\ &=R(\psi(x,t),\psi(x,t)^*). \end{aligned} \tag{3.62}$$

The Lagrangian density of the conservative part of Eq.(3.62) is

$$\begin{aligned} \ell_C &= \frac{\imath}{2}(\psi(x,t)^*_t\psi(x,t)-\psi(x,t)_t\psi(x,t)^*)+|\psi(x,t)|^2-a(t)|\psi(x,t)|^4-4\tau|\psi(x,t)|^6\\ &\quad+(\alpha x^2+\lambda x)|\psi(x,t)|^2. \end{aligned} \tag{3.63}$$

Inserting Eq.(2.2) into Eq.(3.63) and integrating over the spatial coordinate yields the conservative effective Langrangian

$$L_C = N[\phi_t + k^2 + \frac{1}{4}(b_t + 2b^2 + 2\alpha)W^2 + \frac{1}{2W^2} - \frac{aN}{\sqrt{2\pi}W} - \frac{4\tau N^2}{\pi\sqrt{3}W^2}]. \tag{3.64}$$

Using the formula (2.6), we compute the variational equations

$$b = \gamma \tag{3.65}$$

$$k = \frac{4\sqrt{\tau}N}{\sqrt{\pi}W} \tag{3.66}$$

$$\phi_t = \frac{2aN}{\sqrt{2\pi}W} + \frac{12\tau N^2}{\pi\sqrt{3}W^2} - \frac{1}{2W^2} - \frac{16\tau N^2}{\pi W^2} - \frac{1}{2}(\gamma^2 + \alpha)W^2. \tag{3.67}$$

The number of particles is given by $N = N_0 \exp(2\gamma t)$, $N_0$ being the number of particles at the initial time. Equation 3.65 implies that the chirp is related to the amplification or dissipation of the soliton. From Eq.(3.66) and Eq.(3.67) one infers that the linear and homogeneous phases, respectively, change with time and are related to the rate of exchange of atoms. Assuming a fixed width $W$, the soliton is compressed in the feeding regime.

**(a). Numerical stability of bright soliton solutions of the modified GPE II**

The numerical scheme used is the split-step Fourier method. A small amount of random white noise is inserted in order to bring out any instability that may be embedded in the solution.

The numerical simulations begin by considering the case of attractive condensates, with the linear potential being turned out. The initial condition inserted here is the bright soliton given by Eq.(2.2) with the variational parameters selected as $N = 13.82$, $W = 10$, $a_0 = 0.0001$. We display in Figs. 39(a)-(b) a comparison between the variational solution and the exact numerical one at specific times, and one realizes that both solutions agree very well. In addition, the magnitude of the condensate increases with increasing values of $\gamma$ as depicted in Fig. 39(c). These results well recover the variational solution, and was previously obtained with modulated solitons obtained via modulational instability. The spatiotemporal evolution of the condensate's density in Fig. 39(d) also reveals that our variational solution is dynamically stable. This suggests the possibility of controlling the creation of high density condensates in current experiments, without collapse. As well known, the variational approach becomes less valid for very large solitons as shown in Fig. 40. Though the stability of the initial Gaussian soliton is broken, there still remains a compensation between the dispersion and the nonlinearities, which leads to the creation of a time periodic breather soliton. In the regime of loss of atoms, the peaks of the breather soliton periodically form after the period $P = 156$ (see Fig. 40(a)), and the breather soliton created is also dynamically stable and robust as one can see in Fig. 40(b). Things are different for a condensate in the feeding regime. The breathing behavior may be observed for small widths ($W = 15$) and after a relatively shorter time of propagation ($t \approx 400$)

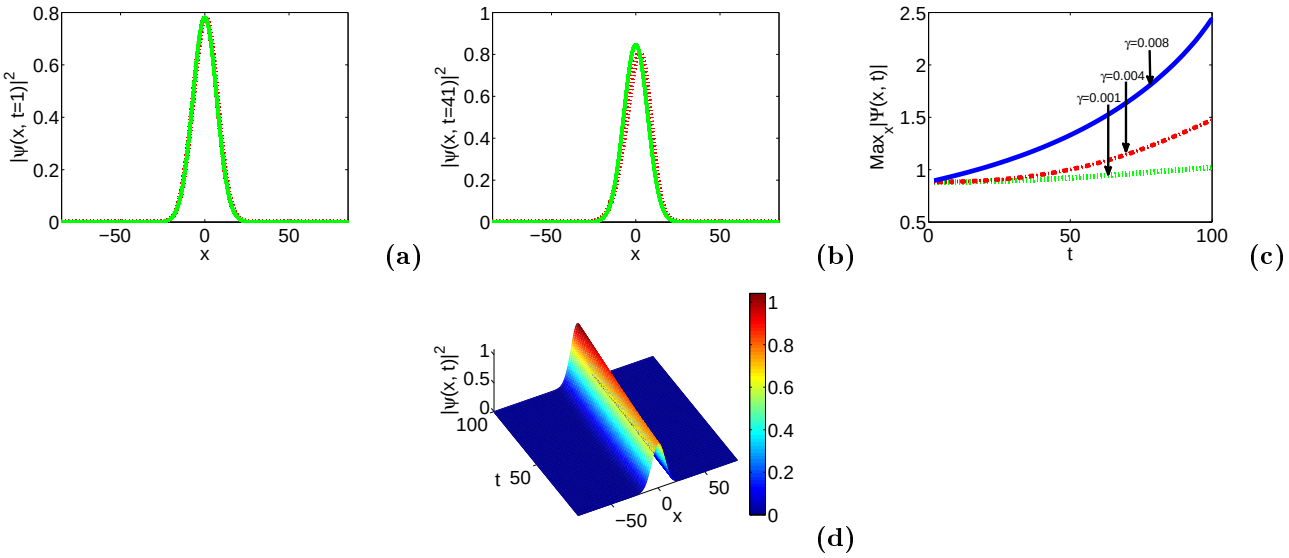


**Figure 39**: (a)-(b) Spatial comparisons between variational solution (solid line) and numerical solution (dotted line) at different times. (c) Feeding atoms to the condensate increases its density. (d) Stable dynamics of a bright soliton in the feeding regime. Parameters are $N = 13.82$, $W = 10$, $a_0 = 0.0001$, $\gamma = 0.001$. Other parameters are $\alpha = 0.0001$, $\tau = 0.00001$.

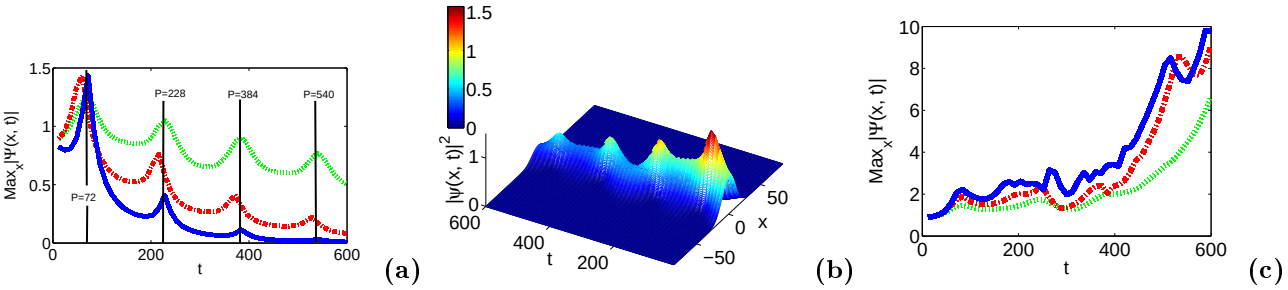


**Figure 40**: (a) Maxima amplitude of breather solitons for $\gamma = -0.001$, $W = 15$ dotted line $N = 20.73$, $W = 20$ dashed-dotted line $N = 207.64$, $W = 25$ solid line $N = 34.54$. (b) Sample of a dynamical stable breather for $\gamma = -0.001$, $W = 15$. (c) Same parameter as in (a) except $\gamma = 0.001$. Other parameters are as in Fig. 39.

(see Fig. 40(c)) the stability is lost. It is likely that, the feeding process plays an important role in the formation of the breather soliton, when the width of the initial condition is large. A soliton with a large width tends to spread due the dispersion, however, adding atoms to the condensate increases its density, meaning a growth of the intensity of the two- and three-body interatomic interactions. As time increases, the strengths of both the two- and three-body interactions increase too, and compensate the dispersion, preventing the collapse of the soliton.

One pitfall of our variational solution is that it fails to provide any information about effects of the linear potential on the properties of our solitons. However, some important effects of the linear potential can be examined numerically. We turn on the linear potential and insert the variational solution of Eq.(2.2) into the modified GPE II with parameters corresponding to Fig. 39. The linear potential induces a gradient field onto the condensate which constrains the soliton to move to the left (−x-direction) part of the axial axis for positive values of $\lambda$, while the soliton is shifted towards the right (+x-direction) for negative values of $\lambda$ (see Fig. 41(a)). Moreover, the linear potential also induces time oscillations which period decreases with increasing values of $\lambda$ (see Fig. 41(a) where $\lambda = 0.1$, $P = 72$ and Fig. 41(b) where $P = 30$ and $\lambda = 0.2$). In the case where the width of the soliton is large, the linear potential alleviates

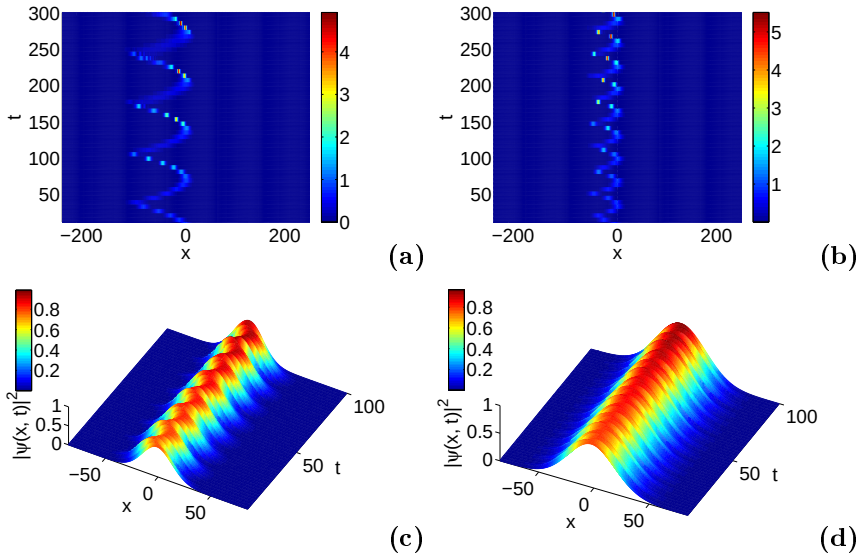


**Figure 41**: Effects of the linear potential on the dynamics of bright solitons in attractive condensates. (a) $\lambda = 0.1$, (b) $\lambda = 0.2$. (c) $W = 20$, $\lambda = 8$. (d) $W = 30$, $\lambda = 12$. Other parameters as in Fig. 39(d).

the instability, and may completely remove it, when the value of $\lambda$ is relatively high as can be seen in Fig. 41(c) ($W = 20$, $\gamma = 8$) and Fig. 41(d) ($W = 30$, $\gamma = 12$); the initial waves rapidly reshape and start oscillating due to the presence of the linear potential. Thus, the linear potential offers the possibility to create stable large solitons. This is an important feature since large solitons transport more energy than narrow ones.

We now confront our variational solution with the numerical exact one in the case of a

repulsive condensate. In Fig. 42(a) ($W = 10$, $N = 14$) the initial condition remains stable when starting with a relatively small density. On the contrary, Fig. 42(b) ($W = 10$, $N = 139$) shows that the initial condition drastically changes its shape, width, and height as time evolves when the initial density is relatively high. As in the attractive condensate case, the repulsive

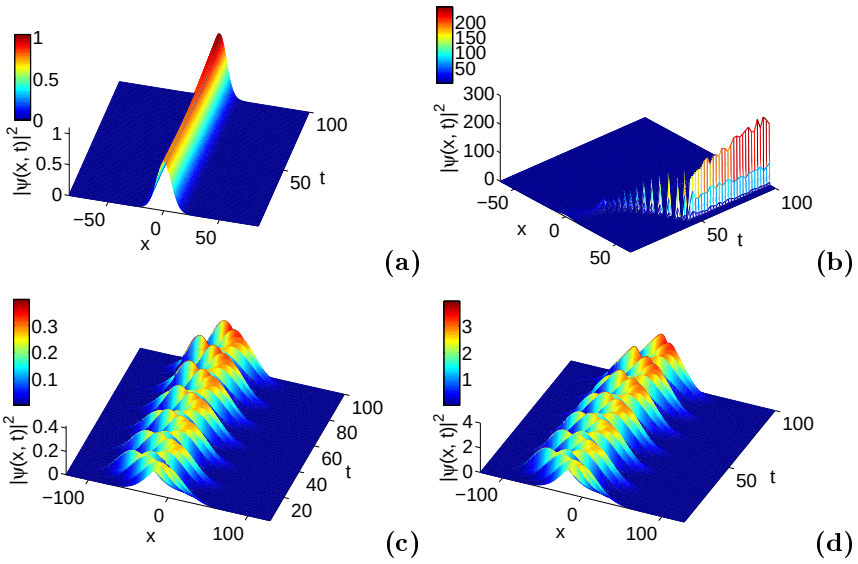


**Figure 42**: (a) $W = 10$, $N = 14$, $\lambda = 0$, stable low density condensate. (b) $W = 10$, $N = 139$, $\lambda = 0$, unstable high density condensate. (c) $W = 30$, $N = 14$, $\lambda = 0.8$. (d) $W = 30$, $N = 139$, $\lambda = 0.8$. Stabilization of unstable large solitons in repulsive condensates starting with low (c) and high (d) densities. In all panels, $a_0 = -0.00049$, $\gamma = 0.001$, $\tau = 0.00001$.

condensate also presents a breathing mode behavior for large solitons. However, turning on the linear potential softens the instability and may even lead to stabilization as depicted in Fig. 42(c) ($W = 30$, $N = 14$, $\lambda = 0.8$) and in Fig. 42(d) ($W = 30$, $N = 139$, $\lambda = 0.8$). Hence, the linear potential is a powerful tool that can be used to stabilize large and high density bright solitons in repulsive condensates.

### 3.4.2 Dynamics of Condensates with three-body interatomic interactions in a complex potential

#### (a). Model and analytical solutions

At the mean-field level, the dynamics of one dimensional Bose-Einstein condensates with both two- and three-body nonlinearities can be described by the following dimensionless GPE [27, 153]

$$\imath\Psi_t(x,t) + \Psi_{xx} - g(t)|\Psi(x,t)|^2\Psi(x,t) - \chi(t)|\Psi(x,t)|^4\Psi(x,t) - (\lambda x + \imath\gamma)\Psi(x,t) = 0, \quad (3.68)$$

where the spatial coordinate $x$ and the time coordinate $t$ are measured in units of $\varsigma = 1\mu m$ (the characteristic length unit in this type of experiment) and $m\varsigma^2/\hbar$ respectively, with $m$

being the mass per particle. The functions $g(t)$ and $\chi(t)$ represent the strengths of the two- and three-body interatomic interactions, respectively, while $\lambda$ corresponds to the strength of a linear potential (or the gravitational field), and $\gamma$ is the rate of exchange of atoms with the thermal cloud [123, 154].

In order to construct analytical solutions of Eq.(3.68), we use the F-expansion method presented in chapter 2, with the Lenard equation as auxiliary equation. So, we first choose the following trial solution of Eq.(3.68)

$$\Psi(x,t) = h(t)\phi(\xi)\exp(\imath\theta(x,t)), \tag{3.69}$$

where $h(t)$ is a real function of time $t$, $\xi = k(t)x + \eta(t)$ is the traveling wave variable, with $k(t)$ controlling the width of the condensate. The overall phase is $\theta = \Gamma(t)x + \Omega(t)$. The function $\Gamma(t)$ is the spatial frequency shift and $\Omega(t)$ is the homogeneous phase shift. Functions $h(t)$, $k(t)$, $\eta(t)$, $\Gamma(t)$, $\Omega(t)$, $\phi(\xi)$, $g(t)$, and $\chi(t)$ are unknown functions to be determined later. The auxiliary equation is the Lenard equation

$$(\frac{d\phi}{d\xi})^2 = b_0 + b_2\phi^2 + b_4\phi^4 + b_6\phi^6. \tag{3.70}$$

Following the steps of the F-expansion method described in the second chapter, Eq.(3.69) is inserted into Eq.(3.68), collecting coefficients of powers $x^n\phi^l$ ($n = 0, 1$, $l = 0, 1, 2, 3, 4, 5$) and $\sqrt{b_0 + b_2\phi^2 + b_4\phi^4 + b_6\phi^6}$, then setting each of the coefficients to zero yields the following set of over-determined partial differential equations where the 'dot' denotes the derivative with respect to time $t$

$$\begin{aligned}
\dot{h} - \gamma h &= 0 \\
h(\dot{\eta} + 2\Gamma k) &= 0 \\
h\dot{k} &= 0 \\
h(-\dot{\Omega} + k^2 b_2 - \Gamma(t)^2) &= 0 \\
h(\dot{\Gamma} + \lambda) &= 0 \\
h(2b_4k^2 - g(t)h^2) &= 0 \\
h(3k^2 b_6 - \chi(t)h^4) &= 0.
\end{aligned} \tag{3.71}$$

The solutions of the set (3.71) are found with MAPLE

$$h(t) = C_5 \exp(\gamma t) \tag{3.72}$$

$$\Gamma(t) = -\lambda t + C_4 \tag{3.73}$$

$$k(t) = C_3 \tag{3.74}$$

$$g(t) = \frac{2b_4 k^2(t)}{h^2(t)} \tag{3.75}$$

$$\chi(t) = \frac{3b_6 k^2(t)}{h^4(t)} \tag{3.76}$$

$$\eta(t) = -2C_3(\frac{-\lambda t^2}{2} + C_4 t) + C_2 \tag{3.77}$$

$$\Omega(t) = -(\frac{\lambda^2 t^3}{3} - C_4 \lambda t^2) + (b_2 C_3^2 - C_4^2)t + \frac{C_4^3}{3\lambda} + C_1. \tag{3.78}$$

Coefficients $C_1, C_2, C_3, C_4, C_5$ are free real constant parameters related to the initial condition of the wave, such as initial coordinate, velocity, shape, amplitude, and overall phase. From Eq.(3.73) and Eq.(3.78), one infers that the overall phase $\theta$ that is essential for reliable solutions does not depend on the rate of exchange of atoms between the condensed and uncondensed fractions. Adding or removing atoms from the condensate does not affect the direction of propagation of solutions. On the contrary, the linear potential deeply affects the overall phase $\theta$ of the condensate. Once the strength of the linear potential is fixed, as time evolves, the deviation of the linear frequency shift from its initial value $C_4$ is proportional to $\lambda$ (see Eq.(3.73)), meanwhile the variation of the homogenous phase clearly depends on $\lambda$ (see Eq.(3.77)). The parameter $b_2$ is related to the solution pattern (see Appendix C). Once the solution pattern is chosen, we can evaluate analytically the overall phase at each time from the initial condition. Hence, Eqs.(3.73)-(3.74) tell us how to adjust the strength of the linear potential in order to obtain a desired phase of the solution during evolution. Equations (3.72), (3.75), (3.76) imply that the two- and three-body interatomic interactions are time-dependent and also depend on the rate of exchange of atoms process with the thermal cloud. During evolution, the interplay between the condensate and the uncondensed fraction modulates the intensity of both two- and three-body interatomic interactions in the condensate. Furthermore, our solutions apply only for specific time-dependent behavior of the strengths of the two- and three-body interatomic interactions given by Eq.(3.75), and Eq.(3.76), respectively. Equation (3.75) is similar to the expression of the scattering length obtained by Kengne and Talla [162] ($g(t) = a_0 \exp(\lambda t)$, $a_0$ being a constant) that was derived from condensate experiments of Bradley, Sackett, Tollet, and Hulet [2, 163] where bright solitons were produced. It has been shown by Li, Li, Li, and Fu [141] that bright and dark solitons may be produced from the experiments of Khaykovich *et al.* and Strecker, Partridge, Truscott, and Hulet [11], provided that the strength of the two-body interatomic interactions takes a mathematical form close to that of Eq.(3.75). By inducing a time modulation, the exchange of atoms process considerably alters the two- and three-body

interatomic interactions. After selecting the values of $b_4$ and $b_6$ which are related to the solution pattern needed (see Appendix C), the experimenter knows how to manage both the two- and three-body interatomic interactions in the condensate. Therefore, we can know how to adjust the related operations to control the evolution of the solutions' overall phase as well as the two- and three-body interatomic interactions. We deduce from Eq.(3.74) that the width of a solution, $1/C_3$, remains constant during evolution leading to the compression of the condensate when atoms are added into the system, while an amplitude dissipation will be observed if atoms are ejected out of the system. On the other hand, the choice of the free parameters $b_4$ and $b_6$ ($b_4$ and $b_6$ may take a wide range of values) and that of $\gamma$ can be done in order to bring the condensate in the range of parameters used in current condensate experiments. Our approach may be used to found out exact solutions of the GPE with different trap geometries, and may also be generalized to higher dimensions as shown by Belobo Belobo, Ben-Bolie, and Kofane [164]. Considering the solutions of the Lenard equation (Eq.(3.70)) given in the Appendix C, we obtain a series of 22 families of exact solutions of Eq.(3.68) as

$$\Psi_{jp}(x,t) = h(t)\phi_{jp}(\xi)\exp[\imath(\Gamma(t)x + \Omega(t))]. \tag{3.79}$$

The integer $j$ corresponds to a family of solutions of Eq.(3.68) and varies from 1 to 11, while the integer $p$ accounts for a particular solution of a specific family and may take the values 1, 2, and 3.

One important aspect is the control of the kinetics of analytical solutions. Setting the traveling variable to zero, $\xi = 0$, enables to derive the position, velocity and the acceleration of the center-of-mass of the matter wave as

$$\begin{aligned} x &= -\lambda t^2 + 2C_4 t - C_2/C_3 \\ \dot{x} &= -2\lambda t + 2C_4 \\ \ddot{x} &= -2\lambda. \end{aligned} \tag{3.80}$$

The set (3.80) tells us important things about the behavior at mean of the solution, starting from the initial condition. First, the relevant physical parameters that affect the motion and velocity of the solution are the strength of the linear potential $\lambda$ and the solution's width. The center-of-mass of the condensate describes a parabola in the plane ($t$, $x$) with a constant acceleration, $2|\lambda|$, which is twice the strength of the linear potential $\lambda$. Secondly, we can compute the velocity and the acceleration of the center-of-mass of the solutions analytically. Thirdly, according to the Newton's second law, the last equation of the set (3.80) formally corresponds to the classical equation of motion of a particle moving in the effective potential $2\lambda x$ with total energy $(1/2)\dot{x}^2 + 2\lambda x$, its only equilibrium point being zero. Hence, the presence of the linear potential induces an acceleration of the condensate. At mean, our solutions are set into motion by the external potential which also induces a gradient on the condensate and finally modifies its trajectory. Besides, the solution (3.79) presents many kinds of solutions with rather different shapes. Let us examine in details some of them.

**(a1). Periodic solutions**

A periodic solution is obtained by setting $j = 2$ and $p = 1$ in Eq.(3.79) for $b_2 = -1$, $b_4 = 3$, $b_6 = -2$, $\gamma = -0.001$, $\lambda = 0.001$. The other parameters are $C_5 = 1$, $C_4 = 0$, $C_2 = 0$, $C_1 = 0$. The condensate is repulsive since $b_4 > 0$, and is in the regime of loss of atoms. We display in Fig. 43 the temporal variations of the strength of the two-body interatomic interactions (Fig. 43(a)), and the strength of the three-body interatomic interactions (Fig. 43(b)). Figure 43 provides a

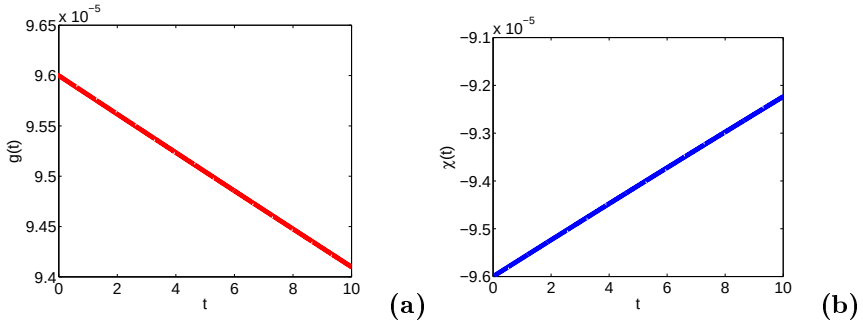


**Figure 43**: Temporal evolutions of (a) repulsive two-body, (b) attractive three-body interactions. Parameters are $\gamma = -0.001$, $C_3 = 0.1$, $b_4 = 3$, $b_6 = -2$.

way to understand how to modulate the two- and three-body interatomic interactions in order to obtain localized solutions. In Fig. 44(a), the spatiotemporal evolution of the condensate's density shows a spatial periodic localized wave packet. The number of solitons, $n$, with the width, $W_s$, available on the cigar-axis of length, $L$, can be determined with the formula

$$n = (\frac{L}{W_s})\alpha, \tag{3.81}$$

where $\alpha$ is a real parameter used to scale the value of $n$. In Figure 44(b) where $C_3 = 0.008$, the number of solitons is twice that in Fig. 44(a), in full agreement with the prediction of Eq.(3.81). It is possible to tune to the desired value the periodicity of the solution.

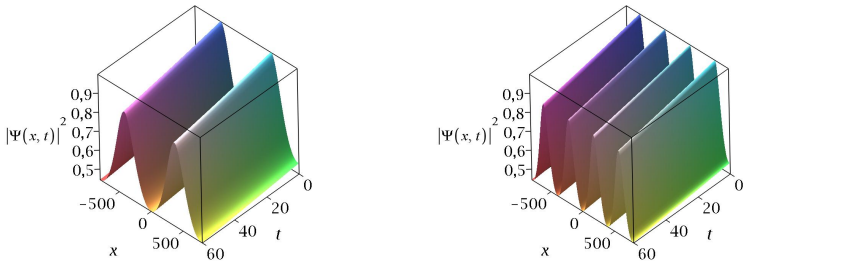


**Figure 44**: Periodic solution of Eq.(3.79) for $j = 2$, $p = 1$, $\lambda = 0.001$, $C_3 = 0.004$, $b_2 = -1$, $C_5 = 1$, $C_1 = C_2 = C_4 = 0$. (a) Spatiotemporal dynamics of the wave function in the regime of atoms loss, $\gamma = -0.001$. (b) Control of the number of solitons, $W = 0.008$. Other parameters as in Fig. 43.

**(a2). Dark profile solutions**

A dark solution is obtained if one fixes in Eq.(3.79) $j = 11$, $b_0 = -4$, $b_2 = -4$, $b_4 = 4$ (repulsive condensate), $b_6 = 4$, $\gamma = 0.001$, $C_3 = 0.1$. Figure 45 exhibits the dynamics of dark profile patterns for two different values of the linear potential's strength $\lambda$ (see panels (a) and (b)). The condensate is drifted towards $-x$-direction when $\lambda$ is positive (see Fig. 45(a) with $\lambda = 0.01$), while the condensate evolves towards $+x$-direction for a negative value of $\lambda$ (see Fig. 45(b) with $\lambda = -0.01$), in conformity with Eq.(3.79). In addition, our dark soliton solutions

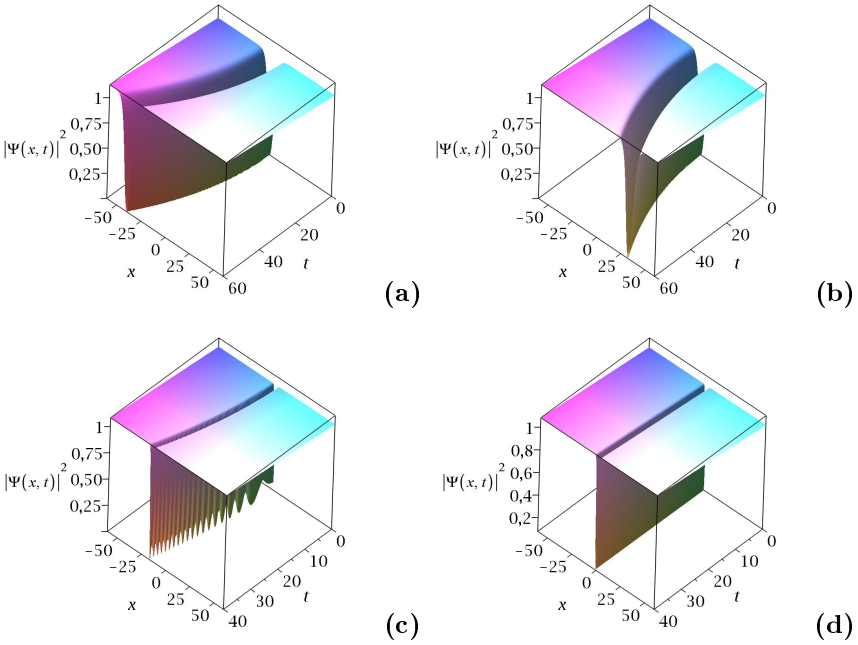


**Figure 45**: Dark profile solutions of Eq.(3.79), with $j = 11$, $b_0 = -4$, $b_2 = -4$, $b_4 = 4$, $b_6 = 4$, $\gamma = 0.001$, $C_3 = 0.1$. (a) $\lambda = 0.01$, (b) $\lambda = -0.01$. (c) $W = 2$. (d) $\lambda = 0$, $W = 2$.

have small amplitude modulations as time increases. The amplitude modulations appear earlier with smaller widths of the solitons. This feature is presented in Fig. 45(c) where $W = 2$. These amplitude modulations are completely absent when the linear potential is turned out as depicted in Fig. 45(d), where the same parameters as in Fig. 45(c) are used except $\lambda = 0$. In order to show the influence the other free parameters have on the dynamics of our solutions, we turn out the linear potential to facilitate interpretations. The parameter $C_4$ not only affects the direction of the solitions, but also induces small amplitude modulations as one can see in Fig. 46(a) ($C_4 = 0.035$), and in Fig. 46(b) ($C_4 = -0.035$). The parameters $C_2$ also changes the direction of propagation of the solutions as shown in Fig. 46(c) ($C_2 = 5$), and Fig. 46(d) ($C_2 = -5$).

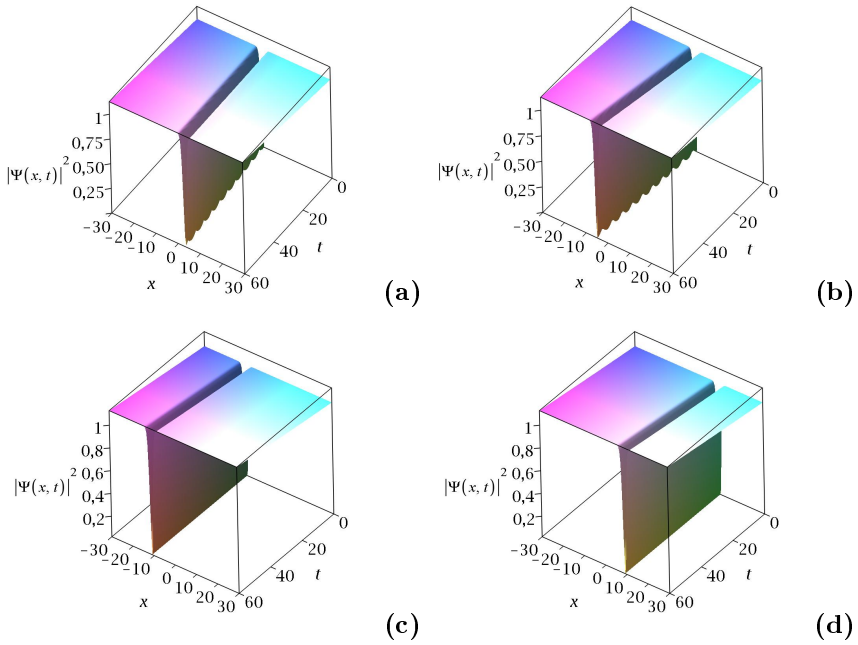


**Figure 46**: (a) $C_4 = 0.035$, (b) $C_4 = -0.035$, prove that $C_4$ deeply affects the direction of propagation of the wavefunction, and also induces a breathing mode behavior ($C_2 = 0$). (c) $C_2 = 5$, and (d) $C_2 = -5$ illustrate the influence $C_2$ has on the direction of propagation of the wave function ($C_4 = 0$).

### (a3). Bright profile solutions

One can obtain bright soliton patterns as displayed in Fig. 47. In Fig. 47(a), in Eq.(3.79), we choose $j = 1$ and $p = 1$, with $b_2 = 2$, $b_4 = -3$ (attractive condensate), $b_6 = -2$, the other parameters are the same as in Fig. 43. A bright structure describing a parabola in the plane ($t$, $x$) is formed, and evolves at the constant acceleration $\ddot{x} = 0.002$. Besides, Fig. 47(b) portrays another bright matter-wave condensate obtained by setting $j = 10$, $b_2 = 2$, $b_4 = 0$, in Eq.(3.79), the other parameters corresponding to those in Fig. 43.

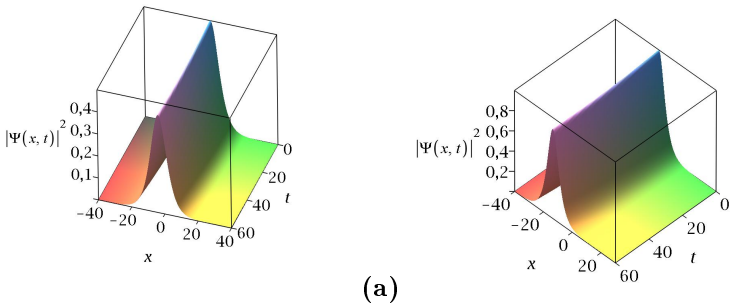


**Figure 47**: Spatiotemporal evolution of the density $|\Psi(x,t)|^2$ of bright solitons. (a) In Eq.(3.79), $j = p = 1$, $b_2 = 2$, $b_4 = -3$, $b_6 = -2$. (b) In Eq.(3.79), $j = 10$, $b_2 = 2$, $b_4 = 0$. Other parameters as in Fig. 43, with $\lambda = 0.001$.

**(a4). Anti-kink and kink like profile solutions**

Different types of solutions patterns can further be obtained for $j = 3$, $p = 1$ in Eq.(3.79), with $b_2 = 2$, $b_4 = -4$, $b_6 = b_4^2/4b_2$, $\gamma = 0.001$, the other parameters taken as in Fig. 45(c). The argument of the tanh function is $-\sqrt{b_2}\xi$ as in Fig. 48(a) for the anti-kink pattern, while it is $\sqrt{b_2}\xi$ in Fig. 48(b) for the kink pattern.

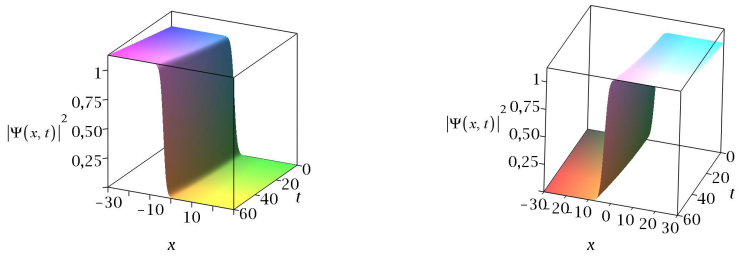


**Figure 48**: Spatiotemporal evolution of the density, $|\Psi(x,t)|^2$ of solutions of Eq.(3.79). (a) Anti-kink-like solution. (b) Kink -like solution. Parameters are $j = 3$, $p = 1$, $b_2 = 2$, $b_4 = -4$, $b_6 = b_4^2/4b_2$, $\gamma = 0.001$, $\lambda = 0.001$, other parameters are as in Fig. 45(c).

**(a5). Linear stability analysis of analytical solutions**

We analyze the stability of our solutions by linearizing the exact solution given by Eq.(3.79) around a small perturbation. The perturbed solution of Eq.(3.68) is written as

$$\Psi(x,t) = (\Psi_1(x,t) + \Psi_2(x,t))\exp(\imath\theta(x,t)), \tag{3.82}$$

where $\Psi_1(x,t)\exp(\imath\theta(x,t))$ is the exact solution of Eq.(3.68), and $\Psi_2(x,t) = R(x,t) + \imath I(x,t)$ represents a small perturbation, i.e. $|\Psi_2(x,t)|^2 \ll |\Psi_1(x,t)|^2$. Inserting Eq.(3.82) into Eq.(3.68) and linearizing around the perturbation, the following system of equations is derived

$$\begin{aligned} R_t &= -I_{xx} + (\theta_t + \theta_x^2 + g(t)\Psi_1(x,t)^2 + \chi(t)\Psi_1(x,t)^4 + \lambda x)I + (\theta_{xx} + \gamma)R - 2\theta_{xx}I_x \\ I_t &= R_{xx} - (\theta_t + \theta_x^2 + 3g(t)\Psi_1(x,t)^2 + 5\chi(t)\Psi_1(x,t)^4 + \lambda x)R - (\theta_{xx} - \gamma)I - 2\theta_{xx}I_x. \end{aligned} \tag{3.83}$$

The analysis of the linear problem given by Eq.(3.83) is a nontrivial task, so we only focus on solutions with zero spatial frequency shift, i.e. $\Gamma(t) = 0$, thus $\lambda = 0$, $C_4 = 0$, $\ddot{x} = \dot{x} = 0$, $\eta = C_2$, $\xi(x,t) \equiv \xi(x) = C_3 x + C_2$, $\theta_t = 2b_2C_3^2$, $\theta_x = \theta_{xx} = 0$. As in all solutions plotted above, we set $C_1 = 0$. Following the work of Bronski, Carr, Deconinck, and Kutz [4], we rewrite the set (3.83) in the form

$$\begin{pmatrix} R_t \\ I_t \end{pmatrix} = J \begin{pmatrix} L_+ & -S \\ S & L_- \end{pmatrix} \begin{pmatrix} R \\ I \end{pmatrix}. \tag{3.84}$$

In Eq.(3.84), $J = \begin{pmatrix} 0 & 1 \\ -1 & 0 \end{pmatrix}$, and

$$\begin{aligned} L- &= -\frac{\partial^2}{\partial x^2} + 2b_2C_3^2 + g(t)\Psi_1(x,t)^2 + \chi(t)\Psi_1(x,t)^4 + \lambda x \\ L_+ &= -\frac{\partial^2}{\partial x^2} + 2b_2C_3^2 + 3g(t)\Psi_1(x,t)^2 + 5\chi(t)\Psi_1(x,t)^4 + \lambda x \\ S &= \gamma. \end{aligned} \tag{3.85}$$

Assuming that the perturbation has the form

$$\begin{aligned} R(x,t) &= r_1(x)\exp(\beta t) \\ I(x,t) &= r_2(x)\exp(\beta t), \end{aligned} \tag{3.86}$$

then substituting Eq.(3.86) into Eq.(3.84) yields the eigenvalue problem given by

$$J\begin{pmatrix} L_+ & -\gamma \\ \gamma & L_- \end{pmatrix}\begin{pmatrix} r_1 \\ r_2 \end{pmatrix} = \beta\begin{pmatrix} r_1 \\ r_2 \end{pmatrix}. \tag{3.87}$$

It is clear that our linear stability analysis can be applied to all families of solutions found above. We consider as examples, the cases of the periodic, anti-kink, kink, and dark solitons presented above. Exploiting theorems presented in the work of Bronski, Carr, Deconinck, and Kutz [4] and applied by Bronski and co-workers in [48], we arrive at the following conclusions: (i) Since in Eq.(3.79), for $j = 2$, $p = 1$ the function $h(t)\phi(\xi) > 0$, the homogenous phase periodic solution is linearly stable in a repulsive condensate, (ii) the homogenous anti-kink-like and kink-like solitons are linearly stable in a repulsive condensate, (iii) the homogenous dark soliton is linearly unstable in the attractive condensate.

**(b). Numerical stability analysis of analytical solutions**

The numerical method used to integrate Eq.(3.68) is the fourth order Runge-Kutta scheme in the interaction picture with large spatial grid in order to prevent problems with the boundaries. Initial solutions are perturbed with a small amount of random white noise. For the sake of clarity, the width of solutions is set to $W = 400$ due to the width of the spatial grid.

We start our numerical simulations by considering the nontrivial phase solution displayed in Fig. 44(a). At $t = 0$, this solution is inserted trough Eq.(3.74). In Figs. 49(a)-(b) one can see a very good agreement between the exact numerical and the analytical solutions, which represent the spatial variation of the density at different times, while Fig. 49(c) displays the spatiotemporal evolution of the linearly and dynamically stable periodic nontrivial phase solution of Fig. 44(a). We also test the validity of the nontrivial phase dark profile solution of Fig. 45(a). Figure. 50(a) proves that the nontrivial phase dark solution is linearly and dynamically

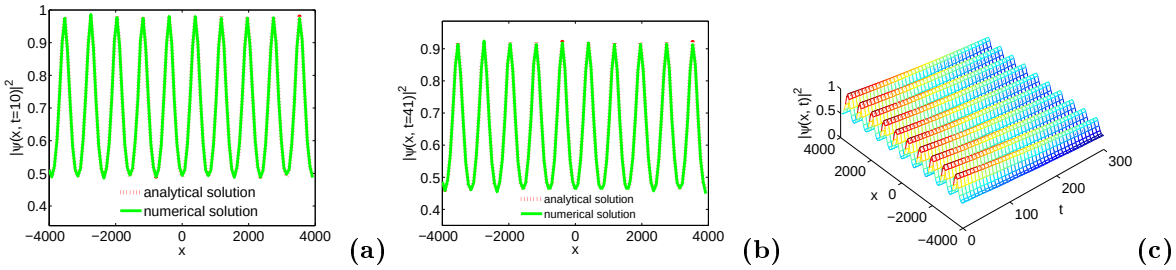


**Figure 49**: (a)-(b) Spatial comparisons between the numerical, and the analytical periodical solutions of Eq.(3.79) for $j = 2$, $p = 1$. (c) Stable density profile of the periodic solution. Same parameters as in Fig. 44(a), except $W = 400$.

stable. For the case of the dark trivial phase solution of Fig. 45(a), we follow the analytical treatment developed above, and set $\lambda = 0$. Then we insert trough Eq.(3.68) the corresponding initial condition with all free parameters selected as in Fig. 45(a). As depicted in Fig. 50(b), the dark trivial phase solution preserves its shape as time increases. However, at the top of the dark trivial phase solution, we observe benign random oscillations. This is a signature of the presence of small instabilities which are consistent with the linear stability analysis carried out above. However, these instabilities do not drastically develop such that the dark trivial phase solution is numerically robust. Further, Fig. 51 proves that the nontrivial phase bright solution

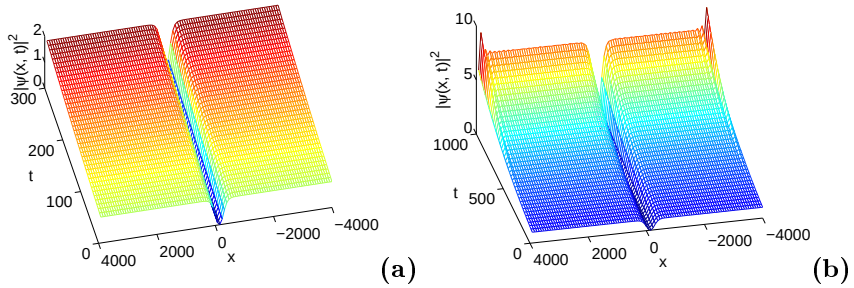


**Figure 50**: (a) Nontrivial phase dark solution. (b) Trivial phase solution. Same parameters as in Fig. 44(a), except $W = 400$.

of Fig. 47(a) is linearly and dynamically stable. Other numerical simulations not shown here

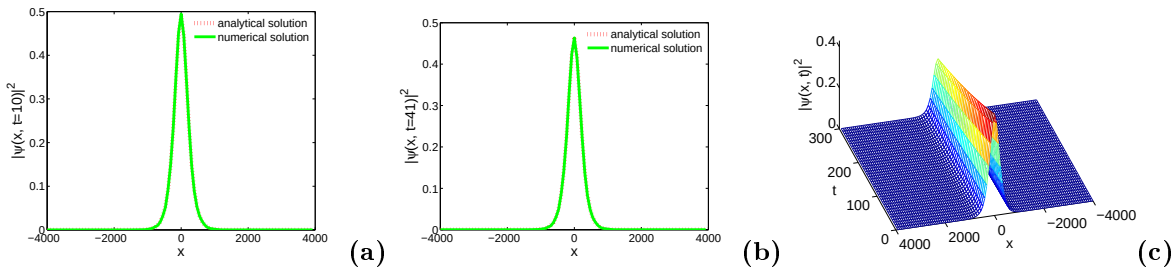


**Figure 51**: (a)-(b) Spatial comparisons between numerical, and analytical bright solutions of Eq.(3.79) for $j = p = 1$. (c) Stable density profile of the bright solution. Same parameters as in Fig. 47(a), except $W = 400$.

also prove that the nontrivial bright profile solution of Fig. 47(b) is also numerically stable. For the nontrivial phase anti-kink-like (Fig. 52(a)) and the kink-like (Fig. 52(b)) solutions, though the presence of small instabilities at the top of density profiles, these solutions are dynamically stable.

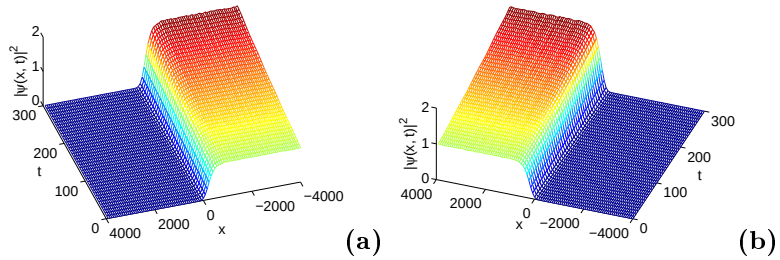


**Figure 52**: Stable propagations of (a) anti-kink and (b) kink solutions. Same parameters in Fig. 43, except $W = 400$.

### 3.4.3 GPE with time-dependent two- and three-body interatomic interactions in a complex potential

#### (a). Model and analytical solutions

Let us consider the dimensionless one dimensional GPE describing the dynamics of condensates with two- and three-body interatomic interactions considered by Mohamadou, Wamba, Lissouck, and Kofane [26]

$$\imath\Psi_t(x,t) + c\Psi_{xx} - g(t)|\Psi(x,t)|^2\Psi(x,t) - \chi(t)|\Psi(x,t)|^4\Psi(x,t) - (\alpha x^2 + \imath\gamma(t))\Psi(x,t) = 0, \quad (3.88)$$

where the time $t$ and the spatial coordinate $x$ are scaled in the harmonic oscillator units. The parameters $\alpha$, $g(t)$, $\chi(t)$, and $\lambda$ are the strengths of harmonic confinement, two- and three-body interatomic interactions, and rate of exchange of atoms with its surroundings, respectively.

In order to find out analytical solutions Eq.(3.88), we follow Mohamadou, Wamba, Lissouck, and Kofane [26] and transform it into a more tractable form with the following modify lens-type transformation

$$\Psi(x,t) = D(t)\Phi(X,T)\exp[\eta(t) + \imath f(t)x^2]. \quad (3.89)$$

In Eq.(3.89), $T$ is a function of time $t$, and $X = \frac{x}{l(t)}$. The function $f(t)$ represents the nonlinear frequency shift, $\eta(t)$ which takes into account the exchange of atoms between the condensate and its surroundings represents the growth ($\eta(t) > 0$) or the loss ($\eta(t) < 0$) of atoms. The

preservation of the scaling implies that $\frac{dT}{dt} = \frac{1}{l(t)^2}$. Further, we request that

$$\begin{aligned}
\frac{df(t)}{dt} &= -4cf(t)^2 - \alpha(t), \\
\frac{dD(t)}{dt} &= -2cf(t)D(t), \\
\frac{dl(t)}{dt} &= 4cf(t)l(t), \\
\frac{d\eta(t)}{dt} &= \gamma(t).
\end{aligned} \tag{3.90}$$

Substituting Eq.(3.89) into Eq.(3.88) and taking into account Eq.(3.90) yield the reduced form of Eq.(3.88) in the rescaled variables $X$ and $T$ [26]

$$\imath\frac{\partial\Phi(X,T)}{\partial T} = -c\frac{\partial^2\Phi(X,T)}{\partial X^2} - P^2|\Phi(X,T)|^2\Phi(X,T) + \chi_0|\Phi(X,T)|^4\Phi(X,T), \tag{3.91}$$

with $D(t) = [|g(t)|l(t)^2\exp[2\eta(t)]]^{-\frac{1}{2}}$, $\chi(t) = \chi_0 g(t)^2 l(t)^2$, $P^2 = -sgn[g(t)]$. The two-body interatomic interactions are attractive if $P^2 = +1$, but are repulsive when $P^2 = -1$. Equation (3.91) is a cubic-quintic GPE with constant parameters. The exact solution of Eq.(3.88) takes the form [26]

$$\Psi(x,t) = \sqrt{|G(t)|}\Phi(X,T)\exp\{\eta(t) + \imath[-\frac{1}{4c}\frac{d}{dt}\ln|G(t)|]x^2\}, \tag{3.92}$$

where $G(t) = g(t)\exp[2\eta(t)]$, $\eta(t) = \int_0^t \gamma(t')dt' + \eta_0$, $\eta_0$ being a constant. The solution given by Eq.(3.92) is obtained by assuming that $l(t) = |G(t)|^{-1}$, $T(t) = \int_0^t G(t')^2 dt'$, $f(t) = \frac{1}{4c}\frac{d}{dt}\ln|G(t)|$.

Analytical explicit solutions of Eq.(3.88) are obtained from the solution of Eq.(3.92) if the explicit form of the function $\Phi(X,T)$ is given. So, we search explicit expressions of $\Phi(X,T)$ with the form

$$\Phi(X,T) = Q(\xi)\exp[i\theta(X,T)], \tag{3.93}$$

where $Q$ represents the amplitude part and $\theta$ accounts for the phase part. The new variables $\xi$ and $\theta$ have the forms

$$\xi = k_0 X - \omega_0 T, \qquad \theta(X,T) = kX - \omega T. \tag{3.94}$$

Parameters $k_0$, $k$, $\omega_0$, and $\omega$ are real constants which account for width, linear frequency shift, velocity, homogenous phase of the wave function $\Phi(X,T)$, respectively. Substituting Eqs.(3.93)-(3.94) into Eq.(3.91), then separating the real and the imaginary parts, respectively read the following set of ordinary differential equations with respect to $Q$

$$(\omega - ck^2)Q + Q^3 - \chi_0 Q^5 + ck_0\frac{d^2Q}{d\xi^2} = 0. \tag{3.95}$$

$$(\omega_0 - 2ckk_0)\frac{d^2Q}{d\xi^2} = 0. \tag{3.96}$$

Assuming the constraint

$$\omega_0 = 2ckk_0, \tag{3.97}$$

means that we only need to solve Eq.(3.95). So far, there are some important physical properties that the complete solutions to be constructed will exhibit. For example, one may be interested in the dynamics of the center-of-mass which characterizes the behavior at mean of the condensate for a specific solution. In term of the dimensionless real physical variables, the position, velocity and acceleration of the center-of-mass are $x_{CM}(t) = (ck/\gamma)\sinh(2\gamma t)$, $\dot{x}_{CM} = 2ck\cosh(2\gamma t)$, $\ddot{x}_{CM} = 4ck\gamma\sinh(2\gamma t)$, respectively. Hence, the behavior at mean of the condensate is affected by the rate of exchange of atoms between the condensate fraction and the uncondensed fraction, and by the linear frequency shift of the initial condition. At initial time, the center-of-mass of the condensate is at the center of the trapping potential with the initial velocity $2ck$ without any acceleration. As time increases, the velocity and acceleration of the center-of-mass increase for negative and positive values of $\gamma$. This implies that the exchange of atoms with the thermal background accelerates the center-of-mass, so that the temperature of the core increases with time, and may lead to the collapse of the condensate. However, for small values of $\gamma$, the acceleration and velocity of the core shall remain small so that the growth of the velocity induced by the atoms pumping, or loss mechanisms shall be negligible, avoiding the collapse of the condensate. The linear frequency $k$ may also be used to control the acceleration and velocity of the condensate's core. So, one has two powerful tools to avoid the collapse of the condensate. The position of the center-of-mass as time evolves also depends on the sign of the linear frequency $k$, so that the condensate moves towards the left side of the axial potential if $k < 0$, while the condensate moves towards the right side of the potential for positive values of $k$. According to the Newton's second law, the condensate can be considered as a classical particle moving in the effective potential $U_{eff} = (-2ck/\gamma)\cosh(2\gamma t)$, with total energy $E = 2[ck\cosh(2\gamma t)]^2 - (2ck/\gamma)\cosh(2\gamma t)$, its only equilibrium point being located at the center of the trap $x = 0$. This means that the solutions constructed in this part of the work are all moving ones. In the following, we use specific auxiliary equations in deriving analytical solutions of Eq.(3.88).

**(a1). The Bernoulli equation as auxiliary equation**

We suppose that the function $Q$ can be written as

$$Q(\xi) = \sum_{i=0}^{M} a_i F^i(\xi), \tag{3.98}$$

where M is a positive integer, $a_i$ are real constants to be determined later. The function $F$ is the solution of the general Bernoulli equation

$$\frac{dF}{d\xi} = aF(\xi) + bF^{\lambda}(\xi), \tag{3.99}$$

parameters $a$, $b$, $\lambda$ being real constants which will also be determined later, with $\lambda \neq 1$. The homogeneous balance yields $\lambda = 2M + 1$. Since $\lambda \neq 1$, then $M \geq 1$. Let us consider the simple

case where $M = 1$, and $\lambda = 3$, we have

$$Q(\xi) = a_0 + a_1 F(\xi), \qquad \frac{dF}{d\xi} = aF(\xi) + bF^3(\xi). \tag{3.100}$$

The explicit expressions of the unknowns are

$$a_0 = 0, \tag{3.101}$$

$$a = \frac{-\sqrt{3}}{4k_0\sqrt{c}\sqrt{\chi_0}}, \tag{3.102}$$

$$b = \pm\frac{a_1^2\sqrt{\chi_0}}{k_0\sqrt{3c}}, \tag{3.103}$$

$$\omega = \frac{-3 + 16ck^2\chi_0}{16\chi_0}. \tag{3.104}$$

Equations (3.101)-(3.104) imply that $c > 0$, and $\chi_0 > 0$, meaning that solutions are valid only for repulsive three-body interatomic interactions. One infers from Eqs.(3.103)-(3.104) that the amplitude and the homogenous phase of the wavefunction are sensitive to the strength of the three-body interatomic interactions $\chi(t)$. It is thus possible to tune to the desired values both the amplitude and the phase of the condensate externally by means of the Feshbach resonance technique. Inserting the solutions of the general Bernoulli equation (Eq.(3.99)) for $\lambda = 3$ given in the Appendix A [116] into Eq.(3.100) leads to explicit expressions of $Q$. Hence, exact explicit solutions of Eq.(3.88) derived by Belobo Belobo, Ben-Bolie and Kofane are [165]

$$\Psi_{1j}(x,t) = \sqrt{\mid G(t) \mid}a_1 F_{1j}(\xi)\exp[\imath\theta(X,T)]\exp\{\eta(t) + \imath[-\frac{1}{4c}\frac{d}{dt}\ln \mid G(t) \mid]x^2\}, \qquad j = 1,2,3. \tag{3.105}$$

Equations (3.100)-(3.104) and solutions of the Appendix A imply that the heights of solutions given by Eq.(3.105) are proportional to the strength of the two-body interatomic interactions, but inversely proportional to the strength of the three-body interatomic interactions. Therefore, the experimenter knows how to manage the two- and three-body interatomic interactions in order to obtain a solution with an assumed amplitude. The density of a solution is subjected to a growth in the feeding regime, while the density decays when atoms are removed from the condensate. This feature has been predicted in [26, 164]. Also, the behavior of the density of the condensate is unchanged both for attractive and repulsive condensates. From Eq.(3.105), one understands that we have constructed three bunches of solutions of Eq.(3.88). In order to represent some samples of these solutions, we choose the following relevant physical parameters: $\alpha(t) = -0.005$, $c = 0.5$, $\gamma(t) \equiv \gamma$, $\eta(t) = \gamma t$ with $\eta_0 = 0$, used in some experimental and theoretical studies [26, 25, 165]. We display in Fig. 53(a) the dynamics of the condensate's wavefunction, where we have set $j = 2$ in the solution of Eq.(3.105) with $\gamma = -0.005$, $\chi_0 = 1/12$, $k = 0.01$. In this case, the solution given by Eq.(3.105) is an anti-kink soliton with initial velocity 0.01. The influence of the linear frequency shift on the direction of the condensate can be seen in Fig. 53(b) where $k = -0.5$. The moving anti-kink soliton evolves towards the left side of

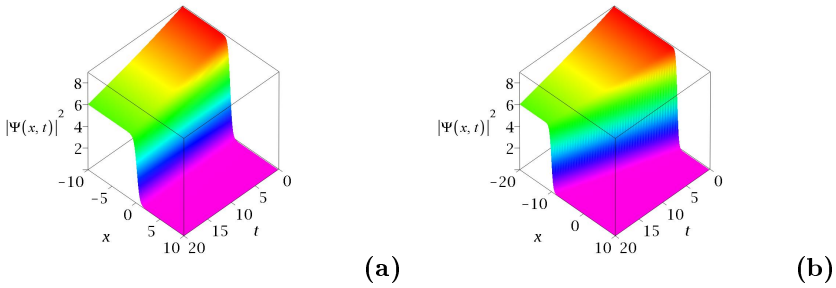


**Figure 53**: Spatiotemporal evolution of the wavefunction of Eq.(3.105) for $j = 2$ for $k_0 = 1$, $\chi_0 = \frac{1}{12}$, $a_1 = 1$, $c = 0.5$, $\eta_0 = 0$, $g(t) = -1$, $\gamma = -0.005$. (a) $k = 0.01$, density profile of an anti-kink soliton with initial speed 0.01. (b) $k = -0.5$, effect of the linear frequency shift on the direction of the moving anti-kink soliton.

the cigar axis and its initial velocity amounts to 0.05. Kink and anti-kink solitons have been predicted in single condensates with two-and three-body interatomic interactions in different trap geometries [26, 164] and in binary condensates with only two-body interatomic interactions [50]. Other nonlinear media also allow the existence of kink and anti-kink solitons such as a layer of binary liquid heated from below, where oscillatory convection sets in via a subcritical bifurcation described by the cubic-quintic Ginsburg-Landau equation [166], optical fibers with elliptical birefringence for the evolution of the state of polarization of counter-propagating waves [167], the nonlinear dispersive fiber optics for the description of wave propagation by including the effects of group-velocity dispersion, self-phase-modulation, stimulated Raman scattering, and self-steepening [168]. The analytical expression of the anti-kink soliton solution found by Mohamadou, Wamba, Lissouck, and Kofane [26] is different from the solution obtained here by using the Bernoulli auxiliary equation. Moreover, with only fewer parameters, i.e., $k$, and $\gamma$, we can characterize the behavior of the condensate at mean.

**(a2). The Riccati equation as auxiliary equation**

We assume that the function $Q$ takes the form

$$Q(\xi) = \sum_{i=-N}^{N} a_i F^i(\xi), \tag{3.106}$$

where the function $F$ is the solution of the following Riccati equation [169]

$$\frac{dF}{d\xi} = MF^{\lambda}(\xi) + \frac{\varepsilon}{1-\lambda} F^{2-\lambda}, \qquad \varepsilon = \pm 1. \tag{3.107}$$

The homogenous balance gives $\lambda = 2N + 1$. We consider the simple case where $N = 1$, and $\lambda = 3$. Equations (3.106)-(3.107) become

$$Q(\xi) = a_0 + a_1 F(\xi) + a_2 F^{-1}(\xi), \qquad \frac{dF}{d\xi} = MF^3(\xi) - \frac{\varepsilon}{2} F(\xi). \tag{3.108}$$

Explicit expressions of the unknowns are

$$\begin{aligned}
a_{11} &= \frac{1}{8c\sqrt{2k_0}}(\frac{3c}{\chi_0})^{\frac{3}{4}}, \quad a_{21} = \sqrt{\frac{k_0}{2}}(\frac{3c}{\chi_0})^{\frac{3}{4}}, \quad M_1 = \frac{3}{128ck_0^2\chi_0}, \quad \omega_1 = ck^2 + \frac{3\varepsilon - 27}{128\chi_0}, \\
a_{12} &= -a_{11}, \quad a_{22} = -a_{21}, \quad M_1, \quad \omega_1, \\
a_{13} &= -\imath a_{11}, \quad a_{23} = \imath a_{21}, \quad M_1, \quad \omega_1, \\
a_{14} &= \imath a_{11}, \quad a_{24} = -\imath a_{21}, \quad M_1, \quad \omega_1, \\
a_{15} &= a_{11}, \quad a_{25} = a_{21}, \quad -M_1, \quad \omega_2 = ck^2 - \frac{(3\varepsilon + 27)}{128\chi_0}, \\
a_{16} &= -a_{11}, \quad a_{26} = -a_{21}, \quad -M_1, \quad \omega_2, \\
a_{17} &= -\imath a_{11}, \quad a_{27} = \imath a_{21}, \quad -M_1, \quad \omega_2, \\
a_{18} &= \imath a_{11}, \quad a_{28} = -\imath a_{21}, \quad -M_1, \quad \omega_2, \\
a_0 &= 0.
\end{aligned} \tag{3.109}$$

The fourth equation of the set (3.109) implies that $c > 0$, and $\chi_0 > 0$ (the three-body interatomic interactions are repulsive). Using Eqs.(3.108)-(3.109), we derive new exact solutions of Eq.(3.88)

$$\Psi_{2nm}(x,t) = \sqrt{\mid G(t) \mid}[a_{1n}F_{2m}(\xi) + a_{2n}F_{2m}^{-1}(\xi)] \exp[\imath\theta(X,T)] \exp\{\eta(t) + \imath[-\frac{1}{4c}\frac{d}{dt}\ln \mid G(t) \mid]x^2\}, \tag{3.110}$$

where, $n$, $m$ are integers, with $n = \overline{1,8}$, and $m = \overline{1,4}$ if $\varepsilon = -1$, $m = \overline{5,7}$ if $\varepsilon = +1$, and $m = 8$ if $\varepsilon = 0$. The solutions of the Riccati equation are given in the Appendix B [169]. Equations (3.109)-(3.110) imply that the amplitudes of solutions given by Eq.(3.110) deeply depend on the values of the width, the strength of the three-body interatomic interactions which is also related to the atoms feeding or loss parameter $\gamma$. The phases of solutions given by Eq.(3.110) are characterized by $\chi_0$ and the free parameter $k$. Hence, after fixing the values of $k_0$, $\chi_0$, and $\gamma$, it is possible to predict the spatiotemporal evolution of the amplitude and the phase of solutions given by Eq.(3.110). Since the latter parameter can be precisely controlled externally in current condensate experiments, one infers that solutions given by Eq.(3.110) are likely to be observed in current or future experiments with condensates. We visualize in Figs. 54(a)-(b) the spatiotemporal evolutions of the wave function for two different cases of solution of Eq.(3.110). In Fig. 54(a), we have set in Eq.(3.110) $n = 5$, $m = 7$, $\varepsilon = 1$. We obtain a multiple bright solitons solution periodically spaced on the axial potential. Multiple bright soliton solutions are usually obtained in condensates via the modulational instability. In the case of Eq.(3.88), multiple bright solitons were generated numerically by Mohamadou, Wamba, Lissouck, and Kofane [26]. Here, we give an analytical expression of a multiple bright solitons solution in the framework of Eq.(3.88). Figure 54(b) portrays the spatiotemporal evolution of a kink soliton obtained for $n = 5$, $m = 3$, $\varepsilon = -1$. This is a novel kink soliton solution of Eq.(3.88) different from that derived by Mohamadou, Wamba, Lissouck, and Kofane [26].

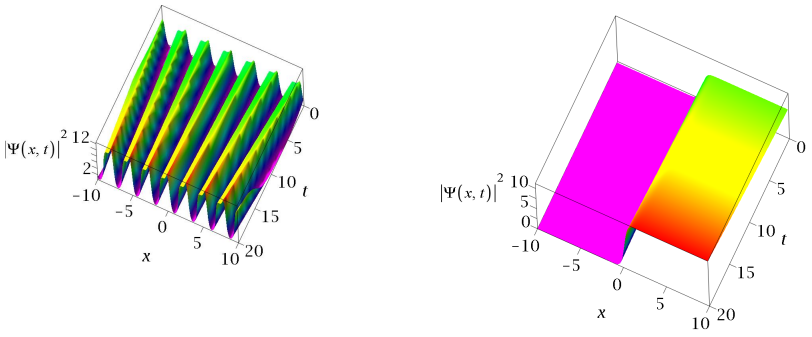


**(a)** **(b)**

**Figure 54**: (a) Density profile of a growing periodic solution for $n = 5$, $m = 7$, $\varepsilon = +1$. (b) Density profile of a moving kink soliton for $n = 5$, $m = 3$, $\varepsilon = -1$. Other parameters are the same as in Fig. 48(a), except $\chi_0 = 0.1$, $\gamma_0 = 0.005$.

**(a3). The Lenard equation as auxiliary equation**

We search a function $Q$ with the form

$$Q(\xi) = \sum_{i=0}^{N} a_i F^i(\xi), \tag{3.111}$$

the function $F$ satisfying the Lenard equation [170]

$$\frac{dF}{d\xi} = \sqrt{b_0 + b_2 F^2(\xi) + b_4 F^4(\xi) + b_6 F^6(\xi)}. \tag{3.112}$$

Solutions of Eq.(3.112) are given in the Appendix C. The homogeneous balance leads to $N = 1$. Explicit expressions of the unknown are

$$\begin{aligned} a_{11} &= \sqrt{k_0}(\frac{cb_6}{\chi_0})^{\frac{1}{4}}, \quad b_4 = -\frac{1}{2ck_0}\sqrt{\frac{2cb_6}{\chi_0}}, \\ a_{12} &= -a_{11}, \quad b_4, \\ a_{13} &= \imath a_{11}, \quad -b_4, \\ a_{14} &= -\imath a_{11}, \quad b_4, \\ a_0 &= 0, \quad \omega = ck^2 - ck_0^2 b_2. \end{aligned} \tag{3.113}$$

The set (3.113) implies that $k_0$ must be positive, both $\chi_0$ and $b_6$ must have the same sign. Inserting Eq.(3.113) into Eq.(3.111), yields explicit solutions of $Q$, which in turn are used to obtain exact solutions of Eq.(3.88), that are

$$\Psi_{3nm}(x,t) = \sqrt{\mid G(t) \mid} a_{1n} F_{3,m}(\xi) \exp[\imath\theta(X,T)] \exp\{\eta(t) + \imath[-\frac{1}{4c}\frac{d}{dt}\ln \mid G(t) \mid]x^2\}, \tag{3.114}$$

where, $n$, $m$ are integers, with $n = \overline{1,4}$, and $m = \overline{1,18}$ for $b_0 = 0$, $m = \overline{19,22}$ for $b_0 = \frac{8b_2^2}{27b_4}$ and $b_6 = \frac{b_4^2}{4b_2}$. The first four relations of the set (3.113) mean that the amplitudes of solutions

given by Eq.(3.114) depend on the values of $k_0$ and $\chi_0$. The last equation of set (3.113) implies that the phases of the solutions of Eq.(3.114) depend on the values of $k$ and $k_0$. After the choice of the parameters $b_i$ $(i = \overline{0,6})$ related to the solution pattern needed, it is possible to precisely manipulate the amplitude and the phase of solutions only with the selection of the values of the width $(1/k_0)$, the linear frequency $k$, the sign of $\chi_0$, and the rate of exchange $\gamma$ of atoms with the surroundings. There are many types of solutions of Eq.(3.88) that can be derived from Eq.(3.114). We present in Fig. 55(a) a bright soliton solution of Eq.(3.114) for $n = 1$, $m = 1$, with $b_2 = 2$, $b_6 = -2$, $\chi_0 = -0.1$, $g(t) = 1$. The other parameters are the same as in Fig. 53(a). To the best of our knowledge, the bright soliton solution of Eq.(3.88) presented in Fig. 55(a) is new. The parameter $k_0$ plays two important roles in the characterization of the solutions: (i) generally speaking, the width of the condensate is $1/k_0$, (ii) for each solution derived from Eq.(3.114), the amplitude is proportional to $\sqrt{k_0}$ as depicted by Eq.(3.113). A comparison between Figs. 55(a) and (b) corroborates the latter effects due to $k_0$.

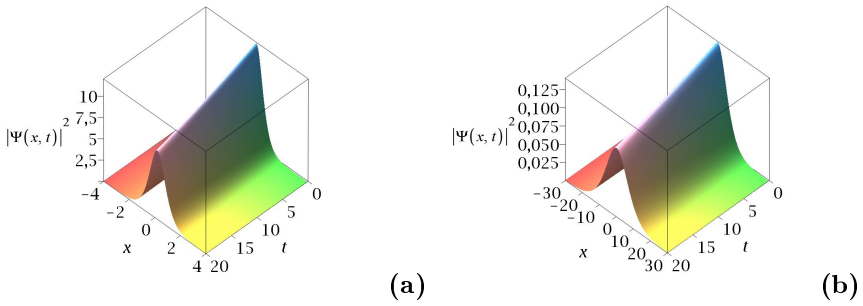


**Figure 55**: (a) Bright soliton solution derived from Eq.(3.114) for $n = 1$, $m = 1$ with $k_0 = 1$, $\chi_0 = -0.1$, $b_2 = 2$, $b_6 = -2$. (b) Same parameters as in panel (a) except $k_0 = 0.1$. $k_0$ affects both the width and the amplitude of the solution. Same parameters as in Fig. 53(a).

One important class of physically relevant solutions of Eq.(3.88) is the Jacobi elliptic function solutions that are missed in the above development. We need to remedy to this by including the generalized Jacobian elliptic solutions. To this end, we resort the same procedure and consider the following special solutions of the Lenard equation [171] which can be found in the Appendix D. The generalized Jacobi exact solutions of Eq.(3.88) can then be expressed as follows

$$\Psi_{3nm}(x,t) = \sqrt{|G(t)|}a_{1n}F_{5,m}(\xi)\exp[\imath\theta(X,T)]\exp\{\eta(t) + \imath[-\frac{1}{4c}\frac{d}{dt}\ln|G(t)|]x^2\}, \qquad (3.115)$$

where, $n$, $m$ are integers, with $n = \overline{1,4}$, and $m = \overline{18,19}$. These solutions have to respect the constraint imposed by the expression of $b_4$ given by Eq.(3.105), and are valid only for negative values of $\chi_0$. Thus, the generalized Jacobi function solutions of Eq.(3.115) are valid provided that the three-body interatomic interactions are attractive, and share the same features with solutions of Eq.(3.114) regarding the behavior of the amplitude and the phase. Subsequently, $k_0$ can be written in terms of the periods $k_1$ and $k_2$ as $k_0 = -\frac{1}{2cb_4}\sqrt{\frac{2cb_6}{\chi_0}}$, with $b_4$ and $b_6$ satisfying Eq.(3.113). In other words, once two periods $k_1$, $k_2$, are fixed, the width $1/k_0$ and the strength

of the three-body interatomic interactions are derived. It is interesting to notice that except the atoms feeding or loss mechanisms that is controlled by $\gamma$, all important features of the solutions described by Eq.(3.115) depend on the values of the periods $k_1$, $k_2$. We plot in Fig. 56(a) the density profile of the generalized Jacobi cosine function, and in Fig. 56(b) the density profile of the generalized Jacobi function of the third kind, in the feeding regime $\gamma = 0.001$, for repulsive condensates $g = 1$. As periodic solutions, the generalized Jacobi elliptic function solutions may

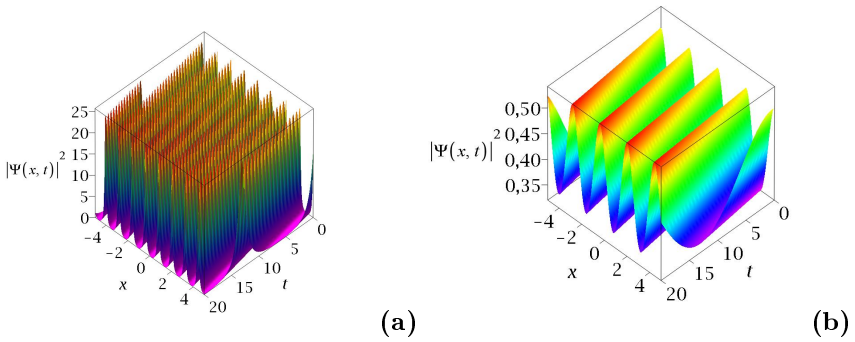


**Figure 56**: Spatiotemporal evolution of density profiles of generalized Jacobi elliptic solutions of Eq.(3.115). (a) $c(\xi, k_1, k2)$, (b) $d_1(\xi, k_1, k2)$. Other parameters are $k_1 = 0.6$, $k_2 = 0.2$, $\chi_0 = -k_1^2 k_2^2$, $\gamma = 0.001$, $k = 0.1$, $g = 1$.

be observed for condensates in optical lattices.

**(a5). The Hyperbolic equation as auxiliary equation**

The function $Q$ is assumed to have the form

$$Q(\xi) = \sum_{i=0}^{N} a_i \sinh^i(F(\xi)), \tag{3.116}$$

where the function $F$ satisfies the Hyperbolic equation [165]

$$\frac{dF}{d\xi} = c_0 + c_2 \sinh^2(\xi). \tag{3.117}$$

The solutions of the Hyperbolic equation are presented in the Appendix E [172]. The homogeneous balance gives $N = 1$, and the unknowns are found to be

$$\begin{aligned}
a_{11} &= \sqrt{k_0 c_2 (\frac{3c}{\chi_0})^{\frac{1}{4}}}, \quad \omega_1 = k_0 c_2 \sqrt{\frac{3c}{\chi_0}} + ck^2 + \frac{3ck_0^2 c_2^2}{4} - \frac{3}{16\chi_0}, \quad c_{01} = \frac{-\sqrt{\frac{3c}{\chi_0}} - 2ck_0 c_2}{4ck_0}, \\
a_{12} &= -a_{11}, \quad \omega_1, \quad c_{01} \\
a_{13} &= \imath a_{11}, \quad \omega_2 = -k_0 c_2 \sqrt{\frac{3c}{\chi_0}} + ck^2 + \frac{3ck_0^2 c_2^2}{4} - \frac{3}{16\chi_0}, \quad c_{02} = \frac{\sqrt{\frac{3c}{\chi_0}} - 2ck_0 c_2}{4ck_0}, \\
a_{14} &= -\imath a_{11}, \quad \omega_2, \quad c_{02}, \\
a_0 &= 0.
\end{aligned} \tag{3.118}$$

Proceeding in a similar way as above, we obtain exact solutions of Eq.(3.88)

$$\Psi_{4nm}(x,t) = \sqrt{\mid G(t) \mid} a_{1n} \sinh_{1,m}[F(\xi)] \exp[\imath\theta(X,T)] \exp\{\eta(t) + \imath[-\frac{1}{4c}\frac{d}{dt} \ln \mid G(t) \mid]x^2\}, \tag{3.119}$$

where $n, m = 1, 2, 3, 4$. From Eqs.(3.118), one realizes that features of the solutions of Eq.(3.119) are related to some experimental parameters such as the strength of the three-body interatomic interactions, the rate of exchange of atoms with the thermal background $\gamma$, and the linear frequency shift $k$. For instance, the amplitudes of solutions of Eq.(3.119) depend on the width $(1/k_0)$, and the strength of the three-body interatomic interactions $\chi_0$ (that depends on the interplay between the condensate and the thermal vapor), whereas the homogenous phase depends on the width, linear phase and $\chi_0$. As already stated above, it is possible to control the amplitude and phase of a solution in nowadays condensate experiments once $1/k_0$, $k$ and $\gamma$ have been fixed. We expect the present work will motivate the quest of hyperbolic solutions in condensate experiments and applications.

**(b). Numerical stability analysis of solutions**

The numerical scheme used is the split-step Fourier method. An initial reasonable small amount of random perturbation is added in order to unveil any instability that may be seeded during the time evolution. We restrict ourselves only on some cases of exact solutions found above.

Let us start with the anti-kink soliton solution of Eq.(3.105) for $j = 2$. In the case where $\gamma = 0$, the number of atoms in the condensate is constant. Figure 57 proves that the initial condition persists without destruction though the insertion of a small initial random perturbation. The long time behavior of the solution displayed in Fig. 57 means that it is linearly and dynamically stable. For a condensate in the regime of loss of atoms, there is also a very good agreement

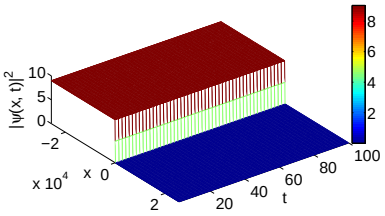


**Figure 57**: Spatiotemporal evolution of the stable anti-kink-like soliton of (3.105). Same parameters as in Fig. 53(a) except $\gamma = 0$.

between the analytical prediction and numerical results as depicted by panels (a)-(b) of Fig. 58, for $\gamma = -0.005$. Figure 58(c) shows that the disturbed initial condition remains stable during evolution. One can then consider that such a solution is a robust physical object that can be observed in a real experiment.

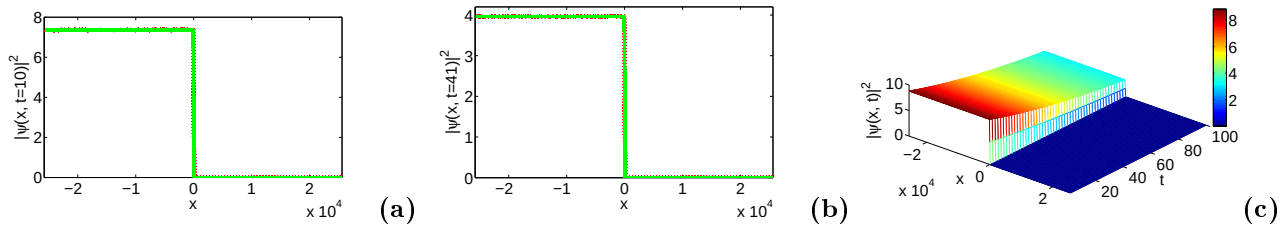


**Figure 58**: (a)-(b) Comparisons between analytical (solid line) and numerical (dotted line) solutions at particular times of the anti-kink-like soliton of Fig. 53(a). (c) Spatiotemporal evolution of the stable anti-kink-like soliton of Fig. 53(a). Other parameters as in Fig. 53(a).

We continue with the kink soliton solution of Fig. 54(b). In Fig. 59(a) ($\gamma = 0$) the amplitude of the condensate stays constant during evolution, while the amplitude increases with time in the feeding regime as shown in Fig. 59(b) ($\gamma = 0.005$). From Figs. 59(a) and 59(b) ($\gamma = 0.005$), one infers that the new derived kink-like soliton solution of Eq.(3.110) for $n = 5$, $m = 3$, $\varepsilon = -1$, is a stable solution.

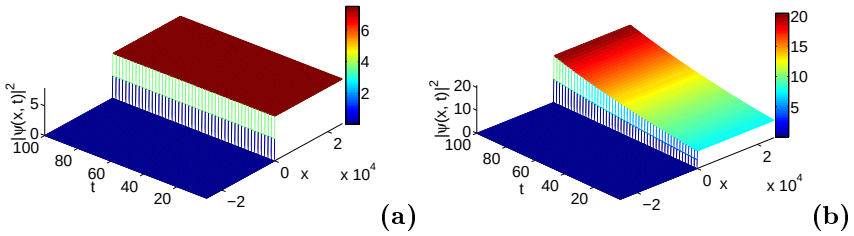


**Figure 59**: (a) Spatiotemporal evolution of stable kink solution of Fig. 54(a), $\gamma = 0$. (b) Spatiotemporal evolution of stable growing kink-like solution of Fig. 54(b), $\gamma = 0.005$. Other parameters as in Fig. 54(a).

The bright soliton solution of Fig. 55(b) obtained by using the Lenard equation is dynamically stable and accurately corroborates its analytical counterpart. Figure 60 displays the agreement between the numerical and analytical solutions, as well as the long time robustness of our bright soliton exhibited in Fig. 60(b).

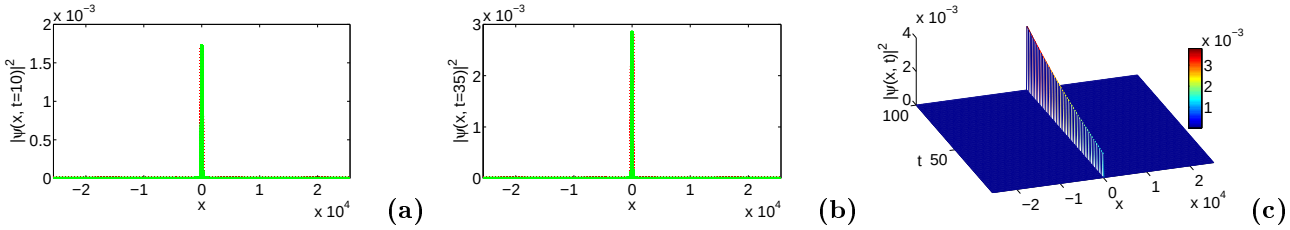


**Figure 60**: (a)-(b) Parallel between analytical (solid line) and numerical (dotted line) solutions at different times of the bright soliton of Fig. 55(b). (c) Spatiotemporal evolution of the stable bright soliton. Same parameters as in Fig. 55(b) except $\gamma = 0.005$.

## 3.5 Conclusion

In conclusion, in this chapter we have dealt with analytical and numerical studies of modulational instability for different models of condensates, and the dynamics of condensates with two- and three-body interatomic interactions, confined in a complex potential.

The chapter begins with the study of condensates confined in a versatile anharmonic optical lattice. Using the variational approach, we have generalized the stability criterion of bright solitons in condensates to the general class of anharmonic periodic potential shapes. Then, full numerical simulations have validated the results obtained analytically.

We have also examined the modulational instability of single trapped condensates, and trapless two-component condensates with two- and three-body interatomic interactions. For the case of single condensates, the external potential consists of a harmonic confinement, a linear part, and a complex one related to the exchange of atoms between the condensate and the thermal background. Different models describing the dynamics of single condensates beyond the mean-field GPE picture are used. Effects of some important quantum properties, such as the quantum fluctuations around the mean-field, the three-body interatomic interactions, on the modulational instability of condensates are considered. Using the linear stability analysis, we have derived the modulational instability criterions and the formulas of the gains of instability. Effects of the complex potential, the quantum fluctuations around the mean-field, and the three-body interactions on the modulational instability are elucidated analytically. Intensive numerical simulations carried out have corroborated the analytical predictions. As far as binary condensates are concerned, we have shown analytically and numerically the impact of the three-body intraspecies and interspecies interactions on the modulational instability and the dynamics of solitons generated.

We have also constructed analytical solutions of condensates for two model equations. The first model is the modified GPE II with a complex potential using the variational approach. The influence of the nature of condensates (attractive or repulsive), and the linear potential on the dynamics of bright solitons are clarified in the variational sense. The second model equation is the GPE with time modulation of the two- and three-body interatomic interactions, confined in a complex potential. Using the F-expansion method, we have constructed many new families of solutions. These solutions have many free parameters which may be used to manipulate many condensate properties. The issue of stability of analytical solutions found here has been addressed analytically and numerically. The numerical investigations conducted have confirmed the reliability and robustness of our solutions.

# General Conclusion

## Summary and Contributions

In this thesis, the generation, structure dynamics, and stability of matter waves of Bose-Einstein condensates, confined in external potentials with different shapes, have been investigated.

The first chapter is devoted to generalities on Bose-Einstein condensation. A description of non-interacting and interacting Bose-Einstein condensed gases has been presented. Using the mean-field theory, we have derived time-dependent and time-independent GPEs that have been used to describe the dynamics of conservative condensates. Some limitations of GPEs have been discussed and some models that go beyond the mean-field GPE have been presented. The first chapter ended up with a description of experimental procedures that lead to experimental observations of Bose-Einstein condensates.

In the second chapter, we first presented some analytical methods used to examine the dynamics of solitons in condensates. These are the variational approach, the modified lens-type transformation, the linear stability analysis, and the F-expansion method. The variational approach has been used to study the stability of bright solitons in condensates. The modified lens-type transformation and the linear stability analysis have been used to investigate the modulational instability of matter waves in condensates. Some numerical methods that are usually used to confirm analytical results have been described. We presented the normalized gradient flow with backward centered finite difference scheme, the split-step Fourier method, the fourth order Runge-Kutta in the interaction picture method, and the MATLAB toolbox PDEPE.

The main results and contributions of this thesis are presented in the third chapter. We started by considering the cubic GPE for attractive condensates trapped in an optical lattice which shape can be varied between the Kronig-Penney and its inverse. Applying the variational approach along with the Vakhitov-Kolokolov criterion, a generalized stability criterion for bright solitons in condensates has been derived. In fact, for too large or too small values of the shape parameter $s$, we have shown that if $V_0 < V_{0crit}$, there is one stable localized state and if $V_{0crit} < V_0$, there are three localized states, two stable and one unstable, some of them present a gap region where there is no solution as $V_0$ increases ($V_{0crit} < V_0$). We have also proved that

for all other values of the shape parameter $s$, if $V_0 < V_{0crit}$, there are three localized states, two stable and one unstable, and for $V_{0crit} < V_0$, there are three localized states with a gap region where the solution does not exist. This gap region gradually increases with $V_0$ (in the case $V_{0crit} < V_0$).

Besides, we have also investigated the generation and structure dynamics of Bose-Einstein condensates via the modulational instability process. Performing a modified lens-type transformation with a linear stability analysis, modulational instability criterions and gains of instability have been derived within each condensate model equation used. For the case of the modified GPE I, it has been shown analytically and confirmed by numerical calculations that the quantum fluctuations, the strength of the parabolic background, and the exchange of atoms with the thermal cloud enhance the loss of stability. Further numerical integrations of the modified GPE I have shown that the linear potential deviates the trail of trains of solitons, enhances the appearance of these trains and reduces the lifetime of the solitons when the absolute value of $\gamma$ is increased. For the case of the modified GPE II, it has been shown analytically and numerically that the three-body interatomic interactions and small values of the strength of the attractive and the expulsive external potentials enhance the instability of the system. Additional numerical simulations have shown that for condensates in an attractive trap, the three-body interatomic interactions significantly changes the trail of solitons generated, and enhances the occurrence of instability, while for condensates in a repulsive potential, the three-body interatomic interactions break up the symmetry of the trail of solitons created, increase the number of solitons produced via the activation of modulational instability and also alter the lifetime of solitons. The modified GPE III has allowed to investigate effects of the quantum fluctuations and the three-body interatomic interactions on the dynamics of condensates beyond the mean-field picture. A systematical theoretical study of the modulational instability of trapless condensates, trapped condensates in attractive and repulsive harmonic potentials has been carried out. Our study has revealed that the three-body interatomic interactions enhance the appearance of solitons, increase the number of solitons generated as well as their lifetime. A new initial condition has also been introduced and has allowed to increase the number of solitons generated via modulational instability. Besides, in two-component condensates, we have thoroughly analyzed the effects of the three-body interspecies and intraspecies interactions of the onset of instability, and on the dynamics of solitons that emerged due to modulational instability. The analytical study has revealed that small attractive and large repulsive three-body interspecies interactions enhance the instability. Moreover, attractive three-body intraspecies interactions more destabilize the binary system, while repulsive ones smoothen its instability. For repulsive three-body intraspecies interactions, the two-component condensate system remains stable for $-\chi^1 < \chi < \chi^1$. Numerical results have proven that two-body interatomic interactions are dominant near the center of the train of solitons, while effects of the three-body interatomic interactions become important at the borders of the trains.

Using the variational approximation, the stability criterion of bright solitons of the modified GPE II with a complex potential has been derived. For attractive and repulsive condensates, the bright soliton solution is stable if the width and the initial density remain relatively small. By means of numerical simulations, it has been shown that the linear potential induces oscillations of solitons and can be used to stabilize the system. We have also constructed analytical solutions of the GPE with time-dependent two- and three-body interatomic interactions, for condensates confined in complex potentials. The analytical method that has been used to find out new matter wave solutions is the F-expansion method along with some auxiliary equations. Many families of solutions have been found among periodic, dark, bright, anti-kink-like and kink-like profile solutions, generalized Jacobi elliptic function solutions and many others. The stability of analytical solutions found in this thesis has been addressed analytically and numerically. Intensive numerical simulations performed have shown that our analytical solutions are robust such that these solutions may be observed in condensate experiments.

## Open problems and future directions

Though this thesis presents many interesting new results, there still remains numerous important issues that need to be addressed in future works.

- In the GPE picture, the gas is at zero temperature where thermal effects are neglected. In this case, the number of particles in the condensate is a conserved quantity. However, condensate experiments are conducted at finite temperatures, and in some regimes, thermal effects are no longer small. Hence, a fraction of the atomic cloud is not condensed and couples to the condensed fraction. This situation may results to a coupling between the condensate and a source of uncondensed atoms at the same temperature and to a sink. Thus, the dynamics of the condensate is described by a dissipative Ginsburg-Landau GPE [44, 45, 46] type. The dissipative Ginsburg-Landau GPE describes the dynamics of opened condensates and have been applied to study some properties of atom lasers [44, 45, 46], solitons and vortices in polariton condensates [47]. The influence of some quantum aspects, such as the quantum fluctuations around the mean-field on the dynamics of atom lasers, polariton condensates in the realm of the dissipative Ginsburg-Landau GPE should be investigated.
- There is an increase of interest in the properties of spinor condensates, where phenomena such as spin domains and spin textures, bright, dark, gap, bright-dark vector solitons, and modulational instability [173] are studied. The effects of the three-body interatomic interactions on the latter phenomena in binary and spinor condensates shall be examined.
- The study of the dynamics of condensates in optical lattices is an important developing issue. We have investigated the stability of bright solitons in a versatile linear continuous optical lattice. Many soliton properties need more investigations in continuous as well as

discrete media [174]. Among problems awaiting further development and analysis are the search for stable soliton complexes and vortices in higher dimensional nonlinear lattices, the study of the soliton mobility and collisions in optical lattices, the effects of the commensurability and incommensurability in mixed linear- nonlinear lattices, the soliton formation in random and quasiperiodic nonlinear landscapes. Such problems can be examined using the general variable optical lattice used above.

- With the experimental realization of condensates made of $^{52}$Cr where long-range dipolar interactions are important [175], there has been a growing interest on the dynamics of dipolar condensates. The dynamics of dipolar condensates in complex potentials and in versatile optical lattices should be examined. Also, there has been an increasing interest in the study of extreme waves described as rogue. Rogue waves have been studied in different media such as water, nonlinear optics, and recently in Bose-Einstein condensates [96] with only two-body interactions. Effects of the three-body interactions on the dynamics of rogue waves should be investigated in future works.
- Bose-Einstein condensates have been realized in accelerated potentials [174] where some important phenomena are observed like matter waves transport, transition from coherent structures to chaos [176]. There is also the possibility to control the dynamics of solitons in condensates by managing the dispersion, and or the two- and three-body interactions in space or in time [174]. The effects of the quantum fluctuations on the latter phenomena shall be examined in future works.

# Bibliography


[1] M.H. Anderson, J.R. Ensher, M.R. Matthews, C.E. Wieman, and E.A. Cornell, Science **269**, 198 (1995).

[2] C.C. Bradley, C.A. Sackett, J.J. Tollett, and R.G. Hulet, Phys. Rev. Lett. **75**, 1687 (1995).

[3] K.B. Davis, M.-O. Mewes, M.R. Andrews, N.J. van Druten, D.S. Durfee, D.M. Kurn, and W. Ketterle, Phys. Rev. Lett. **75**, 2969 (1995).

[4] B.P. Anderson and M.A. Kasevich, Science **282**, 1686 (1998); M. Greiner, O. Mandel, T. Esslinger, T.W. Hänsch and I. Bloch, Nature **415**, 39 (2002); J.C. Bronski, L.D. Carr, B. Deconinck and J.N. Kutz, Phys. Rev. Lett. **86**, 1402 (2001).

[5] D.I. Choi and Q. Niu, Phys. Rev. Lett. **82**, 2022 (1999); C. Orzel, A.K. Tuchman, M.L. Fesenlau, M. Yasuda and M.A. Kasevich, Science **291**, 2386 (2001); M.-O. Mewes, M. Andrews, D.M. Kurn, D.S. Durfee, C.G. Townsend and W. Ketterle, Phys. Rev. Lett. **78**, 582 (1997).

[6] F.S. Cataliotti, S. Burger, C. Fort, P. Maddaloni, F. Minardi, A. Trombettoni, A. Smerzi and M. Inguscio, Science **293**, 843 (2001); L.M. Duan, E. Demler and M.D. Lukin, Phys. Rev. Lett. **91**, 090402 (2003).

[7] J.K. Pachos and P.L. Knight, Phys. Rev. Lett. **91**, 107902 (2003).

[8] S. Burger, F.S. Cataliotti, C. Fort, F. Minardi and M. Inguscio, Phys. Rev. Lett. **86**, 4447 (2001).

[9] E.W. Hagley et al., Science **283**, 1706 (1999); I. Bloch, T.W. Hänsch, and T. Esslinger, Phys. Rev. Lett. **82**, 3008 (1999); A.V Carpentier, H. Michinel, D.N. Olivieri, and D. Novoa, Phys. B: At. Mol. Opt. Phys. **43**, 105302 (2010);

[10] S. Burger, K. Bongs, S. Dettmer, W. Ertmer, K. Sengstock, A. Sanpera, G.V. Shlyapnikov, and M. Lewenstein, Phys. Rev. Lett. **83**, 5198 (1999); B.P. Anderson, P.C. Haljan, C.A. Regal, D.L. Feder, L.A. Collins, C.W. Clark, and E.A. Cornell, Phys. Rev. Lett. **86**, 2926 (2001); J. Denschlag, J.E. Simsarian, D.L. Feder, C.W. Clark, L.A. Collins, J. Cubizolles, L. Deng, E.W. Hagley, K. Helmerson, W. P. Reinhardt, S.L. Rolston, B.I. Schneider, W.D. Phillips, Science **287**, 97 (2000).

[11] K.E. Strecker, G.B. Partridge, A.G. Truscott, R.G. Hulet, Nature (London) **417**, 150 (2002); L. Khaykovich, F. Schreck, G. Ferrari, T. Bourdel, J. Cubizolles, L.D. Carr, Y. Castin, and C. Salomon, Science **296**, 1290 (2002); H. Sakaguchi and B.A. Malomed, Phys. Rev. E **72**, 046610 (2005).

[12] T. Busch and J.R. Anglin, Phys. Rev. Lett. **87**, 010401 (2001).

[13] M.R. Matthews, B.P. Anderson, P.C. Haljan, D.S. Hall, C.E. Wieman, and E.A. Cornell, Phys. Rev. Lett. **83**, 2498 (1999); K.W. Madison, F. Chevy, W. Wohlleben, and J. Dalibard, Phys. Rev. Lett. **84**, 806 (2000); S. Inouye, S. Gupta, T. Rosenband, A.P. Chikkatur, A. Gorlitz, T.L. Gustavson, A.E. Leanhardt, D.E. Pritchard, and W. Ketterle, Phys. Rev. Lett. **87**, 080402 (2001).

[14] J.R. Abo-Shaeer, C. Raman, J.M. Vogels, and W. Ketterle, Science **292**, 476 (2001); J.R. Abo-Shaeer, C. Raman, and W. Ketterle, Phys. Rev. Lett. **88**, 070409 (2002); P. Engels, I. Coddington, P.C. Haljan, and E.A. Cornell, Phys. Rev. Lett. **89**, 100403 (2002).

[15] E.A. Cornell, C.E. Wieman, Rev. Mod. Phys. **74**, 875 (2002); W. Ketterle, Rev. Mod. Phys. **74**, 1131 (2002).

[16] D.M. Stamper-Kurn , M.R. Andrews, A.P. Chikkatur, S.Inouye, M.H. Miesner, J. Stenger, and W. Ketterle Phys. Rev. Lett. **80**, 2027 (1998); M.D. Barrett, J.A. Sauer, and M.S. Chapman Phys. Rev. Lett. **87**, 010404 (2001).

[17] J. Weiner, V.S. Bagnato, S. Zilio, and P.S. Julienne, Rev. Mod. Phys. **71**, 1 (1999); R. Grimm, M. Weidemüller, and Y.B. Ovchinnikov, Adv. At. Mol. Opt. Phys. **42**, 95 (2000).

[18] O. Morsch and E. Arimondo, *in* T. Dauxois, S. Ruffo, E. Arimondo, and M. Wilkens (Eds.), *Dynamics and Thermodynamics of Systems with Long-Range Interactions*, Springer, Berlin, (2002), pp. 312-331.

[19] I. Bloch, J. Phys. B: At. Mol. Opt. Phys. **38**, S629 (2005); I. Bloch, Nature Phys. **1**, 23 (2005); 0. Morsch and M.K. Oberthaler, Rev. Mod. Phys. **78**, 179 (2006).

[20] S. Peil, J.V. Porto, B.L. Tolra, J.M. Obrecht, B.E. King, M. Subbotin, S.L. Rolston, and W.D. Phillips, Phys. Rev. A **67**, 051603(R) (2003); F.W. Strauch, M. Edwards, E. Tiesinga, C. Williams and C.W. Clark, Phys. Rev. A **77**, 050304 (2008).

[21] M.R. Andrews, C.G. Townsend, H-J. Miesner, D.S. Durfee, D.M. Kurn, and W. Ketterle, Science **275**, 637 (1999).

[22] M. Albiez, R. Gati, J. F¨ olling J, S. Hunsmann, M. Cristiani, and M.K. Oberthaler, Phys. Rev. Lett. **95**, 010402 (2005).

[23] C.J. Pethick and H. Smith, *Bose-Einstein Condensation in Dilute Alkali Gases*, Cambridge University Press, Cambridge, (2002); L.P. Pitaevskii and S. Stringari, *Bose-Einstein Condensation*, Clarendon Press, Oxford, (2003).

[24] A. Leggett, Rev. Mod. Phys. **73**, 307 (2001); F. Dalfovo, S. Giorgini, L.P. Pitaevskii, and S. Stringari, Rev. Mod. Phys. **71**, 463 (1999).

[25] S. Inouye, M.R. Andrews, J. Stenger, H-J. Miesner, D.S. Stamper-Kurn, and W. Ketterle, Nature (London) **392**, 151 (1998); Ph. Courteille, R.S. Freeland, D.J. Heinzen, F.A. van Abeelen and B.J. Verhaar, Phys. Rev. Lett. **81**, 69 (1998); J.L. Roberts, N.R. Claussen, J.P. Burke, Jr., C.H. Greene, E.A. Cornell, and C.E. Wieman, Phys. Rev. Lett. **81**, 5109 (1998); V. Vuletić, A.J. Kerman, C. Chin, and S. Chu, Phys. Rev. Lett. **82**, 1406 (1999); S.L. Cornish, N.R. Claussen, J.L. Roberts, E.A. Cornell, and C.E. Wieman, Phys. Rev. Lett. **85**, 1795 (2000).

[26] A. Mohamadou, E. Wamba, D. Lissouck, and T.C. Kofané, Phys. Rev. E **85**, 046605 (2012); E. Wamba, A. Mohamadou, and T.C. Kofané, Chin. Phys. B **21**, 070504 (2012).

[27] F.Kh. Abdullaev, A.A. Abdumalikov, and R.M. Galimzyanov Phys. Lett. A **367**, 149 (2007); U. Al. Khawaja, J. Phys. A: Math. Theor. **39**, 9679 (2006); K.D. Moll, A.L. Gaeta, and G. Fibich, Phys. Rev. Lett. **90**, 203902 (2003); A. T. Avelar, D. Bazeia, and W. B. Cardoso, Phys. Rev. E **79**, 025602(R) (2009).

[28] V.V. Konotop and M. Salerno, Phys. Rev. A **65**, 021602(R) (2002).

[29] A. Smerzi, A. Trombettoni, P.G. Kevrekidis, and A.R. Bishop, Phys. Rev. Lett. **89**, 170402 (2002).

[30] F.S. Cataliotti, L. Fallani, F. Ferlaino, C. Fort, P. Maddaloni, M. Inguscio, A. Smerzi, A. Trombettoni, P.G. Kevrekidis, and A.R. Bishop (2002)., e-print cond-mat/0207139

[31] M. Kasevich and A. Tuchman (private communication).

[32] G. Theocharis, D.J. Frantzeskakis, P.G. Kevrekidis, B.A. Malomed, and Yu.S. Kivshar, Phys. Rev. Lett. **90**, 120403 (2003); G. Theocharis, Z. Rapti, P.G. Kevrekidis, D.J. Frantzeskakis, and V.V. Konotop, Phys. Rev. A **67**, 063610 (2003); J.-K. Xue, Phys. Lett. A **341**, 527 (2005).

[33] F. Kh. Abdullaev, A.A. Abumalikov, R.M. Galimzyanov, Physica D **238**, 1345 (2009); R. Murali, K. Porsezian, Physica D **239**, 1 (2010).

[34] E. Wamba, *Matter waves of Bose-Einstein condensates with two- and three-body interactions*, PhD thesis, University of Yaounde I, (2013).

[35] C.J. Myatt, E.A. Burt, R.W. Ghrist, E.A. Cornell, and C.E. Wieman Phys. Rev. Lett. **78**, 586 (1997); D.S. Hall, M.R. Matthews, J.R. Ensher, C.E. Wieman, and E.A. Cornell, Phys. Rev. Lett. **81**, 1539 (1998).

[36] J. Stenger, S. Inouye, M.R. Andrews, H.-J. Miesner, D.M. Stamper-Kurn, and W. Ketterle, Phys. Rev. Lett. **82**, 4569 (1999); D.M. Stamper-Kurn, A.P. Chikkatur, A.Görlitz, S. Inouye, S. Gupta, D.E. Pritchard, and W. Ketterle, Phys. Rev. Lett. **83**, 2072 (1998).

[37] R. Wynar, R.S. Freeland, D.J. Han, C. Ryu, and D.J. Heinzen, Science **287**, 1016 (2000); G. Modugno, G. Ferrari, G. Roati, R.J. Brecha, A. Simoni, and M. Inguscio, Science **294**, 1320 (2001).

[38] M. Trippenbach , K. Goral, K. Rzazewski, B. Malomed, and Y.B. Band, J. Phys. B: At. Mol. Opt. Phys. **33**, 4017 (2000); I.M. Merhasin, B.A. Malomed, R. Driben, J. Phys. B: At. Mol. Opt. Phys. **38**, 877 (2005); I.M. Merhasin, B.A. Malomed and R. Driben, Phys. Scripta **T116**, 18 (2006).

[39] S. Coen and M. Haelterman, Phys. Rev. Lett. **87**, 140401 (2001).

[40] P. Öhberg and L. Santos, Phys. Rev. Lett. **86**, 2918 (2001).

[41] Th. Busch and J.R. Anglin, Phys. Rev. Lett. **87**, 010401 (2001); C. Becker, S. Stellmer, S. Soltan-Panahi, S. Dorcher, M. Baumert, E.-M. Richter, J. Kronjager, K. Bongs and K. Sengstock, Nature Phys. **4**, 496 (2008).

[42] K. Kasamatsu, M. Tsubota and M. Ueda, Int. J. Mod. Phys. B **19**, 1835 (2005).

[43] W.-P. Hong, Z. Naturforch **60**a, 719 (2005); B.B. Baizakov, A. Bouketir, A. Messikh, and B.A. Umarov, Phys. Rev. E **79**, 046605 (2009); T. Mithun and K. Porsezian, Phys. Rev. A **85**, 013616 (2012).

[44] F.T. Arecchi, J. Bragard, L.M. Castellano, Opt. Commun. **179**, 149 (2000).

[45] B. Kneer, T. Wong, K. Vogel, W.P. Schleich, D.F. Walls, Phys. Rev. A **58**, 4841 (1998).

[46] S. Martellucci, A.N. Chester, A. Aspect, and M. Inguscio, *Bose-Einstein Condensates and Atom Lasers*, Kluwer Academic Publishers, New York, Boston, Dordrecht, London, Moscow (2002).

[47] E.A. Ostrovskaya, J. Abdullaev, A.S. Desyatnikov, M.D. Fraser, and Y.S. Kivshar, Phys. Rev. **86**, 013636 (2012).

[48] J.C. Bronski, L.D. Carr, B. Deconinck, and J.N. Kutz, Phys. Rev. Lett. **86**, 1402 (2001); J.C. Bronski, L.D. Carr, B. Deconinck, and J.N. Kutz, and K. Promislow, Phys. Rev. E **63**, 036612 (2001); B. Deconinck, B. A. Frigyik, and J. N. Kutz, Phys. Lett. A **283**, 177 (2001).

[49] Y.V. Kartashov, B.A. Malomed, L. Torner, Rev. Mod. Phys. **83**, 247 (2011), and references therein.

[50] N. Dror, B. A. Malomed, and J. Zeng, Phy. Rev. E **84**, 046602 (2011).

[51] E. Braaten and A. Nieto, Phys. Rev. B **56**, 14745 (1997); A. Fabrocini and A. Polls, Phys. Rev. A **60**, 2319 (1999); A. Fabrocini and A. Polls, Phys. Rev. A **64**, 063610 (2001); D. Blume and Chris H. Greene, Phys. Rev. A **63**, 063601 (2001); A. Banerjee and M.P. Singh, Phys. Rev. A **64**, 063604 (2001).

[52] H. Fu, Y. Wang, and B. Gao, Phys. Rev. A **67**, 053612 (2003).

[53] W. Bao and Q. Du, SIAM J. SCI. COMPUT. **25**, 1674 (2004).

[54] R. J. Ballagh, "*Partial Differential Equation Algorithm : Conceptual*" unpublished personal papers (1995); B.M. Caradoc-Davies, R.J. Ballagh, and K. Burnett, Phys. Rev. Lett. **83**, 895 (1999); B.M. Caradoc-Davies, R.J. Ballagh, and P.B. Blakie, Phys. Rev. A **62**, 011602(R) (2000);
R.J. Ballagh, *Computation Methods for Solving Nonlinear Partial Differential Equations*, Lecture given at Institute for Theoretical Physics, Innsbruck University, November 2000.

[55] G. Agrawal, *Nonlinear Fiber Optics*, 3rd edition, Academic Press, San Diego, (2001).

[56] A. Einstein, Sitzber. Kgl. Preuss. Akad. Wiss. 261 (1924); A. Einstein, Sitzber. Kgl. Preuss. Akad. Wiss. 3 (1925).

[57] S.N. Bose, Z. Phys. **26**, 178 (1924).

[58] B.H. Bransden and C.J. Joachain, *Quantum Mechanics*, Pearson Education Limited, Essex, England, (2000).

[59] E.A. Donley, N.R. Claussen, S.L. Cornish, J.L. Roberts, E.A. Cornell, and C.E. Wieman, Science **412**, 295 (2001).

[60] K. Huang, *Statistical Mechanics* 2nd ed., John Wiley, (1987).

[61] W. Ketterle and N. J. van Druten, Phys. Rev. A **54**, 656 (1996).

[62] N.N. Bogoliubov, J. Phys. **11**, 23 (1947).

[63] L.D. Landau, J. Phys. USSR **5**, 71 (1941).

[64] S. Inouye, M. R. Andrews, J. Stenger, H. J. Miesner, D. M. Stamper-Kurn, W. Ketterle, Nature **392**, 151 (1998).

[65] J. Stenger, S. Inouye, M.R. Andrews, H-J. Miesner, D.M. Stamper-Kurn, and W. Ketterle, Phys. Rev. Lett. **82**, 2422 (1999).

[66] J.L. Roberts, N.R. Claussen, J.P.Jr. Burke, C.H. Greene, E.A. Cornell, and C.E. Wieman, Phys. Rev. Lett. **81**, 5109 (1998).

[67] S.L. Cornish, N.R. Claussen, J.L. Roberts, E.A. Cornell, and C.E. Wieman, Phys. Rev. Lett. **85**, 1795 (2000).

[68] E.B. Kolomeisky, T.J. Newman, J.P. Straley, and X. Qi, Phys. Rev. Lett. **85**, 1146 (2000).

[69] A.J. Moerdijk, B.J. Verhaar, and A. Axelsson, Phys. Rev. A **51**, 4852 (1995); J.L. Roberts, N.R. Claussen, S.L. Cornish, and C.E. Wieman, Phys. Rev. Lett. **85**, 728 (2000).

[70] P.O. Fedichev, Yu. Kagan, G.V. Shlyapnikov, and J.T.M. Walraven, Phys. Rev. Lett. **77**, 2913 (1996).

[71] K. Huang and C.N. Yang, Phys. Rev. **105**, 767 (1957).

[72] S.A. Morgan, J. Phys. B **33**, 3847 (2000); S.A Morgan, *A Gapless Theory of Bose-Einstein Condensation in Dilute Gases at Finite Temperatures*, PhD thesis, University of Oxford, (1999).

[73] J.R. Taylor, *Scattering Theory*, John Wiley and Sons, Inc, (1972).

[74] M.J. Davis, *Dynamics of Bose-Einstein condensation*, PhD thesis, University of Oxford, (2001); A.A. Norrie, *A classical field treatement for colliding Bose-Einstein condensates*, PhD thesis, University of Otago, (2005).

[75] E. Braaten, H.-W. Hammer, and T. Mehen, Phys. Rev. Lett. **88**, 040401 (2002).

[76] A. Gammal, T. Frederico, and L. Tomio, Phys. Rev. A **64**, 055602 (2001).

[77] T-L. Ho, V.B. Shenoy, Phys. Rev. Lett. **77**, 3276 (1996); P. Öhberg, S. Stenholm, Phys. Rev. A **57**, 1272 (1998); E. Timmermans, Phys. Rev. Lett. **81**, 5718 (1998).

[78] H. Pu, and N.P. Bigelow, Phys. Rev. Lett. **80**, 1134 (1998).

[79] J.J. García-Ripoll, and V.M. Pérez-García, Phys. Rev. Lett. **84**, 4264 (2000).

[80] B.D. Esry, C.H. Greene, Phys. Rev. A **59**, 1457 (1999).

[81] W-P. Hong, Z. Naturforch **60a**, 719 (2005); B. B. Baizakov, A. Bouketir, A. Messikh, and B. A. Umarov, Phys. Rev. E **79**, 046605 (2009).

[82] N.P Proukakis and B. Jackson, J. Phys. B: At. Mol. Opt. Phys. **41**, 203002 (2008).

[83] S. Cowell, H. Heiselberg, I.E. Mazets, J. Morales, V.R. Pandharipande, and C. J. Pethick, Phys. Rev. Lett. **88**, 210403 (2002).

[84] E. Tiesinga, C.J. Williams, F.H. Mies, and P.S. Julienne, Phys. Rev. A **61**, 063416 (2000); D. Blume and C.H. Greene, Phys. Rev. A **65**, 043613 (2002); E.L. Bolda, E. Tiesinga, and P.S. Julienne, Phys. Rev. A **66**, 013403 (2002).

[85] H. Fu, Y. Wang, and B. Gao, Phys. rev. A **67**, 053612 (2003).

[86] C.J. Foot, Contemp. Phys. **32**, 369 (1991); S. Chu, Rev. Mod. Phys. **70**, 685 (1998); C. Cohen-Tannoudji, Rev. Mod. Phys. **70**, 707 (1998); W. D. Phillips, Rev. Mod. Phys. **70**, 721 (1998).

[87] W. Ketterle, K.B. Davis, M.A. Martin, and D.E. Pritchard, Phys. Rev. Lett. **70**, 2253 (1993).

[88] N.R. Newbury and C.E. Wieman, Am. J. Phys. **64**, 18 (1996).

[89] W. Petrich, M.H. Anderson, J.R. Ensher, and E.A. Cornell, Phys. Rev. Lett. **74**, 3352 (1995).

[90] M.-O. Mewes, M.R. Andrews, N.J. van Druten, D.M. Kurn, D.S. Durfee, and W. Ketterle, Phys. Rev. Lett **77**, 416 (1996).

[91] I. Bloch, J. Dalibard, and W. Zwerger, Rev. Mod. Phys. **80**, 885 (2008).

[92] S. Raghanavan, A. Smerzi, S. Fantoni, and S.R. Shenoy, Phys. Rev. A **59**, 620 (1999); M. Albiez, R. Gati, J. Föling, S. Hunsmann, M. Cristiani, and M. Oberthaler, Phys. Rev. Lett. **95**, 010402 (2005).

[93] K. Staliunas, S. Longhi, and G. J. de Valcárcel, Phys. Rev. Lett. **89**, 210406 (2002); P. Engels, C. Atherton, M. Hoefer, Phys. Rev. Lett. **98**, 095301 (2007); A. Balaž, R. Paun, A.I. Nicolin, S. Balasubramanian, and R. Ramaswamy, Phys. Rev. A **89**, 023609 (2014);

[94] F.Kh. Abdullaev, P.G. Kevrekidis, and M. Salerno, Phys. Rev. Lett. **105**, 205313 (2010); Y.V. Kartashov, V.V. Konotop, and L. Torner, Phys. Rev. B **86**, 205313 (2012).

[95] Th. Busch and J.R. Anglin, Lecture Notes in Physiscs **538**, 67 (2000); I. Shomroni, E. Lahoud, S. Levy, and J. Steinhauer, Nature Phys. **5**, 193 (2009).

[96] S. Loomba, H. Kaur, R. Gupta, C.N. Kumar, and T.S. Raju, Phys. Rev. E **89**, 70271 (2014), and references therein.

[97] V. N. Serkina, Akira Hasegawa, and T.L.Belyaeva, Proc. of SPIE **7027**, 70271 (2008), and references therein.

[98] T. Zhang, Z-Y. Yang, L-C. Zhao, and R-H. Yuen, Chin. Phys. B **19**, 070502 (2007).

[99] X-F. Zhang, C-W. Xie, and S-En Wang, Commun. Theor. Phys. **47**, 1063 (2007).

[100] F-H. Qi, Bo Tian, T. Xu, H-Q. Zhang, Li-Li Li, X.H. Meng, X. Lu, W-J. Liu, Int. J. Mod. Phys. B **25**, 1037 (2011)

[101] W.H uang, J.W. Mao, and W.G. Qiu, Acta Phys. Pol. A 119, 294297 (2011).

[102] X-L. Wang, G-H. Wang, C.B. Liu, and H-J. Yang, Commun. Theor. Phys. **59**, 273 (2013).

[103] D.J. Kaup, M.J. Ablowitz, A.C. Newell and H. Segur, Stud. Appl. Math. **53**, 249 (1974).

[104] D.J. Kaup, B.A. Malomed, Physica D **87**, 155 (1995).

[105] M. Bondeson, M. Lisak, and D. Anderson, Phys. Scripta **20**, 479 (1979).

[106] D. Anderson, Phys. Rev. A **27**, 3135 (1983); D. Anderson, M. Lisak, and T. Reichel, J. Opt. Soc. Am. B **5**, 207 (1988).

[107] B.A. Malomed, Prog. Opt. **43**, 71 (2002).

[108] C. Sulem and P.L. Sulem, *The Nonlinear Schrödinger Equation: Self-Focusing and Wave Collapse*, Springer-Verlag, New-York, (1999).

[109] L. Wu, J.-F. Zhang, and L. Li, N. J. Phys. **9**, 69 (2007).

[110] V.M. Pérez Garcá, P.J. Torres, V.V. Konotop, Physica D **221**, 31 (2006).

[111] E. Yomba, Phys. Lett. A **336**, 463 (2005).

[112] H.A. Abdusalam, Int. J. Nonlinear Sci. Numer. Simul. **6**, 99 (2005).

[113] Z.T. Fu, S.K. Liu, Q. Zhao, Phys. Lett. A **289**, 69 (2001); ibid **290**, 72 (2001); E.J. Parkes, B.R. Duffy, P.C. Abbott, Phys. Lett. A **295**, 280 (2002).

[114] S. Sheng, W. Li, F. Zheng, J. Yu, M. Ji, Z. Lü, C. Ma, Int. J. Nonlinear. Sci. **5**, 25 (2007).

[115] Z.Y. Yan, Phys. Lett. A **292**, 100 (2001); J.B. Liu, K.Q. Yang, Chaos, Solitons and Fractals **22**, 111 (2004); S. Zhang, Solitons and Fractals **30**, 1213 (2006); ibid **32**, 847 (2007); ibid **32**, 1375 (2007); J. Chen, H.S. He, K.Q. Yang, Commun. Theo. Phys. **44**, 307 (2005).

[116] W.X. Ma and B. Fuchssteiner, Int. J. Non-Linear Mech. **31**, 329 (1996).

[117] K.E. Strecker, G.B. Partridge, A.G. Truscott, and R.G. Hulet, Nature **417**, 150 (2002).

[118] L.V. Hau, S.E. Harris, Z. Dutton, C.H. Behroozi, Nature **397**, 594 (1999); S.E. Harris, Phys. Today **50**, 36 (1997); C. Liu, Z. Dutton, C.H. Behroozi, L.V. Hau, Nature **409**, 490 (2001); D. Tarhan, A. Sennaroglu,and Ö.E. Müstecaplioğlu, Eur. Phys. J. Special Topics **160**, 399 (2008).

[119] Z. Dutton, L.V. Hau, Phys. Rev. A **70**, 053831 (2004).

[120] J. Klaers, J. Schmitt, F. Vewinger, and M. Weitz, Nature **468**, 545 (2010).

[121] A. Ramanathan, K.C. Wright, S.R. Muniz, M. Zelan, W.T. Hill III, C.J. Lobb, K. Helmerson, W.D. Phillips, and G.K. Campbell, Phys. Rev. Lett. **106**, 130401 (2011).

[122] O. Mandel, M. Greiner, A. Widera, T. Rom, T. W. Hänsch, and I. Bloch, Nature (London) **425**, 937 (2003); O. Mandel, M. Greiner, A. Widera, T. Rom, T. W. Hänsch, and I. Bloch, Phys. Rev. Lett. **91**, 010407 (2003).

[123] I.H. Deutsch, G.K. Brennen, and P.S. Jessen, Fortschr. Phys. **48**, 925 (2000).

[124] J.V. Porto, S. Rolston, B.L. Tolra, C.J. Williams, and W.D. Phillips,Philos. Trans. R. Soc. London, Ser. A **361**, 1417 (2003).

[125] D. Jaksch, Contemp. Phys. **45**, 367 (2004).

[126] R. Carretero-González, D.J. Frantzeskakis, and P.G. Kevrekidis, Nonlinearity **21**, 139 (2008), and references therein.

[127] V.A. Brazhnyi, V.V. Konotop, Mod. Phys. Lett. B **18**, 627 (2004).

[128] M. Theis, G. Thalhammer, K. Winkler, M. Hellwig, G. Ruff, R. Grimm, and J.H. Denschlag, Phys. Rev. Lett. **93**, 123001 (2004).

[129] Y.V. Bludov, V.V. Konotop, and M. Salerno, Eur. Phys. Lett. **93**, 30003 (2011);

[130] V.A. Brazhnyi, V.V. Konotop, V.M. Perez Garcia, and H. Ott, Phys. Rev. Lett. **102**, 144101 (2009).

[131] M. Remoissenet and M. Peyrard, J. Phys. C: Solid State Phys. **14** 481, (1981).

[132] A.J. Tristram, M. Salerno, E.A. Ostrovskaya and Y.S. Kivshar, Phys. Rev. A **77**, 043607 (2008).

[133] D. Belobo Belobo, T.B. Ekogo, G.H. Ben-Bolie, and T.C. Kofané, Far East J. Dynam. Syst. **16**, 107 (2011).

[134] P. Mururaganandam and S.K. Adhikari, Comp. Phys. Comm. **180**, 1888 (2009).

[135] C.G. Latchio Tiofack, T.B. Ekogo, H. Moussambi, A. Mohamadou, T.C. Kofane, Appl. Math. **3**, 844 (2012).

[136] L. Wu and J.-F. Zhang, Chin. Phys. Lett. **24**, 1471 (2007).

[137] H. Fu, Y. Wang and B. Gao, Phys. Rev. A **67**, 053612 (2003).

[138] D. Belobo Belobo, G.H. Ben-Bolie, T.B. Ekogo, and T.C. Kofané, Int. J. Mod. Phys. B **26**, 1250164 (2012).

[139] A. Mohamadou, E. Wamba, S.Y. Doka, T.B. Ekogo, and T.C. Kofané, Phys. Rev. A **84**, 023602 (2011).

[140] V.R. Ramesh, R. Radha, and M. Wadati, J. Phys. Soc. Jpn. **79**, 074005 (2010).

[141] Q-Y. Li, Z-D. Li, L. Li, G-S. Fu, Opt. Commun. **283**, 3661 (2010).

[142] J. Toulouse, J. Lightwave Technol. **23**, 30625 (2005), and references therein.

[143] D. Schneble, G. K. Campbell, E. W. Streed, M. Boyd, D. E. Pritchard, and W. Ketterle, Phys. Rev. A **69**, 041601(R) (2004).

[144] B. W. Shore, *The Theory of Coherent Atomic Excitation, vol. 1 Simple Atoms and Fields*, (John Wiley and Sons, 1990).

[145] K. C. Wright, L. S. Leslie, and N. P. Bigelow, Phys. Rev. A, **77**, 041601(R) (2008).

[146] M.M. Cola and N. Piovella, Phys. Rev. A **70**, 045601 (2004).

[147] D. Belobo Belobo, G.H. Ben-Bolie, T.B. Ekogo, T.C. Kofané, Int. J. Theor. Phys **52**, 1415 (2013).

[148] A. Mohamadou, E.A. Bebe, T.C. Kofane, Phys. Rev. E **74**, 046604 (2006).

[149] D. Belobo Belobo, G.H. Ben-Bolie, and T.C. Kofané, Int. J. Mod. Phys. B **26**, 1250202 (2012).

[150] A. Gammal, T. Frederico, L. Tomio, and Ph. Chomaz, J. Phys. B: At. Mol. Opt. Phys. **33**, 4053 (2000).

[151] W.X. Ma, M. Chen, Appl.Math. Comput. **215**, 2835 (2009).

[152] D. Belobo Belobo, G.H. Ben-Bolie, T.B. Ekogo, and T.C. Kofane, J. Phys. A: Math. Gen. (to be published).

[153] W. Hai, and Q. Xie, Phys. Rev. E **70**, 036213 (2002), and references therein.

[154] A. Maimistov, B. Malomed and A. Desyatnikov, Phys. Lett. A **254**, 179 (1999).

[155] D. Belobo Belobo, G.H. Ben-Bolie, and T.C. Kofané, Int. J. Mod. Phys. B **28**, 1450003 (2014).

[156] A.T. Avelar, D. Bazeia, and W.B. Cardoso, Phys. Rev. E **79**, 025602(R) (2009).

[157] V.N. Serkin and A. Hasegawa, Phys. Rev. Lett. **85**, 4502 (2000).

[158] S. Sabari, R.V.J. Raja, K. Porsezian, and P. Murugunandam, J. Phys. B: At. Mol. Opt. Phys. **43**, 125302 (2010).

[159] J. Zeng and B.A. Malomed, Phys. Rev. A **85**, 023824 (2012).

[160] P.K. Kevrekidis and D.J. Frantzeskakis, Mod. Phys. Lett. B **18**, 173 (2004).

[161] V.S. Filho, S.M. Holz, and L. Tomio, Phys. Lett. A **372**, 6778 (2008).

[162] E. Kengne and P.K. Talla, J. Phys. B: At. Mol. Opt. Phys. **39**, 3679 (2006).

[163] C.C. Bradley, C.A. Sackett, J.H. Tollett, and R.G. Hulet, Phys. Rev. Lett. **79**, 1170(E) (1997).

[164] D. Belobo Belobo, G.H. Ben-Bolie, and T.C. Kofane, Phys. Rev. E **89**, 042913 (2014).

[165] D. Belobo Belobo, G.H. Ben-Bolie, and T.C. Kofane, Phys. Rev. E (to be published).

[166] W. van Saarloos and P.C. Hohenberg, Phys. Rev. Lett. **64**, 749 (1990); V. Hakim, P. Jacobsen, and Y. Pomeau, Europhys. Lett. **11**, 19 (1990); B.A. Malomed and A.A. Nepomnyashchy, Phys. Rev. A **42**, 6009 (1990).

[167] S. Wabnitz, PIERS ONLINE **5**, 621 (2009).

[168] G.P. Agrawal and C. Headley III, Phys. Rev. A **46**, 1573 (1992).

[169] S. Zhang, Y. N. Sun, J. M. Ba and L. Dong, J. Adv. Math. Studies **3**, 125 (2010).

[170] L-H. Zhang, Appl. Math. Comput. **208**, 144 (2009).

[171] E.A-B. Abdel-Salam, Z. Naturforschung a **64**, 639 (2009); P.F. Byrd and M.D. Friedman, Handbook of Elliptic Integrals for Engineers and Physicists, (Springer, Berlin, Germany, 1954).

[172] S. D. Zhu, Chaos Solitons and Fractals **34**, 1608 (2007).

[173] R. Navarro, R. Carretero-González, P.G. Kevrekidis, *Acsess Proceedings* (2009) 0910, and references therein.

[174] P.G. Kevrekidis, *The Discrete Nonlinear Schrödinger Equation: Mathematical Analysis, Numerical Computations and Physical Perspectives* (Springer, Berlin Heidelberg, 2009).

[175] T. Koch, T. Lahaye, J.Metz, B. Frohlich, A. Griesmaier, and T. Pfau, Nature Phys. **4**, 218 (2008); T. Lahaye, C. Menotti, L. Santos, M. Lewenstein, and T. Pfau, Rep. Prog. Phys. **72**, 126401 (2009).

[176] T. Paul, K. Richter, and P. Schlagheck, Phys. Rev. Lett. **94**, 020404 (2005); R. Chacon, D. Bote, and R. Carretero-González, Phys. Rev. E **78**, 036215 (2008), and references therein.

**APPENDICES**

## APPENDIX A: Solutions of the general Bernoulli equation

Solutions of the general Bernoulli equation are [158]:

(A1) $F_{11}(\xi) = (-\frac{a}{2b})^{\frac{1}{2}}$;

(A2) $\xi_0 > 0$: $F_{12}(\xi) = -\frac{a}{2b}[\tanh[a\xi - \frac{\ln(\xi_0)}{2}] + 1]^{\frac{1}{2}}$;

A(3) $\xi_0 < 0$: $F_{13}(\xi) = -\frac{a}{2b}[\coth[a\xi - \frac{\ln(-\xi_0)}{2}] + 1]^{\frac{1}{2}}$.

## APPENDIX B: Solutions of the Ricatti equation

Solutions of the Ricatti equation are [162]:

(B1) $F_{21}(\xi) = \{\sqrt{\frac{-1}{M(\lambda-1)}}\tanh[\sqrt{-M(\lambda-1)}\xi]\}^{\frac{1}{\lambda-1}}$;

(B2) $F_{22}(\xi) = \{\sqrt{\frac{-1}{M(\lambda-1)}}\coth[\sqrt{-M(\lambda-1)}\xi]\}^{\frac{1}{\lambda-1}}$;

(B3) $F_{23}(\xi) = \{\sqrt{\frac{-1}{M(\lambda-1)}}[\sqrt{\frac{-1}{M(\lambda-1)}}\tanh[\sqrt{-M(\lambda-1)}\xi] \pm \imath sech[\sqrt{-M(\lambda-1)}\xi]]\}^{\frac{1}{\lambda-1}}$;

(B4) $F_{24} = \{\sqrt{\frac{-1}{M(\lambda-1)}}[\frac{\sqrt{2}\sqrt{\frac{-1}{M(\lambda-1)}}\tanh[\sqrt{-M(\lambda-1)}\xi]\pm\imath sech[\sqrt{-M(\lambda-1)}\xi]]}{\sqrt{2}-sech[\sqrt{-M(\lambda-1)}\xi]}]\}^{\frac{1}{\lambda-1}}$;

(B5) $F_{25}(\xi) = \{-\sqrt{\frac{-1}{M(\lambda-1)}}\tan[\sqrt{-M(\lambda-1)}\xi]\}^{\frac{1}{\lambda-1}}$;

(B6) $F_{26}(\xi) = \{\sqrt{\frac{-1}{M(\lambda-1)}}\cot[\sqrt{-M(\lambda-1)}\xi]\}^{\frac{1}{\lambda-1}}$;

(B7) $F_{27} = \{-\sqrt{\frac{-1}{M(\lambda-1)}}[\frac{\sqrt{2}\sqrt{\frac{-1}{M(\lambda-1)}}\tan[\sqrt{-M(\lambda-1)}\xi]\pm\imath\sec[\sqrt{-M(\lambda-1)}\xi]}{\sqrt{2}+\sqrt{5}\sec[\sqrt{-M(\lambda-1)}\xi]}]\}^{\frac{1}{\lambda-1}}$;

(B8) $F_{28} = \{\frac{1}{-M(\lambda-1)\xi+p}\}^{\frac{1}{\lambda-1}}$.

$p$ is an arbitrary real constant.

## APPENDIX C: Solutions of the Lenard equation

The Lenard equation admits the following solutions [163]:

(C1) $b_2 > 0$, $b_4 < 0$, $b_6 < 0$, $\delta = b_4^2 - 4b_2b_6 > 0$: $F_{3,1} = \sqrt{\frac{2b_2 sech^2(\sqrt{b_2}\xi)}{2\sqrt{\delta}-(\sqrt{\delta}+b_4)sech^2(\sqrt{b_2}\xi)}}$, $F_{3,2} = \sqrt{\frac{2b_2 csch^2(\pm\sqrt{b_2}\xi)}{2\sqrt{\delta}+(\sqrt{\delta}-b_4)csch^2(\pm\sqrt{b_2}\xi)}}$;

(C2) $b_0 = 0$, $b_2 < 0$, $b_4 \geq 0$, $b_6 < 0$, $\delta > 0$: $F_{3,3} = \sqrt{\frac{-2b_2\sec^2(\sqrt{-b_2}\xi)}{2\sqrt{\delta}-(\sqrt{\delta}-b_4)\sec^2(\sqrt{-b_2}\xi)}}$, $F3,4 =$

$\sqrt{\frac{2b_2\csc^2(\pm\sqrt{-b_2}\xi)}{2\sqrt{\delta}+(\sqrt{\delta}+b_4)\csc^2(\pm\sqrt{-b_2}\xi)}}$;
(C3) $b_6=\frac{b_4^2}{4b_2}$, $b_2>0$, $b_4<0$: $F_{3,5}=\sqrt{\frac{-b_2}{b_4}[1+\tanh(\pm\sqrt{b_2}\xi)]}$, $F_{3,6}=\sqrt{\frac{-b_2}{b_4}[1+\coth(\sqrt{b_2}\xi)]}$;
(C4) $b_2>0$: $F_{3,7}=\sqrt{\frac{-b_2b_4sech^2(\sqrt{b_2}\xi)}{b_4^2-b_2b_6[1+\tanh^2(\sqrt{b_2}\xi)]}}$, $F_{3,8}=\sqrt{\frac{b_2b_4csch^2(\sqrt{b_2}\xi)}{b_4^2-b_2b_6[1+\coth^2(\sqrt{b_2}\xi)]}}$, $F_{3,9}=4\sqrt{\frac{b_2\exp(2\sqrt{b_2}\xi)}{\exp(4\sqrt{b_2}\xi-4C_4)-64b_2b_6}}$;
(C5) $b_2>0$: $F_{3,7}=4\sqrt{\frac{b_2\exp(2\sqrt{b_2}\xi)}{\exp((2\sqrt{b_2}\xi-4C_4)^2-64b_2b_6)}}$;
(C5) $b_2>0$, $\delta>0$: $F_{3,10}=\sqrt{\frac{2b_2}{\sqrt{\delta}\cosh(2\sqrt{b_2}\xi)-b_4}}$;
(C6) $b_2>0$, $\delta<0$: $F_{3,11}=2\sqrt{\frac{2b_2}{\sqrt{-\delta}\sinh(2\sqrt{b_2}\xi)-b_4}}$;
(C7) $b_2<0$, $\delta>0$: $F_{3,12}=\sqrt{\frac{2b_2}{\sqrt{\delta}\sin(2\sqrt{-b_2}\xi)-b_4}}$, $F_{3,13}=\sqrt{\frac{2b_2}{\sqrt{\delta}\cos(2\sqrt{-b_2}\xi)-b_4}}$;
(C8) $b_2>0$, $b_6>0$; $F_{3,14}=\sqrt{\frac{-b_2sech^2(\sqrt{b_2}\xi)}{b_4+2\sqrt{b_2b_6}\tanh(\sqrt{b_2}\xi)}}$, $F_{3,15}=\sqrt{\frac{b_2csch^2(\sqrt{b_2}\xi)}{b_4+2\sqrt{b_2b_6}\coth(\sqrt{b_2}\xi)}}$;
(C9) $b_2<0$, $b_6>0$: $F_{3,16}=\sqrt{\frac{-b_2\sec^2(\sqrt{-b_2}\xi)}{b_4+2\sqrt{-b_2b_6}\tan(\sqrt{-b_2}\xi)}}$, $F_{3,17}=\sqrt{\frac{-b_2\csc^2(\sqrt{-b_2}\xi)}{b_4+2\sqrt{-b_2b_6}\cot(\sqrt{-b_2}\xi)}}$;
(C10) $b_2>0$, $b_4=0$: $F_{18}=4\sqrt{\frac{\pm b_2\exp(2\sqrt{b_2}\xi)}{1-64b_2b_6\exp(4\sqrt{b_2}\xi)}}$;
(C11) $b_2<0$, $b_4>0$: $F_{3,19}=\sqrt{\frac{-8b_2\tanh^2(\pm\sqrt{\frac{-b_2}{3}}\xi)}{3b_4[3+\tanh^2(\pm\sqrt{\frac{-b_2}{3}}\xi)]}}$, $F_{3,20}=\sqrt{\frac{-8b_2\coth^2(\pm\sqrt{\frac{-b_2}{3}}\xi)}{3b_4[3+\coth^2(\pm\sqrt{\frac{-b_2}{3}}\xi)]}}$;
(C112) $b_2>0$, $b_4<0$: $F_{3,21}=\sqrt{\frac{8b_2\tan^2(\pm\sqrt{\frac{b_2}{3}}\xi)}{3b_4[3-\tan^2(\pm\sqrt{\frac{b_2}{3}}\xi)]}}$, $F_{3,22}=\sqrt{\frac{8b_2\cot^2(\pm\sqrt{\frac{b_2}{3}}\xi)}{3b_4[3-\cot^2(\pm\sqrt{\frac{b_2}{3}}\xi)]}}$.
$b_0=0$ corresponds to $F_{3,1}-F_{3,18}$; $b_0=\frac{8b_2^2}{27b_4}$ and $b_6=\frac{b_4^2}{4b_2}$ correspond to $F_{3,19}-F_{3,22}$.

## APPENDIX D: Genaralized Jacobi elliptic function solutions of the Lenard equation

Generalized Jacobi elliptic function solutions of the Lenard equation [164]:
(D1) $b_0=1-k_1^2-k_2^2+k_1^2k_2^2$, $b_2=-1+2k_1^2+2k_2^2-3k_1^2k_2^2$, $b_4=-k_1^2-k_2^2+3k_1^2k_2^2$, $b_6=-k_1^2k_2^2$: $F_{23}=c(\xi,k_1,k_2)$;
(D2) $b_0=-1+k_1^2-k_2^2+k_1^{-2}k_2^2$, $b_2=2-k_1^2+2k_2^2-3k_1^{-2}k_2^2$, $b_4=-1-k_2^2+3k_1^{-2}k_2^2$, $b_6=-k_1^{-2}k_2^2$: $F_{24}=d_1(\xi,k_1,k_2)$.
$c(\xi,k_1,k2)$ is the generalized Jacobi elliptic cosine function, and $d_1(\xi,k_1,k2)$ is the generalized Jacobi elliptic function of the third kind. The generalized Jacobi elliptic functions can be written in terms of the standard Jacobi elliptic functions as:
$c(\xi,k_1,k2)=k_3cn(k_3\xi,k_4)/\sqrt{1-k_2^2cn^2(k_3\xi,k_4)}$,
$d_1(\xi,k_1,k2)=\sqrt{k_1^2-k_2^2}dn(k_3\xi,k_4)/\sqrt{k_1^2-k_2^2dn^2(k_3\xi,k_4)}$,
with $k_3=\sqrt{1-k_2^2}$, $k_4=\sqrt{(k_1^2-k_2^2)/(1-k_2^2)}$, $0\le k_2\le k_1\le 1$. The generalized Jacobi functions degenerate to traditional functions in some limiting cases. For instance, if $k_2\to 0$, one can obtain the usual Jacobi elliptic function solutions: $c(\xi,k_1,0)\to cn(\xi,k_1)$, $d_1(\xi,k_1,0)\to dn(\xi,k_1)$. If $k_1\to 1$, $k_2\to 0$, one obtains hyperbolic solutions: $c(\xi,1,0)$, $d(\xi,1,0)\to sech(\xi)$. For $k_1\to 0$, $k_2\to 0$, the generalized Jacobi elliptic functions degenerate to trigonometric solutions:

$c(\xi,0,0) \to \cos(\xi)$, $d_1(\xi,0,0) \to 1$.

## APPENDIX E: Solutions of the hyperbolic equation

Some solutions of the hyperbolic equation [164]:

(E1) $c_2 > 0$, $c_0c_2 - c_2^2 > 0$, $c_2 - 2c_0 + 2\sqrt{c_0(c_2-c_0)}\tan(\sqrt{[c_0(c_2-c_0)]}\xi) > 0$:

$\sinh_{11}[F(\xi)] = \{\frac{[c_0-\sqrt{c_0(c_2-c_0)}\tan[\sqrt{(c_0(c_2-c_0))}\xi]]^2}{c_2[c_2-2c_0+2\sqrt{c_0(c_2-c_0)}\tan[\sqrt{(c_0(c_2-c_0))}\xi]]}\}^{\frac{1}{2}}$;

(E2) $c_2 > 0$, $c_0c_2 - c_2^2 < 0$, $c_2 - 2c_0 + 2\sqrt{c_0(c_2-c_0)}\cot[\sqrt{[c_0(c_2-c_0)]}\xi] > 0$:

$\sinh_{12}[F(\xi)] = \{\frac{[c_0-\sqrt{c_0(c_2-c_0)}\cot[\sqrt{[c_0(c_2-c_0)]}\xi]]^2}{c_2[c_2-2c_0+2\sqrt{c_0(c_2-c_0)}\cot[\sqrt{[c_0(c_2-c_0)]}\xi]]}\}^{\frac{1}{2}}$;

(E3) $c_2 > 0$, $c_0c_2 - c_0^2 < 0$, $c_2 - 2c_0 - 2\sqrt{c_0(c_2-c_0)}\coth[\sqrt{-[c_0(c_2-c_0)]}\xi] > 0$:

$\sinh_{13}[F(\xi)] = \{\frac{[c_0+\sqrt{-c_0(c_2-c_0)}\coth[\sqrt{-[c_0(c_2-c_0)]}\xi]]^2}{c_2[c_2-2c_0-2\sqrt{-c_0(c_2-c_0)}\coth[\sqrt{-[c_0(c_2-c_0)]}\xi]]}\}^{\frac{1}{2}}$;

(E4) $c_2 < 0$, $c_0c_2 - c_0^2 < 0$, $c_2 - 2c_0 - 2\sqrt{c_0(c_2-c_0)}\tanh[\sqrt{-[c_0(c_2-c_0)]}\xi] < 0$:

$\sinh_{13}[F(\xi)] = \{\frac{[c_0+\sqrt{-c_0(c_2-c_0)}\tanh[\sqrt{-[c_0(c_2-c_0)]}\xi]]^2}{c_2[c_2-2c_0-2\sqrt{-c_0(c_2-c_0)}\tanh[\sqrt{-[c_0(c_2-c_0)]}\xi]]}\}^{\frac{1}{2}}$.

## APPENDIX F: Expression of $\chi^1$

The expression of the parameter $\chi^1$ takes the form:

$A_1 = 2n_1n_2(4n_1^2\eta + 4n_2^2\eta + 6n1n2\eta + n1n2 + n1n2\eta^2)$

$A_2 = g_1n_1^2n_2\eta - 4gn_1^2n_2\eta + g_2n1n_2^2\eta - g_1n1^1n_2\eta^2 - 4gn_1n_2^2\eta + 2\chi_1n_1^3n_2\eta - 2\chi_1n_1^3n_2\eta^2 - 2\chi_2n_2^3n_1 + 2\chi n_1n_2^3\eta - g_2n_1n2^2$

$A_3 = -2g_1^2n_1^4n_2^2\eta^3 + 2g^2n_1^3n_2^3\eta^2 - 2g_2n_1^2n_2^4\eta - 8\chi_1^2n_1^6n_2^2\eta^3 - 2g_1gn_1^4n_2^2\eta^2 - 4g_1g_2n_1^3n_2^3\eta^2 - 2g_1gn_1^3n_2^3\eta^2$

$A_4 = -8g_1\chi_1n_1^5n_2^2\eta^3 + 8g_1\chi_2n_1^3n_2^4\eta^2 - 2gg_2n_1^3n_2^3\eta^2 + 2gg_1n_1^4n_2^2\eta^3 - 4g\chi_1n_1^5n_2^2\eta^3 + 4g\chi_1n_1^5n_2^2\eta^3 + 4g\chi_2n_1^3n_2^4\eta$

$A_5 = -4g\chi 2n_1^3n_2^4\eta^2 + 2gg_2n_1^3n_2^2\eta - 2gg_2n_1^2n_2^4\eta^2 + 8g_2\chi_1n_1^4n_2^3\eta^2 - 8g_2\chi_2n_1^2n_2^5\eta + 2gg_1n_1^3n_2^3\eta^3 - 4g\chi_1n_1^4n_2^3\eta^2$

$A_6 = 4g\chi_1n_1^4n_2^3\eta^3 + 4g\chi_2n_1^2n_2^2\eta - 4g\chi_2n_1^2n_2^5\eta^2 + 2gg_2n_1^2n_2^4\eta + 16\chi_1\chi_2n_1^4n_2^4\eta^2 + 8\chi_1\chi_2n_1^5n_2^3\eta^2 + 4g_2\chi 1n_1^5n_2^2\eta^2$

$A_7 = -4g_2\chi 2n_1^3n_2^4\eta + 4g_1\chi_2n_1^4n_2^3\eta^2 + 2g_1g_2n_1^4n_2^2\eta^2 - 4g_1\chi_1n_1^6n_2\eta^3 + 8\chi_1\chi_2n_1^3n_2^5\eta^2 + 4g_2\chi_2n_1^3n_2^4\eta^2 - 4g_2\chi_2n_1n_2^6\eta$

$A_8 = 4g_1\chi_2n_1^2n_2^5\eta^2 + 2g_1g_2n_1^2n_2^4\eta^2 - 4g_1\chi_1n_1^4n_2^3\eta^3 - 8\chi_2^2n_1^2n_2^6\eta - 4\chi_1^2n_1^7n_2\eta^3 - g_1^2n_1^5n_2\eta^3 - g_2^2n_1^3n_2^3\eta$

$A_9 = -4\chi_2^2n_1^3n_2^5\eta - 4\chi_1^2n_1^5n_2^3\eta^3 - g_1^2n_1^3n_2^3\eta^3 - g_2^2n_1n_2^5\eta - 4\chi_2^2n_1n_2^7\eta - g^2n_1^3n_2^3\eta - g^2n_1^3n_2^3\eta^3$

$\chi^1 = \frac{1}{A_1}[A_2 + 2(A_3 + A_4 + A_5 + A_6 + A_7 + A_8 + A_9)^{\frac{1}{2}}]$

## List of publications

1. **D. Belobo Belobo**, T.B. Ekogo, G.H. Ben-Bolie, T.C. Kofané, "*Solitons in attractive Matter- wave condensates in variable anharmonic periodic potentials*", Far East J. Dynam. Syst. **16**, 107 (2011).
2. **D. Belobo Belobo**, G.H. Ben-Bolie, T.B. Ekogo, C. G. Latchio Tiofack, and T.C. Kofane"*Modulational instability of a Bose-Einstein condensate beyond the Fermi pseudopotential with a time-dependent complex potential*", Int. J. Mod. Phys. B **26**, 1250164 (2012).
3. **D. Belobo Belobo**, G.H. Ben-Bolie, T.C. Kofane, "*Three-body interactions beyond the Gross-Pitaevskii equation and modulational instability of Bose-Einstein condensates*", Int. J. Mod. Phys. B **26**, 1250202 (2012).
4. **D. Belobo Belobo**, G.H. Ben-Bolie, T.B. Ekogo, T.C. Kofané, "*Wave trains generation in a delayed nonlinear response of Bose-Einstein condensates with three-body interactions*", Int. J. Theor. Phys **52**, 1415 (2013).
5. **D. Belobo Belobo**, G.H. Ben-Bolie, T.C. Kofane, "*Generation of bright matter-wave soliton patterns in mixtures of Bose-Einstein condensates with cubic and quintic nonlinearities*", Int. J. Mod. Phys. B **28**, 1450003 (2014).
6. **D. Belobo Belobo**, G.H. Ben-Bolie, T.C. Kofane, "*Dynamics of matter-wave condensates with time-dependent two- and three-body interactions trapped by a linear potential in the presence of atom gain or loss*", Phys. Rev. E **89**, 042913 (2014).
7. **D. Belobo Belobo**, G.H. Ben-Bolie, T.C. Kofane, "*Dynamics of Kink, anti-kink, bright, generalized Jacobi elliptic functions solutions of the Gross-Pitaevskii equation with time-dependent two- and three-body interactions*", Phys. Rev. E **91**, 042902 (2015).
8. **D. Belobo Belobo**, G.H. Ben-Bolie, T.B. Ekogo, T.C. Kofané, "*Phase engineering, modulational instability, and bright solitons of a derivative Gross-Pitaevskii equation type*", Chaos Solitons and Fractals (to be published).

# Dynamics of kink, antikink, bright, generalized Jacobi elliptic function solutions of matter-wave condensates with time-dependent two- and three-body interactions

D. Belobo Belobo,[1,2,*] G. H. Ben-Bolie,[1,2] and T. C. Kofane[2,3,4]

[1]*Laboratory of Atom and Radiation, Department of Physics, Faculty of Science, University of Yaounde I, P.O. Box 812, Yaounde, Cameroon*

[2]*Centre d'Excellence en Technologies de l'Information et de la Communication (CETIC), University of Yaounde I, Yaounde, Cameroon*

[3]*Laboratory of Mechanics, Department of Physics, Faculty of Science, University of Yaounde I, P.O. Box 812, Yaounde, Cameroon*

[4]*The Max Planck Institute for the Physics of Complex Systems Nöthnitzer Strasse 38, 01187 Dresden, Germany*

(Received 27 April 2014; revised manuscript received 25 July 2014; published 7 April 2015)

By using the F-expansion method associated with four auxiliary equations, i.e., the Bernoulli equation, the Riccati equation, the Lenard equation, and the hyperbolic equation, we present exact explicit solutions describing the dynamics of matter-wave condensates with time-varying two- and three-body nonlinearities. Condensates are trapped in a harmonic potential and they exchange atoms with the thermal cloud. These solutions include the generalized Jacobi elliptic function solutions, hyperbolic function solutions, and trigonometric function solutions. In addition, we have also found rational function solutions. Solutions constructed here have many free parameters that can be used to manipulate and control some important features of the condensate, such as the position, width, velocity, acceleration, and homogeneous phase. The stability of the solutions is confirmed by their long-time numerical behavior.

DOI: 10.1103/PhysRevE.91.042902 PACS number(s): 05.45.Yv, 03.75.Lm, 03.75.Kk, 34.20.Cf

## I. INTRODUCTION

The dynamics of Bose-Einstein condensates (BECs) trapped in a harmonic potential and exchanging atoms with the thermal cloud has been a fascinating topic and has attracted much attention in recent theoretical and experimental works [1]. It is well known that the dynamical behavior of a condensate in the mean-field limit is well described by the Gross-Pitaevskii equation (GPE) [1], which is a nonlinear Schrödinger equation with an external potential. Basically, the GPE is a three-dimensional (3D) equation, but in some cases, it may be reduced to a one-dimensional (1D) form. This is possible when the condensate is frozen in two transverse directions by a stronger potential. The dimensionless governing equation of cigar-shaped (1D) BECs with two- and three-body nonlinearities can be written as [1]

$$\iota\Psi_t(x,t) + c\Psi_{xx} - g(t)|\Psi(x,t)|^2\Psi(x,t) - \chi(t)|\Psi(x,t)|^4\Psi(x,t) - (\alpha x^2 + \iota\gamma)\Psi(x,t) = 0. \quad (1)$$

In Eq. (1), the time $t$ and the spatial coordinate $x$ are scaled in the harmonic-oscillator units. The time-dependent cubic nonlinearity coefficient $g(t)$ characterizes the intensity of the two-body interactions. The quintic nonlinearity coefficient $\chi(t)$ characterizes the strength of the three-body interactions. Generally speaking, $\chi(t)$ is a complex quantity, but its imaginary part can be neglected since it is very small compared to the real part [2,3]. Thus, in the following, we consider that $\chi(t)$ is a real-valued expression. Time variations of the cubic and the quintic nonlinearities can be realized in condensates by magnetically or optically induced Feshbach resonances [1]. The parameter $\alpha$ represents the strength of the external magnetic or optical harmonic confinement. The complex quantity $\iota\gamma$, which is a nonconservative term, is introduced phenomenologically in Eq. (1). It takes into account the interaction between the condensate and the noncondensed fraction of the atomic vapor. When $\gamma > 0$, the density of the condensate grows due to an injection of atoms into the condensate from the thermal background or by a pumping mechanism from an atomic reservoir. For $\gamma < 0$, the density of the condensate decays since atoms are expelled out of the harmonic potential. This dissipative process can be explained by inelastic collisions in the BEC due to dipolar relaxation [1]. Hence, $\gamma$ accounts for the exchange of atoms between the pure condensate and its surrounding thermal background. The rate of exchange of atoms is characterized by a temporal scale $\zeta$, which is the time interval between subsequent events of adding or removing individual atoms from the atomic ensemble. The mean-field approximation GPE for BECs is applicable if $\zeta$ is negligible, i.e., $\zeta\omega_\perp \ll 1$, which is verified for typical configurations where $\omega_\perp = 2\pi \times 100$ Hz and $\zeta \sim 10$ $\mu$s [4]. In the absence of the three-body interactions $\chi(t) = 0$, Eq. (1) coincides with the cubic GPE with a gain or loss term ($\gamma$) employed in Refs. [5,6]. In Ref. [6], the cubic GPE with the gain term has been used to model the condensate growth in a trap, and it appears that as the condensate grows, its center of mass oscillates in the trap. In addition, the cubic GPE with the gain or loss term has been proposed to describe the dynamics of atom lasers [7], or light waves in fiber optics in the absence of harmonic confinement [8]. Some exact solutions of the cubic GPE with the gain or loss term $\gamma$ have been reported [9]. In the case in which $\chi(t) = \gamma = 0$, Eq. (1) reduces to the well-known nonlinear Schrödinger equation. In such a case, there exists many kinds of exact solutions with the Hirota method, the inverse scattering method, the Darboux transformation, and the Lax pairs technique for describing bright-bright solitons, dark-dark solitons, bright-dark solitons, and so on in the existing literature.

Equation (1) (and its variant forms) is a nonlinear evolution equation, and it also appears in many fields in physics such as nonlinear optics, biophysics, fluids mechanics, and so on.

*Author to whom all correspondence should be addressed: belobodidier@gmail.com

 

It is rather difficult to solve Eq. (1) analytically, but in recent years many powerful and direct methods for finding exact solutions of Eq. (1) have emerged. Among them are the Bäcklund transformation [10], the tanh-function method [11], the extended tanh-function method [12], the homogeneous balance method [13], the auxiliary equation method [14], the F-expansion method [15], just to name a few. Exact solutions are of a relevant importance in physics in general, since as mathematical models they provide better understandings of physical models, and they may lead to physical applications. In the context of BECs, Mohamadou *et al.* [16] have recently derived exact solutions of Eq. (1) by using the extended-tanh function method with special solutions of an auxiliary equation, i.e., the Lenard equation. In addition, using the same method developed in Ref. [16], exact solutions of Eq. (1) with different geometrical traps have also been proposed by Wamba *et al.* [17] and Belobo *et al.* [18]. We recall that in Ref. [17], the trapping potential consists of a linear magnetic field and a time-dependent laser field, while in Ref. [18] the condensate is confined by a linear field and exchanges atoms with the thermal cloud. If we want to better understand the dynamical behavior of BECs trapped in a harmonic potential and exchanging atoms with the thermal cloud, a detailed investigation of Eq. (1) using more powerful methods to obtain more types of exact solutions containing soliton solutions is needed. Hence, using another method may lead to other solutions of Eq. (1).

The aim of this work is to construct exact solutions of Eq. (1) in the framework of the F-expansion method, combined with four types of auxiliary equations, i.e., the Bernoulli equation, the Riccati equation, the Lenard equation, and the hyperbolic equation.

The rest of the paper is organized as follows. In Sec. II, we present the model. Section III is devoted to deriving exact solutions of Eq. (1) by applying the F-expansion method, combining it with four types of auxiliary equations. We discuss some issues of our exact solutions in Sec. IV. Then, we show that it is possible to significantly increase the number of solutions obtained in Ref. [16] by using other solutions of the Lenard equation. Finally, Sec. V concludes the paper.

## II. KINEMATICS OF THE CENTER OF MASS OF THE CONDENSATE

To derive exact solutions of Eq. (1), we need to transform Eq. (1) into a more tractable and manageable form. Toward that end, we follow Ref. [16] and use the following modified lens-type transformation:

$$\Psi(x,t) = D(t)\Phi(X,T)\exp[\eta(t) + \imath f(t)x^2], \tag{2}$$

where $T$ is a function of time $t$, and $X = \frac{x}{l(t)}$. The function $f(t)$ represents the nonlinear frequency shift, and $\eta(t)$ (which takes into account the exchange of atoms between the condensate and its surroundings) represents the growth $[\eta(t) > 0]$ or the loss $[\eta(t) < 0]$ of atoms. The preservation of the scaling implies that $\frac{dT}{dt} = \frac{1}{l(t)^2}$. Further, we request that

$$\frac{df(t)}{dt} = -4cf(t)^2 - \alpha(t), \tag{3}$$

$$\frac{dD(t)}{dt} = -2cf(t)D(t), \tag{4}$$

$$\frac{dl(t)}{dt} = 4cf(t)l(t), \tag{5}$$

$$\frac{d\eta(t)}{dt} = \gamma. \tag{6}$$

Inserting Eq. (2) into Eq. (1) and using Eqs. (3)–(6) yields the reduced form of Eq. (1) in the rescaled variables $X$ and $T$ (see [16]),

$$\imath\frac{\partial\Phi(X,T)}{\partial T} = -c\frac{\partial^2\Phi(X,T)}{\partial X^2} - P^2|\Psi(X,T)|^2\Phi(X,T) + \chi_0|\Phi(X,T)|^4\Phi(X,T), \tag{7}$$

with $D(t) = [|g(t)|l(t)^2\exp[2\eta(t)]]^{-\frac{1}{2}}$, $\chi(t) = \chi_0 g(t)^2 l(t)^2$, $P^2 = -\mathrm{sgn}[g(t)]$. The two-body interactions are attractive if $P^2 = +1$, but they are repulsive when $P^2 = -1$. Equation (7) is a cubic-quintic GPE with constant parameters. The exact solution of Eq. (1) takes the form [16]

$$\Psi(x,t) = \sqrt{|G(t)|}\Phi(X,T) \times \exp\left\{\eta(t) + \imath\left[-\frac{1}{4c}\frac{d}{dt}\ln|G(t)|\right]x^2\right\}, \tag{8}$$

where $G(t) = g(t)\exp[2\eta(t)]$, $\eta(t) = \int_0^t \gamma dt' + \eta_0$, $\eta_0$ being a constant. Solution (8) is obtained by assuming that $l(t) = |G(t)|^{-1}$, $T(t) = \int_0^t G(t')^2 dt'$, $f(t) = \frac{1}{4c}\frac{d}{dt}\ln|G(t)|$.

Exact explicit solutions of Eq. (1) are obtained from the solution (8) if the explicit form of the function $\Phi(X,T)$ is given. To derive explicit expressions of $\Phi(X,T)$, we assume that it takes the amplitude-phase form and can be written as

$$\Phi(X,T) = Q(\xi)\exp[i\theta(X,T)], \tag{9}$$

where $Q$ represents the amplitude part and $\theta$ accounts for the phase part. The variables $\xi$ and $\theta$ have the forms

$$\xi = k_0X - \omega_0T, \quad \theta(X,T) = kX - \omega T. \tag{10}$$

Parameters $k_0$, $k$, $\omega_0$, and $\omega$ are real constants that account for width, linear frequency shift, velocity, and the homogenous phase of the wave function $\Phi(X,T)$, respectively. Substituting Eqs. (9) and (10) into Eq. (7), and then separating the real and the imaginary parts, respectively, yields the following set of ordinary differential equations with respect to $Q$:

$$(\omega - ck^2)Q + Q^3 - \chi_0Q^5 + ck_0\frac{d^2Q}{d\xi^2} = 0, \tag{11}$$

$$(\omega_0 - 2ckk_0)\frac{d^2Q}{d\xi^2} = 0. \tag{12}$$

Assuming the constraint

$$\omega_0 = 2ckk_0 \tag{13}$$

means that we only need to solve Eq. (11). Thus, in the following, we focus our attention on deriving solutions of Eq. (11). We will assume that the function $Q$ is expandable in a polynomial function $F(\xi)$, where $F$ satisfies an

auxiliary equation. So far, there are some important physical properties that will be exhibited by the complete solutions to be constructed. For example, one may be interested in the dynamics of the center of mass of the condensate for a specific solution. The properties of the center of mass help us to understand the behavior of the condensate at mean. In the rescaled frame, the position, velocity, and acceleration of the condensate center of mass are $X_{\rm CM} = 2ckT$, $\dot{X}_{\rm CM} = 2ck$, and $\ddot{X}_{\rm CM} = 0$, respectively. In terms of the dimensionless physical variables, the position, velocity, and acceleration of the center of mass are $x_{\rm CM}(t) = (ck/\gamma)\sinh(2\gamma t)$, $\dot{x}_{\rm CM} = 2ck\cosh(2\gamma t)$, and $\ddot{x}_{\rm CM} = 4ck\gamma\sinh(2\gamma t)$, respectively. Hence, the behavior at mean of the condensate is affected by the rate of exchange of atoms between the condensate fraction and the uncondensed fraction, and by the linear frequency shift of the initial condition. These features, that are nowadays manageable in BEC experiments with a high accuracy, allow us to understand the influence that the interplay between the condensate and the uncondensed fraction has on the stability and the dynamics of the condensate. At initial time, the center of mass of the condensate is at the center of the trapping potential with the initial velocity $2ck$ without any acceleration. As time increases, the velocity and acceleration of the center of mass increase for negative and positive values of $\gamma$. This implies that the exchange of atoms with the thermal background accelerates the center of mass, such that the temperature of the core increases with time, and it may lead to the collapse of the condensate. However, for small values of $\gamma$, the acceleration and velocity of the core shall remain small such that the growth of the velocity induced by the atoms pumping, or the loss mechanisms, will be negligible, avoiding the collapse of the condensate. The linear frequency $k$ may also be used to control the acceleration and the velocity of the condensate's core. In this work, one has two powerful tools to avoid the collapse of the condensate. The position of the center of mass as time evolves also depends on the sign of the linear frequency $k$, such that the condensate moves toward the left side to the axial potential if $k < 0$, while the condensate moves toward the right side of the potential for positive values of $k$. The features of the parameters $\gamma$ and $k$ may be used in some BEC applications such as the realization of the atomic laser where the velocity of atoms can be tuned by proper choices of the linear frequency and the rate of rate of exchange of atoms between the condensate and its surroundings. Another potential application is the transport of the condensate in experiments driven by the parameters $\gamma$ and $k$. According to Newton's second law, the condensate can be considered as a classical particle moving in the effective potential $U_{\rm eff} = (-2ck/\gamma)\cosh(2\gamma t)$, with total energy $E = 2[ck\cosh(2\gamma t)]^2 - (2ck/\gamma)\cosh(2\gamma t)$, its only equilibrium point being located at the center of the trap, $x = 0$.

## III. EXACT SOLUTIONS

### A. The Bernoulli equation as an auxiliary equation

We suppose that the function $Q$ has the following form:

$$Q(\xi) = \sum_{i=0}^{M} a_i F^i(\xi), \tag{14}$$

where $M$ is a positive integer, $a_i$ are real constants to be determined later, and the function $F$ is the solution of the general Bernoulli equation,

$$\frac{dF}{d\xi} = aF(\xi) + bF^{\lambda}(\xi), \tag{15}$$

the parameters $a$, $b$, and $\lambda$ being real constants that will be also determined later, with $\lambda \neq 1$. Introducing Eq. (14) into Eq. (11) and using the homogeneous balance between the highest-order derivative and nonlinear terms, respectively, yields $\lambda = 2M + 1$. Since $\lambda \neq 1$, then $M \geqslant 1$. Let us consider the simple case in which $M = 1$ and $\lambda = 3$. We have

$$Q(\xi) = a_0 + a_1 F(\xi), \qquad \frac{dF}{d\xi} = aF(\xi) + bF^3(\xi). \tag{16}$$

Inserting Eq. (16) into Eq. (11) and collecting coefficients of powers $F^i(\xi)$, then setting each coefficient to zero, yields a set of overdetermined algebraic equations for the unknowns $a_0$, $a_1$, $a$, $b$, and $\omega$. Solving this set of overdetermined equations with the aid of MAPLE leads to the following solutions:

$$a_0 = 0, \tag{17}$$

$$a = \frac{-\sqrt{3}}{4k_0\sqrt{c}\sqrt{\chi_0}}, \tag{18}$$

$$b = \pm\frac{a_1^2\sqrt{\chi_0}}{k_0\sqrt{3c}}, \tag{19}$$

$$\omega = \frac{-3 + 16ck^2\chi_0}{16\chi_0}. \tag{20}$$

Equations (17) and (18) imply that $c > 0$ and $\chi_0 > 0$, meaning that solutions are valid only for repulsive three-body interactions. One infers from Eqs. (19) and (20) that the amplitude and the homogeneous phase of the wave function are sensitive to the strength of the three-body interaction $\chi(t)$. It is thus possible to tune to the desired values both the amplitude and the phase of the condensate externally by means of the Feshbach resonance technique. Inserting the solutions of the general Bernoulli equation [Eq. (15)] for $\lambda = 3$ [19] given in Appendix A into Eq. (16) leads to an explicit expression of $Q$. Hence, exact explicit solutions of Eq. (1) are

$$\begin{aligned}\Psi_{1j}(x,t) = {} & \sqrt{|G(t)|}a_1 F_{1j}(\xi)\exp[\imath\theta(X,T)] \\ & \times \exp\left\{\eta(t) + \imath\left[-\frac{1}{4c}\frac{d}{dt}\ln|G(t)|\right]x^2\right\}, \\ & j = 1,2,3.\end{aligned} \tag{21}$$

Equations (16)–(20) and the solutions of Appendix A imply that the heights of solutions (21) are proportional to the strength of the cubic nonlinearity, but inversely proportional to the strength of the quintic nonlinearity. Therefore, the experimenter knows how to manage the cubic and quintic nonlinearities in order to obtain a solution with an assumed amplitude. The density of a solution is subjected to a growth in the feeding regime, while the density decays when atoms are removed from the condensate. This feature has been predicted in Refs. [16,18]. In addition, the behavior of the density of the condensate is unchanged both for attractive and

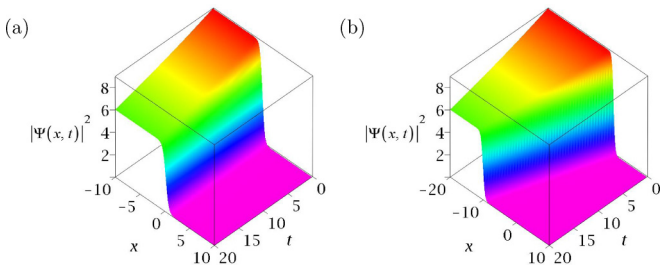


FIG. 1. (Color online) Spatiotemporal evolution of the wave function of Eq. (21) for $j = 2$. The parameters selected are $\alpha = -0.005$, $k_0 = 1$, $\chi_0 = \frac{1}{12}$, $a_1 = 1$, $c = 0.5$, $\eta_0 = 0$, $g(t) = -1$, and $\gamma = -0.005$. (a) $k = 0.01$, density profile of an antikink soliton with initial speed 0.01. (b) $k = -0.5$, effect of the linear frequency shift on the direction of the moving antikink soliton. The initial speed of the soliton is equal to $|k|$, and the direction of the soliton depends on the sign of $k$.

repulsive condensates. From (21), one understands that we have constructed three bunches of solutions of Eq. (1). To represent some samples of the solutions (21), we choose the following relevant physical parameters: $\alpha = -0.005$, $c = 0.5$, and $\eta(t) = \gamma t$ with $\eta_0 = 0$, used in some experimental and theoretical studies [16–21]. (We remind the reader that a slightly expulsive parabolic harmonic potential, negative value of $\alpha$ was used in the experiments of Refs. [20,21] to produce solitons in condensates.) We display in Fig. 1(a) the dynamics of the condensate's wave function, where we have set $j = 2$ in solution (21) with $\gamma = -0.005$, $\chi_0 = 1/12$, and $k = 0.01$. In this case, the solution (21) is an antikink soliton with initial velocity 0.01. The influence of the linear frequency shift on the direction of the condensate can be seen in Fig. 1(b), where $k = -0.5$. The moving antikink soliton evolves toward the left side of the cigar axis and its initial velocity amounts to 0.05. Kink and antikink solitons have been predicted in single condensates with two- and three-body nonlinearities in different trap geometries [16,17,18] and in binary condensates with cubic nonlinearities [22]. Other nonlinear media also allow the existence of kink and antikink solitons such as a layer of binary liquid heated from below, where oscillatory convection sets in via a subcritical bifurcation described by the cubic-quintic Ginsburg-Landau equation [23], optical fibers with elliptical birefringence for the evolution of the state of polarization of counterpropagating waves [24], the nonlinear dispersive fiber optics for the description of wave propagation by including the effects of group-velocity dispersion, self-phase-modulation, stimulated Raman scattering, and self-steepening [25]. The analytical expression of the antikink soliton solution found in Ref. [16] is different from the solution obtained in the present work by using the Bernoulli auxiliary equation. Moreover, with only fewer parameters, i.e., $k$ and $\gamma$, we can characterize the behavior of the condensate at mean.

### B. The Riccati equation as an auxiliary equation

We assume that the function $Q$ takes the form

$$Q(\xi) = \sum_{i=-N}^{N} a_i F^i(\xi), \tag{22}$$

where the function $F$ is the solution of the following Riccati equation [26]:

$$\frac{dF}{d\xi} = MF^{\lambda}(\xi) + \frac{\varepsilon}{1-\lambda} F^{2-\lambda}, \quad \varepsilon = \pm 1. \tag{23}$$

Inserting Eq. (22) into Eq. (11) and considering the homogeneous balance between the highest-order derivative and nonlinear terms, respectively, we obtain $\lambda = 2N + 1$. Let us now consider the simple case in which $N = 1$ and $\lambda = 3$. Equations (22) and (23) become

$$\begin{aligned} Q(\xi) &= a_0 + a_1 F(\xi) + a_2 F^{-1}(\xi), \\ \frac{dF}{d\xi} &= MF^3(\xi) - \frac{\varepsilon}{2} F(\xi). \end{aligned} \tag{24}$$

Introducing Eqs. (24) into Eq. (11), collecting coefficients of powers $F^i(\xi)$, and then setting each coefficient to zero, yields a set of overdetermined algebraic equations for the unknowns $a_0$, $a_1$, $M$, and $\omega$. Solving these equations with the aid of MAPLE, we obtain

$$\begin{aligned} a_{11} &= \frac{1}{8c\sqrt{2k_0}} \left(\frac{3c}{\chi_0}\right)^{\frac{3}{4}}, \quad a_{21} = \sqrt{\frac{k_0}{2}} \left(\frac{3c}{\chi_0}\right)^{\frac{3}{4}}, \\ M_1 &= \frac{3}{128ck_0^2\chi_0}, \quad \omega_1 = ck^2 + \frac{3\varepsilon - 27}{128\chi_0}, \end{aligned} \tag{25}$$

$$a_{12} = -a_{11}, \quad a_{22} = -a_{21}, \quad M_1, \quad \omega_1, \tag{26}$$

$$a_{13} = -\imath a_{11}, \quad a_{23} = \imath a_{21}, \quad M_1, \quad \omega_1, \tag{27}$$

$$a_{14} = \imath a_{11}, \quad a_{24} = -\imath a_{21}, \quad M_1, \quad \omega_1, \tag{28}$$

$$a_{15} = a_{11}, \quad a_{25} = a_{21}, \quad -M_1, \quad \omega_2 = ck^2 - \frac{(3\varepsilon + 27)}{128\chi_0}, \tag{29}$$

$$a_{16} = -a_{11}, \quad a_{26} = -a_{21}, \quad -M_1, \quad \omega_2, \tag{30}$$

$$a_{17} = -\imath a_{11}, \quad a_{27} = \imath a_{21}, \quad -M_1, \quad \omega_2, \tag{31}$$

$$a_{18} = \imath a_{11}, \quad a_{28} = -\imath a_{21}, \quad -M_1, \quad \omega_2, \tag{32}$$

$$a_0 = 0. \tag{33}$$

Equation (28) implies that $c > 0$ and $\chi_0 > 0$ (the three-body interactions are repulsive). Using Eqs. (24)–(33), we derive exact solutions of Eq. (1),

$$\begin{aligned} \Psi_{2nm}(x,t) = \sqrt{|G(t)|}[a_{1n} F_{2m}(\xi) + a_{2n} F_{2m}^{-1}(\xi)] \exp[\imath\theta(X,T)] \\ \times \exp\left\{\eta(t) + \imath\left[-\frac{1}{4c}\frac{d}{dt}\ln|G(t)|\right]x^2\right\}, \end{aligned} \tag{34}$$

where $n,m$ are integers, with $n = \overline{1,8}$, and $m = \overline{1,4}$ if $\varepsilon = -1$, $m = \overline{5,7}$ if $\varepsilon = +1$, and $m = 8$ if $\varepsilon = 0$. The solutions of the Riccati equation are given in Appendix B [26]. Equations (25)–(34) imply that the amplitudes of solutions (34) are highly dependent on the values of the width and the strength

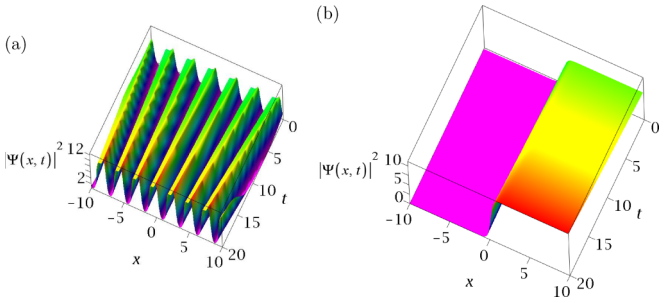


FIG. 2. (Color online) Propagation of the matter wave condensate of the solution given by Eq. (34). (a) Density profile of a growing periodic solution for $n = 5$, $m = 7$, and $\varepsilon = +1$. (b) Density profile of a moving kink soliton for $n = 5, m = 3$, and $\varepsilon = -1$. In both cases, the other parameters are the same as in Fig. 1(a), except $\chi_0 = 0.1$, $\gamma_0 = 0.005$.

of the quintic nonlinearity, which is also related to the atom feeding or loss parameter $\gamma$. The phases of solutions (34) are characterized by $\chi_0$ and the free parameter $k$. Hence, after fixing the values of $k_0$, $\chi_0$, and $\gamma$, it is possible to predict space-time evolution of the amplitude and the phase of solutions (34). Since the latter parameters can be precisely controlled externally in current BEC experiments, we infer that solutions (34) are likely to be observed in current or future experiments with condensates. We visualize in Figs. 2(a) and 2(b) the spatiotemporal evolutions of the wave function for two different cases of solution (34). In Fig. 2(a), we have set in Eq. (34) $n = 5$, $m = 7$, and $\varepsilon = 1$. We obtain a multiple bright soliton solution periodically spaced on the axial potential. The dynamical characteristics of the center of mass of this solution are the same as those of Fig. 1(a) since the same parameters were used. Multiple bright soliton solutions are usually obtained in condensates via the modulational instability. In the case of Eq. (1), multiple bright solitons were generated numerically in Ref. [27]. Here, we give an analytical expression of a multiple bright soliton solution in the framework of Eq. (1). Such moving periodic solutions may be observed in optical lattices, and they can be used to insert atoms onto optical devices, such as atom chips, waveguides, and mirrors [18,28]. Figure 2(b) portrays the spatiotemporal evolution of a kink soliton obtained for $n = 5$, $m = 3$, and $\varepsilon = -1$. This is a kink soliton solution of Eq. (1) that is different from that derived in Ref. [16].

### C. The Lenard equation as an auxiliary equation

We search a function $Q$ that has the form

$$Q(\xi) = \sum_{i=0}^{N} a_i F^i(\xi), \tag{35}$$

the function $F$ satisfying the Lenard equation [29]

$$\frac{dF}{d\xi} = \sqrt{b_0 + b_2 F^2(\xi) + b_4 F^4(\xi) + b_6 F^6(\xi)}. \tag{36}$$

Solutions of (36) are given in Appendix C. Substituting Eq. (35) into Eq. (11) and considering the homogeneous balance between the highest-order derivative and nonlinear terms, respectively, we obtain $N = 1$. Inserting $Q$ into Eq. (11), collecting coefficients of powers $F^i(\xi)$, and then equating each coefficient to zero, yields a set of overdetermined algebraic equations for the unknowns $a_0$, $a_1$, $b_4$, and $\omega$. Solving them with MAPLE, we have

$$a_{11} = \sqrt{k_0}\left(\frac{cb_6}{\chi_0}\right)^{\frac{1}{4}}, \quad b_4 = -\frac{1}{2ck_0}\sqrt{\frac{2cb_6}{\chi_0}}, \tag{37}$$

$$a_{12} = -a_{11}, \quad b_4, \tag{38}$$

$$a_{13} = \iota a_{11}, \quad -b_4, \tag{39}$$

$$a_{14} = -\iota a_{11}, \quad b_4, \tag{40}$$

$$a_0 = 0, \quad \omega = ck^2 - ck_0^2 b_2. \tag{41}$$

Equation (37) implies that $k_0$ must be positive, and both $\chi_0$ and $b_6$ must have the same sign. Inserting Eqs. (37)–(41) into Eq. (35) yields explicit solutions of $Q$, which in turn are used to obtain exact solutions of Eq. (1), which are

$$\Psi_{3nm}(x,t) = \sqrt{|G(t)|}a_{1n}F_{3,m}(\xi)\exp[\iota\theta(X,T)] \times \exp\left\{\eta(t) + \iota\left[-\frac{1}{4c}\frac{d}{dt}\ln|G(t)|\right]x^2\right\}, \tag{42}$$

where $n,m$ are integers, with $n = \overline{1,4}$, and $m = \overline{1,18}$ for $b_0 = 0$ and $m = \overline{19,22}$ for $b_0 = \frac{8b_2^2}{27b_4}$ and $b_6 = \frac{b_4^2}{4b_2}$. Relations (37)–(40) mean that the amplitudes of solutions (42) depend on the values of $k_0$ and $\chi_0$. Equation (41) implies that the phases of the solutions (42) depend on the values of $k$ and $k_0$. After the choice of the parameters $b_i$ ($i = 0,1,2,3,4,5,6$) related to the solution pattern needed, it is possible to precisely manipulate the amplitude and the phase of solutions only with the selection of the values of the width ($1/k_0$), the linear frequency $k$, the sign of $\chi_0$, and the rate of exchange $\gamma$. There are many types of solutions of Eq. (1) that can be derived from Eq. (42). We present in Fig. 3(a) a bright soliton solution of (42) for $n = 1$, $m = 1$, with $b_2 = 2$, $b_6 = -2$, $\chi_0 = -0.1$, and $g(t) = 1$. The other parameters are the same as in Fig. 1(a). Bright solitons have been reported in condensate experiments with a constant two-body nonlinearity [20,21]. The dynamics of the core of this soliton are the same as that of the solution of Fig. 1(a). The parameter $k_0$ plays two important roles in the characterization of the solutions: (i) generally speaking, the width of the condensate is $1/k_0$; (ii) for each solution

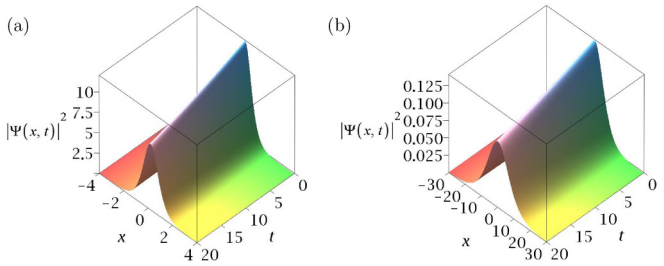


FIG. 3. (Color online) (a) Sample of a bright soliton solution derived from solution (42) for $n = 1, m = 1$ with $k_0 = 1$, $\chi_0 = -0.1$, $b_2 = 2$, and $b_6 = -2$. (b) Same parameters as in panel (a) except $k_0 = 0.1$. The parameter $k_0$ affects both the width and the amplitude of the solution. The other parameters as the same as in Fig. 1(a).

derived from Eq. (42), the amplitude is proportional to $\sqrt{k_0}$ as depicted by Eq. (37). A comparison between Figs. 3(a) and 3(b) corroborates the latter effects due to $k_0$.

One important class of physically relevant solutions of Eq. (1) is the Jacobi elliptic function solutions that are missed in the above development. We need to remedy this by including the generalized Jacobian elliptic solutions of Eq. (1). Toward that end, we resort the same procedure and consider the following special solutions of the Lenard equation [30–33], which can be found in Appendix D. The generalized Jacobi exact solutions of Eq. (1) can then be expressed as follows:

$$\Psi_{3nm}(x,t) = \sqrt{|G(t)|}a_{1n}F_{5,m}(\xi)\exp[\imath\theta(X,T)] \times \exp\left\{\eta(t) + \imath\left[-\frac{1}{4c}\frac{d}{dt}\ln|G(t)|\right]x^2\right\}, \quad (43)$$

where $n,m$ are integers, with $n = \overline{1,4}$ and $m = \overline{18,19}$. These solutions have to respect the constraint imposed by the expression of $b_4$ given by Eq. (37), and they are valid only for negative values of $\chi_0$. Thus, the generalized Jacobi function solutions (43) are valid provided that the quintic interatomic interactions are attractive, and they share the same features with solutions (42) regarding the behavior of the amplitudes and the phase. Subsequently, $k_0$ can be written in terms of the periods $k_1$ and $k_2$ as $k_0 = -\frac{1}{2cb4}\sqrt{\frac{2cb_6}{\chi_0}}$, with $b_4$ and $b_6$ chosen as in Eq. (37) or in Appendix D. In other words, once two periods $k_1,k_2$ are fixed, the width $1/k_0$ and the strength of the three-body interatomic interactions are derived. It is interesting to notice that, except for the atom feeding or loss mechanism that is controlled by $\gamma$, all important features of the solutions (43) depend on the values of the periods $k_1,k_2$. We plot in Fig. 4(a) the density profile of the generalized Jacobi cosine function, and in Fig. 4(b) the density profile of the generalized Jacobi function of the third kind, in the feeding regime $\gamma = 0.001$, for repulsive condensates $g = 1$. As periodic solutions, the generalized Jacobi elliptic function solutions may be observed for BECs in optical lattices [28]. Some particular solutions of (43), the Jacobi elliptic function solutions, have been reported in Jacobian elliptic potentials for condensates with constant cubic and cubic-quintic nonlinearities [34].

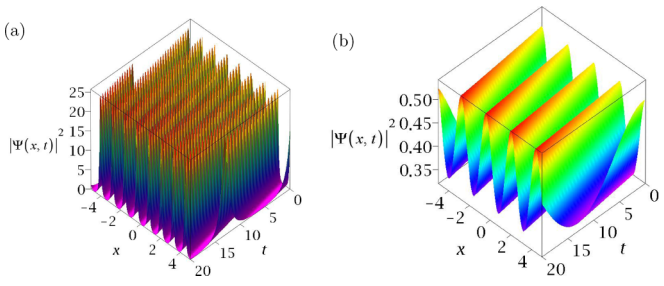


FIG. 4. (Color online) Spatiotemporal evolution of density profiles of generalized Jacobi elliptic solutions of Eq. (1). (a) $c(\xi,k_1,k_2)$, (b) $d_1(\xi,k_1,k_2)$. Parameters are $\alpha = -0.005$, $k_1 = 0.6$, $k_2 = 0.2$, $\chi_0 = -k_1^2k_2^2$, $\gamma = 0.001$, $k = 0.1$, and $g = 1$.

### D. The hyperbolic equation as an auxiliary equation

The function $Q$ is assumed to have the form

$$Q(\xi) = \sum_{i=0}^{N} a_i \sinh^i[F(\xi)], \quad (44)$$

where the function $F$ satisfies the hyperbolic equation [35]

$$\frac{dF}{d\xi} = c_0 + c_2\sinh^2(\xi). \quad (45)$$

The solutions of the hyperbolic equation [35] are presented in Appendix E. Substituting Eq. (44) into Eq. (11) and considering the homogeneous balance between the highest-order derivative and nonlinear terms, respectively, we obtain $N = 1$. Then, introducing the function $Q$ into Eq. (11), collecting all coefficients of powers $\sinh^i[F(\xi)]$, and setting each coefficient to zero yields a set of overdetermined algebraic equations for the unknowns $a_0$, $a_1$, $c_0$, and $\omega$. Solving them with MAPLE, we obtain

$$a_{11} = \sqrt{k_0c_2\left(\frac{3c}{\chi_0}\right)^{\frac{1}{4}}},$$
$$\omega_1 = k_0c_2\sqrt{\frac{3c}{\chi_0}} + ck^2 + \frac{3ck_0^2c_2^2}{4} - \frac{3}{16\chi_0}, \quad (46)$$
$$c_{01} = \frac{-\sqrt{\frac{3c}{\chi_0}} - 2ck_0c_2}{4ck_0},$$

$$a_{12} = -a_{11}, \quad \omega_1, \quad c_{01}, \quad (47)$$

$$a_{13} = \imath a_{11}, \quad \omega_2 = -k_0c_2\sqrt{\frac{3c}{\chi_0}} + ck^2 + \frac{3ck_0^2c_2^2}{4} - \frac{3}{16\chi_0},$$
$$c_{02} = \frac{\sqrt{\frac{3c}{\chi_0}} - 2ck_0c_2}{4ck_0}, \quad (48)$$

$$a_{14} = -\imath a_{11}, \quad \omega_2, \quad c_{02}, \quad (49)$$

$$a_0 = 0. \quad (50)$$

Proceeding in a similar way as above, we obtain exact solutions of Eq. (1) as

$$\Psi_{4nm}(x,t) = \sqrt{|G(t)|}a_{1n}\sinh_{1,m}[F(\xi)]\exp[\imath\theta(X,T)] \times \exp\left\{\eta(t) + \imath\left[-\frac{1}{4c}\frac{d}{dt}\ln|G(t)|\right]x^2\right\}, \quad (51)$$

where $n,m = 1,2,3,4$. From Eqs. (46)–(50), one can realize that features of the solutions (51) are related to some experimental parameters such as the strength of the quintic interatomic interactions, the rate of exchange of atoms with the thermal background $\gamma$, and the linear frequency shift $k$. For instance, the amplitudes of solutions (51) depend on the width $(1/k_0)$ and the strength of the quintic interatomic interactions $\chi_0$ (which depends on the interplay between the condensate and the thermal vapor), whereas the homogeneous phase depends on the width, linear phase, and $\chi_0$. As already stated above, it is possible to control the amplitude and phase

of a solution in current condensate experiments once $1/k_0$, $k$, and $\gamma$ have been fixed. In addition, the kinematics of the center of mass of the solutions (51) are also manageable externally in experiments, as mentioned before. We expect that the present work will motivate the quest of hyperbolic solutions in BEC experiments and applications.

### E. Discussions

In the latter section, we have constructed exact solutions of Eq. (1) using a lens-type transformation with constraints [Eqs. (3)–(6)] also used in Ref. [16]. However, due to the method used in this work, the kinematics of the center of mass of our solutions is rather different from that predicted in Ref. [16]. In addition, we provide many types of solutions that are related to important experimental parameters with BECs. We have also proposed hyperbolic solutions and generalized Jacobi function solutions.

It is well known that the inclusion of quintic nonlinearity alters the behavior of matter-wave condensates. One important issue is to show what effects the quintic nonlinearity has on the formation of matter-wave condensates. To single out these effects, we consider the solutions with and without quintic nonlinearity for the four types of auxiliary equations. In the limit case of vanishing three-body interactions, the solutions found above actually have $\chi(t) = 0$ counterparts, since they exist for any arbitrary nonzero small values of $\chi(t)$, however their counterparts for $\chi(t) = 0$ cannot be expressed analytically simply due to divergence to infinity of some parameters [see Eqs. (18), (25), (37), and (46) for example]. Therefore, we resolve Eq. (1) again with $\chi(t) = 0$. For the case of the Bernoulli equation, the analytical solution is given by Eq. (21), where $a_1 F(\xi)$ is replaced by $a_0 + a_1 F(\xi)$, with $a_0 = \pm ck_0 a/\sqrt{-2c}$, $a_1 = \pm\sqrt{-2c}k_0 b$, and $\omega = \frac{1}{2}c(k_0^2 a^2 + 2k^2)$, $a$ and $b$ being free real parameters. The solutions exist only if the dispersion coefficient $c$ is negative. Such solutions do not describe the evolution of matter-wave condensates, but they may rather describe the evolution of light waves in fiber optics with application to telecommunication transmissions. In addition, from Eq. (18) we know that the solutions with nonzero quintic nonlinearity are valid only for positive values of $c$. Due to the method adopted in the present work, the influence of quintic nonlinearity on the dynamics of waves cannot be determined because the solutions obtained describe two distinct physical situations (positive

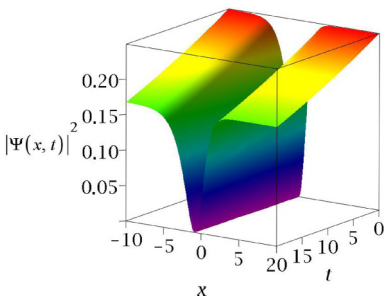


FIG. 5. (Color online) Evolution of the density of a dark soliton of Eq. (1) obtained using the Bernoulli equation, with the same parameters as in Fig. 1(a) except $c = -0.5$, $a = 1$, $b = -1$, and $\chi(t) = 0$.

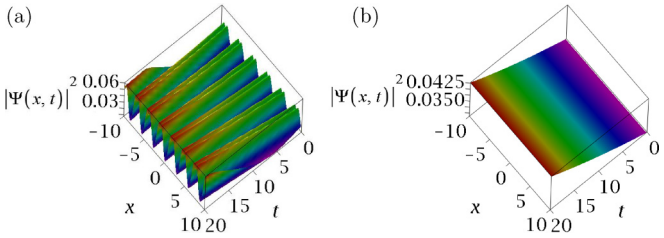


FIG. 6. (Color online) (a) Evolution of the density of a periodic solution of Eq. (1) obtained using the Riccati equation, with same parameters as in Fig. 2(a) except $M = -0.4$, $\chi(t) = 0$. (b) Evolution of the density of a plane-wave solution of Eq. (1) derived using the Riccati equation, with the same parameters as in Fig. 2(b), except $M = -0.4$, $\chi(t) = 0$.

dispersion coefficient $c > 0$ and negative dispersion coefficient $c < 0$). A comparison between Fig. 5 [$\chi(t) = 0$] and Fig. 1(a) confirms that with the inclusion of quintic nonlinearity, the dynamics of waves are different with regard to the shape of the solution, which turns from a dark profile to an antikink profile. When one uses the Riccati equation, the solution of Eq. (1) is given by Eq. (34), where $n = \overline{1,5}$; $m$ and $\varepsilon$ have the same signification. The coefficients are $a_{11} = 0$, $a_{21} = \sqrt{-2c}\varepsilon k_0$, $\omega_1 = ck^2 + 2ck_0^2 M\varepsilon$; $a_{12} = 0$, $a_{22} = -a_{11}$, $\omega_2 = \omega_1$; $a_{13} = -2ck_0^2 M^2$, $a_{23} = 0$, $\omega_3 = \omega_1$; $a_{14} = a_{13}$, $a_{24} = a_{21}, \omega_4 = 6ck_0^3 M^2\sqrt{-2c}\varepsilon + ck^2 + 2ck_0^2 M\varepsilon$; $a_{15} = a_{13}, a_{25} = -a_{24}$, $\omega_5 = -6ck_0^3 M^2\sqrt{-2c}\varepsilon + ck^2 + 2ck_0^2 M\varepsilon$. $M$ is a free real parameter. The expressions of the coefficients $a_{1i}$ and $a_{2i}$ show that only the coefficients for $n = 3$ correspond to matter-wave solutions. The others with a negative dispersion coefficient may rather describe the evolution of light in fiber optics. A comparison between Fig. 6(a) [$\chi(t) = 0$] and Fig. 2(a) implies that the inclusion of quintic nonlinearity modifies the top of the periodic solution. In addition, drawing a parallel between Fig. 6(b) and Fig. 2(b), one realizes that the inclusion of quintic nonlinearity may also induce the localization of matter waves in BECs. Localized solutions are due to a compensation between dispersion and nonlinearity. It is likely that the quintic nonlinearity helps to attain a regime of parameters where the nonlinearities balance the dispersion. Resolving Eq. (1) for $\chi(t) = 0$ with the hyperbolic equation, the solutions are provided by Eq. (51) for the parameters $a_1 = a_2 = 0$ and $\omega = -a_0^2 + ck^2$, where $a_0$ is a free parameter. Once again, due to the reason mentioned above, quintic nonlinearity also induces the localization of solutions since the cubic form

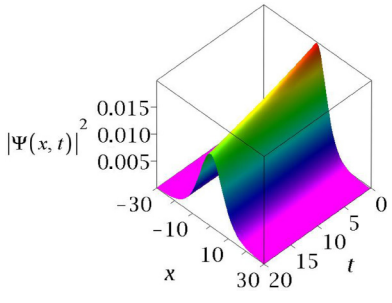


FIG. 7. (Color online) Evolution of the density of a bright solution of Eq. (1) obtained using the ordinary auxiliary equation, with the same parameters as in Fig. 2(a) except $M = -0.4$, $\chi(t) = 0$.

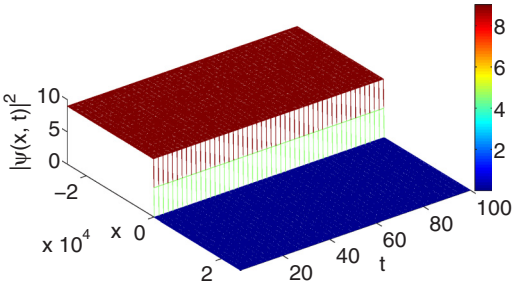


FIG. 8. (Color online) Spatiotemporal propagation of the stable antikink-like soliton of Fig. 1(a). Parameters are the same as in Fig. 1(a) except $\gamma = 0$.

of Eq. (1) only admits plane-wave solutions (due to the fact that $a_1 = a_2 = 0$.) Setting $\chi(t) = 0$ in Eq. (1), the Lenard equation reduces to the ordinary auxiliary equation since one must set $b_6 = 0$ [12]. In this case, it is difficult to check the impact the quintic nonlinearity has on the formation of matter-wave condensates because the ordinary auxiliary equation has different solutions, which are presented in Appendix F [23]. The solutions of the cubic equation found by means of the ordinary auxiliary equation are given by Eq. (43), where $n = 1,2$, with $a_1 = \pm\sqrt{-2cb_4}k_0$ and $\omega = ck^2 - ck_0^2 b_2$. The solutions found may describe the evolution of matter-wave condensates provided that $c > 0$, which implies that $b_4 < 0$. The inclusion of the quintic nonlinearity does not bring significant changes, as can be seen by comparing Figs. 7, 3(a), and 3(b).

## IV. NUMERICAL SIMULATIONS

An important issue concerning exact solutions found with mathematical methods is their stability or robustness in real physical experiments. The physical relevance of an exact solution can be investigated by means of comparisons with the exact numerical solution obtained by a direct integration of the underlying Eq. (1). Here, the numerical method used is the split-step Fourier method [36,37]. The spatial grid is sufficiently large in order to prevent problems with the boundaries [37]. An initial reasonably small amount of random perturbation is added in order to unveil any instability that can be seeded during the time evolution. We restrict ourselves to some of the cases of exact solutions found above.

Let us start with the antikink soliton solution of (21) for $j = 2$. In the case in which $\gamma = 0$, the condensate does not exchange any atoms with a thermal background. Figure 8 proves that the initial condition persists without destruction though the insertion of a small initial random perturbation. For a condensate in the regime of a loss of atoms, there is also very good agreement between the analytical prediction and numerical results, as depicted by Figs. 9(a)–9(c), for $\gamma = -0.005$. Figure 9(d) shows that the disturbed initial condition remains stable during the propagation. One can then consider that such a solution is a robust physical object that can be observed in a real experiment.

Next, we look at the kinklike soliton solution of Fig. 2(b). Two cases are considered, namely the feeding regime and the regime where the condensate does not exchange any atom with its surroundings. In Fig. 10(a) ($\gamma = 0$), the amplitude of the condensate stays constant during the propagation, while the amplitude increases with time in the feeding regime, as shown in Figs. 10(b)–10(d) ($\gamma = 0.005$). From Figs. 10(a) and 10(e) ($\gamma = 0.005$), one infers that the derived kinklike soliton solution of (37) for $n = 5$, $m = 3$, and $\varepsilon = -1$ is a stable solution.

The bright soliton solution of Fig. 3(b) obtained by using the Lenard equation is dynamically stable and accurately corroborates its analytical counterpart. Figure 11 displays the agreement between the numerical and analytical solutions,

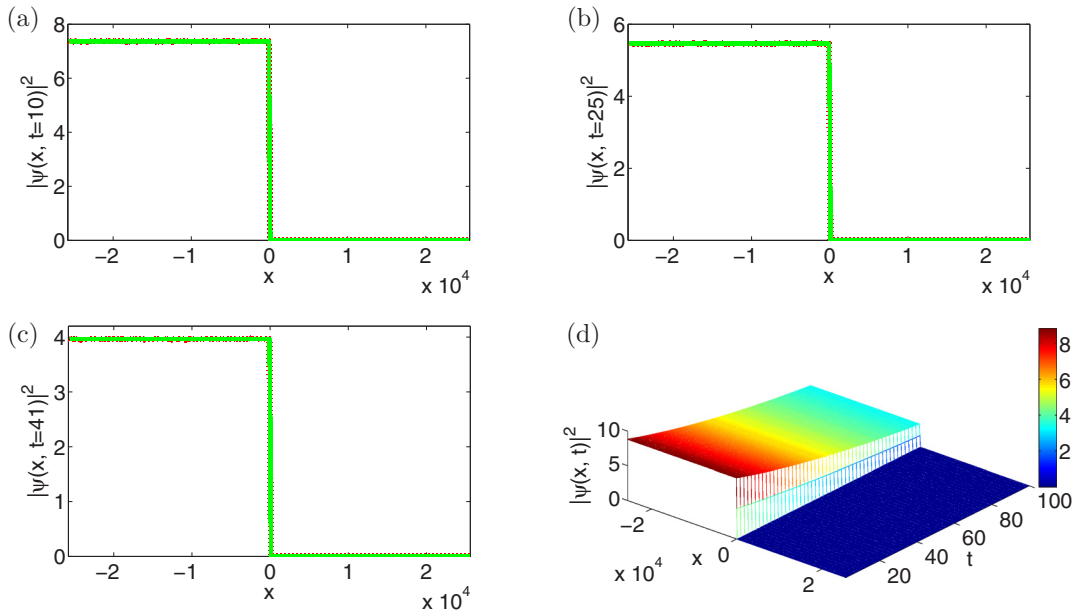


FIG. 9. (Color online) (a)–(c) Comparison between analytical (solid line) and numerical (dotted line) solutions at particular times of the antikink-like soliton of Fig. 1(a). (d) Spatiotemporal evolution of the stable antikink-like soliton of Fig. 1(a). Parameters are the same as in Fig. 1(a).

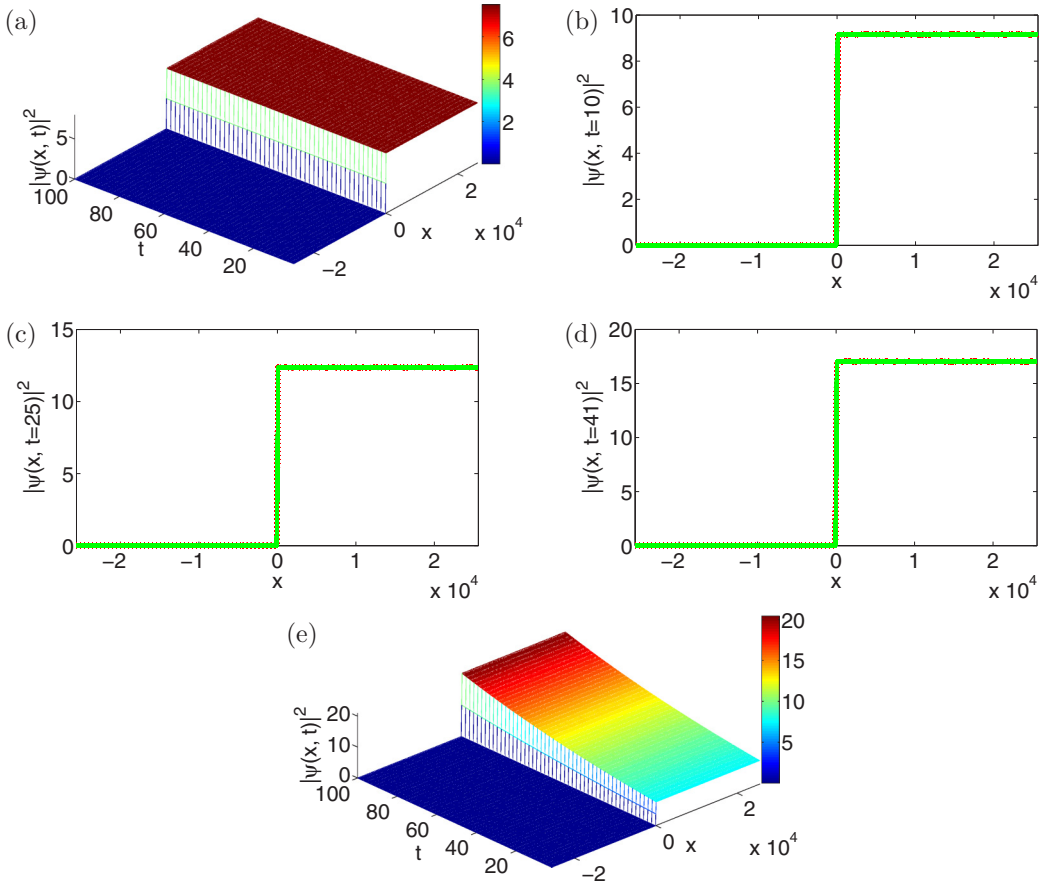


FIG. 10. (Color online) (a)–(c) Parallel between analytical (solid line) and numerical (dotted line) solutions at different times of the kinklike soliton of Fig. 2(b). (d) Spatiotemporal propagation of the stable antikink-like soliton. Parameters are the same as in Fig. 2(a).

as well as the long-time robustness of our bright soliton [Fig. 3(a)].

In the above discussions, we have shown that an analytical solution for the case $\chi = 0$ and $c > 0$ is not available for the physical situation of matter waves in condensates if one uses the Bernoulli equation as an auxiliary equation. To show how far the qualitative behavior changes, we display in Fig. 12 the spatiotemporal evolution of the condensate density with

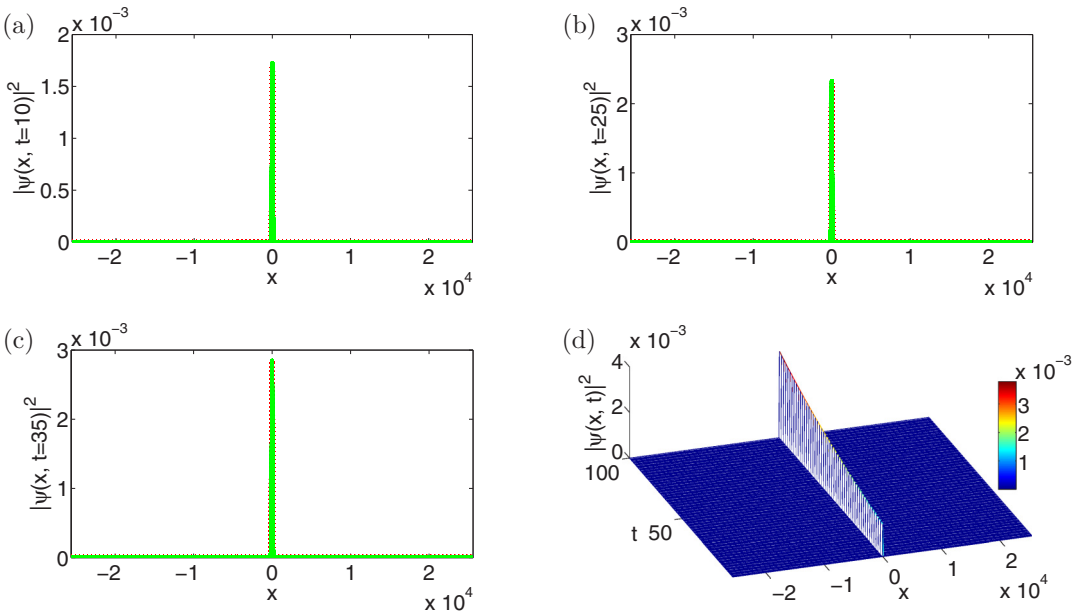


FIG. 11. (Color online) (a)–(c) Parallel between analytical (solid line) and numerical (dotted line) solutions at different times of the bright soliton of Fig. 3(b). (d) Spatiotemporal propagation of the stable bright soliton. Parameters are the same as in Fig. 3(b) except $\gamma = 0.005$.

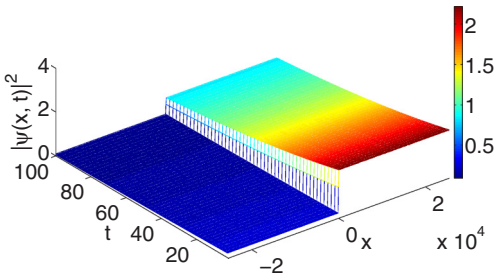


FIG. 12. (Color online) Spatiotemporal evolution of a stable kink solution for $\chi = 0$, $c = 0.5$. The solution is that of Fig. 5 with the same parameters except that of $c$.

the same parameters as in Fig. 5, except $c = 0.5$. As one can see, we obtain a stable kink profile solution, the maximum density of which is 2.21. The analytical solution with $c > 0$ for a (vanishingly) small value of $\chi$ is an antikink solution with very large density, confirming the previous analysis.

The dynamical stability of some trivial-phase dark, kink, and antikink soliton solutions of Eq. (1) has been analyzed mathematically and numerically in Ref. [10]. Here, the dynamical stability of more valuable nontrivial phase solutions is investigated numerically. The stability of the specific solutions that were tested is well verified. Families of solutions constructed here may also be applied in other physical media where Eq. (1) also appears, such as nonlinear fiber optics.

## V. CONCLUSION

In this paper, we have studied the GPE with time-dependent two- and three-body nonlinearities, confined in a harmonic potential and exchanging atoms with the thermal background. By applying the F-expansion method, and taking advantage of solutions of four types of auxiliary equations, i.e., the Bernoulli equation, the Riccati equation, the Lenard equation, and the hyperbolic equation, we have constructed 230 explicit exact solutions of Eq. (1), distributed into 49 families. Among these solutions, we have hyperbolic function solutions and trigonometric functions solutions. Furthermore, we have also found rational function solutions. In comparison with the work done in Ref. [10], we have found more exact solutions of Eq. (1) and we analyzed the stability of some nontrivial phase soliton solutions numerically. The latter nontrivial phase solitons appear to be dynamically stable. The effects of quintic nonlinearity on the formation of matter-wave condensates are also studied in certain cases. It appears that the inclusion of quintic nonlinearity drastically modifies the shape of solutions found with the Riccati and hyperbolic auxiliary equations, and it could lead to localization of solutions. This localization can come from the fact that the inclusion of quintic nonlinearity alters the nonlinearities in such a way that they compensate the dispersion.

When the parameter $\gamma$ is not small, Eq. (1) formally describes the evolution of condensates at finite temperatures where the effects of the thermal cloud become important. Many models have been developed in order to account for the effects of the thermal cloud [38]. Indeed, through a recent self-consistent investigation of the whole thermal cloud part (i.e., the noncondensed and the anomalous densities) by means of a variational time-dependent Hartree-Fock-Bogoliubov theory, the impact of the anomalous density in three- and two-dimensional homogeneous Bose gases at finite temperatures has been analyzed [39,40]. The parameter $\gamma$ can be related to the so-called Keldysh self-energy [41,42]. Comparisons between some finite-temperature BEC models have been performed in Ref. [42]. The dynamics of dark solitons within a finite-temperature BEC model with only two-body interatomic interactions has been reported in Ref. [43]. Nevertheless, many finite-temperature BEC models rarely consider the effects of three-body interactions. For instance, a study of the effects of finite temperature ($\gamma$ large) on the dynamics of solitons in matter waves of BECs with two- and three-body interatomic interactions should be carried out in future works.

## ACKNOWLEDGMENTS

D.B.B. acknowledges the hospitality of the Abdus Salam International Center for Theoretical Physics (Trieste, Italy), where a part of this work was done. D.B.B. is indebted to B. Deconinck and R. Carretero-González for useful discussions on the numerics. T.C.K. is grateful for the hospitality of the Max-Planck Institute for the Physics of Complex Systems in Dresden. The authors acknowledge anonymous reviewers for useful comments and suggestions.

## APPENDIX A: SOLUTIONS OF THE GENERAL BERNOULLI EQUATION

The solutions of the general Bernoulli equation according to Ref. [13] are found to be as follows:

$$F_{11}(\xi) = \left(-\frac{a}{2b}\right)^{\frac{1}{2}}; \tag{A1}$$

$$\xi_0 > 0: F_{12}(\xi) = -\frac{a}{2b}\left[\tanh\left(a\xi - \frac{\ln(\xi_0)}{2}\right) + 1\right]^{\frac{1}{2}}; \tag{A2}$$

$$\xi_0 < 0: F_{13}(\xi) = -\frac{a}{2b}\left[\coth\left(a\xi - \frac{\ln(-\xi_0)}{2}\right) + 1\right]^{\frac{1}{2}}. \tag{A3}$$

## APPENDIX B: SOLUTIONS OF THE RICATTI EQUATION

The solutions of the general Bernoulli equation according to Ref. [20] are found to be as follows:

$$F_{21}(\xi) = \left\{\sqrt{\frac{-1}{M(\lambda-1)}}\tanh[\sqrt{-M(\lambda-1)}\xi]\right\}^{\frac{1}{\lambda-1}}; \tag{B1}$$

$$F_{22}(\xi)=\left\{\sqrt{\frac{-1}{M(\lambda-1)}}\coth[\sqrt{-M(\lambda-1)}\xi]\right\}^{\frac{1}{\lambda-1}}; \tag{B2}$$

$$F_{23}(\xi)=\left(\sqrt{\frac{-1}{M(\lambda-1)}}\left\{\sqrt{\frac{-1}{M(\lambda-1)}}\tanh[\sqrt{-M(\lambda-1)}\xi]\pm\iota\,\mathrm{sech}[\sqrt{-M(\lambda-1)}\xi]\right\}\right)^{\frac{1}{\lambda-1}}; \tag{B3}$$

$$F_{24}=\left\{\sqrt{\frac{-1}{M(\lambda-1)}}\left[\frac{\sqrt{2}\sqrt{\frac{-1}{M(\lambda-1)}}\tanh[\sqrt{-M(\lambda-1)}\xi]\pm\iota\,\mathrm{sech}[\sqrt{-M(\lambda-1)}\xi]}{\sqrt{2}-\mathrm{sech}[\sqrt{-M(\lambda-1)}\xi]}\right]\right\}^{\frac{1}{\lambda-1}}; \tag{B4}$$

$$F_{25}(\xi)=\left\{-\sqrt{\frac{-1}{M(\lambda-1)}}\tan[\sqrt{-M(\lambda-1)}\xi]\right\}^{\frac{1}{\lambda-1}}; \tag{B5}$$

$$F_{26}(\xi)=\left\{\sqrt{\frac{-1}{M(\lambda-1)}}\cot[\sqrt{-M(\lambda-1)}\xi]\right\}^{\frac{1}{\lambda-1}}; \tag{B6}$$

$$F_{27}=\left\{-\sqrt{\frac{-1}{M(\lambda-1)}}\left[\frac{\sqrt{2}\sqrt{\frac{-1}{M(\lambda-1)}}\tan[\sqrt{-M(\lambda-1)}\xi]\pm\iota\,\sec[\sqrt{-M(\lambda-1)}\xi]}{\sqrt{2}+\sqrt{5}\sec[\sqrt{-M(\lambda-1)}\xi]}\right]\right\}^{\frac{1}{\lambda-1}}; \tag{B7}$$

$$F_{28}=\left\{\frac{1}{-M(\lambda-1)\xi+p}\right\}^{\frac{1}{\lambda-1}}. \tag{B8}$$

$p$ is an arbitrary real constant.

## APPENDIX C: SOLUTIONS OF THE LENARD EQUATION

The Lenard equation admits the following solutions [23]:

$$b_2>0,\quad b_4<0,\quad b_6<0,\quad \delta=b_4^2-4b_2b_6>0{:}F_{3,1}=\sqrt{\frac{2b_2\mathrm{sech}^2(\sqrt{b_2}\xi)}{2\sqrt{\delta}-(\sqrt{\delta}+b_4)\mathrm{sech}^2(\sqrt{b_2}\xi)}},$$

$$F_{3,2}=\sqrt{\frac{2b_2\mathrm{csch}^2(\pm\sqrt{b_2}\xi)}{2\sqrt{\delta}+(\sqrt{\delta}-b_4)\mathrm{csch}^2(\pm\sqrt{b_2}\xi)}}; \tag{C1}$$

$$b_0=0,\quad b_2<0,\quad b_4\geqslant 0,\quad b_6<0,\delta>0{:}F_{3,3}=\sqrt{\frac{-2b_2\sec^2(\sqrt{-b_2}\xi)}{2\sqrt{\delta}-(\sqrt{\delta}-b_4)\sec^2(\sqrt{-b_2}\xi)}},$$

$$F3{,}4=\sqrt{\frac{2b_2\csc^2(\pm\sqrt{-b_2}\xi)}{2\sqrt{\delta}+(\sqrt{\delta}+b_4)\csc^2(\pm\sqrt{-b_2}\xi)}}; \tag{C2}$$

$$b_6=\frac{b_4^2}{4b_2},\quad b_2>0,\quad b_4<0{:}F_{3,5}=\sqrt{\frac{-b_2}{b_4}[1+\tanh(\pm\sqrt{b_2}\xi)]},\quad F_{3,6}=\sqrt{\frac{-b_2}{b_4}[1+\coth(\sqrt{b_2}\xi)]}; \tag{C3}$$

$$b_2>0{:}F_{3,7}=\sqrt{\frac{-b_2b_4\mathrm{sech}^2(\sqrt{b_2}\xi)}{b_4^2-b_2b_6[1+\tanh^2(\sqrt{b_2}\xi)]}},\quad F_{3,8}=\sqrt{\frac{b_2b_4\mathrm{csch}^2(\sqrt{b_2}\xi)}{b_4^2-b_2b_6[1+\coth^2(\sqrt{b_2}\xi)]}},$$

$$F_{3,9}=4\sqrt{\frac{b_2\exp(2\sqrt{b_2}\xi)}{\exp(4\sqrt{b_2}\xi-4C_4)-64b_2b_6}}; \tag{C4}$$

$$b_2>0{:}F_{3,7}=4\sqrt{\frac{b_2\exp(2\sqrt{b_2}\xi)}{\exp[(2\sqrt{b_2}\xi-4C_4)^2-64b_2b_6]}};\quad b_2>0,\quad \delta>0{:}F_{3,10}=\sqrt{\frac{2b_2}{\sqrt{\delta}\cosh(2\sqrt{b_2}\xi)-b_4}}; \tag{C5}$$

$$b_2>0,\quad \delta<0{:}F_{3,11}=2\sqrt{\frac{2b_2}{\sqrt{-\delta}\sinh(2\sqrt{b_2}\xi)-b_4}}; \tag{C6}$$

$$b_2<0,\quad \delta>0: F_{3,12}=\sqrt{\frac{2b_2}{\sqrt{\delta}\sin(2\sqrt{-b_2}\xi)-b_4}},\quad F_{3,13}=\sqrt{\frac{2b_2}{\sqrt{\delta}\cos(2\sqrt{-b_2}\xi)-b_4}}; \tag{C7}$$

$$b_2>0,\quad b_6>0;\quad F_{3,14}=\sqrt{\frac{-b_2\mathrm{sech}^2(\sqrt{b_2}\xi)}{b_4+2\sqrt{b_2b_6}\tanh(\sqrt{b_2}\xi)}},\quad F_{3,15}=\sqrt{\frac{b_2\mathrm{csch}^2(\sqrt{b_2}\xi)}{b_4+2\sqrt{b_2b_6}\coth(\sqrt{b_2}\xi)}}; \tag{C8}$$

$$b_2<0,\quad b_6>0: F_{3,16}=\sqrt{\frac{-b_2\sec^2(\sqrt{-b_2}\xi)}{b_4+2\sqrt{-b_2b_6}\tan(\sqrt{-b_2}\xi)}},\quad F_{3,17}=\sqrt{\frac{-b_2\csc^2(\sqrt{-b_2}\xi)}{b_4+2\sqrt{-b_2b_6}\cot(\sqrt{-b_2}\xi)}}; \tag{C9}$$

$$b_2>0,\quad b_4=0: F_{18}=4\sqrt{\frac{\pm b_2\exp(2\sqrt{b_2}\xi)}{1-64b_2b_6\exp(4\sqrt{b_2}\xi)}}; \tag{C10}$$

$$b_2<0,\quad b_4>0: F_{3,19}=\sqrt{\frac{-8b_2\tanh^2\left(\pm\sqrt{\frac{-b_2}{3}}\xi\right)}{3b_4[3+\tanh^2\left(\pm\sqrt{\frac{-b_2}{3}}\xi\right)]}},\quad F_{3,20}=\sqrt{\frac{-8b_2\coth^2\left(\pm\sqrt{\frac{-b_2}{3}}\xi\right)}{3b_4[3+\coth^2\left(\pm\sqrt{\frac{-b_2}{3}}\xi\right)]}}; \tag{C11}$$

$$b_2>0,\quad b_4<0: F_{3,21}=\sqrt{\frac{8b_2\tan^2\left(\pm\sqrt{\frac{b_2}{3}}\xi\right)}{3b_4[3-\tan^2\left(\pm\sqrt{\frac{b_2}{3}}\xi\right)]}},\quad F_{3,22}=\sqrt{\frac{8b_2\cot^2\left(\pm\sqrt{\frac{b_2}{3}}\xi\right)}{3b_4[3-\cot^2\left(\pm\sqrt{\frac{b_2}{3}}\xi\right)]}}. \tag{C12}$$

$b_0=0$ corresponds to $F_{3,1}-F_{3,18}$; $b_0=\frac{8b_2^2}{27b_4}$ and $b_6=\frac{b_4^2}{4b_2}$ correspond to $F_{3,19}-F_{3,22}$.

## APPENDIX D: GENERALIZED JACOBI ELLIPTIC FUNCTION SOLUTIONS OF THE LENARD EQUATION

Some generalized Jacobi elliptic function solutions of the Lenard equation [25–27] are as follows:

$$b_0=1-k_1^2-k_2^2+k_1^2k_2^2,\quad b_2=-1+2k_1^2+2k_2^2-3k_1^2k_2^2,\quad b_4=-k_1^2-k_2^2+3k_1^2k_2^2,\quad b_6=-k_1^2k_2^2: F_{23}=c(\xi,k_1,k_2); \tag{D1}$$

$$b_0=-1+k_1^2-k_2^2+k_1^{-2}k_2^2,\quad b_2=2-k_1^2+2k_2^2-3k_1^{-2}k_2^2,\quad b_4=-1-k_2^2+3k_1^{-2}k_2^2,\quad b_6=-k_1^{-2}k_2^2: F_{24}=d_1(\xi,k_1,k_2). \tag{D2}$$

$c(\xi,k_1,k_2)$ is the generalized Jacobi elliptic cosine function, and $d_1(\xi,k_1,k_2)$ is the generalized Jacobi elliptic function of the third kind. The generalized Jacobi elliptic functions can be written in terms of the standard Jacobi elliptic functions as follows: $c(\xi,k_1,k_2)=k_3cn(k_3\xi,k_4)/\sqrt{1-k_2^2cn^2(k_3\xi,k_4)}$, $d_1(\xi,k_1,k_2)=\sqrt{k_1^2-k_2^2}dn(k_3\xi,k_4)/\sqrt{k_1^2-k_2^2dn^2(k_3\xi,k_4)}$, with $k_3=\sqrt{1-k_2^2}$, $k_4=\sqrt{(k_1^2-k_2^2)/(1-k_2^2)}$, $0\leqslant k_2\leqslant k_1\leqslant 1$. The generalized Jacobi functions degenerate to traditional functions in some limiting cases. For instance, if $k_2\to 0$, one can obtain the usual Jacobi elliptic function solutions: $c(\xi,k_1,0)\to cn(\xi,k_1)$, $d_1(\xi,k_1,0)\to dn(\xi,k_1)$. If $k_1\to 1, k_2\to 0$, one obtains hyperbolic solutions: $c(\xi,1,0), d(\xi,1,0)\to \mathrm{sech}(\xi)$. For $k_1\to 0, k_2\to 0$, the generalized Jacobi elliptic functions degenerate to trigonometric solutions: $c(\xi,0,0)\to\cos(\xi)$, $d_1(\xi,0,0)\to 1$.

## APPENDIX E: SOLUTIONS OF THE HYPERBOLIC EQUATION

Some solutions of the hyperbolic equation [29]:

$$c_2>0,\quad c_0c_2-c_2^2>0,\quad c_2-2c_0+2\sqrt{c_0(c_2-c_0)}\tan\{\sqrt{[c_0(c_2-c_0)]}\xi\}>0:$$
$$\sinh_{11}[F(\xi)]=\left\{\frac{(c_0-\sqrt{c_0(c_2-c_0)}\tan\{\sqrt{[c_0(c_2-c_0)]}\xi\})^2}{c_2(c_2-2c_0+2\sqrt{c_0(c_2-c_0)}\tan\{\sqrt{[c_0(c_2-c_0)]}\xi\})}\right\}^{\frac{1}{2}}; \tag{E1}$$

$$c_2>0,\quad c_0c_2-c_2^2<0,\quad c_2-2c_0+2\sqrt{c_0(c_2-c_0)}\cot\{\sqrt{[c_0(c_2-c_0)]}\xi\}>0:$$
$$\sinh_{12}[F(\xi)]=\left\{\frac{(c_0-\sqrt{c_0(c_2-c_0)}\cot\{\sqrt{[c_0(c_2-c_0)]}\xi\})^2}{c_2(c_2-2c_0+2\sqrt{c_0(c_2-c_0)}\cot\{\sqrt{[c_0(c_2-c_0)]}\xi\})}\right\}^{\frac{1}{2}}; \tag{E2}$$

$$c_2 > 0, \quad c_0c_2 - c_0^2 < 0, \quad c_2 - 2c_0 - 2\sqrt{c_0(c_2-c_0)}\coth\{\sqrt{-[c_0(c_2-c_0)]}\xi\} > 0:$$
$$\sinh_{13}[F(\xi)] = \left\{\frac{(c_0 + \sqrt{-c_0(c_2-c_0)}\coth\{\sqrt{-[c_0(c_2-c_0)]}\xi\})^2}{c_2(c_2-2c_0-2\sqrt{-c_0(c_2-c_0)}\coth\{\sqrt{-[c_0(c_2-c_0)]}\xi\})}\right\}^{\frac{1}{2}}; \tag{E3}$$

$$c_2 < 0, \quad c_0c_2 - c_0^2 < 0, \quad c_2 - 2c_0 - 2\sqrt{c_0(c_2-c_0)}\tanh\{\sqrt{-[c_0(c_2-c_0)]}\xi\} < 0:$$
$$\sinh_{13}[F(\xi)] = \left\{\frac{(c_0 + \sqrt{-c_0(c_2-c_0)}\tanh\{\sqrt{-[c_0(c_2-c_0)]}\xi\})^2}{c_2(c_2-2c_0-2\sqrt{-c_0(c_2-c_0)}\tanh\{\sqrt{-[c_0(c_2-c_0)]}\xi\})}\right\}^{\frac{1}{2}}. \tag{E4}$$

## APPENDIX F: SOLUTIONS OF THE ORDINARY AUXILIARY EQUATION

The auxiliary equation admits the following solutions [23]:

$$b_0 = \kappa^2 - 1, \quad b_2 = 2 - \kappa^2, \quad b_4 = -1{:}F_{3,1} = dn(\xi); \tag{F1}$$
$$b_0 = 1 - \kappa^2, \quad b_2 = 2\kappa^2 - 1, \quad b_4 = -\kappa^2{:}F_{3,2} = cn(\xi); \tag{F2}$$
$$b_0 = -1, \quad b_2 = 2 - \kappa^2, \quad b_4 = \kappa^2 - 1{:}F_{3,3} = 1/dn(\xi); \tag{F3}$$
$$b_0 = 1, \quad b_2 = 2\kappa^2 - 1, \quad b_4 = \kappa^2(-1+\kappa^2){:}F_{3,4} = sn(\xi)/dn(\xi); \tag{F4}$$
$$b_0 = -2\kappa^3 + \kappa^4 + \kappa^2, \quad b_2 = 6\kappa - \kappa^2 - 1, \quad b_4 = -4/\kappa{:}F_{3,5} = \kappa dn(\xi)cn(\xi)/[1+\kappa sn^2(\xi)]; \tag{F5}$$
$$b_0 = 2 - 2\kappa_1 - \kappa^2, \quad b_2 = -6\kappa_1 - \kappa^2 + 2, \quad b_4 = -4\kappa_1{:}F_{3,6} = \kappa^2 sn(\xi)cn(\xi)/[\kappa_1 + dn^2(\xi)]; \tag{F6}$$
$$b_0 = (\kappa^2-1)/4\left(D_3^2\kappa^2 - D_2^2\right), \quad b_2 = (\kappa^2+1)/2, \quad b_4 = \left(D_3^2\kappa^2 - D_2^2\right)(\kappa^2-1)/4:$$
$$F_{3,7} = \sqrt{\left(D_2^2 - D_3^2\right)/\left(D_2^2 - D_3^2\kappa^2\right)}sn(\xi); \tag{F7}$$
$$b_0 = (2\kappa - \kappa^2 - 1)/D_2^2, \quad b_2 = 2\kappa^2 + 2, \quad b_4 = -D_2^2\kappa^2 - D_2^2 - 2D_2^2\kappa^2{:}F_{3,8} = [\kappa^2 sn^2(\xi) - 1]/D_2[\kappa sn^2(\xi) + 1]; \tag{F8}$$
$$b_0 = -(2\kappa + \kappa^2 + 1)/D_2^2, \quad b_2 = 2\kappa^2 + 2, \quad b_4 = -D_2^2(\kappa^2 + 1 + 2\kappa){:}F_{3,9} = [\kappa sn^2(\xi) + 1]/D_2[\kappa sn^2(\xi) - 1]; \tag{F9}$$
$$b_0 = b_4 = (\kappa^2-1)/4, \quad b_2 = (\kappa^2+1)/2{:}F_{3,10} = dn(\xi)/[1 \pm \kappa sn(\xi)], \quad F_{3,11} = \kappa sd(\xi) \pm nd(\xi); \tag{F10}$$
$$b_0 = -(1-\kappa^2)/4, \quad b_2 = (\kappa^2+1)/2, \quad b_4 = -1/4{:}F_{3,12} = \kappa sd(\xi) \pm nd(\xi); \tag{F11}$$
$$b_0 = 0, \quad b_2 > 0, \quad b_4 < 0{:}F_{3,13} = \sqrt{-b_2/b_4}\,\mathrm{sech}(\sqrt{b_2}\xi); \tag{F12}$$

where $\kappa$ $(0 < \kappa < 1)$ denotes the modulus of the Jacobi elliptic function, $\kappa_1 = \sqrt{1-\kappa^2}$, and $D_2$, $D_3$ $(D_2D_3 \neq 0)$, and $D_4$ are arbitrary constants.


[1] *Emergent Nonlinear Phenomena in Bose-Einstein Condensates. Theory and Experiment*, edited by P. G. Kevrekidis, D. J. Frantzeskakis, and R. Carretero-González (Springer-Verlag, Berlin, 2008), and references therein.

[2] C. P. Search, W. Zhang, and P. Meystre, Phys. Rev. Lett. **92**, 140401 (2004).

[3] K. M. R. van der Stam, R. Meppelink, J. M. Vogels, and P. van der Straten, Phys. Rev. A **75**, 031602 (2007).

[4] V. A. Brazhnyi, V. V. Konotop, V. M. Pérez-García, and H. Ott, Phys. Rev. Lett. **102**, 144101 (2009).

[5] C. Yuce and A. Kilic, Phys. Rev. A **74**, 033609 (2006); L. Wu, R-J. Jiang, Y. H. Pei, and J-F. Zhang, *ibid.* **75**, 037601 (2007).

[6] P. D. Drummond and K. V. Kheruntsyan, Phys. Rev. A **63**, 013605 (2000).

[7] B. Kneer, T. Wong, K. Vogel, W. P. Schleich, and D. F. Walls, Phys. Rev. A **58**, 4841 (1998); A. M. Guzman, M. Moore, and P. Meystre, *ibid.* **53**, 977 (1996).

[8] R. Atre, P. K. Panigrahi, and G. S. Agarwal, Phys. Rev. E **73**, 056611 (2006); V. N. Serkin and A. Hasegawa, Phys. Rev. Lett. **85**, 4502 (2000); V. I. Kruglov, A. C. Peacock, and J. D. Harvey, *ibid.* **90**, 113902 (2003).

[9] L.-C. Zhao, Z.-Y. Yang, T. Zhang, and K.-J. Shi, Chin. Phys. Lett. **26**, 120301 (2009).

[10] *Bäcklund and Darboux Transformations*, edited by A. Coely *et al.* (American Mathematical Society, Providence, RI, 2001), and references therein.

[11] H. A. Abdusalam, Int. J. Nonlin. Sci. Numer. Simul. **6**, 99 (2005).

[12] Z. Y. Yan, Phys. Lett. A **292**, 100 (2001).

[13] M. L. Wang, Phys. Lett. A **213**, 279 (1996).

[14] E. Yomba, Chaos Solitons Fractals **21**, 75 (2004).

[15] Y. B. Zhou, M. L. Wang, and Y. M. Wang, Phys. Lett. A **308**, 31 (2003).

[16] A. Mohamadou, E. Wamba, D. Lissouck, and T. C. Kofane, Phys. Rev. E **85**, 046605 (2012).

[17] E. Wamba, T. C. Kofane, and A. Mohamadou, Chin. Phys. B **21**, 070504 (2012).
[18] D. Belobo Belobo, G. H. Ben-Bolie, and T. C. Kofane, Phys. Rev. E **89**, 042913 (2014).
[19] W. X. Ma and B. Fuchssteiner, Int. J. Nonlin. Mech. **31**, 329 (1996).
[20] L. Khaykovich, F. Schreck, G. Ferrari, T. Bourdel, J. Cubizolles, L. D. Carr, Y. Castin, and C. Salomon, Science **296**, 1290 (2002).
[21] K. E. Strecker, G. B. Partridge, A. G. Truscott, and R. G. Hulet, New J. Phys. **5**, 73 (2003).
[22] N. Dror, B. A. Malomed, and J. Zeng, Phys. Rev. E **84**, 046602 (2011).
[23] W. van Saarloos and P. C. Hohenberg, Phys. Rev. Lett. **64**, 749 (1990); V. Hakim, P. Jacobsen, and Y. Pomeau, Europhys. Lett. **11**, 19 (1990); B. A. Malomed and A. A. Nepomnyashchy, Phys. Rev. A **42**, 6009 (1990).
[24] S. Wabnitz, PIERS ONLINE **5**, 621 (2009).
[25] G. P. Agrawal and C. Headley III, Phys. Rev. A **46**, 1573 (1992).
[26] S. Zhang, Y. N. Sun, J. M. Ba, and L. Dong, J. Adv. Math. Studies **3**, 125 (2010).
[27] A. Mohamadou, E. Wamba, S. Y. Doka, T. B. Ekogo, and T. C. Kofane, Phys. Rev. A **84**, 023602 (2011).
[28] O. Morsch and M. Oberthaler, Rev. Mod. Phys. **78**, 179 (2006); G. K. Campbell, Ph.D. thesis, MIT, 2006.
[29] L-H. Zhang, Appl. Math. Comput. **208**, 144 (2009).
[30] E. A-B. Abdel-Salam, Z. Naturforsch. a **64**, 639 (2009).
[31] H. F. Baker, *Abelian Functions* (Cambridge University Press, Cambridge, 1897).
[32] P. F. Byrd and M. D. Friedman, *Handbook of Elliptic Integrals for Engineers and Physicists* (Springer, Berlin, 1954).
[33] E. T. Whittaker and G. N. Watson, *A Course of Modern Analysis. An Introduction to the General Theory of Infinite Processes and of Analytic Functions* (Cambridge University Press, Cambridge, 1996).
[34] J. C. Bronski, L. D. Carr, B. Deconinck, and J. N. Kutz, Phys. Rev. Lett. **86**, 1402 (2001); J. C. Bronski, L. D. Carr, B. Deconinck, J. N. Kutz, and K. Promislow, Phys. Rev. E **63**, 036612 (2001); B. Deconinck, B. A. Frigyik, and J. N. Kutz, Phys. Lett. A **283**, 177 (2001).
[35] S. D. Zhu, Chaos Solitons Fractals **34**, 1608 (2007).
[36] D. Belobo Belobo, G. H. Ben-Bolie, T. B. Ekogo, and T. C. Kofane, Int. J. Theor. Phys. **52**, 1415 (2013).
[37] G. P. Agrawal, *Nonlinear Fiber Optics* (Academic, San Diego, 2006), and references therein.
[38] N. P. Proukakis and B. Jackson, J. Phys. B **41**, 203002 (2008), and references therein.
[39] A. Boudjemâa and M. Benarous, Phys. Rev. A **84**, 043633 (2011).
[40] A. Boudjemâa, Phys. Rev. A **86**, 043608 (2012).
[41] H. T. C. Stoof, J. Low Temp. Phys. **114**, 11 (1999).
[42] S. P. Cockburn, A. Negretti, N. P. Proukakis, and C. Henkel, Phys. Rev. A **83**, 043619 (2011).
[43] S. P. Cockburn, H. E. Nistazakis, T. P. Horikis, P. G. Kevrekidis, N. P. Proukakis, and D. J. Frantzeskakis, Phys. Rev. Lett. **104**, 174101 (2010).